VULNERABILITY OF TRANSBOUNDARY RIVER BASINS IN A CHANGING CLIMATE: A CASE STUDY OF THE SASKATCHEWAN RIVER BASIN

A Thesis Submitted to the College of
Graduate and Postdoctoral Studies
In Partial Fulfillment of the Requirements
For the Degree of Master of Environment and Sustainability
In the School of Environment and Sustainability
University of Saskatchewan
Saskatoon
Canada

By
KASRA KESHAVARZ

PERMISSION TO USE

In presenting this thesis in partial fulfillment of the requirements for a Postgraduate degree from the University of Saskatchewan, I agree that the Libraries of this University may make it freely available for inspection. I further agree that permission for copying of this thesis in any manner, in whole or in part, for scholarly purposes may be granted by the professor or professors who supervised my thesis work or, in their absence, by the Head of the Department or the Dean of the College in which my thesis work was done. It is understood that any copying or publication or use of this thesis or parts thereof for financial gain shall not be allowed without my written permission. It is also understood that due recognition shall be given to me and to the University of Saskatchewan in any scholarly use which may be made of any material in my thesis.

Requests for permission to copy or to make other uses of materials in this thesis in whole or part should be addressed to:

Director
School of Environment and Sustainability
University of Saskatchewan
117 Science Place, Kirk Hall
Saskatoon, Saskatchewan, S7N 5C8, Canada

OR

Dean
College of Graduate and Postdoctoral Studies
University of Saskatchewan
116 Thorvaldson Building, 110 Science Place
Saskatoon, Saskatchewan, S7N 5C9, Canada

ABSTRACT

About half of the Earth's land surface is covered by transboundary water resources. Approximately 40 percent of the world's population relies on water resources crossing political borders. Within transboundary river basins, allocating these limited and often depleting resources to states is challenging due to various, and often conflicting interests of stakeholders. Treaties and River Basin Organizations (RBOs) provide the primary means of cooperation between states, building institutional capacity, and lowering the likelihood of hydropolitical tensions. A resilient transboundary river system should be able to tolerate the pressures from different stressors to provide a reliable source of water. However, geopolitical, socio-economic, and biophysical stressors threaten the governance of these basins. Climate change is one of the biophysical stressors which is likely to increasingly challenge transboundary river systems. A thorough understanding of climate-change-induced vulnerabilities of a transboundary system, therefore, can help decision and policy makers to plan for adaptive measures to avoid hydropolitical tensions. The Saskatchewan River Basin, located in western Canada and shared amongst the three Canadian provinces of Alberta, Saskatchewan, and Manitoba and also the American state of Montana, is used as a case study. In particular, this thesis assesses the viability of the 1969 Master Agreement on Apportionment that provides the basis for water allocation of eastward flowing interprovincial streams in face of deep uncertainty around future climate change. To this end, a vulnerability assessment methodology consisting of three main components is proposed. First a large set of plausible weather scenarios is generated by perturbing important features of climate including winter precipitation, summer precipitation, annual temperature, and the annual number of dry days. Second, the weather scenarios are fed into a conceptual hydrological model calibrated to historical record to generate a wide range of plausible future streamflow scenarios. Third, the streamflow scenarios are used as input to a water resources management model that distributes the water throughout the transboundary river system. Results show a moderate risk of failure in the southern part of the basin in meeting the criteria established in the apportionment agreement under certain possible changes in climate regime of the region. The risk of not meeting the minimum flow is accompanied by major deficits to irrigation and non-irrigation demands as well as minimum environmental flows. A lower risk is observed in other parts of the basin, mainly due to lower water usage and abstraction.

Keywords: transboundary river basin, climate change, institutional capacity, vulnerability assessment, stochastic weather generator, HBV-SASK.

ACKNOWLEDGMENTS

First and foremost, I would like to express my sincere gratitude to my advisor, Dr. Saman Razavi, for his continuous support during my research and study, and also for his patience and mentorship. Also, I would like to appreciate him for his personal care in helping me settle in Canada and giving me the opportunity to pursue my graduate studies. Most importantly, he helped me to become an independent researcher that is much appreciated.

Besides my advisor, it is my pleasure to thank my advisory committee members for their support, insightful comments, and challenging questions: Dr. Howard Wheater, Dr. Mohamed Elshamy, Dr. Colin Whitfield, and also Dr. Yanping Li. My sincere gratitude goes to my fellow colleagues and lab mates for their support, stimulating discussion and efforts: Dr. Shervan Gharari, Mustakim Ali, Leila Eamen, Hayley Carlson, Mohamed Abdelhamed, Dr. Amin Haghnegahdar, Dr. Jefferson Wong, Dr. Andrew Slaughter, Dr. Do Nhu and Dr. Fuad Yassin. Furthermore, I would like to personally thank Michelle Martel-Andre, Sherry Olauson, Mark Ferguson, Viet Truong, Jordan Becker, Kelly McShane, and Dr. Phani Adapa at the Global Institute for Water Security (GIWS).

Also, I must thank my course instructors for providing a joyful scientific atmosphere and their teaching efforts: Drs. Helen Baulch, Philip Loring and Jeffrey McDonnell from the School of Environment and Sustainability (SENS), and Dr. Margot Hurlbert and Wayne Dybvig from the Johnson Shoyama Graduate School of Public Policy (JSGS). Furthermore, I would like to thank Drs. Hossein Alizadeh, Abbas Afshar, and Ali Kaveh from the Iran University of Science and Technology (IUST) for their recommendations which provided me with an opportunity, in the first place, to study at this great university. And finally, I would like to thank my friends and family who supported me spiritually throughout my life, and especially, during the past three years.

My graduate studies at the University of Saskatchewan were financially supported by the Global Water Futures (GWF) and the Integrated Modelling Program for Canada (IMPC) which, hereby, are acknowledged.

DEDICATION

To my family.

TABLE OF CONTENTS

LIST OF TABLES

LIST OF FIGURES

LIST OF ABBREVIATIONS

AB	Province of Alberta
ACF	Autocorrelation Function
AET	actual evapotranspiration
°C	degrees Celsius
CA	Canada
cdf	cumulative distribution function
cms	cubic meters per second
CMIP5	Coupled Model Inter-comparison Project Phase 5
DDS	dynamically dimensioned search
DJF	December, January, February
ecdf	empirical cumulative distribution function
ET	evapotranspiration
FDC	flow duration curve
g	grams
GHGES	greenhouse gas emission scenario
ICJ	International Court of Justice
IIL	Institute of International Law
IJC	International Joint Commission
ILA	International Law Association
ILC	International Law Commission
Info-Gap	information gap theory
IPCC	Intergovernmental Panel on Climate Change
IRCC	International River Basin Conflict and Cooperation
IWED	International Water Event Database
IWMSask	Integrated Water Management Model of the SaskRB
JJA	June, July, August

km	kilometres
LP	Linear Programming
OA/GCM	ocean-atmosphere/general circulation model
MAM	March, April, May
mb	millibar
MB	Province of Manitoba
mm	millimetre
MODIS	Moderate Resolution Imaging Spectroradiometer
MT	State of Montana
NFA	Network Flow Algorithm
NSR	North Saskatchewan River
PET	potential evapotranspiration
pdf	probability distribution function
PIC	Permanent Indus Commission
PPWB	Prairie Provinces Water Board
rad	radian
RBO	river basin organization
RCM	regional climate model
RCP	representative concentration pathway
RF	Reference Flow
SaskRB	Saskatchewan River Basin
SK	Province of Saskatchewan
SON	September, October, November
SR	Saskatchewan River
SRD	Saskatchewan River Delta
SSR	South Saskatchewan River
TFDD	Transboundary Freshwater Dispute Database
UN	United Nations

UNECE	United Nations Economic Commission for Europe
UNEP	United Nations Environment Programme
US	United States
WG	weather generator

1 CHAPTER 1: INTRODUCTION

1.1 Background

Water is one of the most valuable substances on Earth, enabling the formation of life and an integral part of humans' technological and socio-economic developments. While much of the world's surface is covered by water, only 2.5 percent of it is in the form of freshwater (Gleick 2003). Moreover, much of the freshwater is stored in glaciers and deep groundwater, and only a small fraction of it is available for direct use (Shiklomanov 1993). Rivers are the major source of easily accessible freshwater and humans have historically relied on them for their various needs. Nowadays, rivers provide approximately 47 000 km^3 of this limited resource to societies on average each year (Shiklomanov 1993), which are used for both navigational and non-navigational purposes. Like any other natural resource, waters flowing in the rivers are managed by humans based on their various, competing interests. The impacts of human management measures are usually sensed across an entire river basin. Managerial measures, such as the construction of hydraulic infrastructures on the river system or land-use change to expand agricultural activities, can significantly change the spatial and temporal availability of freshwater flow along with its quality throughout the river basin.

Managing freshwater resources, however, is not an easy task. Water management problems are deemed to be wicked in nature (Reed and Kasprzyk 2009; Rittel and Webber 1973) due to competing interests and contrasting perceptions of stakeholders in a river basin (Islam and Repella 2015). The more stakeholders' interests and incentives differ, the less are the chances that consensus could be achieved over a specific management scheme. Political boundaries add another layer of complexity in water management as the incentives of each state to cooperate could differ significantly (Barua et al. 2019; Wolf et al. 2005). Transboundary water resources, which can be broadly defined as "any surface … waters which mark, cross or are located on boundaries between two or more States" (UNECE 2013), pose nontrivial challenges to international relations.

Currently, 310 internationally-shared river basins have been recognized covering nearly half of the Earth's land surface (McCracken and Wolf 2019). As nearly 40 percent of the world's population rely on the water resources of these basins (UNEP-DHI and UNEP 2016; World Bank 2019), policymakers are required to select sustainable and resilient governance mechanisms to foster water security. Apart from internationally-shared basins, there are many inter-provincial and inter-state basins within each country that can also be categorized as transboundary. Therefore, the total number and spatial coverage of these basins are potentially well above the mentioned statistics.

Security of water resources in transboundary basins could be promoted by constructive cooperation between states (UNECE 2013); however, conflict is often inevitable in this context (Petersen-Perlman et al. 2017; Spector 2000; Zeitoun and Mirumachi 2008). To promote cooperation between states, transboundary water institutions are employed in many river basins around the globe (Norman and Bakker 2015). Institutional governance of transboundary river systems plays an important role in increasing the resiliency of these systems in the face of endogenous and exogenous stressors (Giordano and Wolf 2003; De Stefano et al. 2012, 2017; Wolf et al. 2005).

One of the concerning stressors to river systems in today's world is anthropogenic climate change[1] (UNECE 2016). Climate change is suggested to adversely impact the environment and nature resulting in declining human, food, and water security around the globe (IPCC 2018). A recent IPCC report (2018) suggests that a global warming of 1.5°C above pre-industrial levels can potentially have irreversible impacts on the environment by negatively affecting natural and human systems. Milly et al. (2008) claim that climate change is already impacting hydrology in an unprecedented way with significant impacts observable in various river basins around the world (for example, see Olsson et al. 2015; Shrestha et al. 2016; Steele-Dunne et al. 2008; Zhuang et al. 2017). However, the future conditions of this phenomenon and its impact on hydrology remain uncertain (for example, see Hagemann et al. 2013; Milly and Dunne 2017; Refsgaard et al. 2016; Shen et al. 2018; Winter et al. 2015). This uncertainty can lower the resiliency of transboundary river systems in the face of climate change and significantly complicate management and cooperation in internationally-shared basins (Dinar et al. 2015, 2019; De Stefano et al. 2012, 2017; Tir and Stinnett 2012). Therefore, understanding the vulnerabilities of a transboundary river

[1] *Hereinafter, "climate change".*

system and its pre-existing adaptive capacity in regard to climate change is of utmost importance (UNECE 2016).

1.2 Thesis Objective and Outline

The overall purpose of this research is to propose an approach to conduct vulnerability assessments in transboundary river basins. To this end, firstly, a literature review is conducted to understand the status quo of vulnerability assessment in transboundary river basins. Secondly, three different computer models are used to construct a methodology and framework for vulnerability assessment. Thirdly, a transboundary river basin deemed susceptible to future climatic changes is chosen to demonstrate the application of the methodology.

After conducting a literature review in Chapter 2, the details of the selected transboundary basin are described in Chapter 3. The proposed methodology of this research begins with constructing several climate change scenarios. A stochastic weather generator is used to generate long, synthetic weather time-series reflecting plausible changes in several climate attributes. The details of weather generation and perturbation of weather time-series are explained in Section 4.2 of Chapter 4. Thereafter, a hydrological model is utilized to translate the weather time-series into river flows. In doing so, a variant of the well-known HBV model is employed, the details of which are presented in Section 4.3. Next, a water resources management model is employed to distribute the river flows throughout the selected river basin. Thereafter, the effects of changes in climate attributes on the amounts of water crossing political borders are assessed, and whether a water-sharing agreement is violated or not is examined. The results of the analysis are demonstrated in Chapter 5 for each component of the methodology. Finally, in Chapter 6 a discussion is developed, and thereafter, final conclusions and limitations are discussed.

2 CHAPTER 2: LITERATURE REVIEW

2.1 Transboundary Water Governance

As mentioned earlier, transboundary river basins are providing water to at least half of the world's population and need a resilient governance mechanism to promote water security. Wheater and Gober (2013) define water security as "sustainable use and protection of water resources, safeguarding access to water functions and services for humans and the environment, and protection against water-related hazards (flood and drought)." Security of water resources in transboundary basins could be promoted by constructive cooperation between states (UNECE 2013), while conflict is always the flip side of the coin (Petersen-Perlman et al. 2017; Spector 2000; Zeitoun and Mirumachi 2008). Diplomacy can play a key role in elevating the level of cooperation (McCracken and Meyer 2018) and lowering potential hydro-political tensions. 'Water diplomacy' aims at the stewardship of multilateral relationships by encouraging states to take peaceful measures towards conflict resolution (Schmeier and Shubber 2018). The outcome of constructive water diplomacy is various institutional frameworks including River Basin Organizations (RBOs) and treaties.

Treaties and negotiated agreements around water resources lie at the heart of promoting institutionalized cooperation between states. Shared water resources issues have rarely been the source of violent conflict throughout history (Zeitoun and Mirumachi 2008), and instead have mostly led to cooperative relationships (Kalbhenn and Bernauer 2012); based on the Transboundary Freshwater Dispute Database (TFDD 2017), 600 international treaties regarding transboundary rivers were signed between 1820 and 2007. The extensive work of the Institute of International Law (IIL), the International Law Association (ILA), and the International Law Commission (ILC) provide a comprehensive basis to catalyze initial negotiations over shared water treaties (Salman 2007; Troell and Swanson 2014). The efforts of these institutions have resulted in several guidelines and commitments, such as the 1966 Helsinki Rules on the Use of

Waters of International Rivers[1] (ILA 1966), the Berlin Rules on Water Resources[2] (ILA 2004), and the United Nations Convention on the Law of the Non-navigational Uses of Transboundary Watercourses[3] (UN 1997). Notably, except for the 1997 UN Watercourses Convention which came into force in 2014, none of these international guidelines have legally binding effects per se (Caponera 1985). However, even before 2014, the UN Watercourses Convention gained prominence within international law; the International Court of Justice (ICJ) explicitly referred to the 1997 UN Watercourses Convention in the Gabĉìkovo-Nagymaros case (International Court of Justice 1997 p. 53) highlighting the Convention's importance. It is worth mentioning that the fundamental philosophy behind the modern international water law is the principle of limited territorial sovereignty (see Salman 2007). This principle calls upon states to "equitably" and reasonably utilize shared water resources and "prevent significant harm" to other states (Rieu-Clarke 2019; Troell and Swanson 2014). These two concepts constitute Articles 6 and 7 of the UN Watercourses Convention. As explained thus far, international water law could be a starting point for further diplomatic negotiations between states to locally establish institutional arrangements and treaties. Upon signing a treaty, further collaboration is required to enforce treaty commitments, share information related to transboundary river management, resolve prospective conflicts in the basin, and in general, foster water diplomacy (Gerlak et al. 2011; Mitchell and Zawahri 2015; Schmeier and Shubber 2018).

River Basin Organizations (RBOs), alongside treaties, provide such mechanisms, and not surprisingly, are highly encouraged by the aforementioned guidelines. RBOs are "institutionalized forms of cooperation that are based on binding international agreements covering the geographically defined area of international river or lake basins characterized by principles, norms, rules and governance mechanisms" (Schmeier et al. 2016). Schmeier and Shubber (2018) have called RBOs 'institutional anchors' letting water diplomacy flourish if clear and enough legal duties are associated with them. These organizations are an indispensable part of cooperation as they pave the way for stakeholder and public engagement, data sharing, and at the same time, providing a framework for further dialogue and negotiation (Gerlak et al. 2011; Mitchell and Zawahri 2015; De Stefano et al. 2017; Troell and Swanson 2014). Not surprisingly, the interest in the establishment of RBOs has grown significantly over the course of the 19th and 20th centuries

[1] *Hereinafter "Helsinki Rules"*
[2] *Hereinafter "Berlin Rules"*
[3] *Hereinafter "UN Watercourses Convention"*

(Giordano et al. 2014). Nowadays, RBOs and treaties are indispensable parts of institutional transboundary river governance. In North America, the 1909 Boundary Waters Treaty governs the shared water resources between Canada and the United States and suggests the establishment of the International Joint Commission (IJC) to foster further cooperation (Grover and Krantzberg 2015). In Europe, the Convention on Co-operation for the Protection and Sustainable Use of the Danube River provides regulations on the non-navigational water uses of the river and proposes an RBO to ease further negotiations between states (Gerlak 2004). In the Middle East, the Afghan-Iranian Helmand River Water Treaty oversees the management of the Helmand River and recommends the establishment of the Helmand River Delta Commission for further collaboration (Giordano et al. 2014). In South Asia, the Indus Water Treaty settles water disputes between India and Pakistan and suggests the foundation of the Permanent Indus Commission (PIC) to engage both nations in collaboration over shared water issues (Miner et al. 2009).

Nation-state-driven treaties and RBOs are the primary means of collaboration within the transboundary river basins in today's world (Norman and Bakker 2015). Building institutional capacity by signing treaties and setting up RBOs increases the resiliency of transboundary river systems in the face of various stressors and potentially lowers the likelihood of hydropolitical tensions (Giordano and Wolf 2003; De Stefano et al. 2017; Wolf et al. 2005). Nevertheless, "the likelihood and intensity of conflict within a basin increase as the magnitude or amount of physical or institutional change [due to stressors] exceeds the capacity within the basin to absorb that change" (Yoffe et al. 2003). Landovsky (2006) categorizes stressors threatening transboundary river systems as being: 1) geopolitical, 2) socioeconomic, and 3) biophysical. In this discourse, Iyob (2010) defines resilience as the "ability of a transboundary water management system to maintain its basic functions when subjected to biophysical, socioeconomic, and geopolitical [stressors]." While geopolitical stressors directly target the institutional capacity of transboundary river systems, socioeconomic and biophysical stressors first target the basin's ecosystem and landscape which indirectly impacts the institutional capacity (Landovsky 2006, 2011). A resilient transboundary river system has the potential capacity to lower hydropolitical disputes between states to the lowest degree. Therefore, it is mandatory to grasp the prospective impacts of different stressors and how they can challenge the institutional and ecosystem capacities of transboundary river systems.

In the literature, several inventories have been developed to provide a historical overview of cooperative and conflictive relations in transboundary river systems influenced by different types of stressors: the International Water Event Database (IWED, De Stefano et al. 2010; Wolf et al. 2003), the International River Basin Conflict and Cooperation (IRCC, Kalbhenn and Bernauer 2012), and the Issue Correlates of War – River Claims database (Hensel et al. 2008). In addition to the mentioned inventories, De Stefano et al. (2017) provide a global analysis of the impact of the three types of stressors – with a focus on river damming – and qualitatively describe the risk of potential future hydro-political conflicts. Besides, Farinosi et al. (2018) analyze the stressors which were historically more influential in conflictive and cooperative relations and examine the likelihood of future potential tensions worldwide by considering socioeconomic and biophysical stressors. Notwithstanding the existence of these global inventories, a more detailed analysis of each transboundary basin is mandatory (Farinosi et al. 2018). Many researchers have tried to analyze the impact of different stressors within a particular transboundary river basin: some focus on geopolitical stressors, such as institutional fragmentation (Jetoo et al. 2015), the peacefulness of states' interrelations (Abdolvand et al. 2015; Brichieri-Colombi and Bradnock 2003; Jetoo et al. 2015; Subramanian et al. 2014), the existence of RBOs (Odom and Wolf 2011), foreign interventions (Nagheeby and Warner 2018), lack of treaties (Atef et al. 2019; Tir and Stinnett 2012), etc.; many have considered socioeconomic stressors, such as river damming (Al-Faraj and Scholz 2015), increased hydropower demands (Kuenzer et al. 2013; McNally et al. 2009; Wyatt and Baird 2007), population growth (Bakker and Duncan 2017), etc. Also, many have analyzed biophysical stressors, such as water quality degradation (Shmueli 1999), and climate change (De Stefano et al. 2012), which exacerbates the frequency and intensity of extreme climatic events, such as flood (Bakker 2009) and drought (Do Ó 2012; Sapountzaki and Daskalakis 2016; Ward 2013).

2.2 Anthropogenic Climate Change

This research is focused on one of the most critical biophysical stressors, climate change. Climate change is a direct result of greenhouse gas emissions, land-use change and aerosol releases into the atmosphere. A recent IPCC report (2018) asserts that the average global temperature is projected to increase by 1.5°C above pre-industrial levels by 2030. This global warming will likely

result in negative impacts on ecosystems, sea-level rise, and an increase in the frequency and intensity of extreme weather events with increasing risks to human, food, and water security (IPCC 2018). This stressor threatens transboundary river systems, challenging their institutional and ecosystem capacities (UNECE 2016). Water supply in transboundary rivers is undoubtedly affected by this phenomenon. Milly et al. (2008) claim that climate change falsifies the conventional assumption of hydro-climate stationarity, as the hydro-climate no longer fluctuates within its historical envelope of variability. This could pose a great risk to the water supply which is of high importance in the transboundary context. A resilient institutional capacity can potentially prevent financial losses and hydropolitical tensions (World Bank 2019). Building resilience against climate change by adaptive planning can sustain ecosystems, economies, and interrelations. Whereas, maladaptation can result in negative impacts that can be felt across borders affecting several states, stakeholders, and political systems (World Bank 2019). The first step towards adaptation is understanding the climate-induced vulnerabilities. UNECE (2016) recently has called for "a vulnerability assessment … at the transboundary basin scale" as it can bring about common understandings of river basin system settings amongst states and can avert maladaptation and hydropolitical tension due to disintegration. Nevertheless, uncertainties associated with future changes in climate can diminish decision-makers' ability to fully understand areas of vulnerability of a transboundary river system. A comprehensive vulnerability assessment approach must be able to address a broad spectrum of associated uncertainties to provide analysts and decision-makers with a thorough understanding of system susceptibilities.

Walker et al. (2013) define uncertainty as "limited knowledge about future, past, or current events." In the context of climate change, the uncertainty regarding how the future climate conditions will unfold is of main concern. A spectrum of future uncertainties, including five levels ranging from "complete certainty" to "total ignorance" is conceptualized according to the literature. Table 2.1 describes these five levels as being: 1) complete certainty, 2) shallow uncertainty, 3) medium uncertainty, 4) deep uncertainty, and 5) total ignorance. The level one uncertainty (or recognized uncertainty) signifies the situation where the future is crystal clear. However, it is acknowledged that a true realization of the future requires a high degree of knowledge about the system as well as the characteristics of the uncertain phenomenon. Level two uncertainty (shallow uncertainty) denotes the condition where single or multiple futures could be realized, each associated with objective (or subjective) probabilities (Kwakkel et al. 2010). In the

climate change context, as an example, an ensemble of ocean-atmosphere/general circulation models (OA/GCMs) projections are used to provide a set of probabilistic futures. However, this is not the only level of uncertainty imaginable for climate change in the literature (Maier et al. 2016). Turning to the level three uncertainty (medium uncertainty), it expresses the situation where a set of futures could be realized and ranked based on the perceived likelihood of possibility (Walker et al. 2013). However, in this case, no probability is associated with each case due to the higher level of uncertainty, but the realized futures could be ranked qualitatively using descriptive language (Patt and Schrag 2003). For example, IPCC uses descriptive terminology in explaining the likelihood of future climate conditions (see IPCC 2018) using phrases such as "high confidence", "very high confidence", etc. A deeper level of uncertainty is level four uncertainty (deep uncertainty) which suggests the condition where "it is impossible to form a group of instances because the situation dealt with is in a high degree unique" (Knight 1921). In this type of uncertainty, many plausible futures must be enumerated, while they cannot be ranked or associated with a probability (Kwakkel et al. 2010). The extreme case is the level five uncertainty (total ignorance) that manifests the case in which unknowns are unknown. Taleb (2007) claims that this type of future "lies outside the realm of regular expectations … [and] carries an extreme impact", making surprises or 'Black Swans' inevitable. An example of a Black Swan is the terror attack of 11 September 2001 in New York City (Taleb 2007). Table 2.1 and Figure 2.1 summarize the described levels of future uncertainty.

Based on the perceived level of uncertainty of future climatic changes, analysts determine the method of vulnerability assessment and adaptation planning. In general, two approaches exist to address climate-induced vulnerabilities and adaptation planning (Dessai and Hulme 2004; Lempert and Collins 2007): 1) top-down, and 2) bottom-up.

The top-down method follows a predict-then-act paradigm where the level of future uncertainty is assumed to be shallow based on the classification of Table 2.1. In this approach, physically-based OA/GCMs play a key role as they are considered to provide reliable multi-decadal global-scale climate change projections based on assumed greenhouse gas emission scenarios (GHGESs). Although they are beneficial for vulnerability assessment studies at the global scale (for example, see Farinosi et al. 2018), their spatial scale is too coarse for impact asse-

Table 2.1. Levels of uncertainty (A synthesis of Kwakkel et al. (2010), Walker et al. (2013), and Thissen et al. (2017) with editions)

Level of uncertainty	Description	Example
Level 1 (complete certainty)	One can explicitly measure uncertainties or ignore them due to their negligibility.	The errors of a measurement practice using a calliper.
Level 2 (shallow uncertainty)	One can enumerate multiple futures and associate a probability to each.	The ensembles of OA/GCM projections to get probabilistic futures of climate events
Level 3 (medium uncertainty)	One can enumerate multiple futures and rank them using qualitative likelihood.	The descriptive future climate conditions in the IPCC reports
Level 4 (deep uncertainty)	One can enumerate multiple plausible futures without associating probabilities or rankings.	Field Training Exercise (FTX) (in which military troops face as much war scenarios as possible)
Level 5 (total ignorance)	Surprises and Black Swans which are not imaginable.	11 September 2001 terror attack in New York City (as was seen before that date)

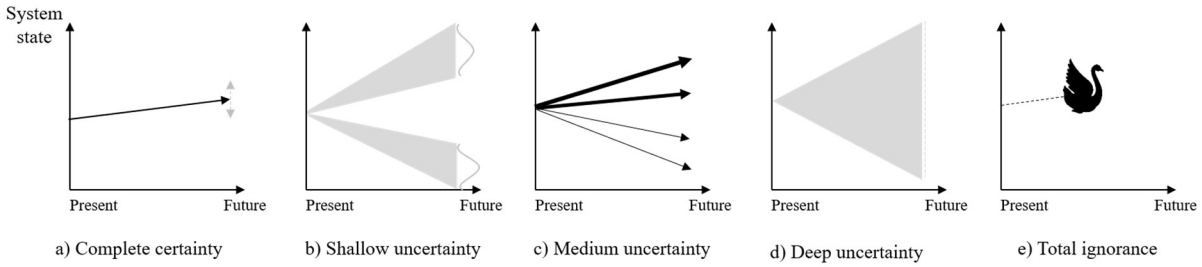

Figure 2.1. Future uncertainty levels: a) level 1 uncertainty where future is clear enough and the uncertainty is small and measurable, b) level 2 uncertainty where several futures could be imagined quantified by probability distributions, c) level 3 uncertainty where several futures could be imagined and ranked (the thickest arrow indicates the most probable future), d) level 4 uncertainty where several plausible futures could be imagined but cannot be ranked or be associated with a probability and e) level 5 uncertainty where surprises or Black Swans are inevitable. (A synthesis of Walker et al. (2013), Maier et al. (2016) and Taleb (2007)).

ssments at regional scales (Ahmed et al. 2013). This issue has led to investments in downscaling techniques which are used to increase the spatial resolution of OA/GCMs for regional studies. Once downscaled, the projections are utilized to assess the impact of climate change at local scales. The hierarchical use of models in this order is the reason this approach is termed ‘top-down’. Nevertheless, several drawbacks are associated with this framework in the literature and the

reliability of the projections is questioned; OA/GCMs structure is based on the physical formulations of the Earth's climate and atmosphere. Undoubtedly, many of the processes could not be perfectly modelled due to the imperfection of the current knowledge base (Foley 2010; Knutti and Sedláček 2013; Oreskes et al. 1994).

In addition, these models need tuning (or parametrization) based on historical climate observations which again limits OA/GCMs credibility (Dommenget and Rezny 2018). Furthermore, the future of socioeconomic developments is known to be deeply uncertain hindering analysts to agree upon GHGESs (Lempert et al. 2004). In addition to these flaws of OA/GCMs, the downscaling techniques have their drawbacks which add other layers of inaccuracy to regional projections. In general, two general downscaling techniques exist: 1) dynamical and 2) statistical. On one hand, in dynamical downscaling, the regional climate models (RCMs) are developed for a specific region relying on the global-scale projections of OA/GCMs. RCMs' projections are shown to be very sensitive to their parametrization which can reduce the overall credibility of regional climate projections (Feser et al. 2011; Tariku and Gan 2018). Yet downscaled, the fine-scale projections are often still too coarse for a climate change impact assessment within a river basin (Chen et al. 2011).

On the other hand, statistical downscaling relies on the concept of hydro-climate stationarity (Schoof 2013), a concept which is proposed to not be credible anymore (Milly et al. 2008). Because of these inaccuracies cascading through different models and assumptions (Smith et al. 2018; Wilby and Dessai 2010), the final results are most often biased. Bias-correction and post-processing of regional climate projections are still a mandate (Maraun 2016; Maraun et al. 2017), even though it "impair[s] the advantages of circulation models by altering spatiotemporal field consistency … and violating conservation principles" (Ehret et al. 2012). All these inaccuracies can lower the reliability of climate change projections and their applicability in regional impact assessments. Unfortunately, high reliance on climate models encourages analysts to consider their projections as nearly accurate and implement them in regional impact analyses.

In the top-down impact assessment approach, an ensemble of future climate projections is usually used, and several futures are assumed. Uncertainties around each future are expressed with probability distribution functions, i.e., level two uncertainty (see Figure 2.1 and Table 2.1, and also Lempert et al. (2004)). However, climate science still needs to make a lot of progress to reliably project trustworthy futures at regional scales. Planning adaptation based on best-guess future

conditions leaves climate-sensitive systems vulnerable to unpredictable changes in climate (Lempert et al. 2010).

The drawbacks associated with using climate models in regional climate change impact assessment should not prevent decision-makers from taking adaptive measures. As opposed to the top-down approach, in the bottom-up one, the level of uncertainty is realistically considered to be deep (see Figure 2.1 and Table 2.1). This implies that there is a fundamental disagreement upon which climate model to choose and how to demystify future uncertainties using probability distributions (Lempert et al. 2003). To deal with this deeply uncertain future, scenario analysis gives a deeper perspective in grasping vulnerabilities by exposing systems to multiple plausible futures (Bankes 1993; Gober 2014). Maier et al. (2016) assert that bottom-up approaches favour explorative scenarios providing multiple plausible futures from a 'what can happen?' standpoint. Thereby, explorative scenarios can embrace a wide range of future uncertainty, although neither a probability distribution nor a ranking system could be associated with them, making them "neutral". Scenario-neutral vulnerability assessment is considered as the primary step in bottom-up adaptation planning by many analysts (Ben-Haim 2001; Brown et al. 2011; Guo et al. 2017; Haasnoot et al. 2013; Kasprzyk et al. 2012; Lempert et al. 2003; Ray and Brown 2015). It is worth mentioning that the term 'neutral' is employed to reflect the idea that each climate future is viewed as having an equal likelihood of occurrence in the exploratory scenario analysis.

Overall, in bottom-up planning, the focus is on robust strategies that are least sensitive to a wide spectrum of climate change scenarios (Herman et al. 2015; McPhail et al. 2018). Not only sensitivities of a system to future climatic changes could be assessed, but also the robustness of a system in face of technological, socio-economic and political shifts could be tracked (Maier et al. 2016). Although almost all bottom-up methods begin with a vulnerability test, each method utilizes a different strategy to propose robust solutions. As this research is only focused on understanding the vulnerabilities of a transboundary system, and does not aim to propose solutions for different problems that may arise due to climate change, further review of the bottom-up methods that address decision-making is beyond of the scope of this research, nonetheless, the literature has provided several reviews and comparisons of these methods (see Dittrich et al. 2016; Hall et al. 2012; Kwakkel et al. 2016; Matrosov et al. 2013; Moallemi et al. 2020a, b; Roach et al. 2016; Weaver et al. 2013).

Despite many advantages associated with the scenario-neutral method, this approach has its own drawbacks; for example, robustness evaluations commonly require a large set of plausible scenarios that are usually produced via stochastic scenario generation models (Bartholomew and Kwakkel 2020). These models often need parametrization based on historical records, similar to OA/GCMs, which lowers their credibility given the non-stationary nature of the current changing climate (Milly et al. 2008). Besides, the computational costs imposed by such large number of evaluations are usually much greater compared to similar top-down evaluations. Furthermore, subjective assumptions regarding the range and independence of uncertain factors impacting the system may not be in line with physical realities that can potentially result in implausible scenarios (Quinn et al. 2020). Given these facts, Conway et al. (2019) have highlighted the use of bottom-up approaches along with the top-down technique in assessing vulnerabilities of climate-sensitive systems.

2.3 Knowledge Gap

Thus far, the scenario-neutral method is proposed to be proper for impact assessments at regional scales. Furthermore, it is shown that this method is capable of embracing a wide range of uncertainties associated with future climatic conditions. Synthetically generated scenarios can play a key role in this method as they provide the flexibility to mirror a wide range of perturbations in various climate attributes. It is worth mentioning that the information gained from OA/GCMs are crucial in informing the scenario generation process, highlighting the complementary relationship of the top-down and bottom-up methods in a vulnerability assessment study.

In the literature, two general methods exist to synthetically generate climate change scenarios, which are: 1) perturbed flow time-series, and 2) perturbed weather time-series. Both perturbed flow time-series (e.g. Borgomeo et al. 2015; Herman et al. 2016; Kirsch et al. 2013; Nazemi et al. 2013; Quinn et al. 2018; Zeff et al. 2016) and weather time-series (e.g. Apipattanavis et al. 2007; Guo et al. 2017; Prudhomme et al. 2010; Ray et al. 2018; Steinschneider and Brown 2013) are extensively used in the literature as means for constructing scenarios reflecting plausible future changes in climate and streamflow. Turning to the transboundary river context, several studies exist in the literature that use perturbed flow scenarios to assess possible susceptibility of different sectors, such as agriculture (Hadjimichael et al. 2020b; a; Quinn et al. 2020) and hydropower

(Quinn et al. 2018; Wild et al. 2019) within a transboundary system. Nonetheless, a deeper understanding could be gained by assessing the vulnerability of a water-sharing agreement and its relation to other sectors under stressed climate conditions. In an effort to address this matter, a few studies employed perturbed flow scenarios to specifically assess the vulnerability of a multi-jurisdictional water-sharing agreement; Nazemi et al. (2013) and Hassanzadeh et al. (2016) evaluated the vulnerability of the Master Agreement on Apportionment – an interprovincial water-sharing agreement in western Canada – using a set of perturbed flow scenarios. Although these two studies inform decision-makers about vulnerabilities associated with the water-sharing agreement, a lack of basin-wide analyses, the absence of linkage between the discovered vulnerabilities and changes in climate variables, and a lack of impact analysis on other sectors in relation to satisfying (or failing) the agreement could be noticed.

Perturbed weather scenarios, on the other hand, provides the capability of directly linking the detected vulnerabilities to the changes in climate signatures. Although weather scenarios have occasionally been used to focus on a certain part or a specific sector of a transboundary river system in the literature (e.g., Ray et al. 2018; Schlef et al. 2018), to the best of the author's knowledge, no extensive study exists in the literature that uses a large set of weather scenarios on a basin-wide scale to assess the vulnerability of a water-sharing agreement within a transboundary basin. To tackle this gap, this study uses a methodology to conduct such a basin-wide vulnerability assessment and applies it to a case study. The employed methodology could be categorized as bottom-up as a wide range of neutral, synthetic climate scenarios (in this study, weather time-series) are used to conduct the vulnerability assessment. The scenarios are only used to detect the climate-change-induced susceptibilities of the chosen case study area and are not meant to follow a predict-then-act paradigm, common in the top-down approach. Following a predict-then-act paradigm does not aim to find the vulnerabilities of a system, instead focuses on finding optimized solutions for the futures that are projected by climate models; this is not the focus of the current study.

Finally, I briefly investigate the vulnerabilities of other sectors in relation to satisfying (or failing) the chosen water-sharing agreement under stressed conditions.

In a nutshell, the importance of a basin-wide scenario-neutral vulnerability assessment in a transboundary river basin is highlighted. The literature review demonstrates the sparsity of such studies (or even lack thereof) in the transboundary river basin research literature. To display the

effectiveness of the employed methodology, the Saskatchewan River Basin (SaskRB), located in western Canada, is chosen as a case study, the details of which are explained in the following chapter.

3 CHAPTER 3: CASE STUDY

3.1 General Overview

This research is focused on the Saskatchewan River Basin (SaskRB), Canada (Figure 3.1). SaskRB is a large, transboundary basin with an area of approximately 400 000 km^2 shared between the three Canadian Provinces of Alberta (AB), Saskatchewan (SK), and Manitoba (MB) as well as the American State of Montana (MT). The main rivers of this basin – North and South Saskatchewan Rivers (NSR and SSR, respectively) – and most of their tributaries originate from the eastern slopes of the Canadian Rocky Mountains with the exception of only three tributaries of the Oldman River – Waterton, Belly, and St. Mary River – initiating from the American portion of the basin. These rivers flow eastward across the three Canadian Provinces and finally drain into Lake Winnipeg in the eastern part of the SaskRB. Before entering the Province of Saskatchewan (SK), the Bow, Red Deer, and Oldman rivers merge into the South Saskatchewan River (SSR) later joining NSR to form the Saskatchewan River (SR) upstream of MB. After crossing the common boundary of SK and MB, and before draining into Lake Winnipeg, the SR forms the Saskatchewan River Delta (SRD) with an area of about 10 000 km^2, making it the largest inland delta in North America (Abu et al. 2020; MacKinnon et al. 2015).

Much of the water flowing in the SaskRB main rivers comes directly from the Canadian Rocky Mountains area (Fang and Pomeroy 2020; Pomeroy et al. 2005; Wheater and Gober 2013). Melting of winter snow accumulations in the Rockies contributes the most to the annual runoff during spring and summer in the Prairie Provinces of western Canada (Shook and Pomeroy 2012). Further downstream, however, the contribution of snowmelt to the flow is negligible as it mostly goes to recharge soil moisture and fill depression storage. Apart from snowmelt, precipitation events in spring and summer also contribute to annual runoff; however, their impact is less than that of snowmelt (Shook and Pomeroy 2012). Additionally, SaskRB is characterized by extreme climate, facing an 80°C daily maximum/minimum temperature change between winter and summer

seasons (Wheater and Gober 2013). The special hydrology, climate, multi-jurisdictional nature, and its vast area, make the SaskRB a unique transboundary basin.

As the water management of this basin is politically shared amongst six different jurisdictions (i.e., Alberta, Saskatchewan, Manitoba, Montana, and the Federal Governments of Canada and the United States), the allocation of water between the states needs a robust means of governance resilient to stressors explained earlier (Section 2.2). SaskRB states have already come up with two means of water sharing governance mechanisms; 1) the Boundary Waters Treaty targeting transboundary waters shared between Canada and the United States, and 2) the Master Agreement on Apportionment[1] stipulating water sharing amongst the relevant Canadian Provinces. In the following, each treaty is discussed, and their water allocation requirements are detailed.

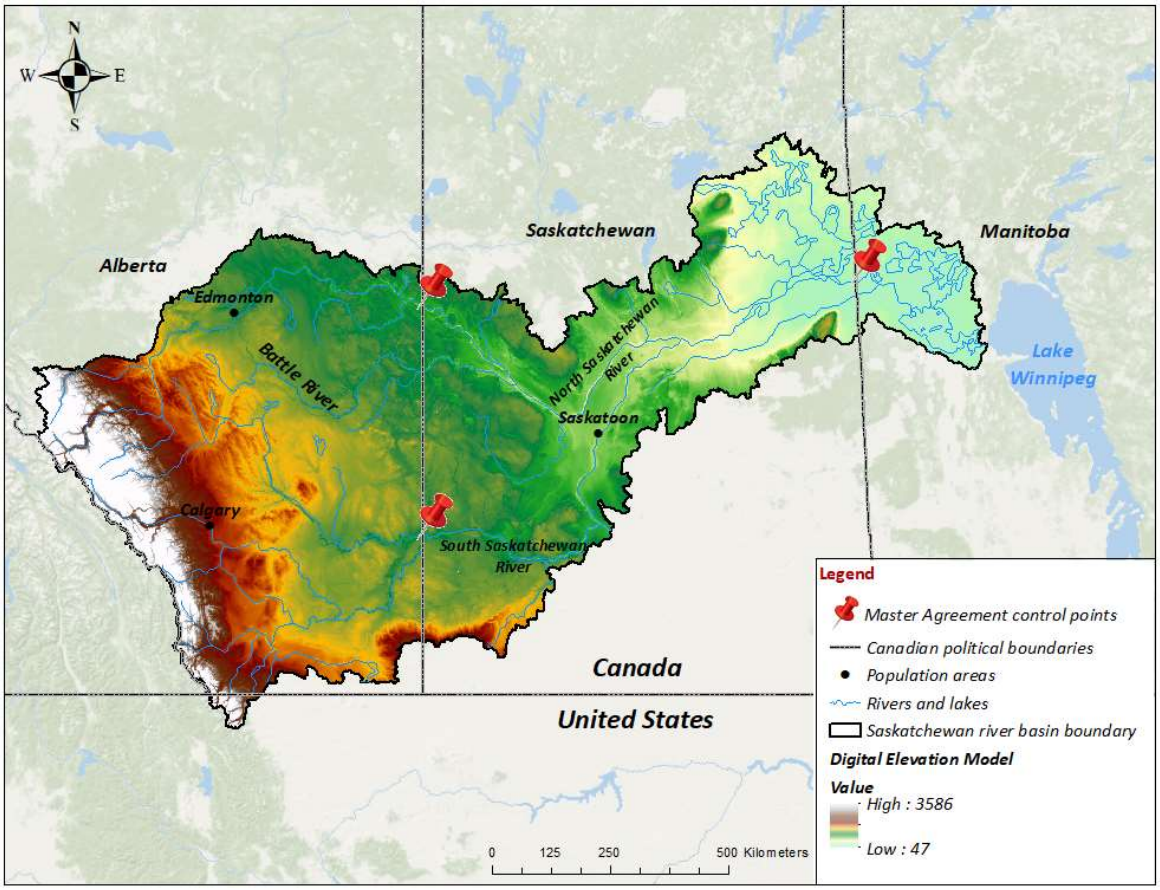

Figure 3.1. The location of the Saskatchewan River Basin, a transboundary river basin shared between the Canadian provinces of Alberta, Saskatchewan, and Manitoba as well as the American State of Montana. The red pins show the control points where the Master Agreement is evaluated.

[1] *Hereinafter "Master Agreement"*

3.2 Boundary Waters Treaty

The Boundary Waters Treaty, signed in 1909, stipulates the allocation of the water resources shared between Canada and the United States. For the case of the SaskRB, it specifically stipulates the water allocation of the St. Mary River shared between the two countries (Figure 3.2). The St. Mary River originates in the American portion of the SaskRB, flows north into Canada, and finally joins the Oldman River upstream of Lethbridge, AB. Before entering Canada, its waters are partially diverted to the Milk River to provide more reliable flows during the irrigation season, i.e., April to October, for the arable lands located in the adjacent Milk River Basin (Halliday and Faveri 2007a). Additionally, another diversion channel, located farther downstream in Canada, transfers waters from St. Mary to Milk River for the same purpose (channel not shown in the figure). For a brief history of diversions, water uses and allocation policies in these basins see Wolfe (1992).

Due to these existing diversions, Article VI of the treaty asserts that the "St. Mary and Milk Rivers and their tributaries … are to be treated as one stream" for the purpose of transboundary water allocation (IJC 1909). It also states that the waters of the two rivers "shall be apportioned equally between the two countries", while allowing both parties to use "more than half … from one river and less than half from the other … to afford a more beneficial use to each." Additionally, the Article specifies the details during the irrigation season entitling the United States to "a prior appropriation of … [14.16 cubic meters per second] of the waters of the Milk River, or so much of such amounts as constitutes three-fourths of its natural flow," and similarly, bounding Canada to a prior appropriation of the same amount (and ratio) of St. Mary River natural flows during the same period.

The second paragraph of the Article suggests that the trans-basin canal located within Canada can be used for the American interests, while any damages incurred by the exercise are addressed under the provisions outlined in Article II of the treaty (see IJC (1909) for details). This is due to the geographical landscape of the Milk River which enters Canada, flows some 340 km within the Canadian territory and then flows back into the United States. Finally, Article VI invites the representatives of both countries to measure and apportion the flows "from time to time … under the direction of the International Joint Commission."

To further clarify Article VI, the IJC issued an Order in 1921. The Order explains that the location to measure and apportion the waters of St. Mary and Milk rivers is set at the international

border. Besides, it declares, during the irrigation season, the waters of the two rivers, after the prior apportionments, must be divided equally between the two countries (IJC 1921). These two remarks were the points of ambiguity of the Article VI language, that the Order clarified, to settle a dispute that arose in the early years after signing the treaty (Halliday and Faveri 2007a).

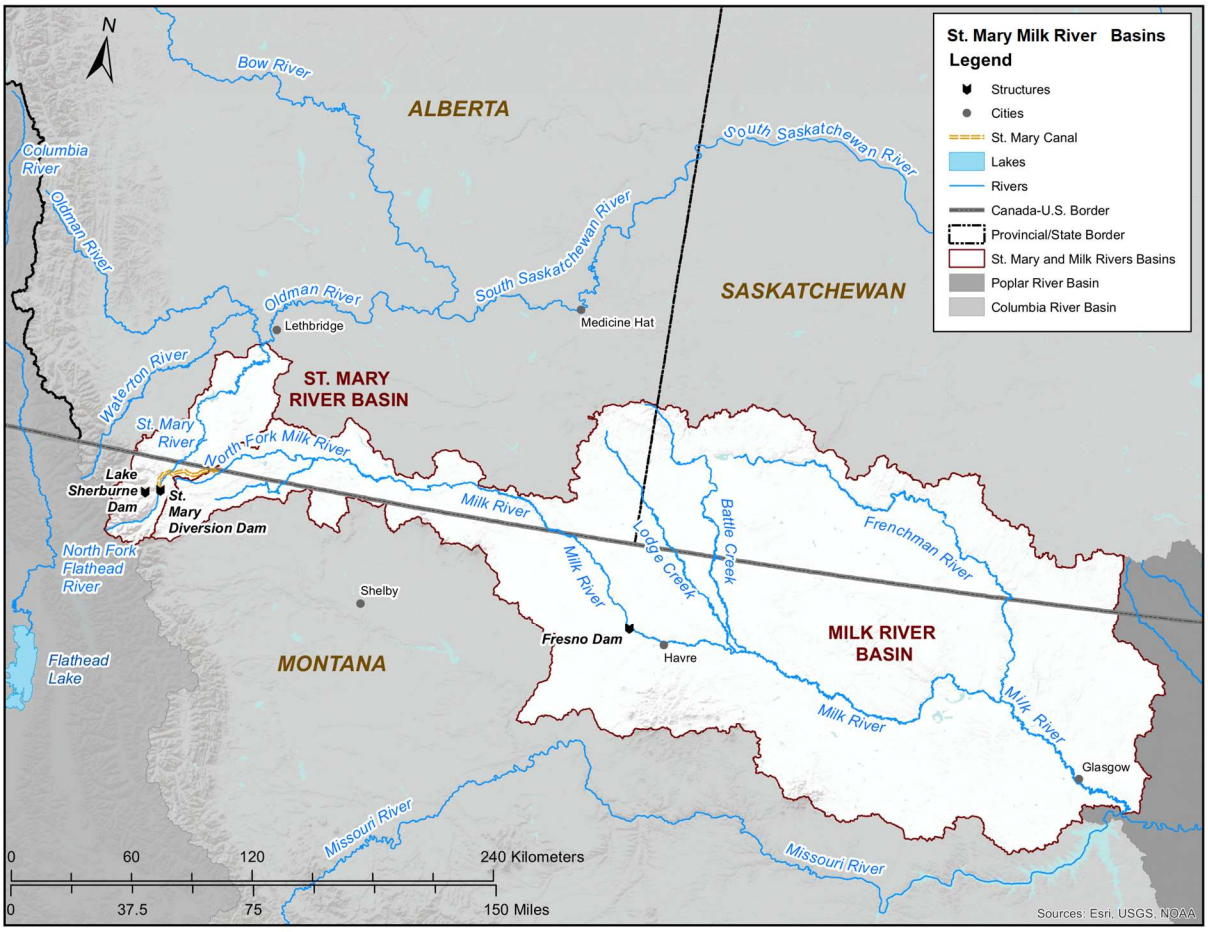

Figure 3.2. The St. Mary and Milk River Basins shared between Canada and the United States. The map is obtained from IJC (2020) and is freely available to the public.

Since the 1921 Order, the two countries worked closely, under IJC's direction, to promote cooperation and contain any conflicts arising in water allocation practices of St. Mary and Milk rivers (Heinmiller 2020). One example is the 2001 Letter of Intent allowing both countries to accumulate deficits in delivering water to the downstream state "allowing each country to use more of its allotted share during seasonal low flow periods" (Government of Alberta 2020a) while minimizing unnecessary surplus deliveries (McLane 2010). Currently, the waters are apportioned

based on 15- or 16-day adjustment periods (Pietroniro and Kilpatrick 2020) providing enough time (considering natural flow calculations, flow routing, etc.) for both states to transfer appropriate amounts of water to the other side of the border.

In another example, in 2003-4 the Governor of Montana asked IJC to revise the "evaluation of the assumptions, methods and parameters that are used to establish natural flows, depletions, and apportionments." In response, the IJC held several public meetings with the stakeholders to contain the dispute and address the concerns of both parties. Halliday and Faveri (2007a, b) provide a complete analysis of the challenges raised by the participants, and whether it is beneficial for both countries to revise the Article VI and 1921 Order.

It is worth noting that apart from St. Mary River, two other tributaries of the Oldman River – Waterton and Belly rivers – cross the international border of Canada and the United States (Belly River not shown in the figure). The apportionment of these rivers, on the contrary, does not follow any official procedure (see IJC Docket No. 57R (1948)), and they mostly flow to Canada without major upstream interventions. This is due to the fact that the lands around their headwaters are not arable, therefore, their waters are not significantly altered in the American portion of the SaskRB (Heinmiller 2020).

3.3 Master Agreement on Apportionment

The Master Agreement was signed in 1969 between the Provincial Governments of Alberta, Saskatchewan, and Manitoba and the Federal Government of Canada (PPWB 2015) to set forth the water allocation scheme amongst the Provinces. The Master Agreement establishes an RBO, i.e., the Prairie Provinces Water Board (PPWB), to "monitor and report on the apportionment of waters as set out in the provisions … ratified by this Master Agreement" (PPWB 2015). The Board consists of five members; two members are appointed by the Federal Government and one member from each of the relevant Provincial Governments (PPWB 2015). Also, the Board founds four Standing Committees to provide technical details on the hydrology, groundwater, water quality and flow forecasting of the interprovincial watercourses. Similar to the Board, each Standing Committee comprises five members appointed from their respective governments. Schedule C of the Master Agreement specifically defines all the duties of the Board; for example, it suggests data

sharing and information exchange between the states, calls for regular meetings of the Board members and additionally explains means of conflict resolution in case of hydro-political tensions.

This agreement, also, describes the details of water sharing between the Canadian provinces; under Schedule A, the government of Alberta (AB) "shall permit a quantity of water equal to one-half the natural flow of each watercourse to flow into the Province of Saskatchewan, and the actual flow shall be adjusted from time to time on an equitable basis during each calendar year" (PPWB 2015). In addition to this annual apportionment commitment, the government of Alberta must also deliver an actual instantaneous minimum flow of 42.5 m^3s^{-1} through the SSR to the Province of Saskatchewan (SK) as long as the natural flow at the border for this river is equal or greater than 85 m^3s^{-1}. Should the natural flow drops below 85 m^3s^{-1}, Alberta is permitted to compromise the minimum flow requirement to half of the amount available (Government of Alberta 2020b).

Meanwhile, the government of Saskatchewan undertakes a similar annual apportionment commitment; under Schedule B, the government of Saskatchewan (SK) must deliver "one-half the water flowing into the Province of Saskatchewan … from [AB]" in addition to the "one-half of the natural flow arising in the Province of Saskatchewan" to the province of Manitoba (MB). Furthermore, "any water which would form part of the natural flow [in the Province of Alberta] … but does not flow into the Province of Saskatchewan" due to separate existing agreements between the three provinces, must be considered in the annual delivery commitment of SK (PPWB 2015). Finally, the Master Agreement does not express any provisions pursuant of a minimum flow mandate through the NSR and SR.

Finally, Schedule D of the Master Agreement gives an overview of interprovincial transboundary water allocations prior to 1969 and Schedule E gives the details on water quality objectives that must be met in the transboundary watercourses of the SaskRB.

Although the Master Agreement suggests means of conflict resolution in case of hydro-political tensions, it does not explicitly guide water allocation under heightened hydrological variability due to climate change. As mentioned earlier, the idea of hydroclimate stationarity is not valid anymore (Milly et al. 2008). Bonsal et al. (2019) affirm this idea by suggesting that increasing temperatures have already caused changes in the attributes of surface water flow in Canada; seasonal timing of peak flow has already shifted due to the warming climate and the volume of summer flow has been reduced compared to the historical records in many parts of Canada. The recent Canada's Changing Climate Report confirms that the flow in the southern Canadian basins

(including SaskRB) will likely to be driven mostly by rainfall events rather than snowmelt in the future (Bonsal et al. 2019). The report also asserts that the warming climate has already caused a declining trend in the annual volume of flow in the main SaskRB rivers since the 1960s and 70s. In short, climate change has already impacted the surface water flow in SaskRB, altering the seasonality of peak flow, and also decreasing the annual volume of flow. These changes are prone to be intensified as the Earth's climate gets warmer in the coming decades (IPCC 2018). Although setting a proportion of flow or a minimum flow to be delivered to the downstream states – as stated in the Master Agreement – could be considered as means of climate proofing the transboundary river agreements (Cooley and Gleick 2011), a comprehensive basin-wide vulnerability assessment is still a mandate (UNECE 2016).

To date, many have already tried to study the impact of climate change in different parts of the SaskRB. Literature is abundant with top-down impact assessments of the hydrology (Burn 1994; Dibike et al. 2017; Islam and Gan 2015a; Kienzle et al. 2012; MacDonald et al. 2012; Pomeroy et al. 2009; Tanzeeba and Gan 2012; Westmacott and Burn 1997), water management (Islam and Gan 2012, 2016; Sauchyn et al. 2016), water quality (Morales-Marín et al. 2018; Schindler et al. 2012), and soil moisture (Cohen 1991; Islam and Gan 2015b) of the basin. However, as mentioned in Chapter 2, a basin-wide scenario-neutral vulnerability assessment (as part of a bottom-up planning method) to evaluate the Master Agreement under stressed conditions, and the impact of its satisfaction (or failure) on the other sectors is needed.

As previously described, only a few bottom-up vulnerability assessments have been conducted thus far in the SaskRB: the studies by Nazemi et al. (2013) and Hassanzadeh et al. (2016) are the only ones that used a set of perturbed flow scenarios to examine the requirements of the Master Agreement for the SSR (at the AB-SK border) and SR (at the SK-MB border), respectively. However, as noted earlier in Chapter 2, using perturbed flow scenarios limits the linkage of detected vulnerabilities to changes in climate attributes and variables. Therefore, this research aims at using several weather scenarios to assess the vulnerability of the Master Agreement on a basin-wide scale for the current water management scheme of the basin. The Master Agreement requirements are evaluated for three control points (see Figure 3.1) where the transboundary rivers of the basin – SSR, NSR, and SR – cross the provincial borders. It may be noted that, the Battle River, another major river of the SaskRB, is excluded from the analysis, as water abstractions from

this river in the AB portion of the basin is insignificant relative to its natural flow volume at the provincial border (Government of Alberta 2020b).

4 CHAPTER 4: METHODOLOGY AND DATASETS

4.1 General Overview

To conduct a scenario-neutral vulnerability assessment, several components were needed. Figure 4.1 displays a general overview of the methodology applied to the SaskRB. In this climate change assessment study, first, a set of plausible climate change scenarios were generated using a multi-site stochastic weather generator (WG). A simple hydrological model was followed to translate each climate scenario into river flow. Thereafter, the simulated flow was fed into a water resources management model that distributed the water throughout the water management system of the basin. The vulnerability of the Master Agreement (see Section 3.3) was assessed in terms of the amount of water flowing at points where transboundary rivers cross political borders. In the following, first, each component of the applied scenario-neutral vulnerability assessment methodology is described, and the datasets used in each section are briefly remarked. Second, the measure of vulnerability is described. And, finally, the complete details of the datasets used throughout this chapter are detailed.

4.2 Generation of Weather Scenarios

As mentioned in Section 2.2, in a bottom-up vulnerability assessment, scenarios play a key role. Through a scenario-neutral vulnerability assessment, several plausible future scenarios are generated to test whether policies under question can meet their predefined objectives (Parker et al. 2015). In order to create scenarios, this study used a stochastic multi-site weather generator that allowed the generation of long, synthetic daily weather time-series. As noted in earlier chapters, the use of weather time-series facilitates the linkage of detected vulnerabilities to changes in climate variables. Meanwhile, this potentially allows the comparison of the bottom-up vulnerability assessment results to those of the top-down approach (Brown et al. 2012); simply,

the prediction of climate models could be added to the map showing the vulnerabilities derived from the vulnerability assessment.

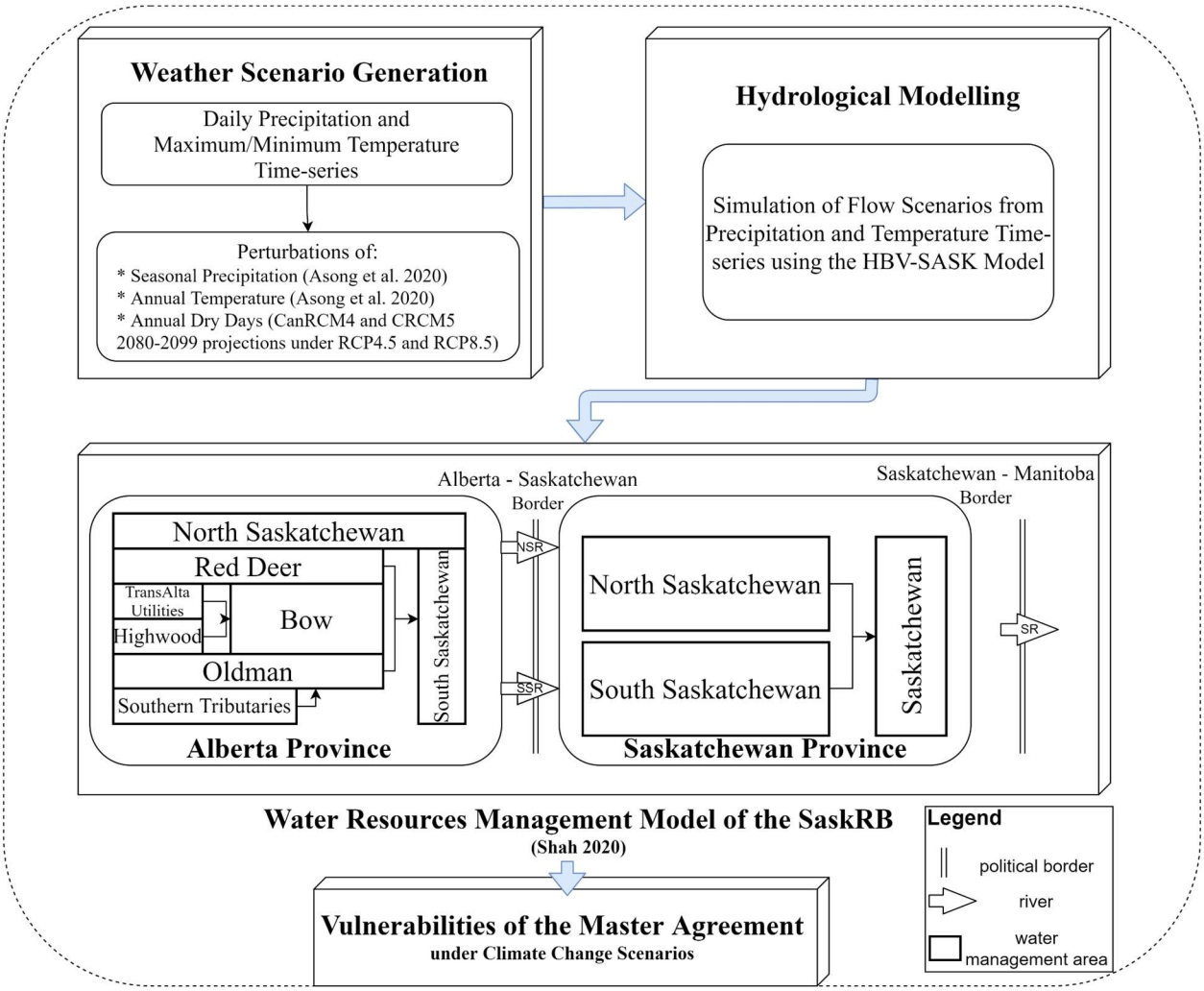

Figure 4.1. Flowchart of the methodology. The vulnerability of the Master Agreement for the transboundary river of the basin – NSR (North Saskatchewan River), SSR (South Saskatchewan River), and SR (Saskatchewan River) – at points where the rivers cross political borders. In the Weather Scenario Generation component the sources used to inform the process are mentioned in the figure and further detailed in Section 4.6.

Weather generators are usually designed to generate weather time-series for a single site (e.g. Racsko et al. 1991; Richardson 1981; Richardson and Wright 1984; Schlabing et al. 2014). They can generate stationary weather scenarios while preserving historical weather attributes, such as time and inter-variable dependence structures. However, their applicability is limited in large basins impacted by different atmospheric systems, such as SaskRB, because single-site weather

generators are unable to preserve the spatial dependence of climate variables (Asong et al. 2016). Multi-site weather generators are designed to overcome this shortcoming (Apipattanavis et al. 2007; Steinschneider and Brown 2013; Wheater et al. 2005). These generators can be employed to produce weather data across several weather stations and basins, and even to synthetize gridded weather scenarios.

Due to the large area of the SaskRB, a multi-site weather generator is selected to produce spatially coherent weather scenarios. As stated earlier, much of the SaskRB river flow initiates from the eastern side of the Canadian Rocky Mountains (Fang and Pomeroy 2020; Pomeroy et al. 2005; Wheater and Gober 2013). Therefore, it is rational to only focus on the climate and hydrology of the SaskRB headwaters. Due to the simplicity of producing weather scenarios for each catchment, the weather generator is used to produce weather time-series for each site of this study. Moreover, site-based weather generation has a lower cost compared to producing gridded weather scenarios due to lower number of areas (compared to many grids) to be considered in the generation process.

Figure 4.2 shows headwater catchments located upstream of the main SaskRB rivers – Bow, Oldman, Red Deer, and North Saskatchewan River (NSR). Each headwater catchment was considered as a site in the weather generation process. Table 4.1 details the location and area of each catchment. As is obvious from the table, some catchments are nested within one another. However, catchments are treated independently and different weather scenarios were produced for each.

Although the selected sites do not cover the entire headwater area, the outflow from each catchment, which is subsequently simulated by the hydrological modelling component (Section 4.2.4) provides the necessary inputs to be fed to the water management model of this study (see Sections 4.4). Same as weather scenario generation process, the flow from each nested catchment is calibrated and used separately in this study. Needless to say, the climate and hydrology in the downstream of these sites were not part of the weather generation process. However, the downstream climate is not entirely ignored and its impact on the downstream contributing flows was modelled using regression, as further described in Section 4.4 and Appendix B.

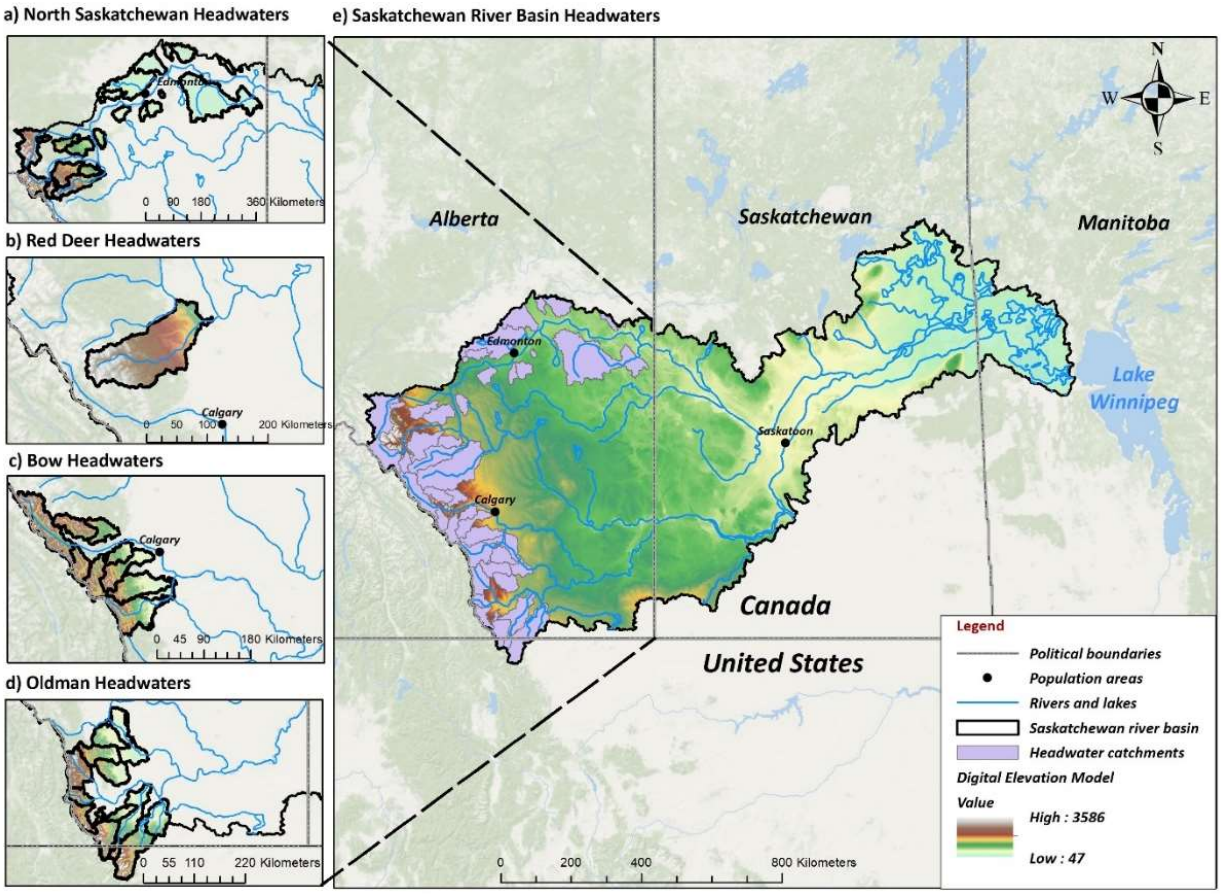

Figure 4.2. Headwater catchments of the SaskRB. The weather generation model is used to produce weather time-series for each. Subsequently, a hydrological model is used to translate the weather of each site to river flows. The flows are served as input to the water management component of this study which covers the rest of the area of the SaskRB.

The procedure to generate multiple plausible climate change scenarios is indicated in Figure 4.3. The first step in the scenario generation part was to set up a weather generator for the SaskRB headwater catchments. To this end, the daily historical time-series of precipitation and minimum/maximum temperature for the baseline period of 1980 to 2013 were extracted from the gridded ANUSPLIN climate dataset (see Section 4.6 for data sources). This observationally-based dataset is selected mainly because it is solely dependant on the gauge observations recorded in the National Climate Data Archive of Environment and Climate Change Canada[1] and suggested to be "the most accurate source of information on precipitation in Canada" (Wong et al. 2017).

[1] *"In Canada, climate data collection is coordinated by the federal government, which is made available by the National Climate Data Archive of Environment and Climate Change Canada" (Wong et al. 2017).*

Thereafter, the parameters of the weather generator were fitted for each site based on the historical time-series. A complete description of the chosen weather generator and its parameters is detailed in Section 4.2.1.

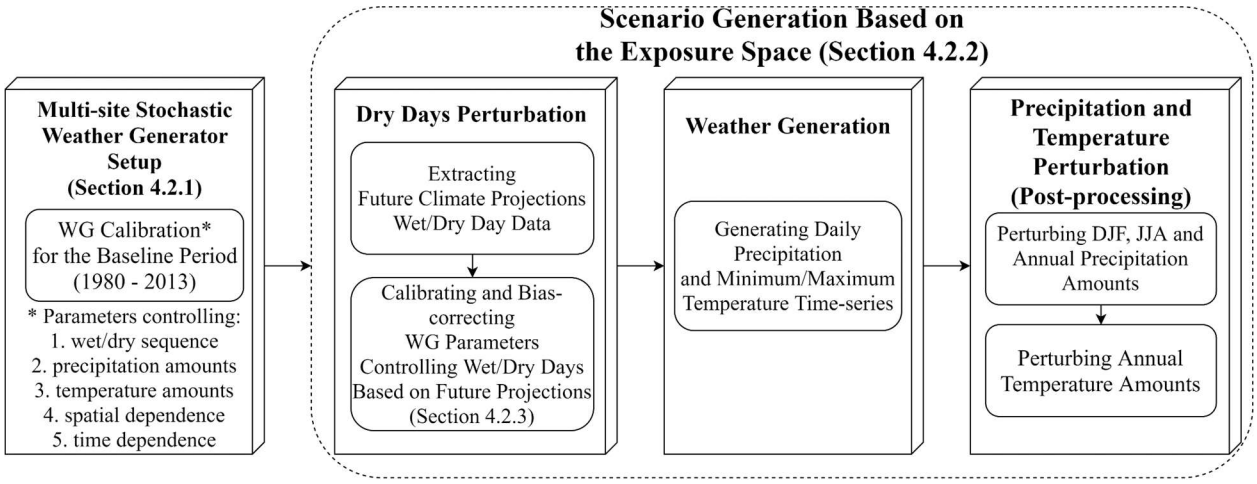

Figure 4.3. Scenario generation flowchart. First, the weather generator is calibrated to historical observations. Thereafter, the weather generator is used to generate perturbed climate scenarios to be used in the vulnerability assessment.

Once calibrated, 40 different realizations of 20-year scenarios (to match the length of scenarios later used for the final vulnerability assessment) were generated to validate the calibration process. These realizations are long enough to allow the validation of different outputs that are produced based on the baseline period (i.e., 1980–2013) properties. Upon validation, the weather generator was then employed to produce perturbed weather scenarios reflecting plausible future climatic changes. These scenarios targeted the plausible changes in several attributes, such as the annual number of dry days, mean seasonal precipitation amounts and mean annual temperature. These target attributes form the 'exposure space' that generally refers to plausible future climatic conditions that a policy will be exposed to, so as to investigate its vulnerability (Guo et al. 2018). Following the developed exposure space (Section 4.2.2), the targeted perturbations in annual dry days were implemented by manipulating the specific parameters of the weather generator controlling the generation of wet/dry day sequences. Subsequently, the weather generator was run with the perturbed parameter sets to produce daily precipitation and minimum/maximum temperature time-series for each site with a varying number of annual dry days. Afterwards, the produced time-series is segmented into 20-year pieces, with each of them

being post-processed to mirror changes in precipitation and temperature attributes. The parameter manipulation and post-processing to generate climate change scenarios are described in Sections 4.2.2 and 4.2.3, respectively. A 0.5 mm trace precipitation value was selected to distinguish between wet and dry days that is justified in Section 4.2.4.

Literature is abundant with different methods of weather generation. Unsurprisingly, several weather generators have been previously employed in Canada and also the SaskRB region; Asong et al. (2014, 2016) used the Generalized Linear Model-based Rglimclim package (for mathematical details, see Chandler and Wheater (2002); Chandler (Chandler 2014)) to produce synthetic climate time-series for several weather sites within the Canadian Prairies, including some located in the SaskRB. McKague et al. (2005) used the ClimGen weather generator to produce time-series of several climate variables across a number of sites in southern Ontario. Recently, Chen et al. (2014) proposed a multi-site weather generator, MulGETS, to produce synthetic weather data over several sites in Quebec, Canada. This study used this specific weather generator since its parameters provide enough flexibility to perturb one of the desired climate attributes of this study, i.e., the annual number of dry days. Moreover, it has been successfully employed in parts of the SaskRB, such as the Red Deer River area (see Dai and Qin 2019). In the following section, the mathematical details of the model are explained.

Table 4.1. The location and area of SaskRB headwater catchments.

Number	Outlet gauge code	Centroid latitude (°)	Centroid longitude (°)	Area (km^2)	Number	Outlet gauge code	Centroid latitude (°)	Centroid longitude (°)	Area (km^2)
1	05AB028	+50.219	−114.363	155.35	**37**	05BH008	+51.179	−115.359	7808.97
2	05BG001	+51.308	−115.065	666.03	**38**	05AD005	+48.951	−113.744	318.53
3	05BC001	+50.926	−115.446	745.32	**39**	GSHMOU	+50.695	−114.451	1579.93
4	05CK004	+51.615	−113.102	45641.92	**40**	GMOSMO	+50.357	−113.891	1039.98
5	05CB007	+51.752	−115.154	5584.75	**41**	GHISQA	+50.415	−114.515	1895.69
6	05BL024	+50.550	−114.428	3983.96	**42**	GLBMOS	+50.517	−113.645	948.01
7	05BL004	+50.417	−114.493	1990.27	**43**	GRDBIG	+52.083	−114.370	17554.69
8	05AA002	+49.622	−114.439	606.67	**44**	GRDJEN	+51.686	−113.377	39978.45
9	05AB002	+50.046	−113.918	2305.96	**45**	05DE007	+52.771	−114.910	546.84
10	05BF001	+50.782	−115.157	907.05	**46**	05EC002	+54.286	−112.903	334.17
11	05BG002	+51.345	−115.359	209.79	**47**	05DD009	+52.678	−115.931	861.70
12	05AA004	+49.373	−114.053	159.32	**48**	05DD007	+52.618	−116.976	2590.94
13	05CD004	+52.031	−114.576	15198.03	**49**	05BJ010	+50.888	−114.705	1183.90
14	05BD002	+51.345	−115.523	883.24	**50**	05DF004	+53.208	−114.289	594.35
15	05AC003	+50.346	−113.670	2746.32	**51**	05DE003	+53.535	−114.513	532.89
16	05CE001	+51.990	−114.032	24971.36	**52**	05DA002	+51.854	−116.366	514.02
17	05AB007	+49.671	−114.205	5640.44	**53**	05EB902	+53.539	−113.094	99.40
18	05BH004	+51.178	−115.346	7890.19	**54**	05EC005	+54.054	−113.444	1603.32
19	05EE007	+53.464	−111.591	7210.47	**55**	05ED002	+54.040	−111.174	355.31
20	05BH009	+51.053	−114.745	563.08	**56**	05DF006	+53.228	−113.621	366.65
21	05CC002	+51.906	−114.781	11693.16	**57**	05DE009	+53.449	−114.838	94.51
22	05BE006	+51.185	−115.500	6596.89	**58**	05EA001	+53.713	−114.039	3298.81
23	05AA024	+49.698	−114.328	4335.87	**59**	05DF003	+53.296	−113.342	629.18
24	05BL009	+50.446	−114.430	2332.39	**60**	05EC006	+54.260	−112.447	1020.57
25	05AB021	+50.155	−114.050	1151.83	**61**	05ED003	+53.976	−110.781	38.85
26	05AD032	+48.908	−113.751	192.30	**62**	05DD004	+52.752	−116.568	214.15
27	05AD041	+49.091	−113.673	687.93	**63**	05AA022	+49.374	−114.368	823.87
28	GBWCON	+49.196	−113.541	1275.85	**64**	05AA023	+49.962	−114.474	1425.49
29	05AD008	+49.204	−113.843	1783.16	**64**	05DA009	+51.962	−116.862	1904.81
30	05AE027	+48.811	−113.523	1212.09	**65**	05DB002	+52.187	−115.234	756.61
31	GSTDAM	+48.953	−113.407	2306.80	**66**	05DC012	+52.605	−115.482	1241.22
32	05AD002	+49.186	−113.552	1234.63	**67**	05DB006	+51.937	−115.627	2108.97
33	05AE006	+49.089	−113.235	3547.70	**68**	05BB001	+51.367	−116.036	2049.64
34	GBEMOU	+49.277	−113.637	3722.68	**69**	05DC006	+52.148	−115.932	1876.05
35	05AD007	+49.424	−113.673	14545.23	**70**	05AB028	+50.219	−114.363	155.35
36	05AD026	+49.119	−113.920	1255.23					

4.2.1 MulGETS Multi-site Stochastic Weather Generator

This study used an improved version of a weather generation model proposed by Wilks (1998)[1], a multi-site stochastic weather generator with the potential to be used in scenario-neutral vulnerability assessments. The Wilks model is largely based on the single-site Richardson (1981)[2] model, which itself and its variants are extensively used in many areas of research, such as hydrological climate impact studies (Caron et al. 2008), statistical downscaling of OA/GCM outputs (Wilby et al. 2002), and evaluating agricultural processes (Wallis and Griffiths 1995). The original Richardson model can generate daily sequences of precipitation and other dependent climate variables, such as maximum and minimum temperature values while preserving historical attributes like inter-variable and time dependence structures. The model is composed of three main components to produce 1) precipitation occurrences, 2) precipitation amounts, and 3) other dependent variable time-series, such as temperature or solar radiation.

Based on Richardson (1981), the precipitation occurrence component generates sequences of wet/dry days using a first-order two-state Markov Chain model which has two independent parameters:

$$P_{01} = 1 - P_{00}, \tag{4.1}$$

$$P_{11} = 1 - P_{10}, \tag{4.2}$$

where P_{01} is the transition probability of a wet day following a dry day, and P_{11} is the probability of a wet day following a wet day. Similarly, P_{00} is the probability of a dry day following a dry day and P_{10} is the probability of a dry day following a wet day. In order to create sequences of wet/dry days (Y_i), a uniform random number is generated for day i (u_i) and is compared with the threshold transition probability values (Equations 4.1 or 4.2) of the day. The threshold transition probability, i.e., critical probability, on a given day is selected based on the wet/dry condition of the previous day:

$$P_c = \begin{cases} P_{01}, & Y_{i-1} = 0 \\ P_{11}, & Y_{i-1} = 1 \end{cases}, \tag{4.3}$$

[1] *Hereinafter, "Wilks model"*
[2] *Hereinafter, "Richardson model"*

where P_c is the critical probability on a given day, which is chosen to be P_{01} if the previous day was dry, otherwise P_{11}. If the random number (u_i) is smaller than the critical probability, the day is considered as wet, otherwise dry. The first day was assumed to be dry in this study.

Once sequences of wet/dry days are generated, the next step is determining the amount of precipitation on wet days which is randomly sampled from a probability density function fitted to the historical observations. Many distribution functions are used to this date in the literature, such as Exponential (Foufoula-Georgiou and Lettenmaier 1987) and Gamma (Chen et al. 2010), and also a mixture of distribution functions like Mixed Exponential (Wilks 1998). Other dependent climate variables, such as minimum and maximum temperature or solar radiation sequences are generated conditional on the precipitation concurrence time-series based on the rationale that precipitation events dominantly control other environmental processes (Wilks and Wilby 1999). To generate the time-series of dependent variables, first, the historical record of each is standardized to calculate the residuals using the following equation:

$$x_i(j) = \frac{X_i(j) - \mu_i^k(j)}{\sigma_i^k(j)}, \tag{4.4}$$

where $\mu_i^k(j)$ and $\sigma_i^k(j)$ are the mean and standard deviation for the variable j on day i for wet ($k = 1$) or dry ($k = 0$) days, $X_i(j)$ is the observed value of the variable of interest, and $x_i(j)$ is the corresponding residual component. Given the equations above, the residuals of each variable could be stochastically generated based on a weakly-stationary generating process (see Matalas (1967)):

$$x_{p,i} = Ax_{p,i}(j) + B\varepsilon_{p,i}(j), \tag{4.5}$$

where p denotes the year, i the day, j the variable of interest and ε denotes a random number sampled from a standard normal probability distribution function. The A and B matrices are defined as follows:

$$A = M_1 M_0^{-1}, \tag{4.6}$$

$$BB^t = M_0 - M_1 M_0^{-1} M_0^T, \tag{4.7}$$

where -1 and T superscripts stand for inverse and transpose of a matrix, respectively, and M_0 and M_1 matrices contain the lag 0 and lag 1 cross-correlation coefficients of the dependent variables of interest. Once the residuals are generated, the time-series of dependent variables could be created using the inverse of Equation 4.5.

The Richardson weather generator needs to be calibrated, a process in which the transition probabilities and probability distribution functions are fitted to the historical data. The calibration of the model's transition probabilities (Equations 4.1 and 4.2) was on a monthly basis. The monthly fitting is suggested to lower the count of model parameters to a reasonable number while minimizing the loss of data for a daily time resolution weather generation (Chen et al. 2014; Richardson 1981; Wilks 1998). Using the chosen trace precipitation (detailed in Section 4.2.4) and upon obtaining monthly transition probabilities, the calibration process continues with fitting Mixed Exponential probability distribution functions to the precipitation amounts across each weather site, and subsequently, determining the matrices to generate maximum/minimum temperature time-series (Equation 4.6 and 4.7) as the last step of the WG calibration. Once calibrated, the three components of the model work sequentially in each time-step to generate stochastic time-series of weather variables.

This single-site weather generator is applicable in a multi-site platform if the historical spatial correlation of weather events at different locations is preserved. To this end, Wilks (1998) proposed a methodology to drive multiple Richardson models at different sites using fields of spatially correlated random numbers that follow the correlation structures of observed precipitation data. In doing so, first, the spatial correlation matrix of precipitation occurrences at different sites is formed based on daily data (notation follows Brissette et al. (2007)):

$$C = \begin{bmatrix} 1 & r_{1,2} & \cdots & r_{1,n-1} & r_{1,n} \\ r_{2,1} & 1 & \cdots & r_{2,n-1} & r_{2,n} \\ \vdots & \vdots & \ddots & \vdots & \vdots \\ r_{n-1,1} & r_{n-1,2} & \cdots & 1 & r_{n-1,n} \\ r_{n,1} & r_{n,2} & \cdots & r_{n,n-1} & 1 \end{bmatrix}, \tag{4.8}$$

where C is the spatial correlation matrix, n is the number of sites, and r is the cross-correlation of daily precipitation between pairs of sites. Using the method of matrix decomposition, spatially correlated random fields are produced using the matrix C (see Brissette et al. (2007)). Once generated, the random numbers for day i and site n ($u_{i,n}$) are used to produce sequences of wet/dry days ($Y_{i,n}$) in a multi-site platform.

Regarding the precipitation amounts, Wilks (1998) used a Mixed Exponential distribution function for each site to generate spatially correlated precipitation amounts. Nonetheless, a shortcoming of the Wilks approach is that it "did not produce dependence between the synthetic precipitation amounts and occurrences that are as strong as in the observations" (Wilks 1998). This

is a common issue known as 'spatial intermittence' (Bardossy and Plate 1992). To address this shortcoming, Brissette et al. (2007) further developed the Wilks model and additionally established a link between the precipitation amount at each site and precipitation occurrences at the basin scale. I used the same approach and used a multi-exponential pdf to simulate precipitation amounts randomly. Additionally, Chen et al. (2014) enhanced the Wilks model by contributing a method to generate spatially coherent maximum and minimum temperature values; a correlation matrix of maximum and minimum temperature values (same as Equation 4.8) is used, and again, n sets of random fields drive separate Richardson weather generators at different sites to produce spatially correlated temperature time-series.

This study uses the final version of Chen et al.'s (2014) weather generator, named MulGETS, which is available via a MATLAB® package capable of generating spatially correlated precipitation and maximum/minimum temperature time-series. MulGETS is applied to the SaskRB headwater catchments in the eastern slope of the Canadian Rocky Mountains (see Figure 4.2 and Table 4.1) to produce synthetic, stationary precipitation, as well as maximum and minimum temperature time-series.

4.2.2 Climate Change Exposure Space

As mentioned in Section 2.2, climate change is suggested to globally alter the current climate state in the coming decades. Not only will it likely change the overall magnitude of precipitation and temperature around the globe (Bush et al. 2018; IPCC 2018), but also alters several other attributes, such as extremes (Fischer and Knutti 2015; O'Gorman 2015; Trenberth 2011; Westra et al. 2014), seasonal and inter-annual variability (Dong et al. 2019; Fatichi et al. 2012; Feng et al. 2013), wet and dry distributions (Giorgi et al. 2018; Shabbar and Bonsal 2003; Sushama et al. 2010), etc. Considering a broad spectrum of changes in different climate variables and their attributes leads to constructing a rich, high-dimensional exposure space. This aids in revealing as many vulnerabilities of a system as possible.

This research considered changes in four attributes of climate variables, which are: 1) average summer precipitation amount (P_{JJA}), 2) average winter precipitation amount (P_{DJF}), 3) average annual temperature (T_{Ann}), and 4) yearly average number of dry days (N_{dry}). In doing so, I use

OA/GCM projections over the 2080–2099 horizon to inform the exposure space formation. The chosen plausible perturbation bounds (relative to the baseline period) are detailed in Table 4.2.

In order to reflect perturbations in the number of dry days (N_{dry}), the transition probabilities of the stochastic weather generator (Equations 4.1 and 4.2) are adjusted according to the projected N_{dry} of two Canadian RCMs, which are: 1) CanRCM4, and 2) CRCM5 (see Section 4.6 for data sources). These two RCMs showed two different distributions in terms of the projected number of dry days for the future, and therefore were employed in this study. It is worth mentioning that in future research more RCMs could be used to construct the exposure space. Each RCM provides projected climate data based on two representative concentration pathways (RCPs)[1], namely RCP4.5 and RCP8.5. As mentioned earlier in Section 2.2, almost all climate model projections are biased, thus, a simple bias-correction method (see Section 4.2.3) is employed to remove the biases using the calibrated transition probabilities based on ANUSPLIN observations. Adjustments of transition probabilities based on the aforementioned projections mirror plausible shifts in N_{dry}.

Table 4.2. Plausible perturbation bounds of the chosen climate attributes relative to the baseline period. The number of samples and the perturbation scale of each attribute are detailed.

Climate variable	Climate attribute	Perturbation range	Number of samples	Perturbation scale
Precipitation	PJJA	−50 to +20 % (10% step)	8	Seasonal
Precipitation	PDJF	−20 to +40 % (10% step)	7	Seasonal
Temperature	TAnn	−2 to +10 °C (2 °C step)	7	Annual
Precipitation	Ndry	Baseline Ndry plus 4 different RCM projections over 2080-2099 horizon	1 (baseline case) + 4 (RCM projections)	Monthly
			Π(samples) = 1,960	

This study uses the uncertainty ranges proposed by Asong et al. (2020) as an initial range of perturbation for precipitation and temperature values. They recently analyzed shifts in seasonal and annual precipitation and temperature values projected by Coupled Model Intercomparison Project Phase 5 (CMIP5) OA/GCMs across major Canadian river basins. Nevertheless, as ensembles of OA/GCMs only demonstrate the "lower bound on the maximum range of

[1] *RCPs manifest "four different 21st century pathways of [greenhouse gas] … emissions and atmospheric concentrations, air pollutant emissions and land-use" (IPCC Panel 2014). RCP2.6 indicates a strictly mitigated greenhouse gas concentration, RCP4.5 and RCP6.0 demonstrate an intermediate and RCP8.5 represents a high concentration of greenhouse gases in the atmosphere.*

uncertainty" (Stainforth et al. 2007), wider, plausible ranges of perturbation bounds are considered to construct the exposure space.

Two scaling factors are used to perturb the precipitation amounts in summer (i.e., P_{JJA} for the months of June, July, and August) and winter (i.e., P_{DJF} for the months of December, January, and February) seasons. The average of P_{JJA} and P_{DJF} is used as a scaling factor to perturb precipitation amounts for these two seasons. These factors are applied to the stationary, synthetic precipitation time-series to mirror changes in the future climate. Furthermore, to clearly reflect the effects of N_{dry} perturbations in scenarios with identical P_{JJA} and P_{DJF} values, another scaling factor is uniformly applied to the precipitation scenarios to assure their annual average precipitation amounts (P_{Ann}) are comparable. Last but not least, one additive factor is also used to uniformly perturb annual temperature values (T_{Ann}). It should be noted that the post-processed perturbations are uniformly applied to all weather sites in the SaskRB headwaters.

A total number of 1,960 scenarios were generated as a result of different combinations of exposure space targets (see Table 4.2). It should be pointed out that due to the inherent stochasticity of weather generators, slight differences in terms of statistical properties of the generated time-series compared to the historical ones are expected. In other words, produced climate change scenarios might follow a marginally different exposure space.

4.2.3 Transition Probability Bias-correction

As mentioned earlier, OA/GCM and RCM climate outputs are biased relative to historical observations (Cannon et al. 2020). Hence, the biases of the transition probabilities (Equations 4.1 and 4.2) that were calculated based on the time-series of future projections used in this study (see Section 4.2.2) must be corrected. It should be noted that, these biases could also potentially include errors resulting from resolution differences between the datasets used to obtain climate forcing time-series for each catchment (see Section 4.6 for data sources). A simple 'delta method' has been employed to carry out the bias-correction procedure. In the context of bias-correction, the delta method generally refers to using a simple change factor representing the difference between projected and baseline values of a climate variable. Later, the factor is added to the baseline period observations to compute bias-corrected values. The delta method is widely used in the literature to correct biases of precipitation and temperature averages (e.g. Navarro-Racines et al. 2020). This

study uses a delta factor to correct the biases associated with the transition probability of the weather generator. In doing so, firstly, the change factor is calculated:

$$\delta = P_{xy,future} - P_{xy,future}, \tag{4.9}$$

where δ is the change factor, P is the transition probability on a given day, x and y represent the wet/dry status of the day i and $i-1$, respectively. It is worth mentioning that the two probabilities used in Equation 4.9 were calculated based on the RCM outputs. Secondly, the change factor is added to the baseline values that are calculated based on the ANUSPLIN observations:

$$P_{xy,bias-corrected} = P_{xy,baseline} + \delta. \tag{4.10}$$

Once the transition probabilities are bias-corrected, they will be used in the weather generation process. It should be stated that an additive delta method was preferred, since a multiplicative change factor can potentially result in unrealistic transition probabilities, if the difference between $P_{xy,future}$ and $P_{xy,future}$ values is significant.

4.2.4 Trace Precipitation Value

A minimum reportable precipitation amount of 0.5 mm (i.e., trace precipitation) was assumed to distinguish between wet and dry days. This value was selected based on an analysis of the proportion of wet days (P_w) calculated for all the climate forcing datasets used in this study (see Section 4.2.2) across a range of different trace precipitation thresholds. This measure is simply calculated as follows:

$$P_w = \frac{n(Day_{wet})}{n(Day_{all})}, \tag{4.11}$$

where n gives the cardinality of a given set, $Day_{wet}$is the set of days that precipitation amounts greater than the selected threshold occur, and Day_{all} is the set of all days of a given time-series. Figure 4.4 shows the results of the analysis, where a 0.5 mm is the least value which resulted in approximately similar P_ws across all the weather sites and datasets for the baseline period of 1980–2013.

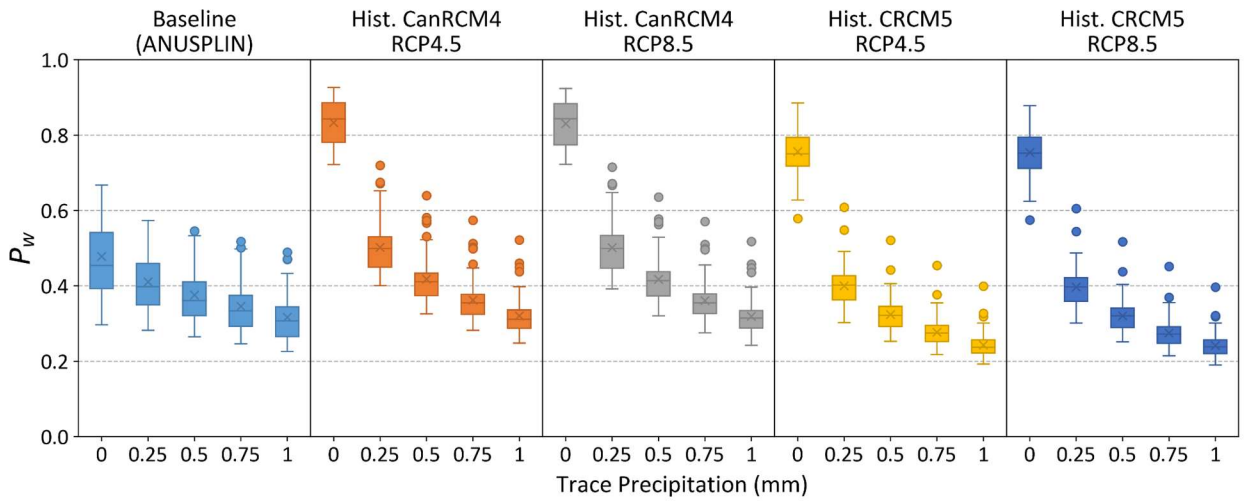

Figure 4.4. P_w calculated for different trace precipitation thresholds ranging from 0 to 1 mm for the daily precipitation data of the baseline period – 1980 to 2013 – of the ANUSPLIN dataset (i.e., observations) and 4 other RCM products: 1) CanRCM4 RCP4.5, 2) CanRCM4 RCP8.5, 3) CRCM5 RCP4.5, and 4) CRCM5 RCP8.5. Each box-and-whisker indicates the distribution of P_ws across the 70 headwater catchments of the case study. Within each box, the horizontal line and cross indicate the median and mean, respectively.

4.3 Hydrological Modeling

In this Section, the chosen hydrological model, its components and the calibration and validation strategies are described.

4.3.1 HBV-SASK Model

This study uses a variation of the well-known HBV hydrologic model. Its simplicity and small computational cost are the reasons that this class of hydrological models is employed in this scenario analysis and vulnerability assessment study given the large number of scenarios to run (i.e., 1,960). Moreover, the HBV-SASK model is only dependant on two input variables, i.e., mean daily temperature and precipitation, that makes the model very suitable for this study. The first version of this model was developed in the early 1970s (Bergström 1995; Bergström and Forsman 1973). Since then, many modified versions came into existence (e.g. Aghakouchak and Habib 2010; Lindström et al. 1997), nonetheless, all of them maintain the same concepts in their structure. This study uses a variation of the original model called HBV-SASK (Gupta and Razavi 2018;

Razavi and Gupta 2019). HBV-SASK has shown good performance in previous studies for the catchments located in the Canadian Rocky Mountains (Gupta and Razavi 2018; Razavi and Gupta 2019). The structure of the model is schematically shown in Figure 4.5.

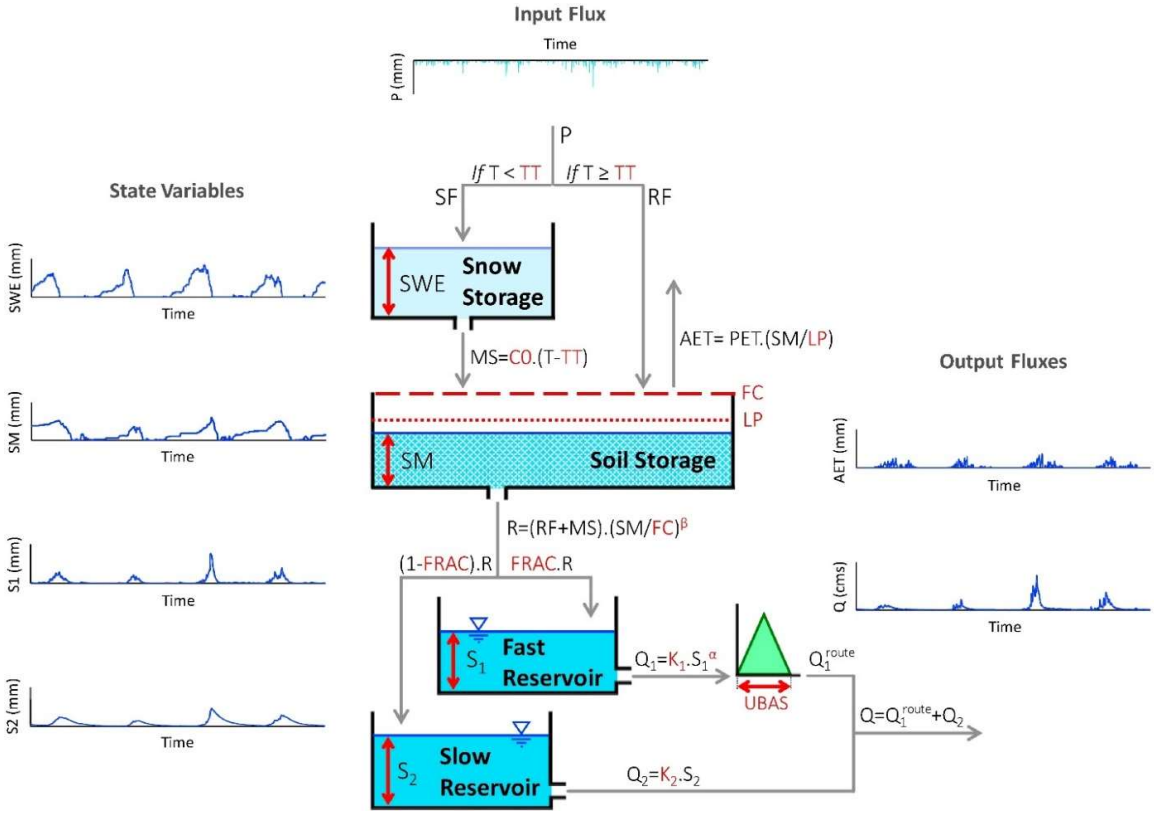

Figure 4.5. The schematic view of the structure of the HBV-SASK conceptual hydrology model (obtained from Razavi et al. (2019) published under the Creative Commons License (CC BY-NC-ND 4.0)). The inputs of the model are daily precipitation and temperature time-series. The output fluxes are streamflow and actual evapotranspiration. The abbreviations are: P (precipitation), T (temperature), SF (snowfall), RF (rainfall), SWE (snow water equivalent), MS (melted snow), AET (actual evapotranspiration), PET (potential evapotranspiration), SM (soil moisture), R (soil release), S1 and S2 (storage in fast and slow reservoirs), Q1 and Q2 (flow from fast and slow reservoirs), $Q1^{route}$ (flow Q1 routed by the watershed unit hydrograph) and Q is total simulated streamflow.

4.3.2 Calibration and Validation

Like any conceptual hydrological model, this model needs to be calibrated for the catchments of interest (Gupta et al. 1998). The dynamically dimensioned search (DDS) algorithm (Tolson and Shoemaker 2007) is used to calibrate parameter values of the model for the headwater catchments

(see Figure 4.2 and Table 4.1). The DDS algorithm is a parsimonious stochastic search algorithm that has shown promising performance in the calibration of hydrological models (Asadzadeh et al. 2014; Haghnegahdar et al. 2014, 2015; Razavi et al. 2014). For data sources of the calibration process see Section 4.6.

The initial calibration ranges of the HBV-SASK parameters and their descriptions are detailed in Table 4.3. The objective function in the calibration process is chosen to be:

$$Objective\ Function = 0.5 \times NSE + 0.5 \times |BIAS|, \tag{4.12}$$

where NSE is the Nash-Sutcliffe Efficiency (Nash and Sutcliffe 1970) metric and $BIAS$ is the absolute value of the volume bias (Gupta et al. 1998). Nash-Sutcliffe efficiency metric is a common metric to evaluate the goodness-of-fit of hydrologic models (e.g., Efstratiadis and Koutsoyiannis 2010; Gaborit et al. 2017; Haghnegahdar et al. 2014) defined as follows:

$$NSE = 1 - \frac{\sum(Q_{obs} - Q_{sim})^2}{\sum(Q_{obs} - \overline{Q_{obs}})^2}, \tag{4.13}$$

where Q_{obs} is the observed flow, Q_{sim} is the simulated flow by the model, and $\overline{Q_{obs}}$ is the average observed flow. The range of this metric is $-\infty < NSE < 1$, and it should be maximized for an optimal solution. Furthermore, the $|BIAS|$ metric can be computed as follows (Gupta et al. 1998):

$$|BIAS| = \left|\frac{\sum(Q_{sim} - Q_{obs})}{\sum(Q_{obs})}\right|. \tag{4.14}$$

The theoretical range of this metric is $0 < |BIAS| < \infty$, however, the practical limit is usually $0 < |BIAS| < 1$. An equal weight for the two metrics has been considered in the calibration of the HBV-SASK for the headwater catchments; the NSE component focuses on the goodness-of-fit of the hydrograph, while the $|BIAS|$ component is used to minimize the total volume bias of the HBV-SASK output.

It should be noted that, the calibrated HBV-SASK is used to simulate flow scenarios from each perturbed weather time-series generated in this study. It is acknowledged, however, the impact of climate change on the model parameters is not considered in this vulnerability assessment study. In future research, the potential changes for each parameter of the HBV-SASK model, such as soil field capacity (FC), can be further pursued.

Table 4.3. The parameters of the HBV-SASK model, including their description and bounds in the calibration process (obtained from Razavi et al. (2019) with modifications.) The table is published under the Creative Commons License (CC BY-NC-ND 4.0)

Number	Parameter	Lower Bound	Upper Bound	Description
1	TT	-4.00	+4.00	Air temperature threshold for melting/freezing of water (°C)
2	C0	0.00	10.00	Base melt factor (mm/°C)
3	ETF	0.00	1.00	Temperature anomaly correction factor for potential evapotranspiration (1/°C)
4	LP	0.00	1.00	Limiting factor for PET as a multiplier to FC
5	FC	50.00	500.00	Field capacity of the soil (mm)
6	β (beta)	1.00	3.00	Shape parameter for soil release Equation (unitless)
7	FRAC	0.10	0.90	The fraction of soil release entering fast reservoir (unitless)
8	K1	0.05	1.00	Fast reservoir coefficient (unitless)
9	α (alpha)	1.00	3.00	Shape parameter for fast reservoir Equation (unitless)
10	K2	0.00	0.05	Slow reservoir coefficient (unitless)
11	UBAS	1.00	3.00	The base of unit hydrograph for watershed routing in day
12	PM	1.00	1.00	Precipitation multiplier for uncertainty analysis

For the calibration process, the daily, natural flow data is employed. However, for a number of catchments where the daily flow data are unavailable, the weekly naturalized flow data were used for calibration (see Table 4.4). In addition to the details of the calibration time resolution, the spin-up, calibration and validation periods of each catchment are listed in Table 4.4. Based on PPWB (1976), the 'project depletion' method was employed to calculate the natural flows at points of interest. Simply, this method "involves identification and measurement or computation of depletions due to storage, diversion, evaporation and consumptive use, and routing these depletions to the point of apportionment where they are applied to the recorded flows at the point to produce natural flows" (PPWB 1976).

Table 4.4. The time resolution of the calibration process for each catchment. The spin-up, calibration, and validation periods are detailed for the two categories of the calibration process.

Number	Catchments with Daily Time-step Calibration⸸		Catchments with Weekly Time-step Calibration⸸	
1	05AA022	05EA001	05AA002	05BG001
2	05AA023	05EB902	05AA004	05BG002
3	05BB001	05EC002	05AA024	05BH004
4	05BJ010	05EC005	05AB002	05BH008
5	05DA002	05EC006	05AB007	05BH009
6	05DA009	05ED002	05AB021	05BL004
7	05DB002	05ED003	05AB028	05BL009
8	05DB006		05AC003	05CB007
9	05DC006		05AD002	05CC002
10	05DC012		05AD005	05CD004
11	05DD004		05AD007	05CE001
12	05DD007		05AD008	05CK004
13	05DD009		05AD026	GBE MOU
14	05DE003		05AD032	GBW CON
15	05DE007		05AD041	GHI SQA
16	05DE009		05AE006	GLB MOS
17	05DF001		05AE027	GMO SMO
18	05DF003		05BC001	GRD BIG
19	05DF004		05BD002	GRD JEN
20	05DF006		05BE006	GSH MOU
21	05EE007		05BF001	GST DAM
Spin-up Period	1980 to 1982		1970 to 1971	
Calibration Period	1982 to 1990, plus 1995 to 2013*		1972 to 1990, plus 1995 to 2001	
Validation Period	1990 to 1994		1990 to 1994	

* The calibration length could be shorter in case the observed flow data are not entirely available.

⸸ The catchments are listed based on the code name of their outlet gauge defined by the Water Survey of Canada and Alberta Environment.

4.3.3 Potential Evapotranspiration (PET) Estimation

The actual evapotranspiration (AET) component in the HBV-SASK model is calculated using a simple relation with the potential one: $AET = PET \times (\frac{SM}{LP})$, where PET is the potential evapotranspiration, SM is the soil moisture, and LP is the limiting factor for PET. The daily potential evapotranspiration (PET) component of the model is estimated using the Hamon (1960) equation which has shown an acceptable performance in the Canadian Rockies (Safaei 2018). Furthermore, it only is dependant on daily mean temperature, that can be calculated for the weather scenarios generated in this study. Hamon (1960) proposes the following equation in order to estimate the potential evapotranspiration:

$$E_p = CD^2P_t, \tag{4.15}$$

where E_p is the potential evapotranspiration in the unit of $^{inch}/_{day}$, D is the possible daily sunshine in units of 12 hours, P_t is the saturated water vapour concentration at the mean temperature in $^{g}/_{m^3}$, and C is an empirical constant of 0.0055. Hamon (1963) modified Equation 4.15, and came up with a slightly different version of the PET equation:

$$E_p = CDP_t, \tag{4.16}$$

where in the modified version, the value of C has been changed to 0.0065. Both versions estimate very similar PET values in a study by McCabe et al. (2015), however, as the Equation 4.16 underwent additional testing by Hamon (1963), this modified version to estimate PET was used. By multiplying the modified version by 25.4 (for metric system unit conversion) the equation could be expanded as follows:

$$E_p = 0.1651 \times D \times \rho_{sat} \times K \tag{4.17}$$

where D is again the daily hours of sunlight in units of 12 hours, ρ_{sat} is the saturated vapour density ($^{g}/_{m^3}$), and K is the calibration coefficient (selected as 1.2 as suggested by Lu et al. (2005)), which all result in the estimation of potential evapotranspiration in the unit of $^{mm}/_{day}$. The components of the equation above are provided in the following (Forsythe et al. 1995; Lu et al. 2005):

$$\rho_{sat} = 216.7 \times \frac{E_{sat}}{T + 273.3} \tag{4.18}$$

$$E_{sat} = 6.108 \times e^{\frac{17.26939 \times T}{T+273.3}} \tag{4.19}$$

$$D = 24 - \frac{24}{\pi} cos^{-1}\left[\frac{sin\frac{p\pi}{180} + sin\frac{L\pi}{180} sin\phi}{cos\frac{L\pi}{180} cos\phi}\right] \tag{4.20}$$

$$\phi = sin^{-1}[0.39795 \times cos\theta] \tag{4.21}$$

$$\theta = 0.2163108 + 2tan^{-1}\left[0.9671396 \times tan[0.00860\ \times (J - 186)]\right] \tag{4.22}$$

where E_{sat} (mb) is the saturated vapour pressure, T (℃) is the daily mean temperature, θ (rad) is the revolution angle based on the day of the year (J, 1 to 365), ϕ (rad) is the sun's declination angle, L $(degree)$ is the latitude, and p $(degree)$ is the day-length coefficient, which is selected to be 0.8333. The last constant is "the summation of the radius of the sun (in degrees as seen from Earth) plus the adopted value for the refraction of the light through the atmosphere of 34 minutes" which reflects the official definition of day-length by the US Government; the definition is simply the time span between the sunrise and sunset when "the top of the sun is apparently even with the horizon" (Forsythe et al. 1995).

The potential evapotranspiration estimates cannot be directly validated since PET values cannot be measured. However, in order to indirectly verify Hamon's evapotranspiration (ET) estimates, the AET values of the HBV-SASK model output could be instead used as a proxy. In doing so, the HBV-SASK AET values were verified using the Moderate Resolution Imaging Spectroradiometer (MODIS) ET estimates. MODIS estimates "provide unexampled information regarding vegetation and surface energy, which can be used for regional and global scale actual ET estimation in near real-time" (Safaei 2018). MODIS's fine resolution — about 1 km^2 — and its valid ET estimates that could be found in the literature (e.g., Bhatti et al. 2016; Cleugh et al. 2007; Kim et al. 2012; Zhang et al. 2008) are the main reasons that it was used in this research. A complete description of the MODIS model could be found in Mu et al. (2013) and its data source in Section 4.6. It should be noted that as the time intervals of the HBV-SASK AET and the MODIS ET estimates are different, i.e., daily and 8-day, respectively, values of both were summed up on a monthly basis for further investigation.

It should be noted that the MODIS ET estimates are not the truth themselves, and they also must be verified using in-situ observations. However, for the sake of simplicity, the validation process was carried on solely using MODIS ET data.

4.4 Water Resources Management Model of the SaskRB

Water resources management modelling is introduced to satisfy the need to simulate different allocation schemes and deficit-sharing policies of different water users within a basin (Farjad et al. 2017; Ilich 2008). These models allocate water based on a priority associated with each water user. Conventionally, this resource allocation problem is solved via Linear Programing (LP), needing an optimization engine in the background to optimize the water allocation throughout the basin according to a set of priorities associated with every user. However, due to the complexity of water management modelling, not all components of the model could be realized as linear functions. In this case, a common approach is simplifying non-linear ones through linearization, for example by using piece-wise linear functions (e.g. Pingale et al. 2014). Network Flow Algorithms (NFAs), such as out-of-kilter (Fulkerson 1961), were amongst the first methods used to solve water management problems. NFAs are widely used in many water resources management models as an optimization engine, such as WRMM (Ilich 1992), KCOM (Andrews et al. 1992), MODSIM (Labadie 2010), etc. LP solvers are also extensively used (e.g., in WEAP (SEI 2020)) to solve water allocation problems, mainly due to their higher efficiency. Nonetheless, both approaches have their own advantages and shortcomings (see Ilich (2008, 2009)).

State-of-the-art water management models are extensively used today. They are means of testing different strategies and assumptions regarding water management decisions. Water management models can simulate different components of a water resources system, such as reservoir operation, diversion channels, demand nodes, water treatment plants, return flows, hydropower plants, etc. In order to understand how different climate change scenarios (Section 4.2) affect the amount of flow crossing political borders of the SaskRB, an integrated water resources model is needed.

Shah (2020) has recently developed a basin-wide, integrated water management model for the SaskRB, named IWMSask, within the MODSIM decision support system. This model served as the water management model component in this study (see Figure 4.1). IWMSask is the most up-to-date model in terms of including the recent water management policies of the SaskRB. Moreover, it is the only available tool that represents the water management of the whole SaskRB. The IWMSask model incorporates rule curves of 59 reservoirs and 29 hydropower plants in the area, as well as the demand data of 160 irrigation and 217 non-irrigation user nodes. The details

of modelled components can be viewed in Figure 4.6. As IWMSask operates on weekly time-steps, the daily simulated flow from the HBV-SASK model for each headwater catchment (Figure 4.2 and Table 4.1) was weekly-averaged to be fed into the model. To better represent the full water budget of the system, several incremental flows have been considered in the initial setup of the IWMSask. In this scenario assessment study, these flows that are contributing to the system in the farther downstream of the chosen headwater catchments (Figure 4.2) were estimated using simple linear regression models, the detail of which are described in Appendix B.

The original IWMSask model has been set up from 1928 to the end of 2018, however, this study only focused on the operation policies and the SaskRB water management scheme of the last 20 years (i.e., 1999 to 2018). This consideration was to account for the water management policies of the SaskRB in response to the recent extreme climatic events in the area, such as the 1999−2005 Prairie drought (Hanesiak et al. 2011) and the 2013 flood (Whitfield and Pomeroy 2016) in the Bow River Basin. Also, in general, the most recent management policies of the basin were of interest in this vulnerability assessment study. For the complete detail on setting up and validating the IWMSask, see Shah (2020).

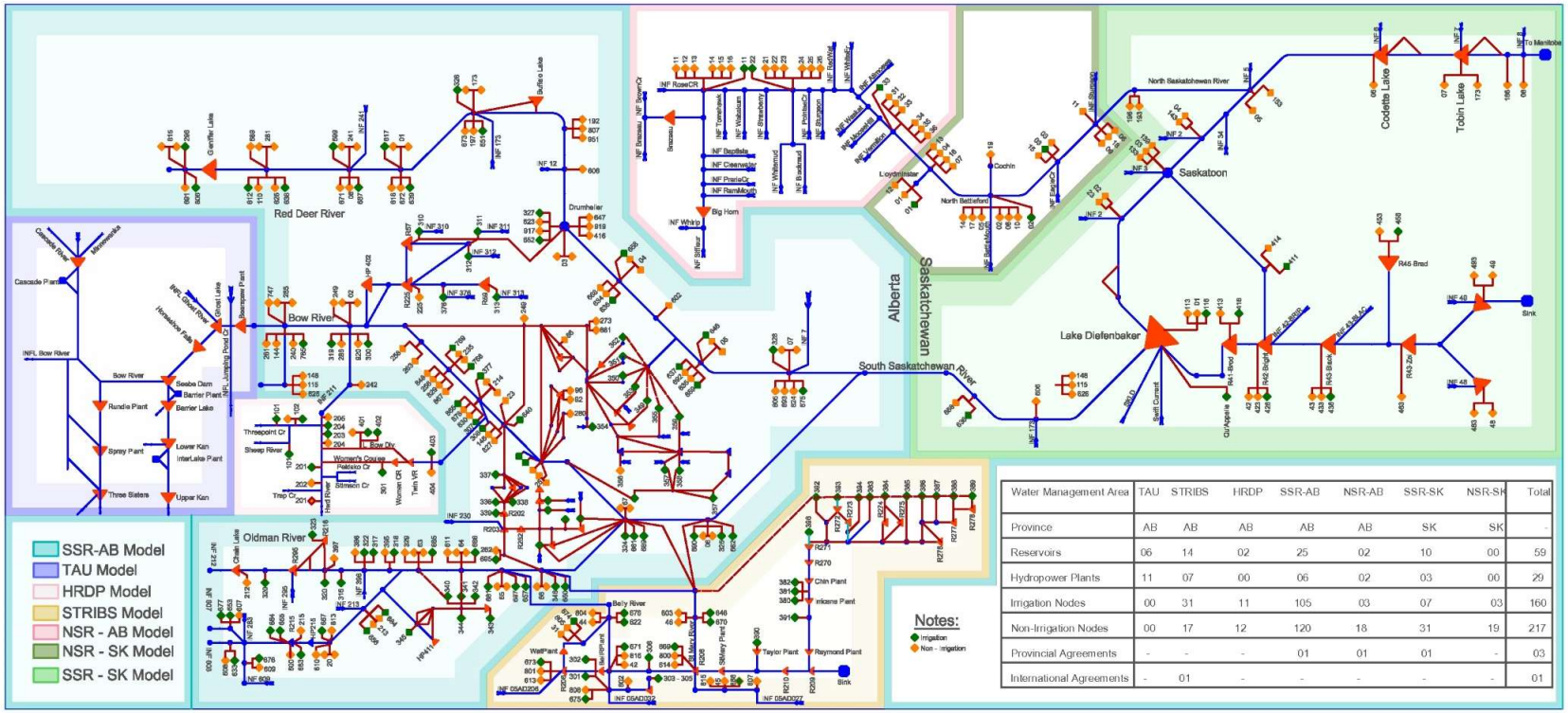

Water Management Area	TAU	STRIBS	HRDP	SSR-AB	NSR-AB	SSR-SK	NSR-SK	Total
Province	AB	AB	AB	AB	AB	SK	SK	-
Reservoirs	06	14	02	25	02	10	00	59
Hydropower Plants	11	07	00	06	02	03	00	29
Irrigation Nodes	00	31	11	105	03	07	03	160
Non-Irrigation Nodes	00	17	12	120	18	31	19	217
Provincial Agreements	-	-	-	01	01	01	-	03
International Agreements	-	01	-	-	-	-	-	01

Figure 4.6. The schematic view of the water management components of the SaskRB (from Shah 2020). Please refer to the digital version of the thesis for higher resolution and colour information

4.4.1 Priority-based Water Allocation

As mentioned earlier, the water allocation process of the IWMSask model is based on a set of priorities associated with each user in the modelled area summarized in Figure 4.7. The separated modelling practice for each water management area stems from the fact that, in real world, each area is managed independently from the others (Shah et al. 2021). This is mainly because each province has its own water allocation strategy. Once the model is set up, IWMSask distributes the available water in each time-step between the defined users in the whole SaskRB for each scenario.

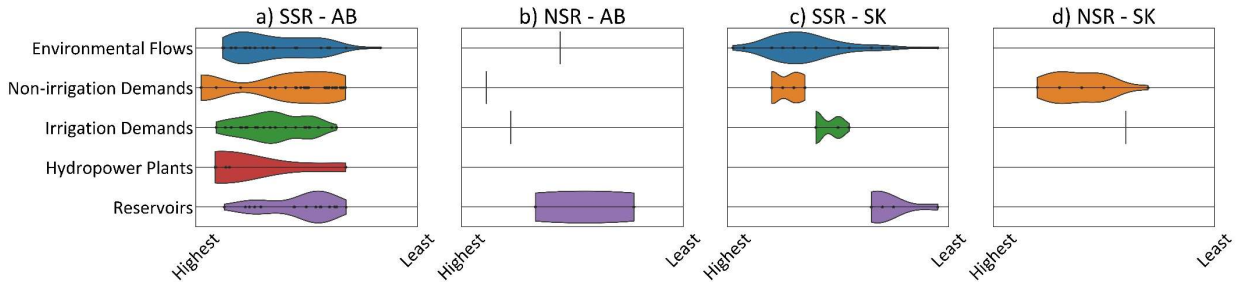

Figure 4.7. The priorities of different sectors in the IWMSask model. Each subplot displays sectoral priorities via violin plots for different areas of the SaskRB: a) SSR portion within southern AB, b) NSR portion within northern AB, c) SSR portion within southern SK, and d) NSR portion within northern SK. The coding of the areas is in line with naming of Figure 4.6 components.

From the figure, it could be viewed that, a portion of the non-irrigation demand users have mostly the highest priorities compared to other sectors (except for the SSR-SK case), as they correspond to municipal and industrial sectors within the SaskRB. Therefore, non-irrigation demands usually first receive water amongst other sectors, however, the location of each user also impacts how much water it receives. The irrigation users, on the other hand, are prioritized based on the water licenses issued by their respective provincial governments. The prioritization of the irrigation users in Alberta follows the concept of 'first in time, first in right' allocation scheme. This concept prioritizes users based on the date each license is issued. Nevertheless, the irrigation sector in Saskatchewan is prioritized based on both 'first in time, first in right' and 'equal sharing' concepts. The latter basically means in case of deficit, the users will suffer equally. A brief description of these concepts is detailed in Shah et al. (2021). The IWMSask model incorporates all these licensing details in allocating water between different irrigation demand nodes in the

SaskRB. The priorities associated with all other sectors, i.e., hydropower plants, reservoirs, and environmental flows, are also detailed in Shah (2020).

4.4.2 IWMSask Automation

Each water management area modeled in IWMSask (highlighted with different colors in Figure 4.6) were interconnected using a simple programming script. To this end, the Python programming language (see https://www.python.org/) was chosen due to its simplicity of syntax and the existence of necessary computational libraries to conduct this automation. Several third-party Python libraries were employed to this end, such as NumPy (Harris et al. 2020), SciPy (Virtanen et al. 2020), and pythonnet (see http://pythonnet.github.io/). The first package was mainly used to read and write flow data within the IWMSask model by manipulating data arrays. The second library was mostly employed to implement mathematical operations on each data array. And the latter provided an interface to communicate with the MODSIM model which serves as the main development tool for the IWMSask water management model.

4.4.3 Implementation of the Master Agreement in IWMSask

As a contribution to IWMSask by this research, a numerical method was incorporated into the water management model ensuring the requirements of the Master Agreement were implemented into water allocation simulations. As mentioned in Chapter 3, the Master Agreement stipulates two types of requirement for eastward flowing rivers of the SaskRB, that are: 1) an instantaneous minimum flow of 42.5 $m^3 s^{-1}$ or 50 percent of natural flow, whichever is less, through the SSR at the border of AB and SK (one objective for SSR), and 2) delivery of 50 percent of the natural flows of the SSR and NSR arising in AB (one objective for SSR and NSR each), and 50 percent of the actual flow delivered from AB plus 50 percent of the local flows arising within SK through SR (one objective for SR) in each calendar year. In the following, the details of the numerical method are described.

4.4.3.1 Instantaneous Minimum Flow Requirement

In this study, the natural flow of the river R at time-step t ($Q_{nat\ R,t}$) was simply calculated by the sum of all the headwater (and incremental) flows contributing to a river up to a point of interest, expressed by the following equation:

$$Q_{nat\ R,t} = \sum_{r=1}^{n} (Q_{r,t} + Q'_t), \tag{4.23}$$

where $Q_{r,t}$ is the flow of the headwater catchment r at time-step t, n represents the number of headwater catchments contributing to the river R, and Q'_t is the incremental flows of river R up to the point of interest.

For the purpose of apportionment of the SSR at the AB and SK border, the American entitlement of the St. Mary River must not be considered as part of the AB's share (Berry 1979). The American entitlement, $Q_{US,t}$, was computed following the procedure displayed in Figure 4.8; during the irrigation season in each calendar year (i.e., April to October), United States takes up to 25 percent of the natural flows of the St. Mary River up to natural flows of 18.9 $m^3 s^{-1}$; for the amounts above this threshold, US is entitled to half of the remaining natural flows available. The equal division of flows also applies to the periods before and after the irrigation season.

Since this study only focused on the Master Agreement objectives and, for the sake of simplicity, further considerations in allocating the St. Mary River waters described in Section 3.2 were not implemented. However, it is acknowledged that the water management operations within St. Mary and Milk river basins can directly impact AB's capability in meeting the Master Agreement's requirements (Halliday and Faveri 2007a). This matter could be further pursued in future studies.

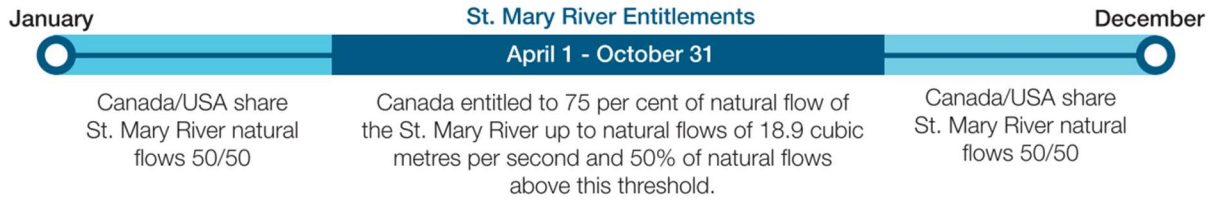

Figure 4.8. The water allocation procedure of the St. Mary River shared between Canada and the United States in each calendar year (the figure contains information licensed under the Open Government Licence – Alberta (Government of Alberta 2020a)).

Upon the calculation of $Q_{US,t}$, the apportionable flow for SSR, i.e., natural flow minus US entitlement, could be computed as follows:

$$Q_{appr\ SSR,t} = Q_{nat\ SSR,t} - Q_{US,t}, \tag{4.24}$$

where $Q_{appr\ SSR,t}$ is the SSR apportionable flow, $Q_{nat\ SSR,t}$ is the SSR natural flow, and $Q_{US,t}$ is the US entitlement of the St. Mary River at time-step t. Thereafter, the instantaneous minimum flow objective for SSR at the AB-SK border could be defined as:

$$Q_{minflow\ SSR,t} = \begin{cases} 42.5\ cms, & Q_{appr.SSR,t} \geq 85\ cms, \\ Q_{nat\ SSR,t} \times 0.5, & Q_{appr.SSR,t} < 85\ cms \end{cases}, \tag{4.25}$$

where $Q_{minflow,SSR,t}$ is the instantaneous minimum flow objective for the SSR at time-step t. This objective is violated, if the actual flow passing the AB-SK border at each time-step ($Q_{\ SSR,t}$) is less than $Q_{minflow,SSR,t}$. The IWMSask mechanism in response to violations of the Master Agreement is further described in the following subsection.

4.4.3.2 Annual Apportionment Requirement

For the annual apportionment objective, however, a more flexible approach was implemented because each upstream jurisdiction is mandated to match the downstream entitlements, not necessarily at each time-step (i.e., weekly in IWMSask), but at the end of an 'apportionment period', which in the case of the Master Agreement is one calendar year. In doing so, the approach of the Alberta Environment and Parks WRMM model (1993) was adopted and implemented in the IWMSask model designed to address the same problem. In the following, the numerical detail is explained.

First, the accumulated volume curve of the 'downstream entitlement' for each time-step of the year was calculated as follows:

$$AV_n = K \times \sum_{t=1}^{n} \left(Q_{appr\ R,t} \times \Delta t\right), \tag{4.26}$$

where AV_n is the accumulated volume of the downstream entitlement up to week number n, K is the fraction (here 0.5) of the apportionable flows of river R ($Q_{appr\ R,t}$) entitled to the downstream jurisdiction, and Δt is the time interval value. A sketch of the calculations is shown in Figure 4.9.

To evaluate whether the downstream deliveries during the year are on the path to meet AV_{52} volume by the year's end, "the [deliveries] … shall be adjusted from time to time on an equitable basis" (PPWB 2015). Thereby, to emulate the timely adjustments in IWMSask, a 'balancing period' equal to 13 weeks was considered (i.e., dividing the year into quarters). The balancing periods helped to instruct the IWMSask with the least target volumes necessary to meet in each time interval to smoothly achieve the overall annual apportionment objective by the year's end. In doing so, first, linear interpolations between the AV_n values for the beginning and end of each balancing period were calculated (blue line in Figure 4.9). The weekly accumulated volumes obtained from the linear interpolations were termed as AV_n'. The target volume path to smoothly meet the annual apportionment objective, was derived by the following equation:

$$TV_n = \min(AV_n\,, AV_n') \tag{4.27}$$

where TV_n is the target volume for week n. As the natural flows were known prior to the simulations of IWMSask (outputs of the HBV-SASK component), TV_n values were calculated beforehand. Once the IWMSask simulations began, the model was instructed with the following target flows in each time-step to achieve the annual apportionment objective:

$$TQ_n = \begin{cases} {(TV_n - DV_{n-1})}/{\Delta t}\,, & if\ (TV_{n-1} - DV_{n-1}) > 0 \\ 0, & if\ (TV_n - DV_{n-1}) \leq 0 \end{cases} \tag{4.28}$$

where TQ_n is the target flow for week n and DV_{n-1} is the accumulated volume delivered up to week $(n-1)$. Unsurprisingly, in the case of water abundance, the surplus of water was allowed to be passed to the downstream jurisdiction and no action was required. However, if the delivered volume dropped below the target volume at a given time step, i.e., $(TV_{n-1} - DV_{n-1}) > 0$, then the model was instructed to attempt to compensate the deficit volume in the succeeding time intervals. The attempts continued as long as the deficit was compensated, or the apportionment period ended. If the annual apportionment objective was violated, i.e., $(TV_{52} - DV_{52}) > 0$, a warning was issued by the IWMSask. It may be noted that the deficits and surpluses of an apportionment year could not be carried over to the next.

The described approach was used to assure the model was provided with enough flexibility to achieve the Master Agreement requirements for SSR and NSR (at the AB-SK border), and SR (at the SK-MB border). Although the Master Agreement is also applicable to the Battle River (see

Figure 4.2), due to insignificant consumptive water use from this river (Government of Alberta 2020b), it has not been considered in this study.

4.5 Vulnerability Assessment

The vulnerability of the Master Agreement was assessed, in particular for three control points. As mentioned in Chapter 3, these points were chosen where the transboundary rivers of the SaskRB – SSR, NSR, and SR – cross the political borders of the Canadian provinces. The four requirements of the Master Agreement studied in this research are described in Section 4.4.1. In this section, violations of the mentioned objectives under the perturbed climate change scenarios are investigated.

In doing so, a general performance metric was defined to quantify the number of violations of each objective. The risk-related performance metric was described as:

$$J_k = Prob[X_t \in F] \tag{4.29}$$

where J_k is the function for the k-th objective, X_t is a random variable which denotes the state of the system on time-step t, while all possible states of the system on each time-step could be categorized into S (i.e., success), or F (i.e., failure) sets. The performance metric is known as 'risk' in the literature and suggested as the opposite of 'reliability' (Hashimoto et al. 1982). Therefore, the performance metric could be applied for each of the Master Agreement objectives which, in this study, are referred to as 1) $J_{minflow,SSR}$, 2) $J_{0.5(nat.flow),SSR}$, 3) $J_{0.5(nat.flow),NSR}$, and 4) $J_{0.5(nat.flow),SR}$. The output of each scenario was evaluated and presented in Section 5.4.

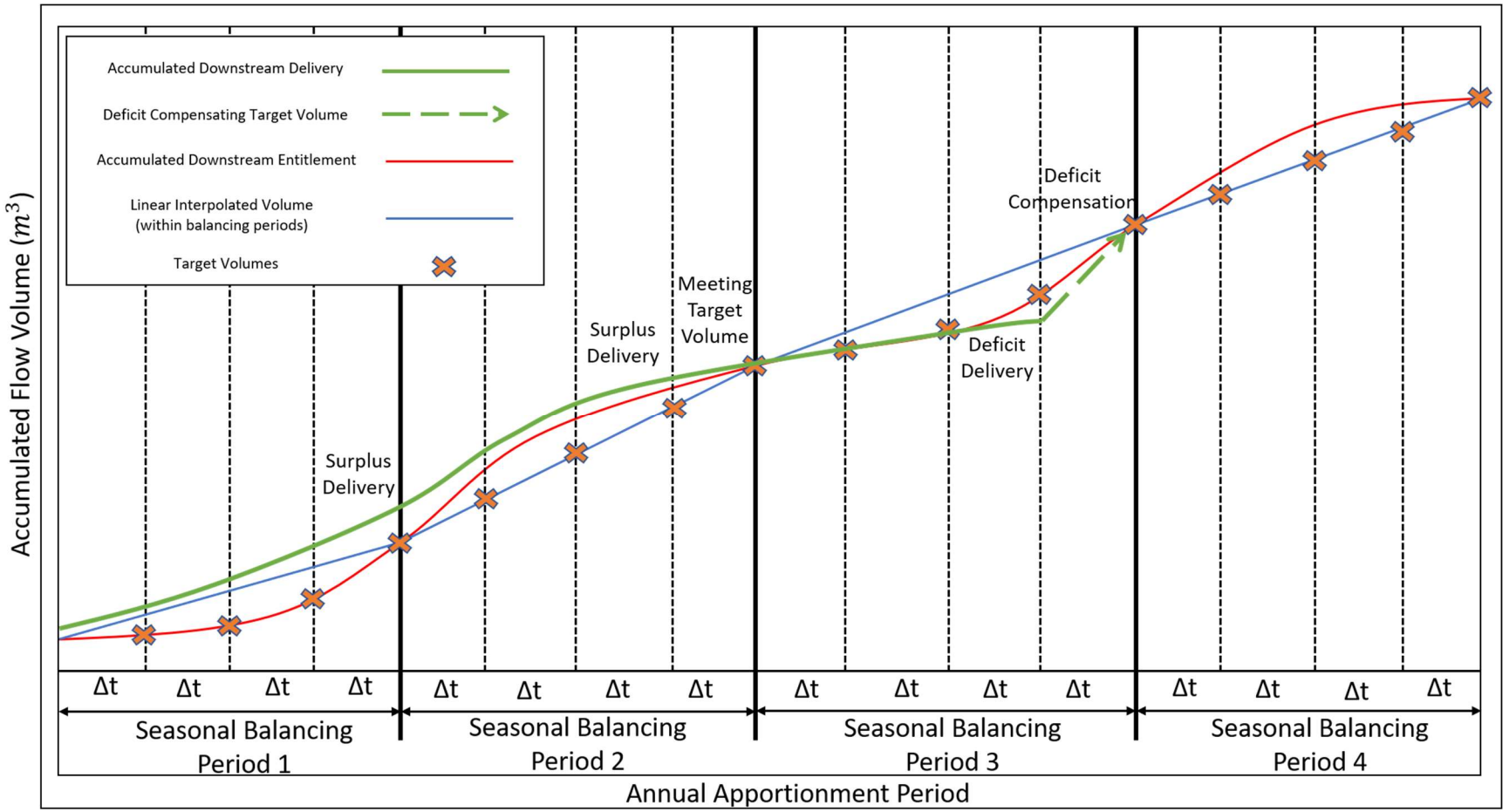

Figure 4.9. Sketch of the annual apportionment procedure implemented in IWMSASK. The figure is reproduced (with modifications) from the Alberta Environment and Parks manual on the WRMM model (Alberta Environmental Protection 1993).

4.6 Data Sources

Several data sources have been used for each part of the applied methodology which are detailed in the following:

1) weather scenario generation:
    a. baseline period observations (see Section 4.2): the daily historical precipitation, minimum and maximum temperature values for the period of 1980 to the end of 2013 have been extracted from the Canadian ANUSPLIN climate dataset. This gridded dataset has a resolution of 0.0833° (~10 km^2) produced using the Australian National University Spline (ANUSPLIN) model (Hutchinson et al. 2009; Wong et al. 2017).
    b. future climate projections for N_{dry} adjustments (see Section 4.2.2): the daily projected precipitation values for the period of 2080 to the end of 2099 were extracted from two Canadian RCM outputs, which were used to calculate future N_{dry}: 1) CanRCM4, and 2) CRCM5. Both of these RCMs have produced future climate projection for two RCPs: 1) RCP4.5, and 2) RCP8.5. Each projection has a rotated grid system with a resolution of 0.44° (~50 km) produced using the CanESM2 OA/GCM as the driver (Mearns et al. 2020; Scinocca et al. 2016).
    c. the initial uncertainty ranges used to construct the exposure space (see Section 4.2.2) for P_{JJA}, P_{DJF}, and T_{Ann}: Asong et al. (2020) recently analyzed shifts in seasonal and annual precipitation and temperature values projected by Coupled CMIP5 OA/GCMs across major Canadian river basins. The work is unpublished.
2) hydrological modelling:
    a. calibration and validation period climate forcing data (see Section 4.3): for those headwater catchments, which were entirely located within Canada (see Figure 4.2), the daily historical precipitation, minimum and maximum temperature time-series were extracted from the Canadian ANUSPLIN dataset. If the catchment was partially located within the United States, then the Princeton dataset was employed. The Princeton dataset is a global reanalysis product developed by the Princeton University with a resolution of 0.5° (~50 km) and spanning from 1901 to the end of 2012 (Sheffield et al. 2006; Wong et al. 2017).
    b. Calibration and validation period streamflow time-series (see Section 4.3): for those headwater catchments, which the natural daily data were available, the streamflow data were acquired from the Water Survey Canada through the HYDAT database. Otherwise, the weekly naturalized flow was obtained from the Alberta Environment and Parks.

c. MODIS ET estimations (see Section 4.3.3): the MOD16A2 dataset provides 8-day estimates of the MODIS evapotranspiration values with a resolution of 0.5° (~1km^2) on a global scale. The MODIS ET data are produced using the Mu et al. (2011) model spanning from 1980 to present. The data are accessible from https://modis.gsfc.nasa.gov/data/dataprod/mod16.php.

5 CHAPTER 5: RESULTS

5.1 General Overview

In this chapter, firstly, the results of the scenario generation process are presented (Section 5.2). Secondly, the HBV-SASK model is evaluated for the headwater catchments of this study in Section 5.3. Finally, the results of the vulnerability assessment study are illustrated, and a discussion is developed in Section 5.4.

5.2 Generation of Weather Scenarios

This section describes the process of generating multiple plausible future scenarios used in this research. First, the MulGETS weather generator is tested to validate its credibility to be used in basin-wide vulnerability assessment studies (Section 5.2.1). Second, the transition probabilities of the weather generator are fitted to the future climate projections and also bias-corrected, which is further described and analyzed in Section 5.2.2. Finally, the exposure space of this study, reporting the properties of the produced, perturbed weather scenarios is described in Section 5.2.3.

5.2.1 Calibration and Validation of the Weather Generator

As mentioned earlier, to test the performance of the generator, the model was employed to produce 40 ensembles of 20-year scenarios. Various statistical properties, such as time and spatial dependence, distributional assumptions, and seasonal extremes, are reported for both the generated and observed time-series. The properties are described for all sites and further scrutinized for four selected individual catchments. These catchments are each located upstream of the four main SaskRB rivers, i.e., Bow, Oldman, Red Deer, and North Saskatchewan River (NSR) the details of which can be found in Table 4.1.

5.2.1.1 Distributional Assumptions

The performance of the model in generating precipitation amounts is evaluated in Figure 5.1, where the observed and generated values across all weather sites are compared for 6 selected quantiles. The figure shows an underestimation in reproducing small (i.e., 10^{th} and 25^{th} quantiles) and extreme (i.e., 99^{th} quantile) precipitation amounts for most sites, though, the model's performance is deemed acceptable in capturing the historical amounts for the quantiles in between (i.e., 50^{th}, 75^{th}, and 95^{th}). It is noteworthy that only the time-series of precipitation amounts greater than the trace precipitation value (i.e., 0.5 mm) is considered in the distributional assessments of this subsection.

Figure 5.2 further illustrates selected statistical properties, including mean, median and standard deviation of the generated daily precipitation for each season of the year across all weather sites. All three statistics of the generated scenario is comparable to that of the observed for almost all sites.

Given the overall preview of the WG's performance in generating precipitation amounts in all weather sites, Figure 5.3 further illustrates the distributional assumptions for four selected catchments in detail. The figure shows the Q-Q plot of the observed and generated precipitation, along with their histogram, empirical cumulative distribution functions (i.e., ecdf), and other relative statistical properties, such as mean, median, and standard deviation. In Figure 5.3a, it could be viewed that, for most quantiles, the data points are lying along the ideal line, especially for low and medium precipitation amounts. Nonetheless, as mentioned earlier, the model's performance diminishes for the heavier precipitation quantiles, with an overestimation in the Red Deer River and Oldman River sites, and an underestimation in the Bow River and North Saskatchewan River ones. In addition, Figure 5.3b and c give a visual view of the goodness-of-fit between the generated and observed precipitation amounts. And finally, Figure 5.3d summarizes the mean, median, and standard deviation of the observed and generated values.

This set of charts is repeated for maximum (Figure 5.4 to Figure 5.6) and minimum (Figure 5.7 to Figure 5.9) temperature variables. Both temperature variables show a slight deviation from the ideal line in the overall quantile figures (i.e., Figure 5.4 and Figure 5.7); the deviation is significantly lower for middle quantiles (i.e., 50^{th} and 75^{th}) of the maximum temperature, and higher quantiles (i.e., 95^{th} and 99^{th}) of the minimum temperature variables. Similar to the

precipitation amounts scenario, the seasonal daily mean and median of the temperature time-series (i.e., Figure 5.5 and Figure 5.8) are comparable to that of the observed. However, the standard deviation of the generated temperature values shows a mismatch for the minimum temperature during winter and maximum temperature during summer seasons. This mismatch could be traced back to the differences that were detected between the distribution of the observed and generated temperature values. The slight discrepancies seen in the Q-Q plot could be further investigated by analyzing the temperature distributions for the four selected sites in Figure 5.6 and Figure 5.9. These differences could be attributed to the assumption of the unimodal distribution of temperature values in generating data; in Equation 4.5 a standard normal pdf is assumed to generate the residuals, as opposed to the bimodal nature of the observed distribution (i.e., Figure 5.6c and Figure 5.9c). This assumption has potentially resulted in slight deviations in lower, middle, and high quantiles of the Q-Q plots (i.e., Figure 5.6a and Figure 5.9a) and ecdf plots (i.e., Figure 5.6b and Figure 5.9b).

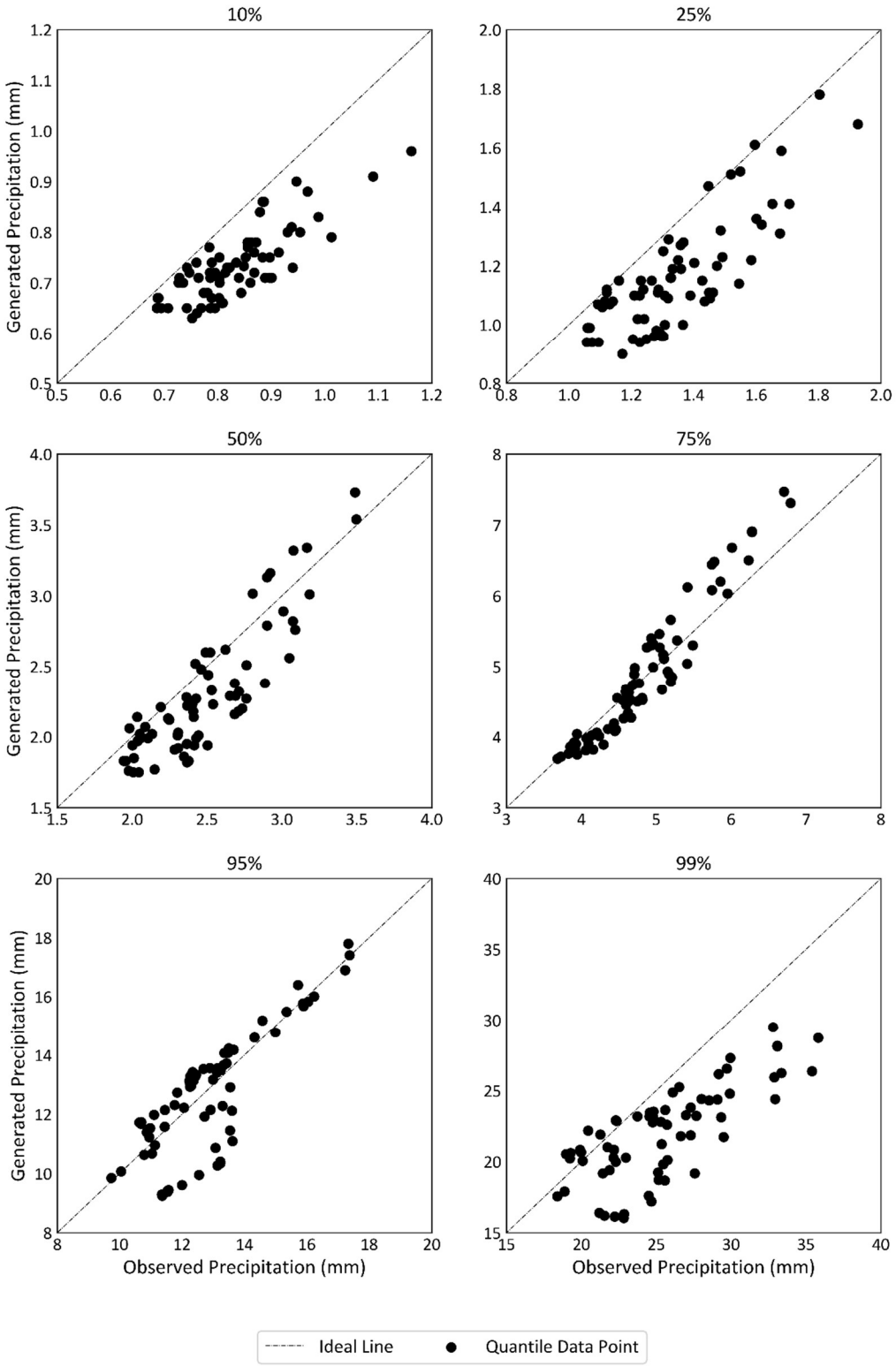

Figure 5.1. The scatter plot of the observed versus generated precipitation amounts across all weather sites for 6 selected quantiles, i.e., 10th, 25th, 50th, 75th, 95th, and 99th. Each circle corresponds to the quantile data of the observed/generated daily precipitation amounts for one weather site (i.e., catchment).

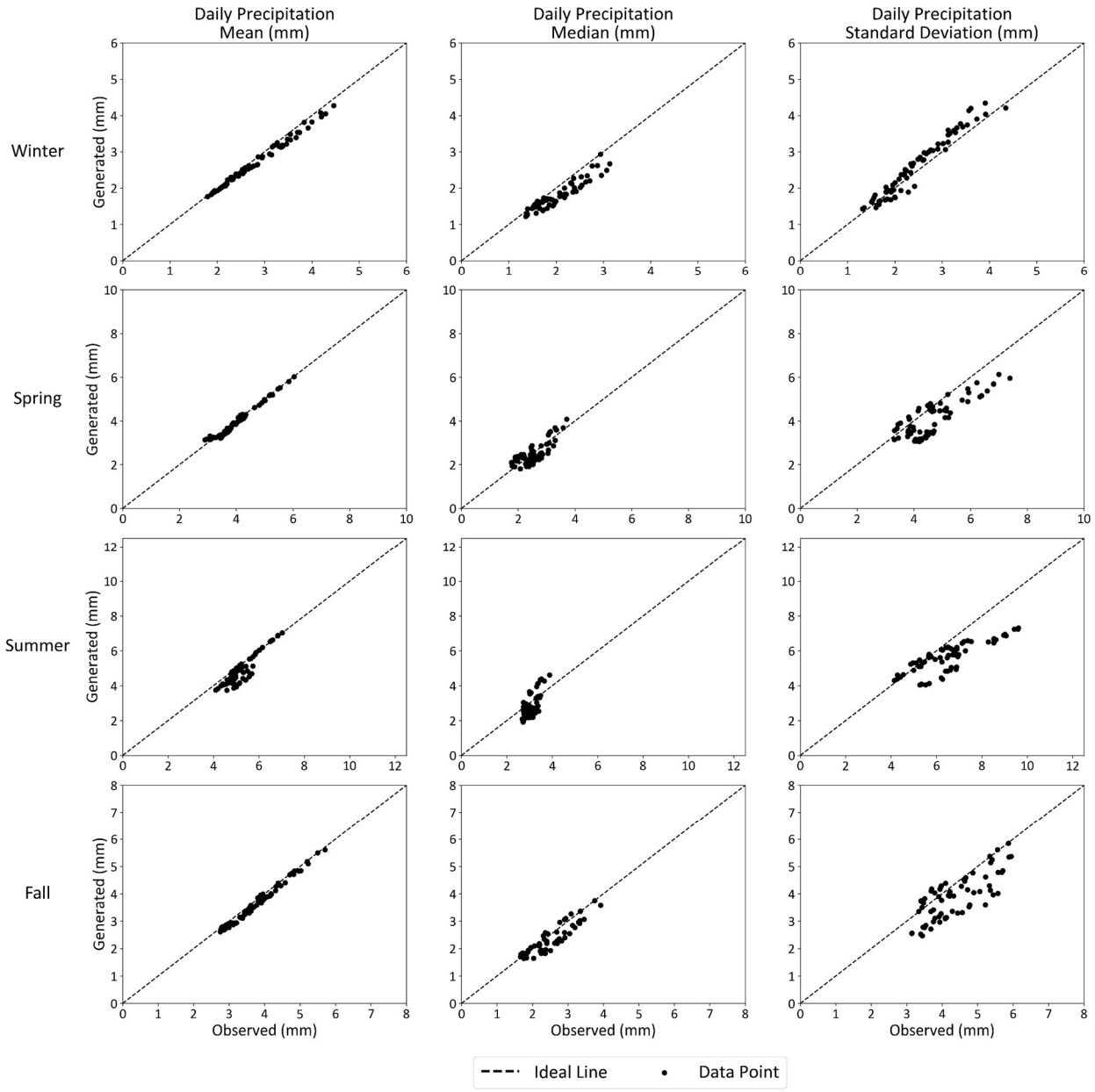

Figure 5.2. Mean, median, and standard deviation of the observed versus generated daily precipitation over all weather sites for four seasons of the year, i.e., spring (MAM), summer (JJA), fall (SON), and winter (DJF). Each circle corresponds to the selected statistics of the observed/generated daily precipitation amounts for one weather site.

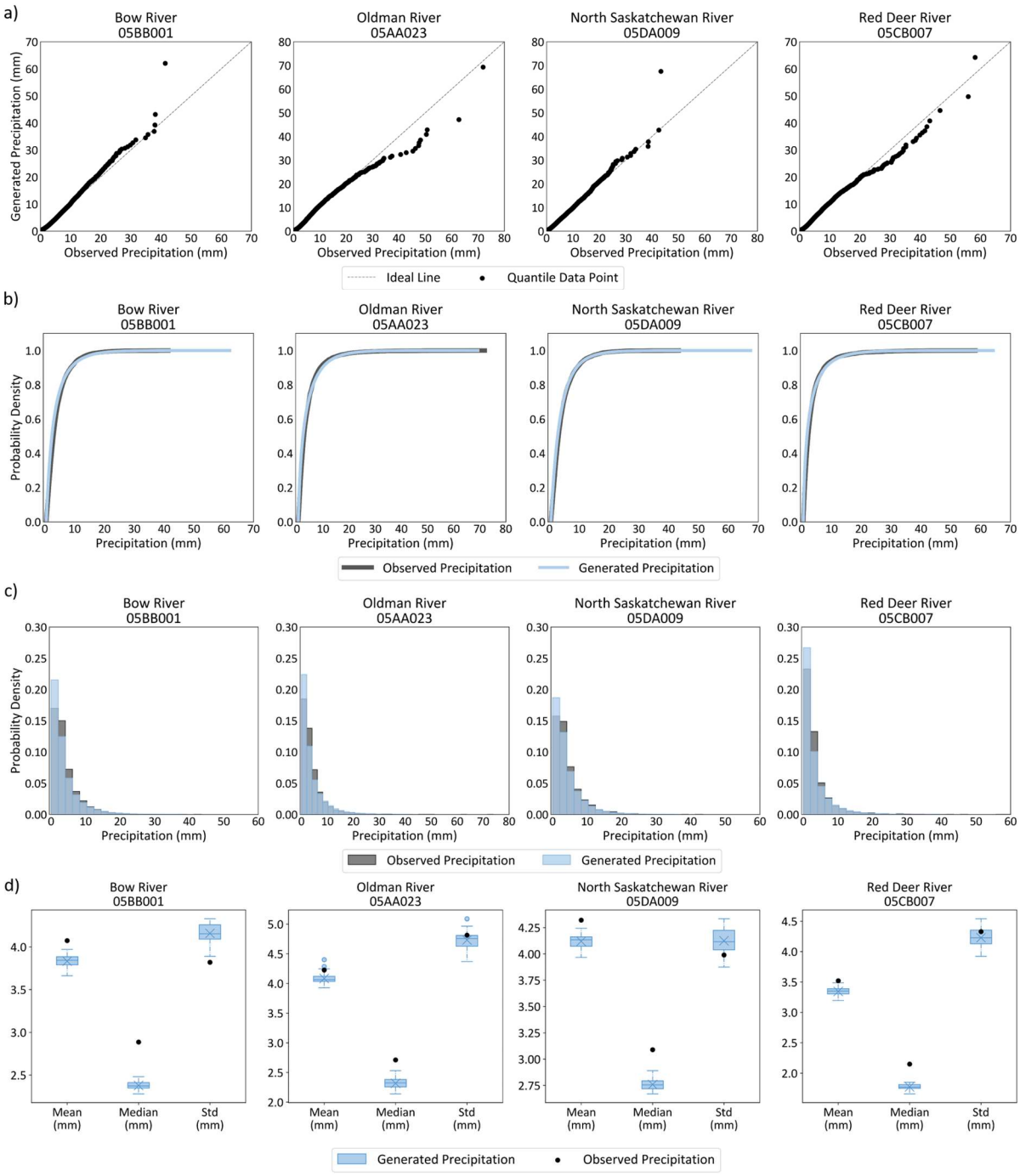

Figure 5.3. The a) Q-Q plot, b) ecdf, c) histogram, and d) general statistical properties of the observed versus generated precipitation amounts for four selected headwater catchments with the following outlet gauges: 1) Bow River at Banff (05BB001), 2) Oldman River near Waldron's Corner (05AA023), 3) North Saskatchewan River (NSR) at Whirlpool Point (05DA009), and 4) Red Deer River at the Dickson Dam Tunnel Outlet (05CB007). Each box-and-whisker contains a horizontal line and a cross indicating the median and mean of the statistic of interest, respectively, for each site. The time resolution of the used observed/generated precipitation amounts is daily.

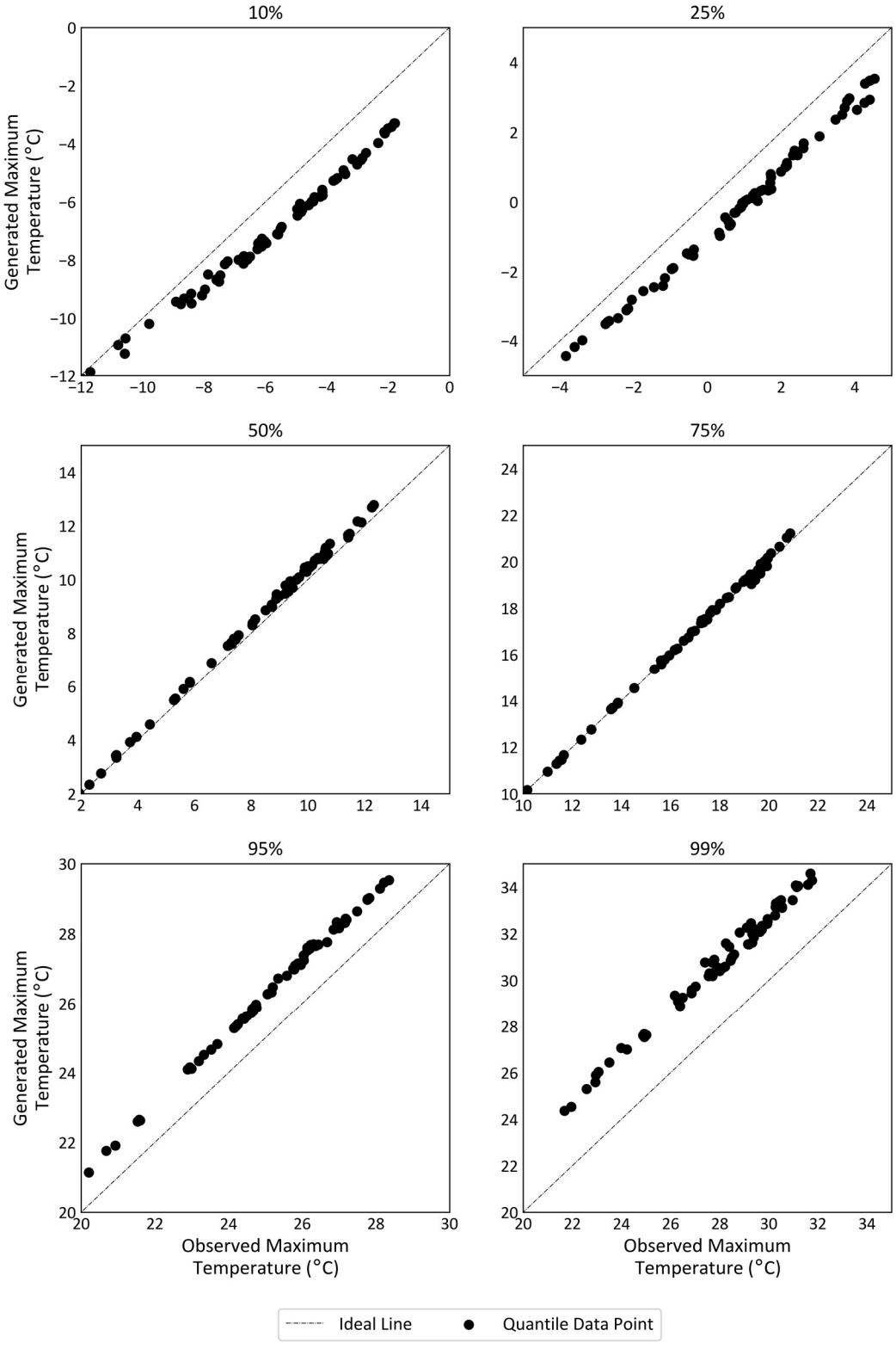

Figure 5.4. The scatter plot of the observed versus generated maximum temperature across all weather sites for 6 selected quantiles, i.e., 10th, 25th, 50th, 75th, 95th, and 99th. Each circle corresponds to the quantile data of the observed/generated daily maximum temperature for one weather site (i.e., catchment).

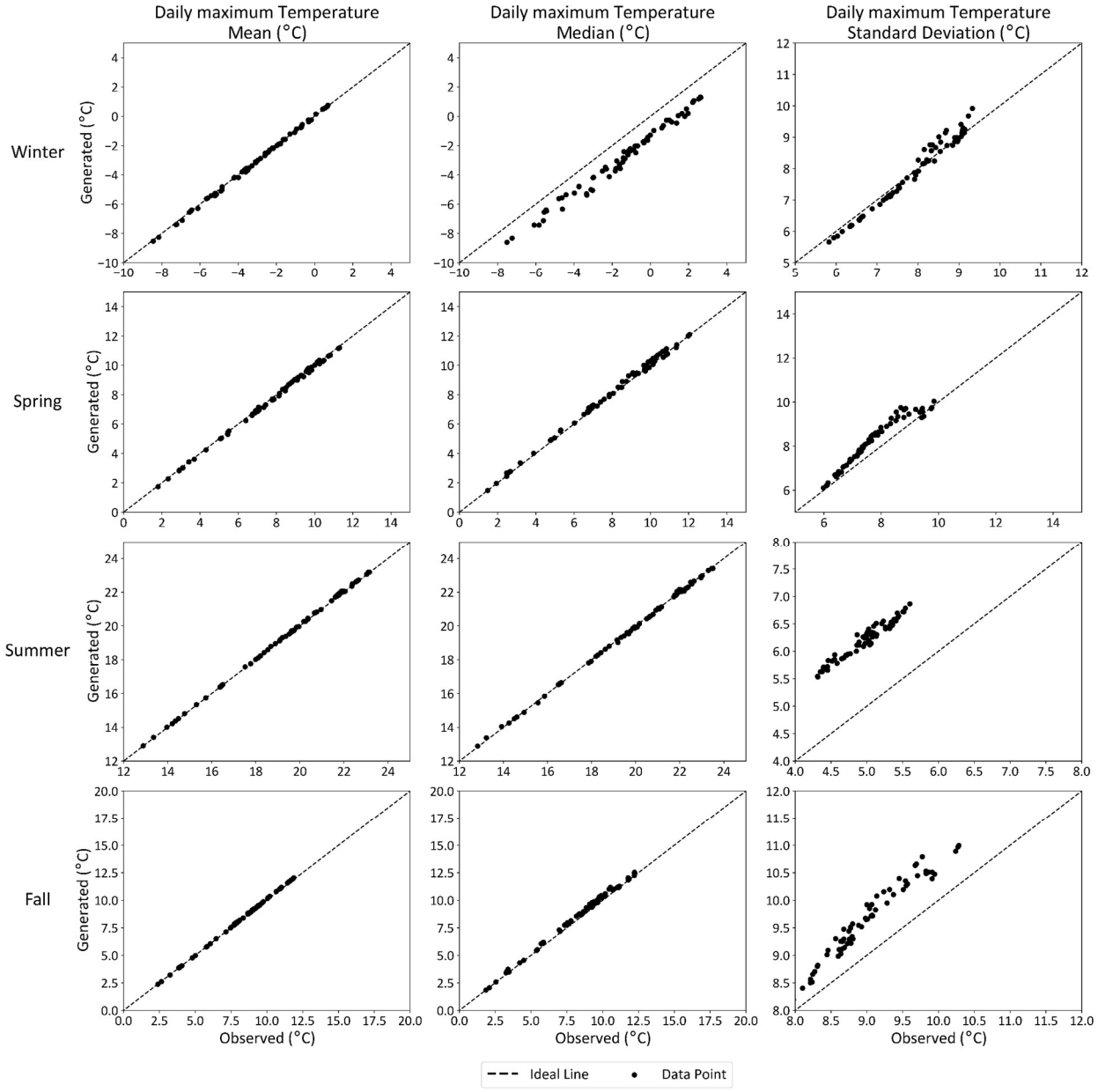

Figure 5.5. Mean, median, and standard deviation of the observed versus generated maximum temperature over all weather sites for four seasons of the year, i.e., spring (MAM), summer (JJA), fall (SON), and winter (DJF). Each circle corresponds to the selected statistics of the observed/generated daily maximum temperature for one weather site.

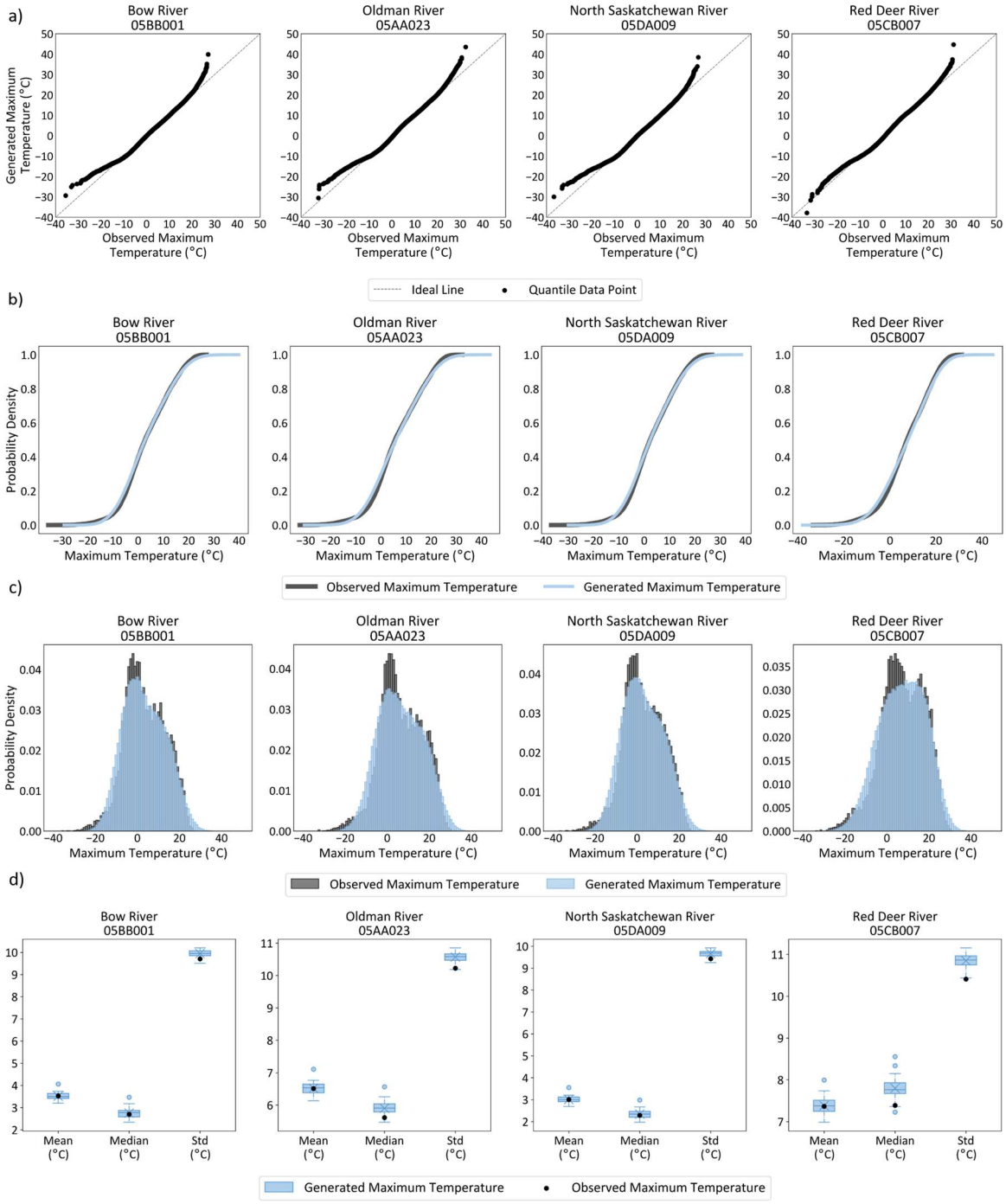

Figure 5.6. The a) Q-Q plot, b) ecdf, c) histogram, and d) general statistical properties of the observed versus generated maximum temperature for four selected headwater catchments with the following outlet gauges: 1) Bow River at Banff (05BB001), 2) Oldman River near Waldron's Corner (05AA023), 3) North Saskatchewan River (NSR) at Whirlpool Point (05DA009), and 4) Red Deer River at the Dickson Dam Tunnel Outlet (05CB007). Each box-and-whisker contains a horizontal line and a cross indicating the median and mean of the statistic of interest, respectively, for each site. The time resolution of the used observed/generated maximum temperature is daily.

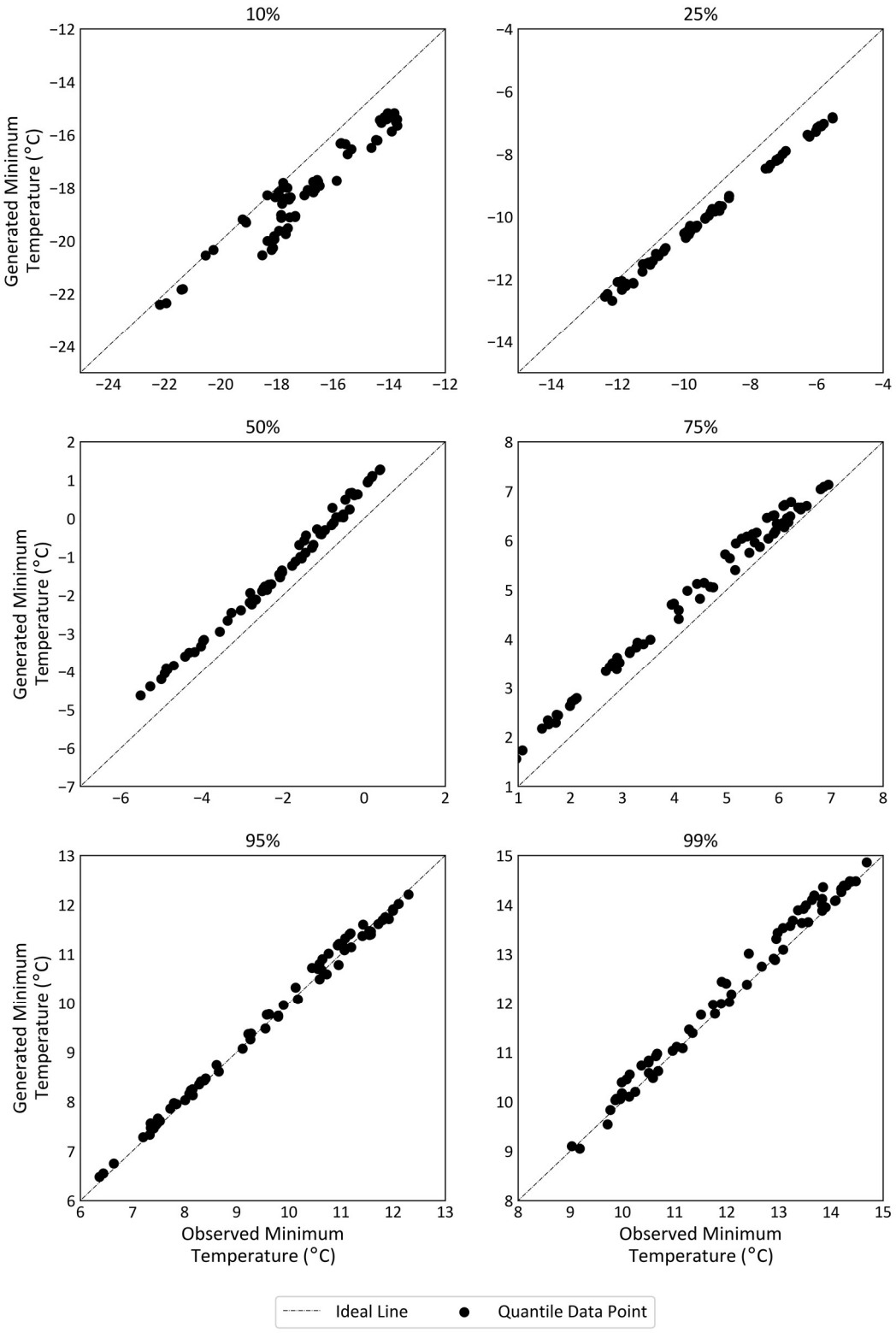

Figure 5.7. The scatter plot of the observed versus generated minimum temperature across all weather sites for 6 selected quantiles, i.e., 10th, 25th, 50th, 75th, 95th, and 99th. Each circle corresponds to the quantile data of the observed/generated daily minimum temperature for one weather site (i.e., catchment).

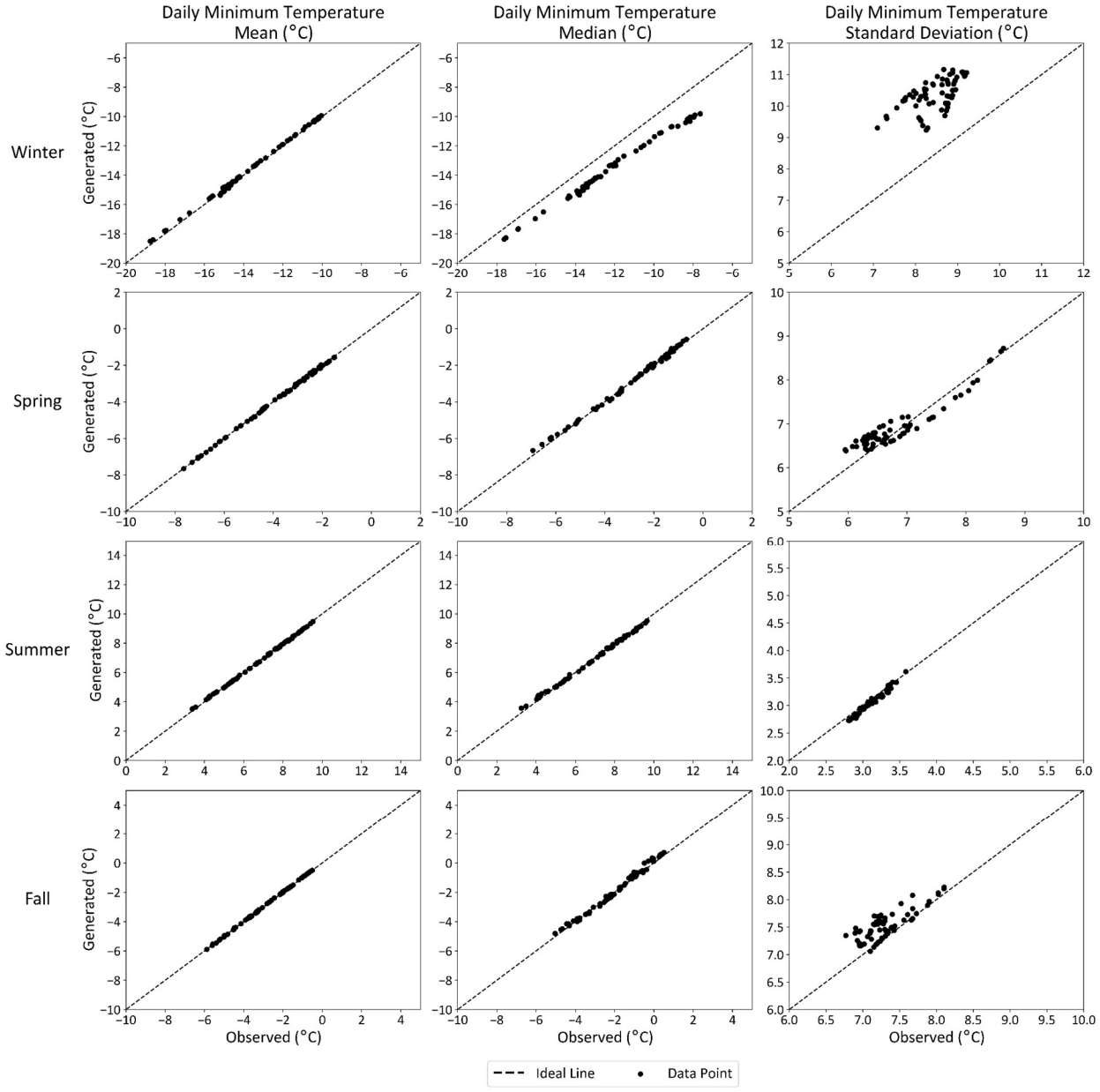

Figure 5.8. Mean, median, and standard deviation of the observed versus generated minimum temperature over all weather sites for four seasons of the year, i.e., spring (MAM), summer (JJA), fall (SON), and winter (DJF). Each circle corresponds to the selected statistics of the observed/generated daily minimum temperature for one weather site.

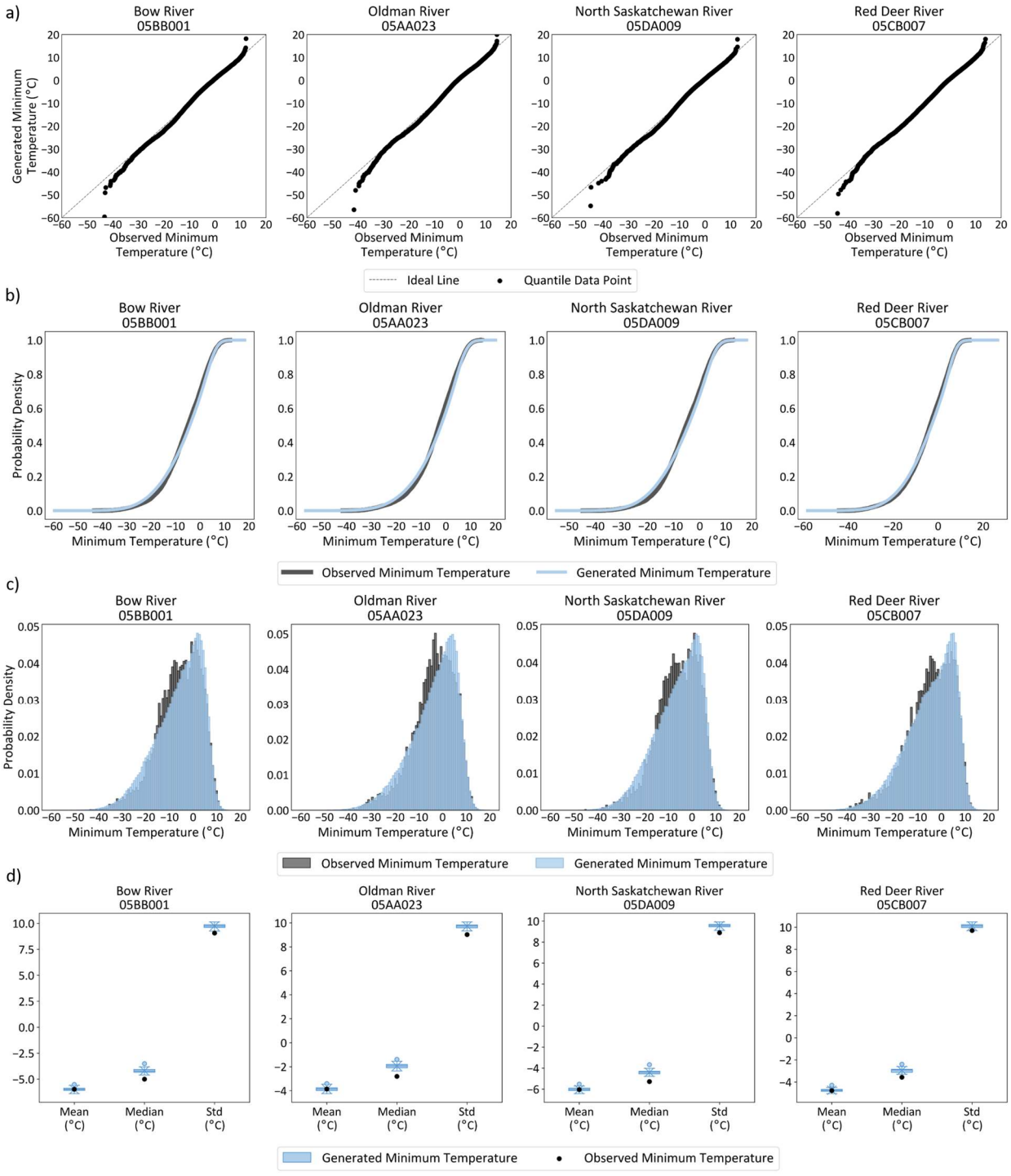

Figure 5.9. The a) Q-Q plot, b) ecdf, c) histogram, and d) general statistical properties of the observed versus generated minimum temperature for four selected headwater catchments with the following outlet gauges: 1) Bow River at Banff (05BB001), 2) Oldman River near Waldron's Corner (05AA023), 3) North Saskatchewan River (NSR) at Whirlpool Point (05DA009), and 4) Red Deer River at the Dickson Dam Tunnel Outlet (05CB007). Each box-and-whisker contains a horizontal line and a cross indicating the median and mean of the statistic of interest, respectively, for each site. The time resolution of the used observed/generated minimum temperature is daily.

5.2.1.2 Time and Spatial Correlation Structures

5.2.1.2.1 Time Correlation Structure

The 40 sample scenarios are also employed to assess the time dependence structure of the generated variables. To assess this property, Figure 5.10 shows the Autocorrelation Functions (ACFs) of the generated and observed precipitation a) occurrences and b) amounts for 6 different time lags (i.e., 1 to 6 days) summarized for each month of the year. The distributions of the observed ACFs across the weather sites are reported using box-and-whiskers, whereas the distributions of the generated ones across all weather sites and the 40 sample scenarios using violin plots. Figure 5.10a shows the good performance of the Markov Chain component in capturing the time dependence structure of the observed precipitation occurrences for all time lags. However, as is evident in Figure 5.10b, the model fails at replicating the dependence structure of the observed amounts for the 1-day lag, mainly due to lacking a mechanism to preserve its autocorrelation structure in the first place. An evaluation of the correlograms for the four selected weather sites (Figure 5.11) further validates the knowledge gained from the overall ACF assessments. Also, it is expected that the model fails at capturing the observed inter-monthly and inter-annual variability, as no mechanism is implemented in the current weather generation model; this issue has been addressed in the literature (see Chen et al. (2019)). It is worth mentioning that dry days (less than 0.5mm of precipitation amount) have been considered in the calculation of ACFs for the precipitation amounts.

The overall ACF charts (Figure 5.12) and correlograms (Figure 5.13) are again reported for the a) maximum and b) minimum temperature variables. Due to the assumption of normally distributed temperature variables (see Section 5.2.1.1), slight deviations from the observed autocorrelation functions are observable in Figure 5.12, especially for the summer months (JJA, i.e., months of June, July, and August) for the maximum temperature, and the months of November to March for the minimum temperature. However, the correlograms indicate an acceptable performance of the model in preserving the time dependence structure of the observed temperature time-series. The confidence bands in the individual ACF figures are calculated using $\pm \frac{1.96}{\sqrt{L}}$, where L is the length of the time-series used.

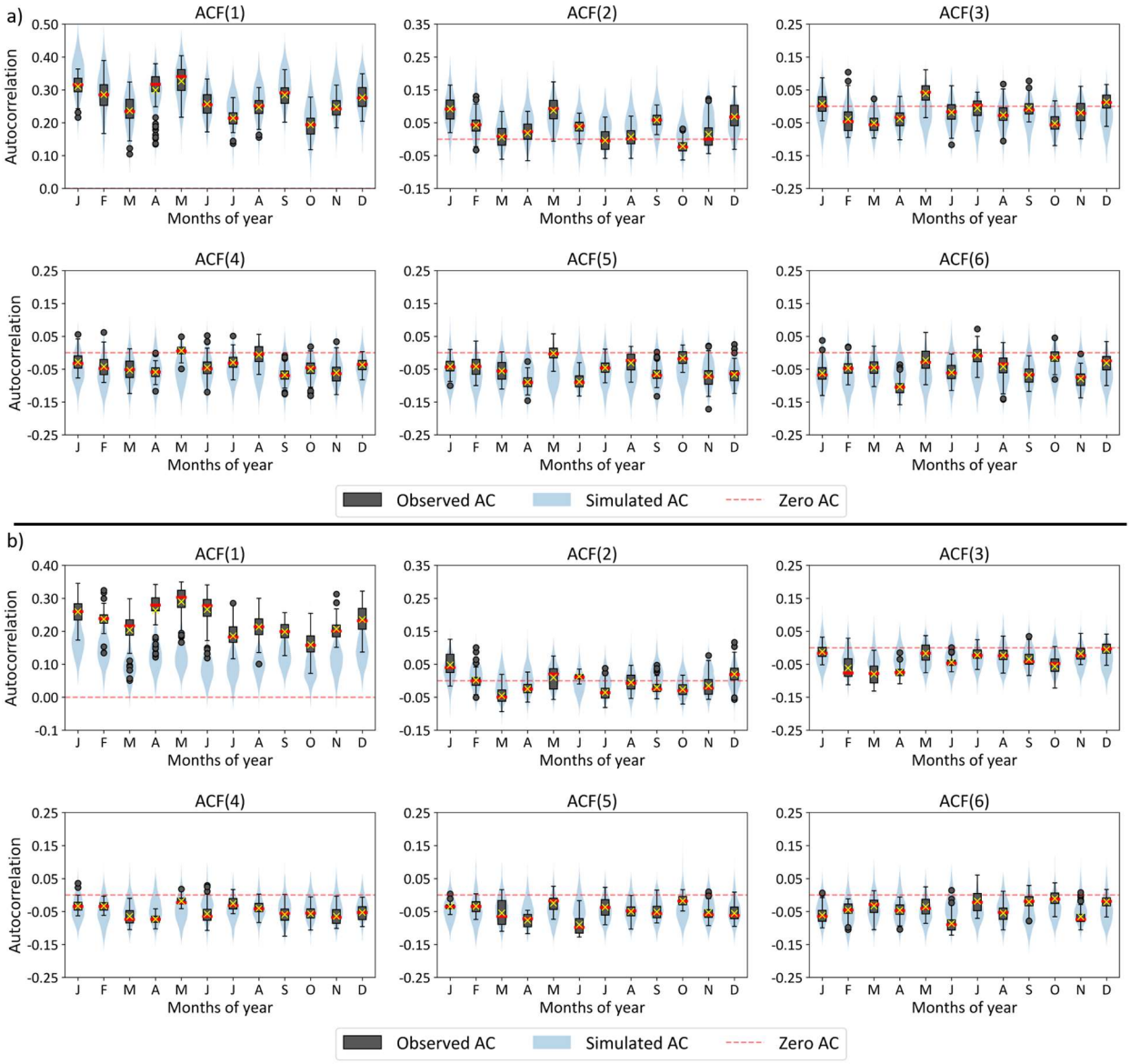

Figure 5.10. The Autocorrelation Function (ACF) of the: a) precipitation occurrences and b) precipitation amounts, for 6 different time lags (in days) and 12 months of the year. Each box-and-whisker indicates ACF for the 70 weather sites. Within each box, the horizontal line and cross correspond to the median and mean of the 70 sites, respectively. Each violin plot indicates the distribution of ACFs across the 40 scenarios pooled over all weather sites. The time resolution of the observed and generated time-series is daily.

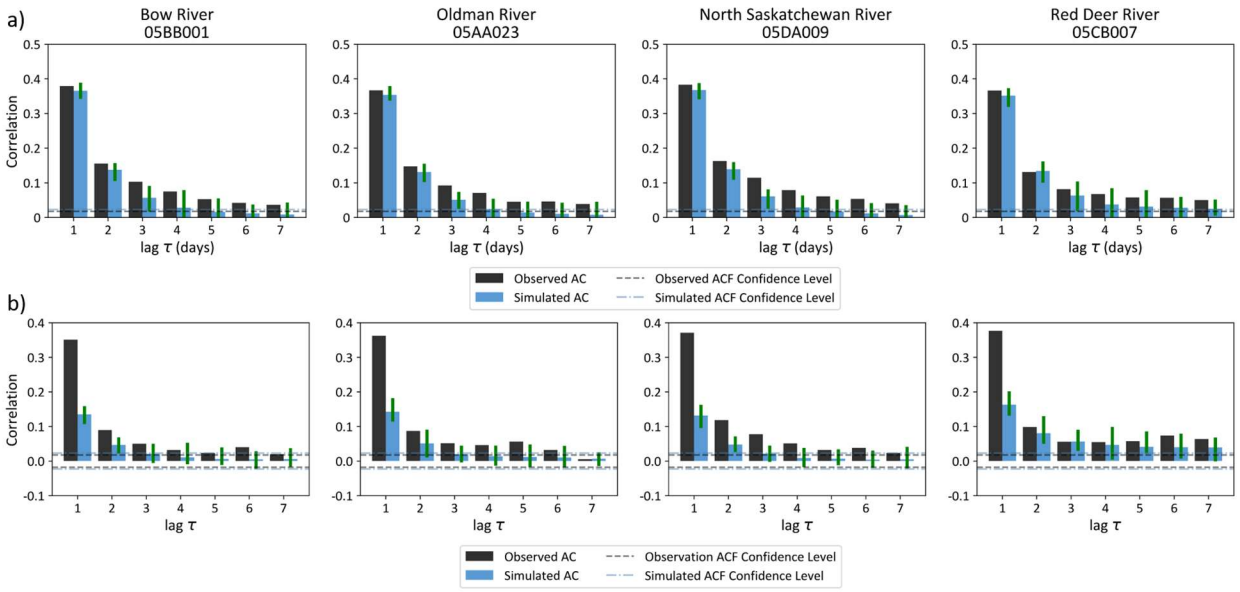

Figure 5.11. Correlograms of the observed versus generated precipitation: a) occurrences and b) amounts for 1- to 7-day time lags. Black bars indicate the observed ACFs, while the blue bars indicate the mean ACF of the 40 generated time-series with their range shown using a green bar on the top. The time resolution of the observed and generated time-series is daily.

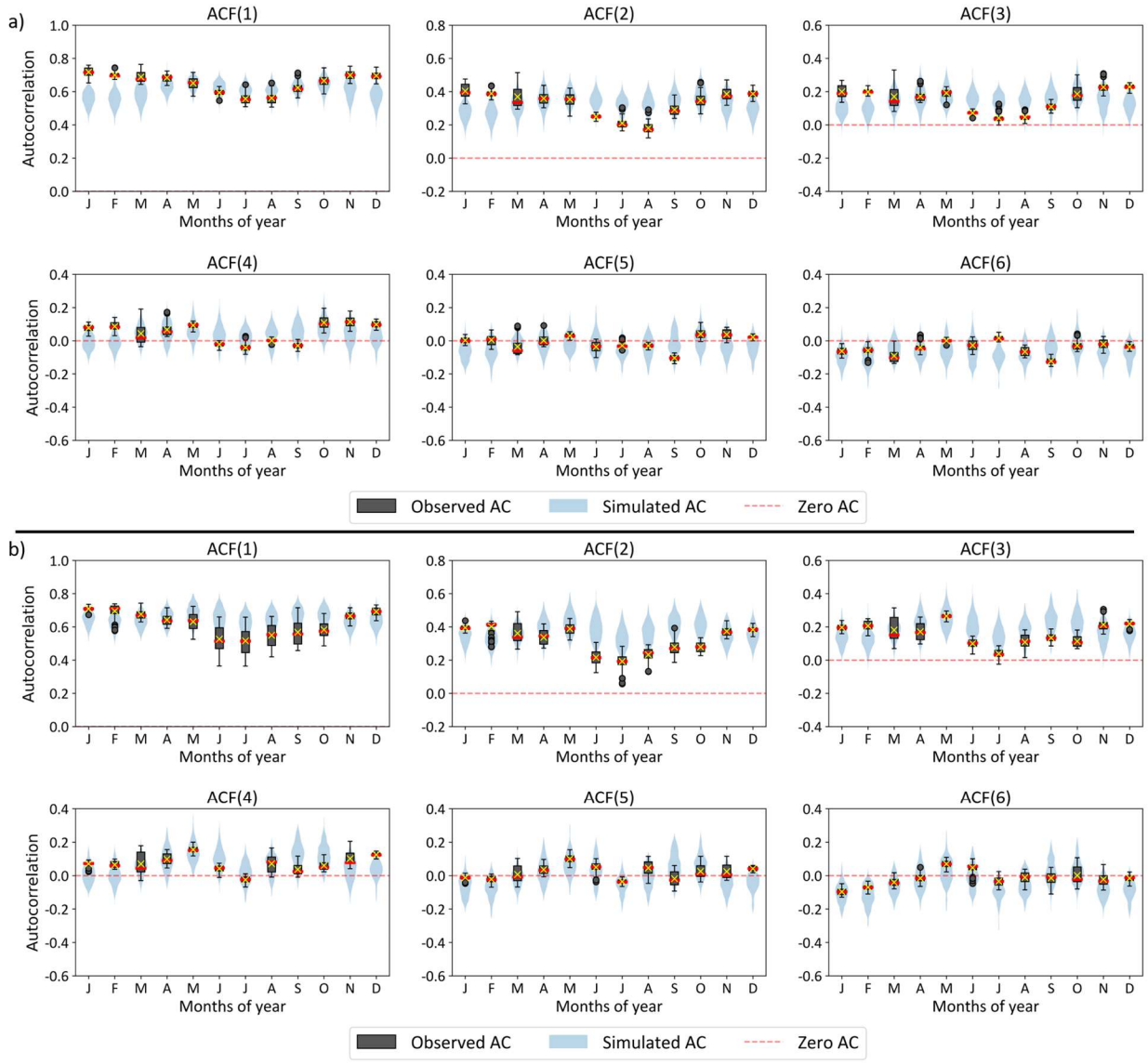

Figure 5.12. The Autocorrelation Function (ACF) of the: a) maximum and b) minimum temperature, for 6 different time lags (in days) and 12 months of the year. Each box-and-whisker indicates ACF for the 70 weather sites. Within each box, the horizontal line and cross correspond to the median and mean of the 70 sites, respectively. Each violin plot indicates the distribution of ACFs across the 40 scenarios pooled over all weather sites. The time resolution of the observed and generated time-series is daily.

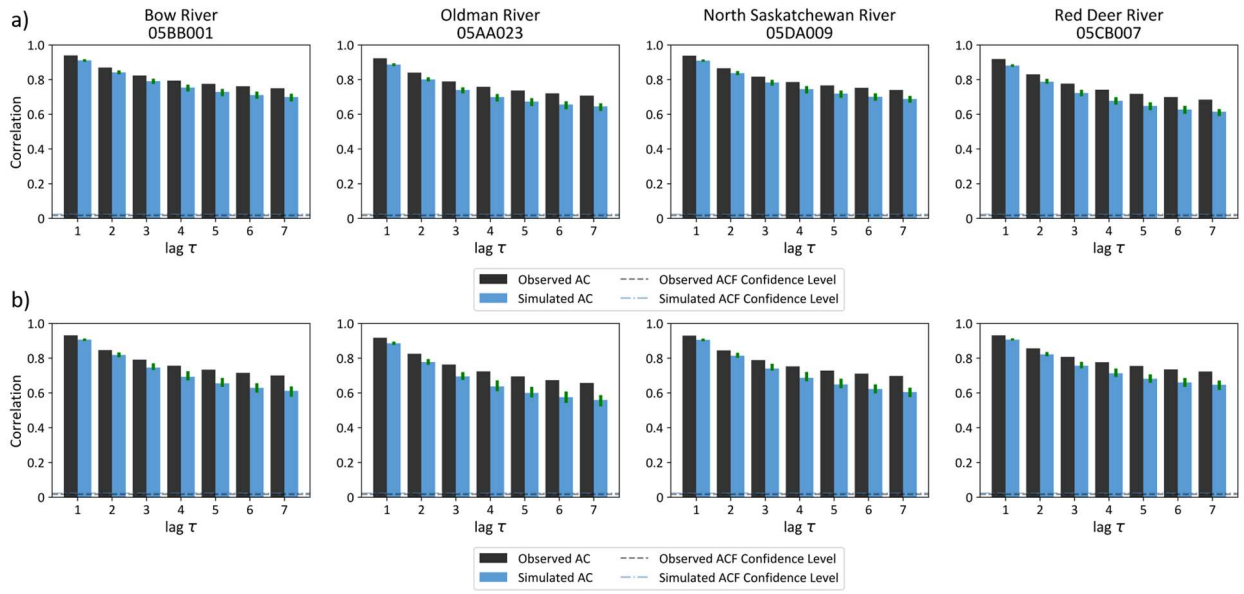

Figure 5.13. Correlograms of the observed versus generated: a) maximum and b) minimum temperature for 1- to 7-day time lags. Black bars indicate the observed ACFs, while the blue bars indicate the mean ACF of the 40 generated time-series with their range shown using a green bar on the top. The time resolution of the observed and generated time-series is daily.

5.2.1.2.2 Spatial Correlation Structure

The spatial dependence structure is evaluated for all weather sites of the study using the produced 40 sample realizations. Figure 5.14 shows the spatial correlation structure of daily precipitation amounts and occurrence between all sites and Figure 5.15 and 16 breaks down the spatial correlations structure into monthly and seasonal time scales. A variety of cross-correlation values are observed from nearly 0 (weak correlation) up to close to 1.0 (strong correlation). The data points around the 45° line are less dispersed compared to the precipitation occurrences values. And finally, a strong cross-correlation is seen between the temperature values of all sites that is perfectly preserved by the weather generator (Figure 5.17). The cross-correlation values range from 0.9 to 1.0 indicating the homogeneity of temperature across the headwater catchments of the SaskRB.

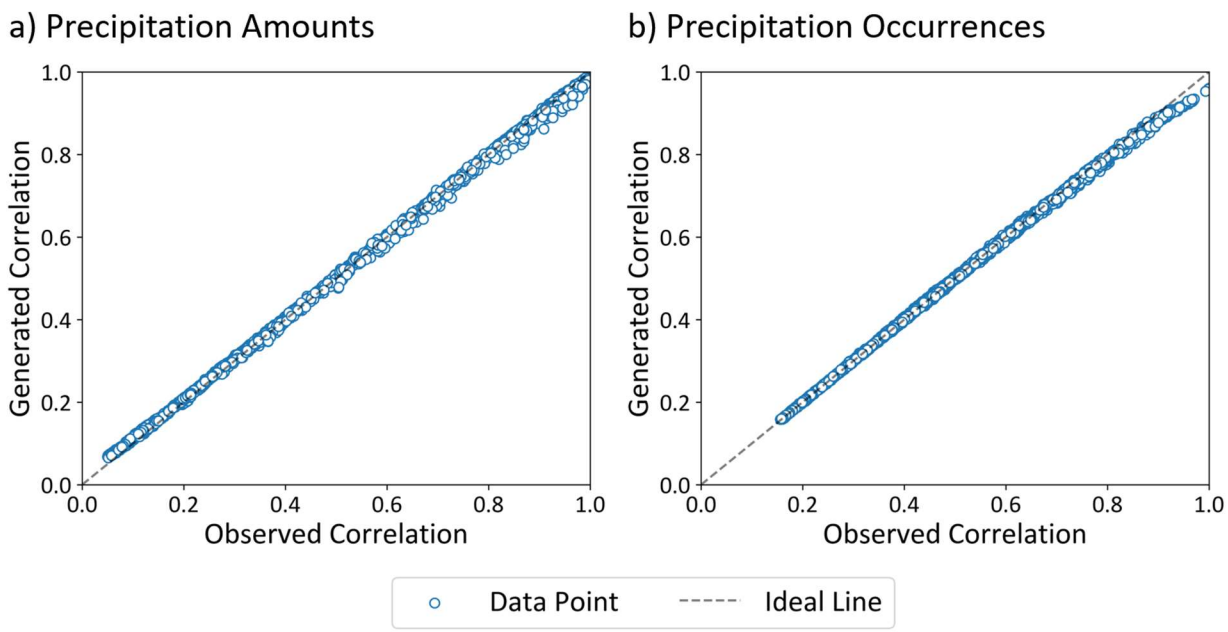

Figure 5.14. The scatter plot of the observed versus generated cross-correlation values of daily precipitation a) amounts and b) occurrences for all possible unique pairs of weather sites reported over the entire time-series of both the generated and observed precipitation values.

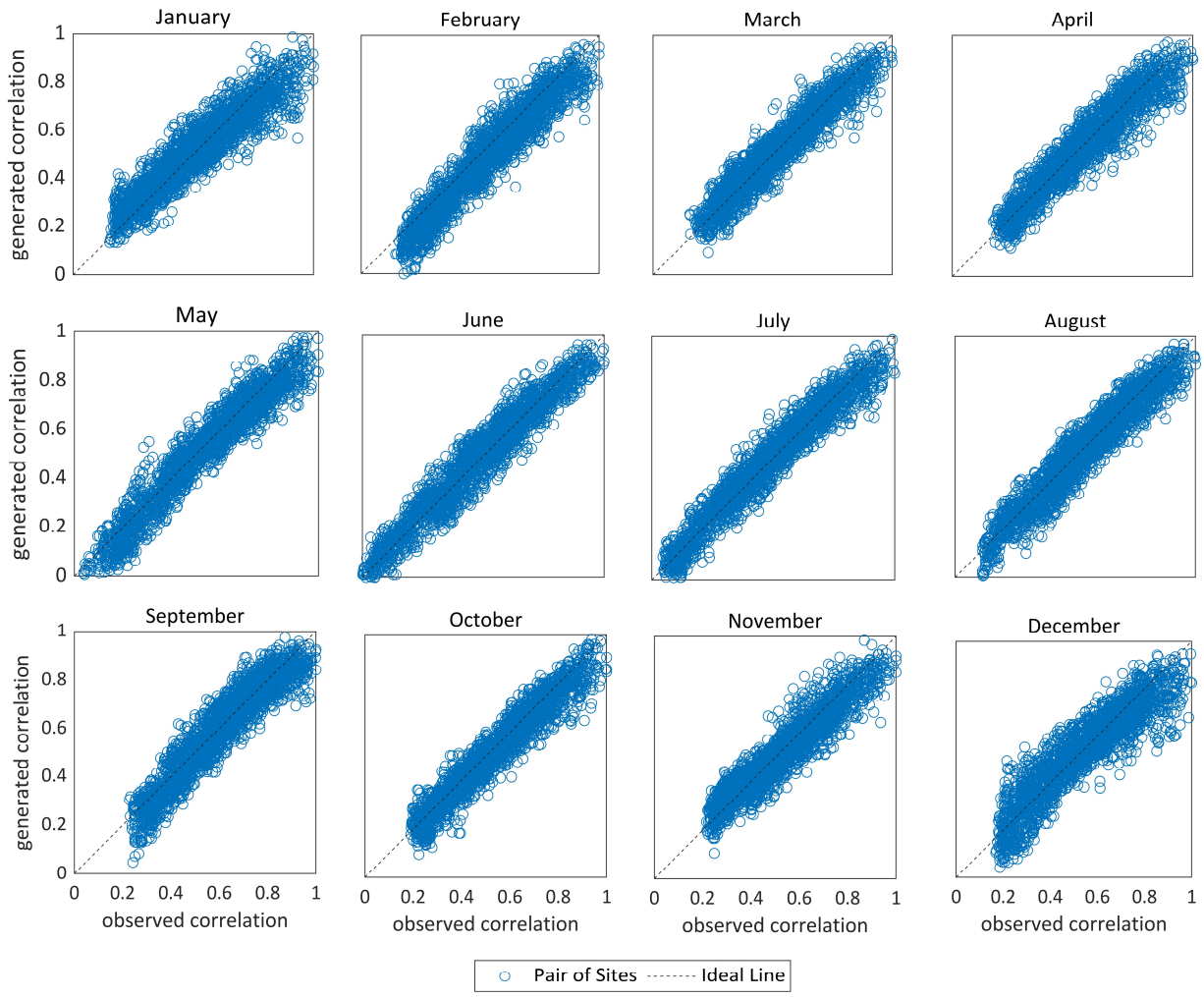

Figure 5.15. The scatter plot of the observed versus generated cross-correlation values of daily precipitation occurrences for all possible unique pairs of weather sites reported for each month of the year.

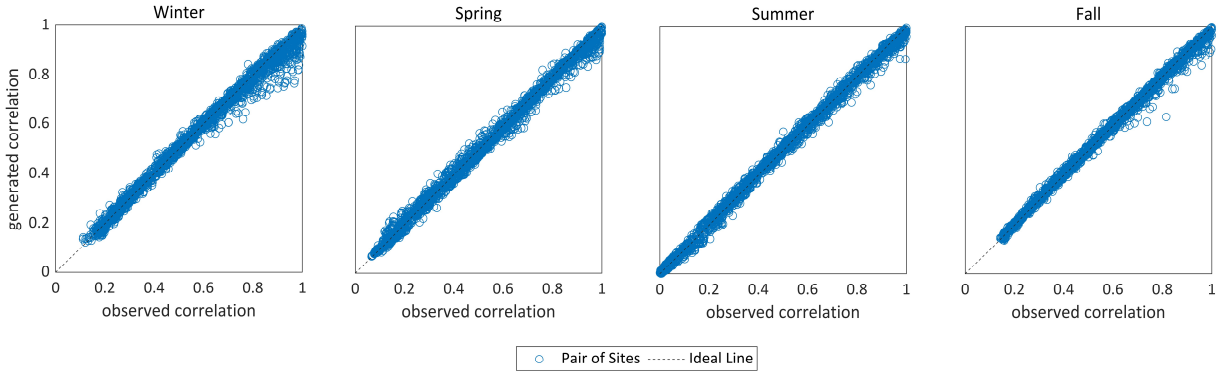

Figure 5.16. The scatter plot of the observed versus generated cross-correlation values of daily precipitation amounts for all possible unique pairs of weather sites reported for each season of the year.

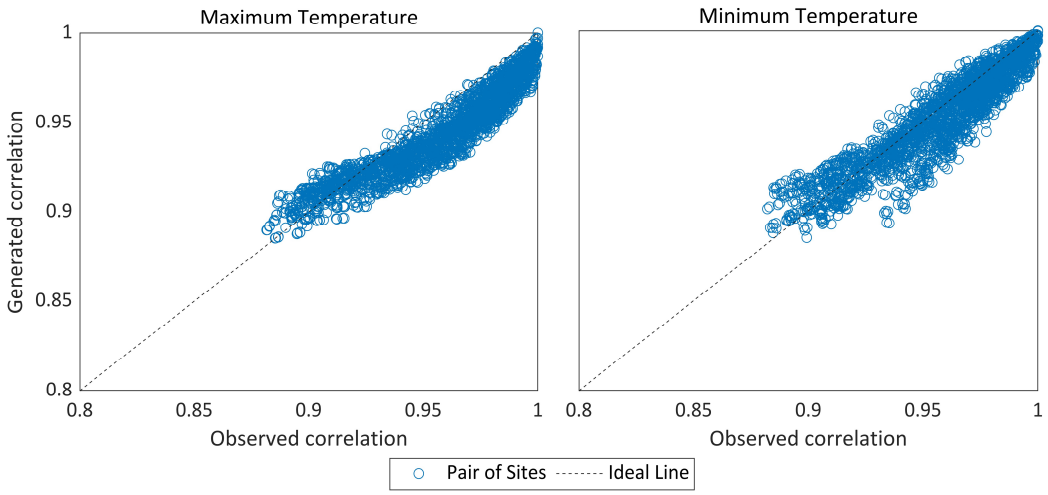

Figure 5.17. The scatter plot of the observed versus generated cross-correlation values of the daily maximum and minimum temperature variables for all possible unique pairs of weather sites.

5.2.1.3 Seasonal Extremes

The 40 sample scenarios are again employed to assess the performance of the WG in reproducing seasonal extremes. The 95th and 99th quantiles of the generated versus observed values of the precipitation amounts and maximum temperature for each season of the year are reported in Figure 5.18 and Figure 5.19. It could be viewed that the seasonal precipitation extremes are mostly reproduced in the four sites since the box-and-whiskers mostly envelop the observed data point. However, some deviations are observable in the spring and fall seasons of both quantiles calculated over the Red Deer River site, and also the 99th quantile over the fall season in the Oldman River catchment.

In terms of maximum temperature, the deviations are more significant in most seasons over all sites, where the climate variable is overestimated by the weather generator. Nonetheless, in Figure 5.20, where the 1st and 5th quantiles of the minimum temperature are reported, the observed seasonal extremes of the variable are well-captured by the weather generator.

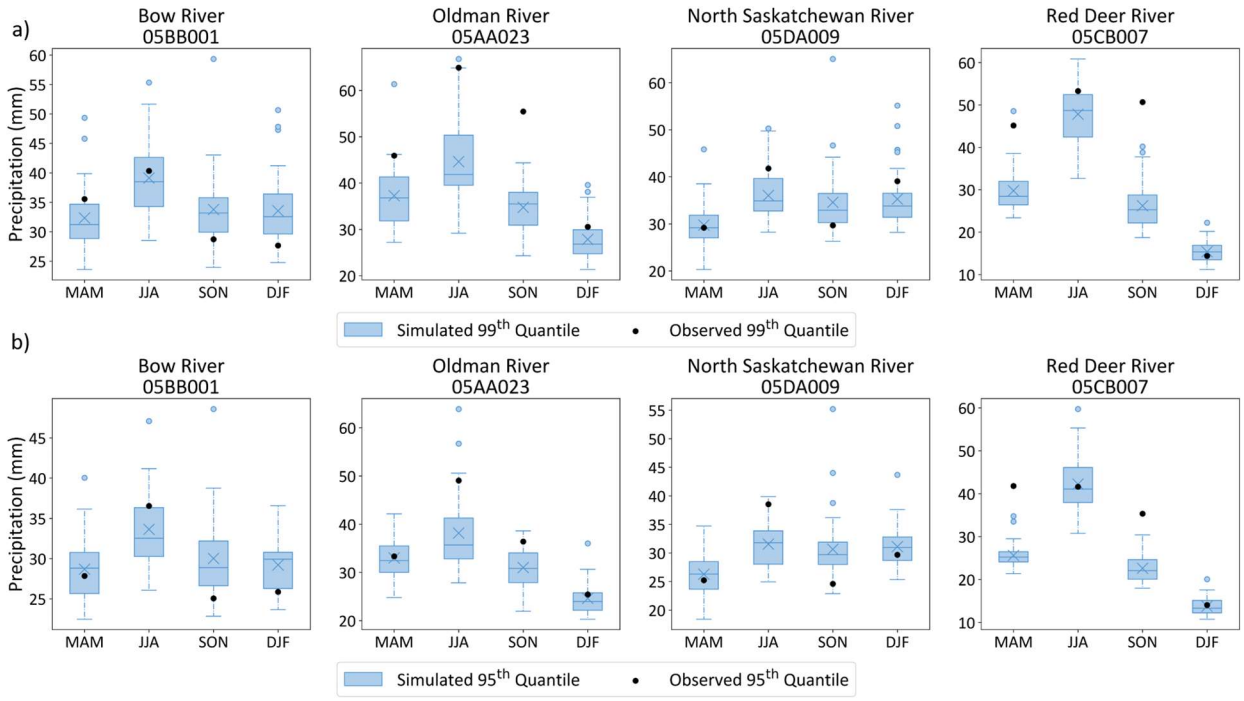

Figure 5.18. The a) 99th and b) 95th quantiles of the observed versus generated daily precipitation quantiles for the four selected sites indicating seasonal extremes. Each box-and-whisker indicates the distribution of seasonal extremes of the 20-year scenarios for the site of interest. Within each box, the horizontal line and cross correspond to the median and mean of the 20-year scenarios' extremes, respectively.

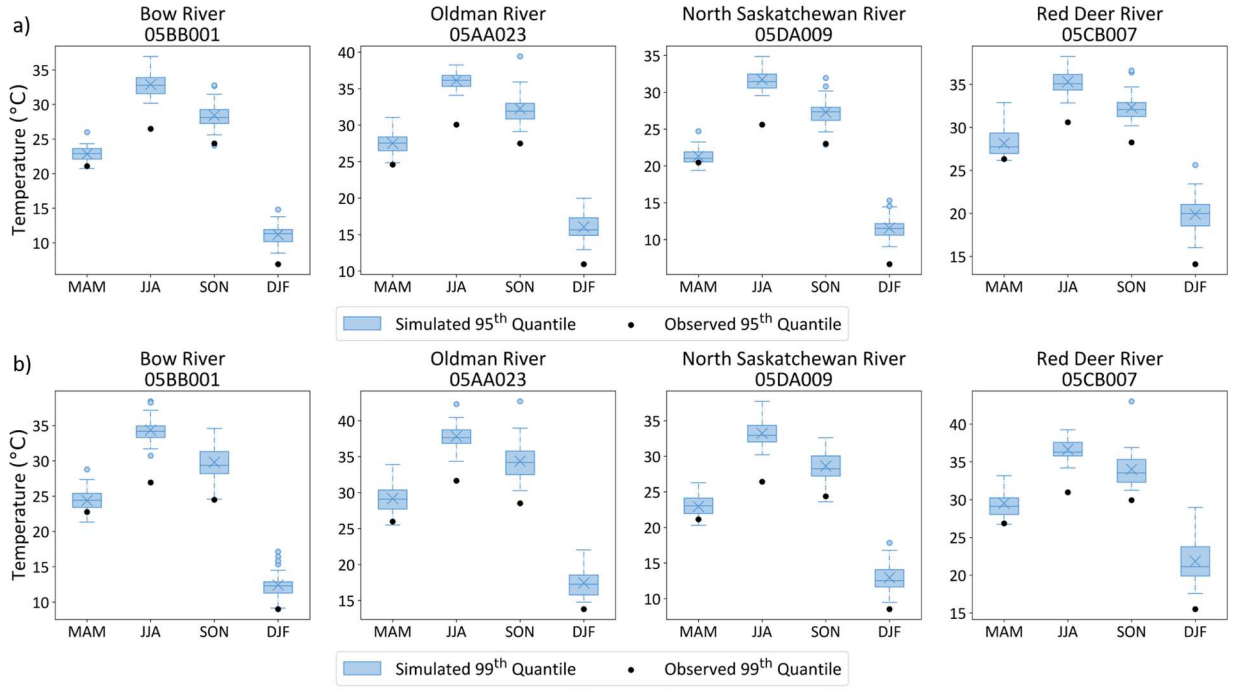

Figure 5.19. The a) 95th and b) 99th quantiles of the observed versus generated daily maximum temperature quantiles for the four selected sites indicating seasonal extremes. Each box-and-whisker indicates the distribution of seasonal extremes of the 20-year scenarios for the site of interest. Within each box, the horizontal line and cross correspond to the median and mean of the 20-year scenarios' extremes, respectively.

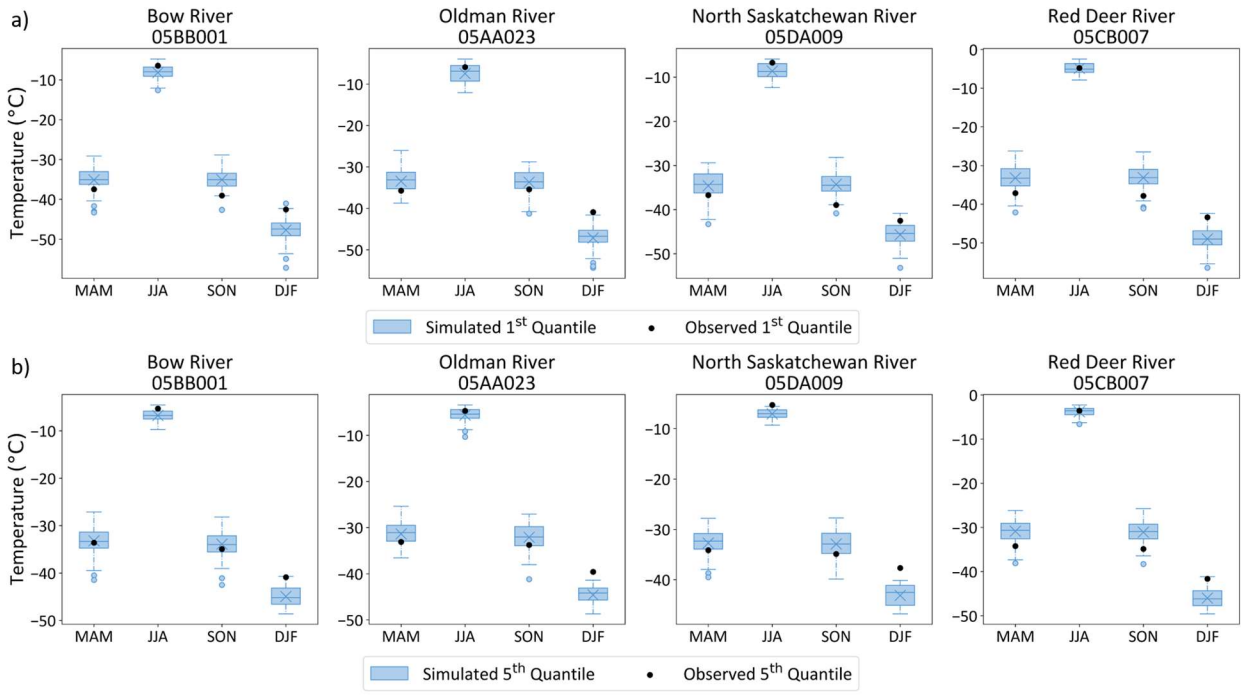

Figure 5.20. The a) 1st and b) 5th quantiles of the observed versus generated daily minimum temperature for the four selected sites indicating seasonal extremes. Each box-and-whisker indicates the distribution of seasonal extremes of the 20-year scenarios for the site of interest. Within each box, the horizontal line and cross correspond to the median and mean of the 20-year scenarios' extremes, respectively.

5.2.2 Transition Probability Bias-correction

As mentioned in Section 4.2.2, the parameters of the weather generator controlling the precipitation occurrences were modified to mirror perturbations in the number of dry days. In doing so, first, the transition probabilities of the weather generator are fitted to 4 different RCM products for the baseline period, i.e., 1980–2013, to understand the biases associated with the precipitation occurrences of each. The biases of the RCM products are shown in Figure 5.21, where the transition probabilities fitted to each product — for the baseline period — are compared to that of the observational ANUSPLIN dataset. As shown in Figure 5.21a, for the P_{00} parameter, both RCM products show negligible biases for almost all months, except for the summer months when both CanRCM4 products suggest major negative biases. For the P_{10} parameter (Figure 5.21b), both RCM products show positive biases for the entire year, except for the summer months during which CRCM5 products indicate significant negative bias.

As described in Section 4.2.3, the biases are corrected using a simple delta factor. The bias-corrected values of the transition probabilities projected by each RCM product for the horizon of 2080–2099 are shown in Figure 5.22 and compared to the baseline period values. Looking at the P_{00} probability (Figure 5.22a), CanRCM4 products generally propose lower probabilities year-round compared to the baseline period conditions, especially in spring (MAM, months of March, April, and May) and fall (SON, months of September, October, and November) seasons. On the other hand, CRCM5 products demonstrate almost identical probabilities to that of the baseline period, with the exception of the CRCM5 RCP8.5 product for July and September with marginally higher and the month of May with lower probabilities.

Moving to the bias-corrected P_{10} probability results (Figure 5.22b), all RCM products indicate

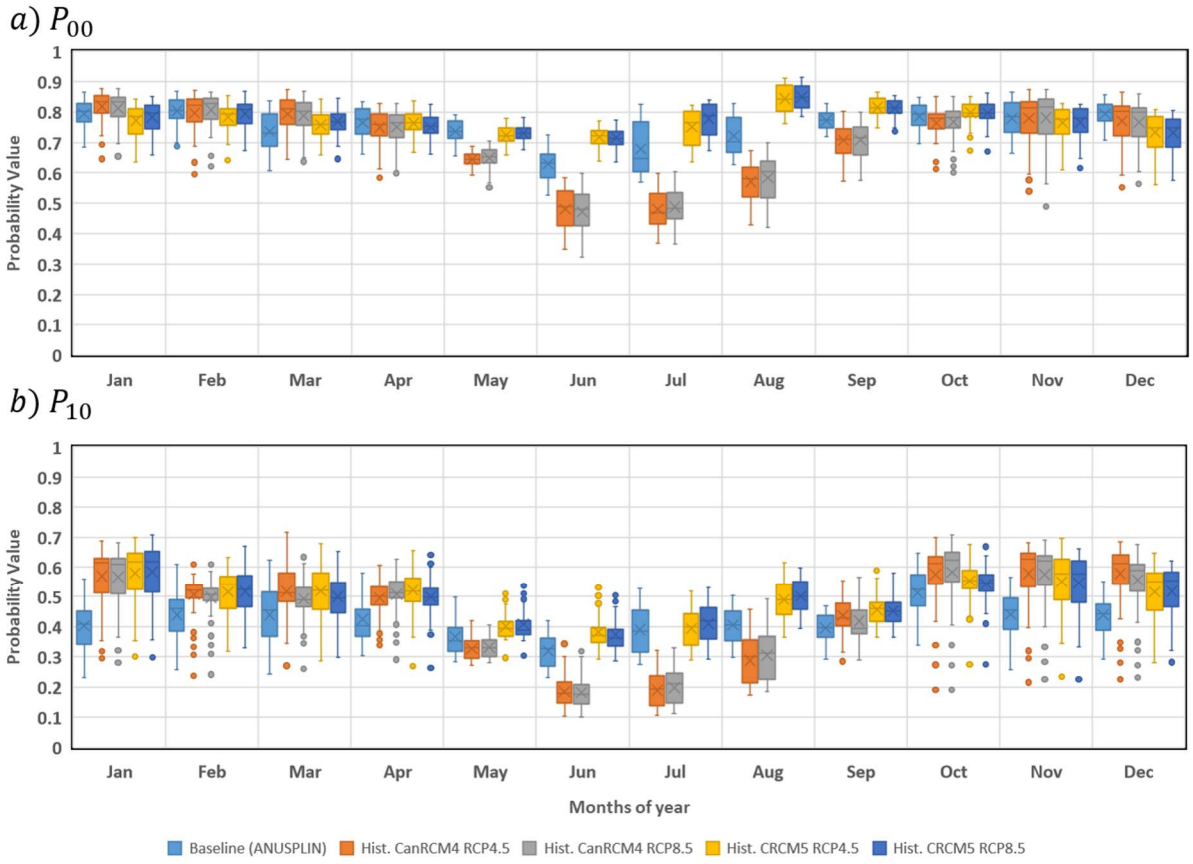

Figure 5.21. The baseline values of the fitted transition probabilities – a) P_{00} and b) P_{10} – of the weather generator. The transition probabilities are fitted to the daily precipitation data of the baseline period – 1980 to 2013 – for the ANUSPLIN dataset (i.e., observations) and 4 other RCM products: 1) CanRCM4 RCP4.5, 2) CanRCM4 RCP8.5, 3) CRCM5 RCP4.5, and 4) CRCM5 RCP8.5. Each box-and-whisker indicates the values of the corresponding transition probability for the 70 headwater catchments of the case study. Within each box, the horizontal line and cross indicates the median and mean of 70 site values, respectively.

similar values for the months of November till March. Moreover, all RCM products show lower values in April and May, while for the other months, they do not follow any regular pattern.

The bias-corrected transition probabilities are employed to create 1,960 weather scenarios across the SaskRB headwaters using the weather generator. The overall result of this parameter manipulation is interpreted in Figure 5.23, where the yearly average number of dry days of all the generated scenarios is demonstrated. It could be interpreted that, the CanRCM4-derived scenarios project a lower number of dry days compared to the baseline period scenarios. Moreover, the CanRCM4 RCP8.5-derived scenarios suggest more frequent wet days than that of the RCP4.5 ones. On the other hand, the CRCM5-derived scenarios suggest similar properties to the baseline period. Also, the majority of the generated scenarios in this study have an average of 225 to 230 dry days per year.

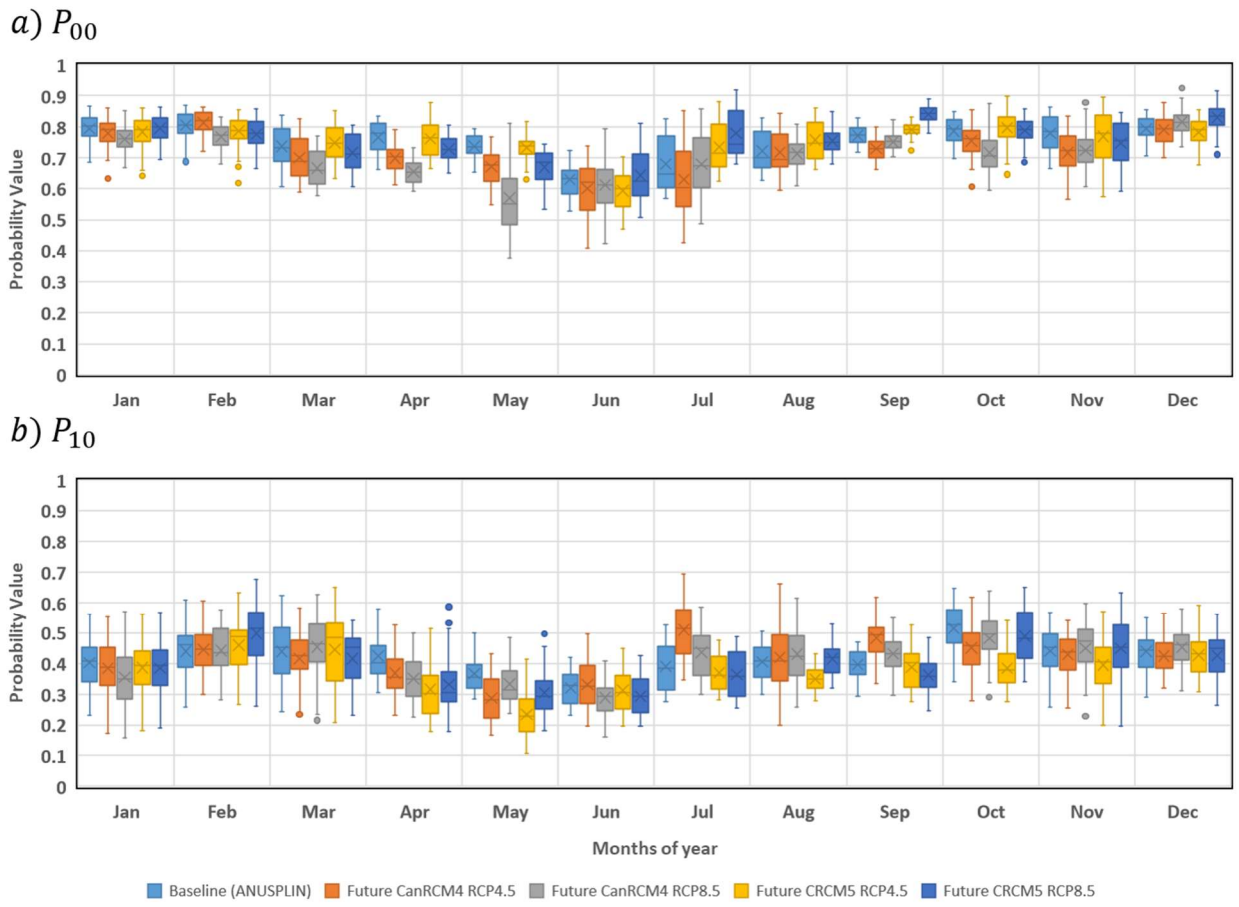

Figure 5.22. The bias-corrected values of the fitted transition probabilities – a) P_{00} and b) P_{10} – of the weather generator. The transition probabilities are fitted to the daily precipitation data of the baseline period – 1980 to 2013 – for the ANUSPLIN dataset (i.e., observations) and the 2080-2099 horizon of 4 other RCM products: 1) CanRCM4 RCP4.5, 2) CanRCM4 RCP8.5, 3) CRCM5 RCP4.5, and 4) CRCM5 RCP8.5. Each box-and-whisker indicates the values of the corresponding transition probability for the 70 headwater catchments of the case study. Within each box, the horizontal line and cross indicates the median and mean, respectively.

5.2.3 Produced Climate Change Exposure Space

After the preliminary generation of the weather scenarios, the post-processing perturbations of precipitation and temperature values are maintained (see Section 4.2.2). Figure 5.24 shows the overall results of the scenario generation process. In the figure, each lower-triangular box represents perturbations in terms of two climate attributes (mapped from the diagonal boxes) and their axes indicate perturbation bounds. Also, each box contains 1,960 dots representing the produced weather scenarios. The top lower-triangular box indicating perturbed P_{JJA} and P_{DJF}

attributes depicts the cloud of scenarios with low density. As mentioned earlier in Section 4.2.2, due to the inherent stochasticity of the weather generator, the produced exposure space is slightly different from the original one. The middle row lower-triangular boxes display perturbed attributes of precipitation and temperature values. Seven discrete clusters within each box are visible which

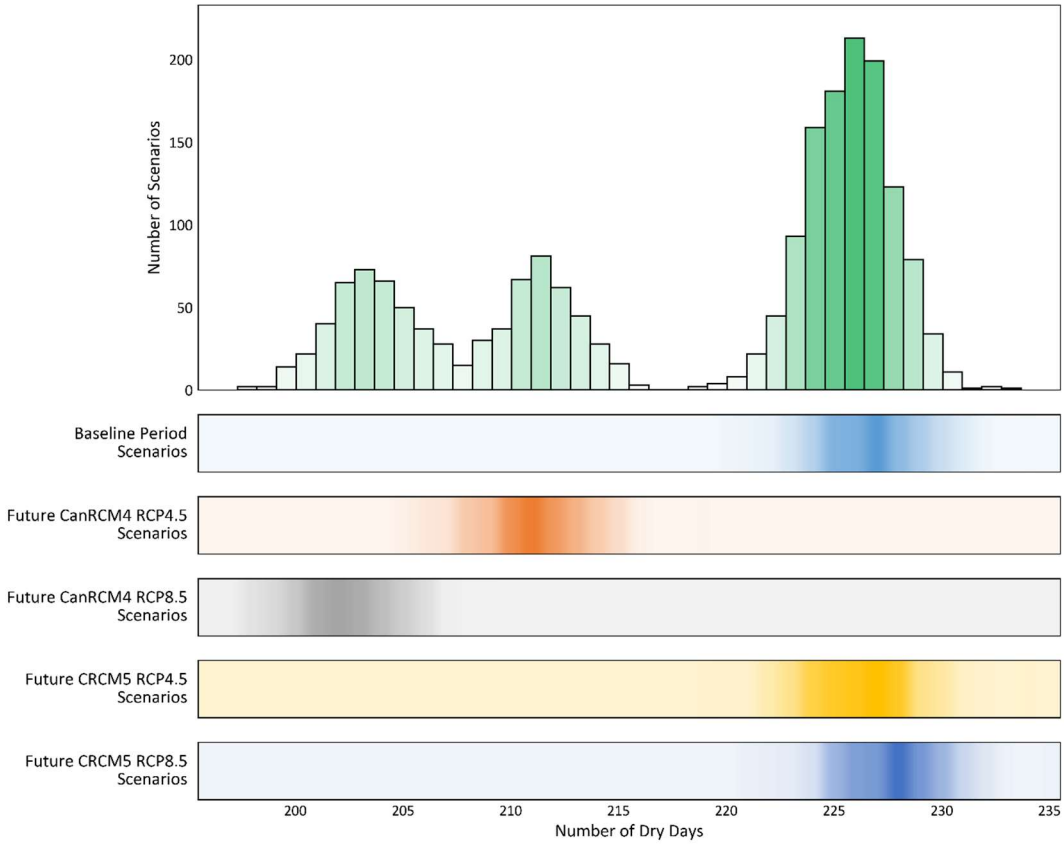

Figure 5.23. The overall result of the dry day perturbations; the top plot indicates the distribution of the generated scenarios in terms of their yearly average of the number of dry days. The five bottom rug plots indicate how each set of bias-corrected transition probabilities fitted to each RCM products, have resulted in scenarios over the spectrum of the plausible number of dry days. The weather generation derived by CanRCM4 transition probabilities results in scenarios with a yearly average of 200 – 215 dry days. Whereas the condition for that of the CRCM5 products is close to the baseline period properties. The darker the colour, the denser population of scenarios in the spectrum of the plausible number of dry days.

is the direct result of the low stochasticity of the weather generator in producing temperature values. Finally, the bottom boxes show changes in N_{dry} and the rest of the chosen attributes.

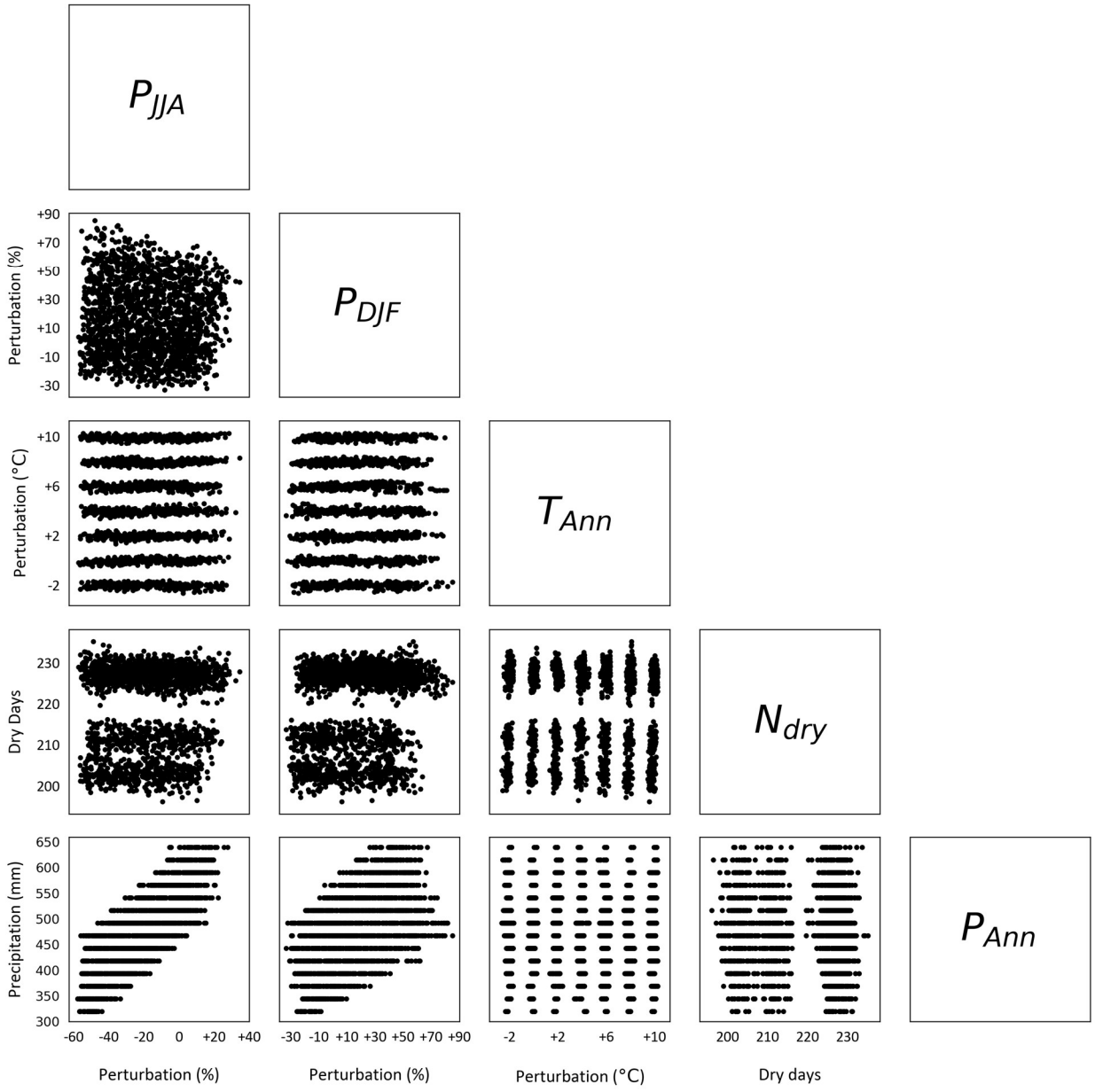

Figure 5.24. The climate change exposure space consisting of four climate attributes (see Section 4.2.2). Each box demonstrates perturbations in terms of two attributes for the 1,960 generated scenarios. In addition to the four climate attributes, the annual average precipitation amounts (P_{Ann}) are also shown, highlighting the importance of N_{dry} attribute and the intensity of precipitation in scenarios with equal annual average precipitation.

5.3 Hydrological Modelling

5.3.1 Calibration and Validation

As mentioned in Section 4.3, the generated weather scenarios are translated into flow using the HBV-SASK hydrological model. This model is calibrated and validated for each catchment based on the observed daily flow at the outlet of each site for the duration of the baseline period, i.e., 1980 to 2013. The results of the calibration and validation for the SaskRB headwater catchments are illustrated in Figure 5.25. Each catchment is calibrated independently; the numerical values of the calibrated parameters of the model are detailed in Appendix A. The hyeto- and hydrographs of the calibrated HBV-SASK output for the four selected catchments (see Section 5.2) are depicted in Figure 5.26 to Figure 5.29.

As could be viewed in Figure 5.25, the model for ~60% of the catchments attained an NSE of 0.7 or greater in both calibration and validation, which is typically considered a good performance in the hydrologic modelling context. For ~20% of the catchments, the model attained an NSE in the range of 0.5 to 0.7, which is typically considered acceptable. For the remaining catchments, the NSE was lower than 0.5, which is an indication of the model's poor skills in reproducing observations. Further examination of the model and data for these catchments indicates a lack of confidence in the available data in some small headwater tributaries and improving the fit to observations might result in possible over-fitting errors in data.

Moreover, this research investigated the volume bias in modelling results, which has significant implications for water supply studies. According to Figure 5.25b, the model shows very good $BIAS$ values for ~90% of the catchments (i.e., within ±10% tolerance) in calibration. In the validation, however, the model demonstrates a bias in that range in only ~50% of the catchments, and in a few of the catchments, the bias is unacceptably large in the validation. To address this issue for the purpose of this water supply vulnerability study, a simple remedy for bias correction based on using multipliers was adopted. For each basin, a multiplier is applied to the whole output flow time-series of the model to compensate for the biases of simulated flow. The black line in Figure 5.25b shows the corrected $BIAS$ values after using the multipliers.

One important remark is the performance of the calibrated HBV-SASK model for the 05DA009 catchment (Figure 5.28). The suggested TT parameter from the calibration experiment

($TT = 2.83$) caused the SWE component to behave abnormally (for a list of parameters see Table 4.3). By setting the TT parameter to zero, as an experiment, the SWE behaved as expected (shown with the dashed line in the bottom panel.) By this correction, the NSE value has been lowered to 0.53 (from 0.8), but the $|BIAS|$ remained almost unchanged.

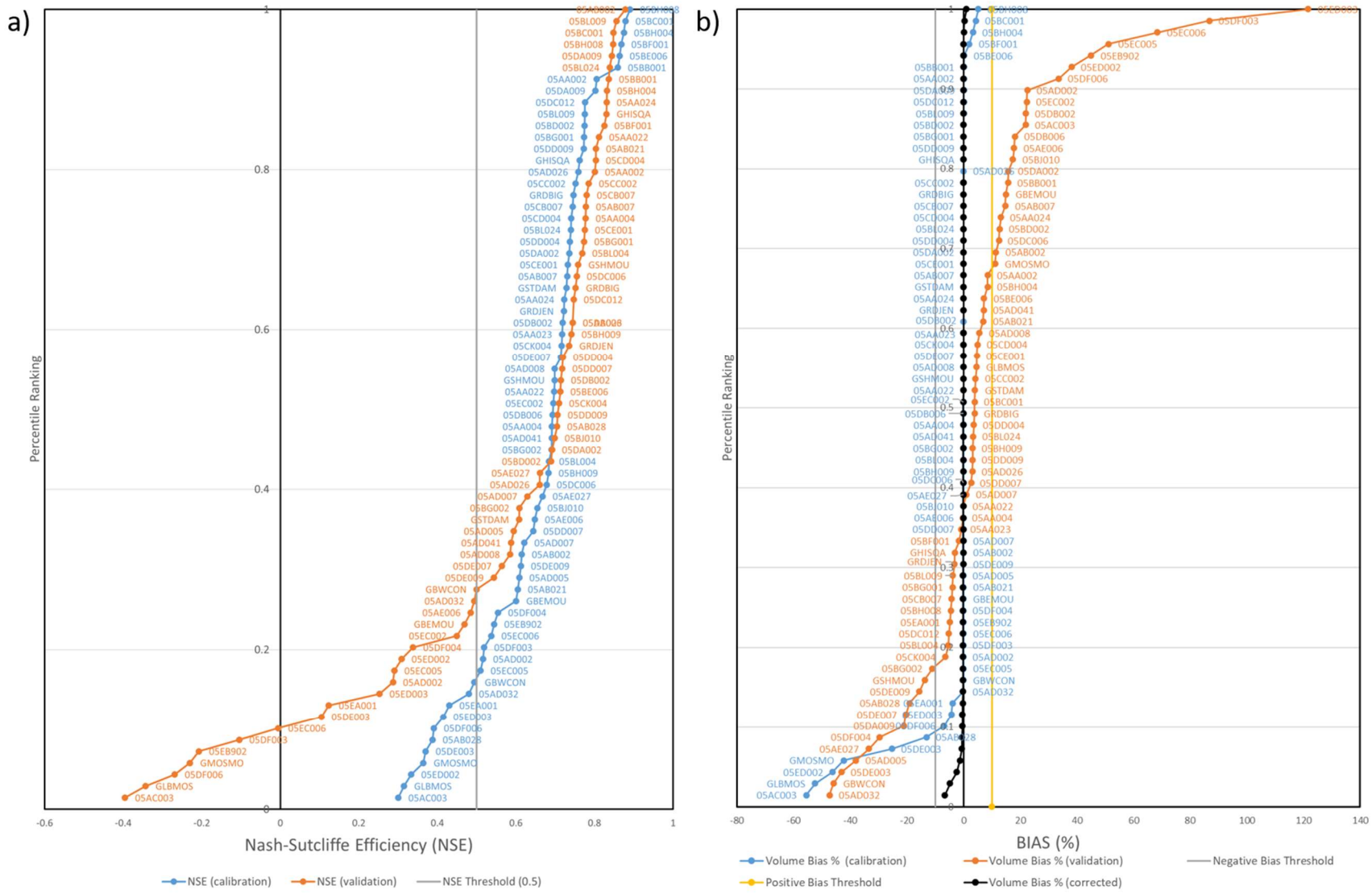

Figure 5.25. The results of the a) NSE, and b) $|BIAS|$ objective function for the calibration and validation experiments of the HBV-SASK model applied to the SaskRB headwater catchments.

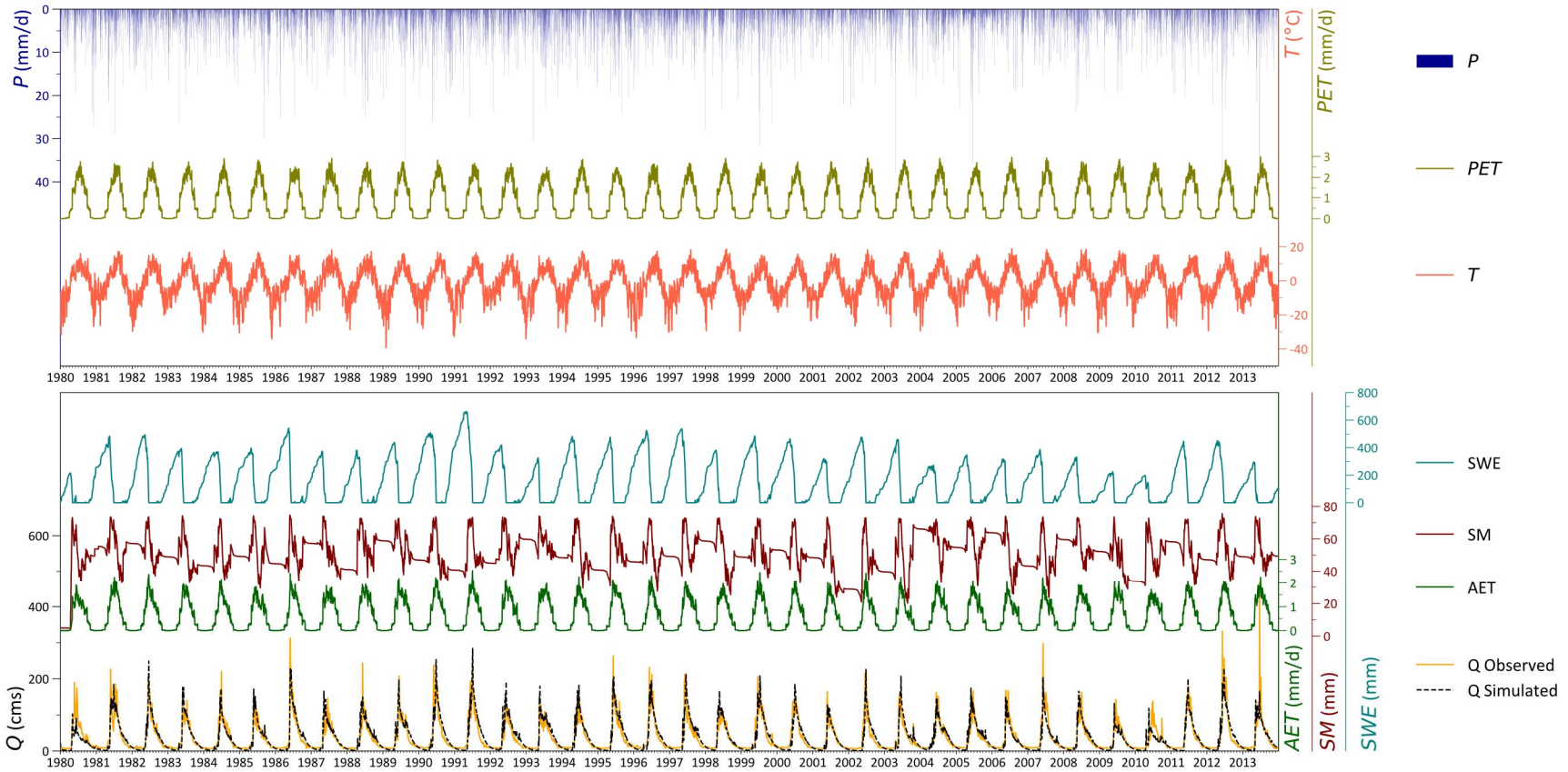

Figure 5.26. The daily hyeto- and hydrograph of the Bow River (at Banff, 05BB001) catchment from 1980 to the end of 2013. The top panel shows the amounts of observed mean daily precipitation (P), temperature (T) and computed Hamon's PET (see Section 4.2.4). The bottom panel shows the observed flow ($Q\ Observed$), as well as the calibrated flow ($Q\ Simulated$). The time-series of the simulated snow water equivalent (SWE), soil moisture (SM), and actual evapotranspiration (AET) components of the model are demonstrated, too. The styling of the graph is adopted from Széles et al. (2020). (The format of the figure is vector-based; in case of software incompatibility, the author should be contacted.)

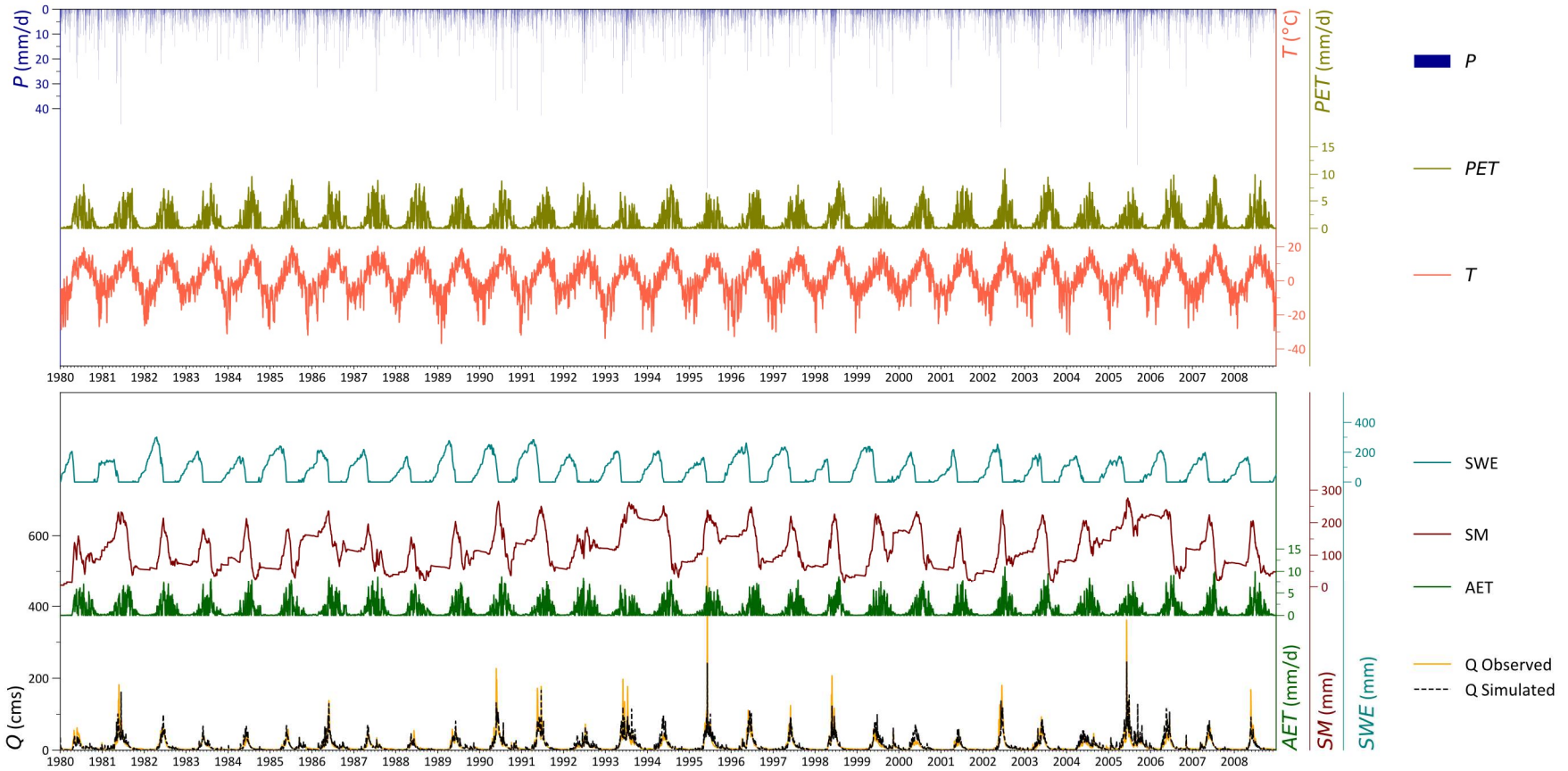

Figure 5.27. The daily hyeto- and hydrograph of the Oldman River (near Waldron's Corner, 05AA023) catchment from 1980 to the end of 2013. The top panel shows the amounts of observed mean daily precipitation (P), temperature (T) and computed Hamon's PET (see Section 4.2.4). The bottom panel shows the observed flow ($Q\ Observed$), as well as the calibrated flow ($Q\ Simulated$). The time-series of the simulated snow water equivalent (SWE), soil moisture (SM), and actual evapotranspiration (AET) components of the model are demonstrated, too. The styling of the graph is adopted from Széles et al. (2020). (The format of the figure is vector-based; in case of software incompatibility, the author should be contacted.)

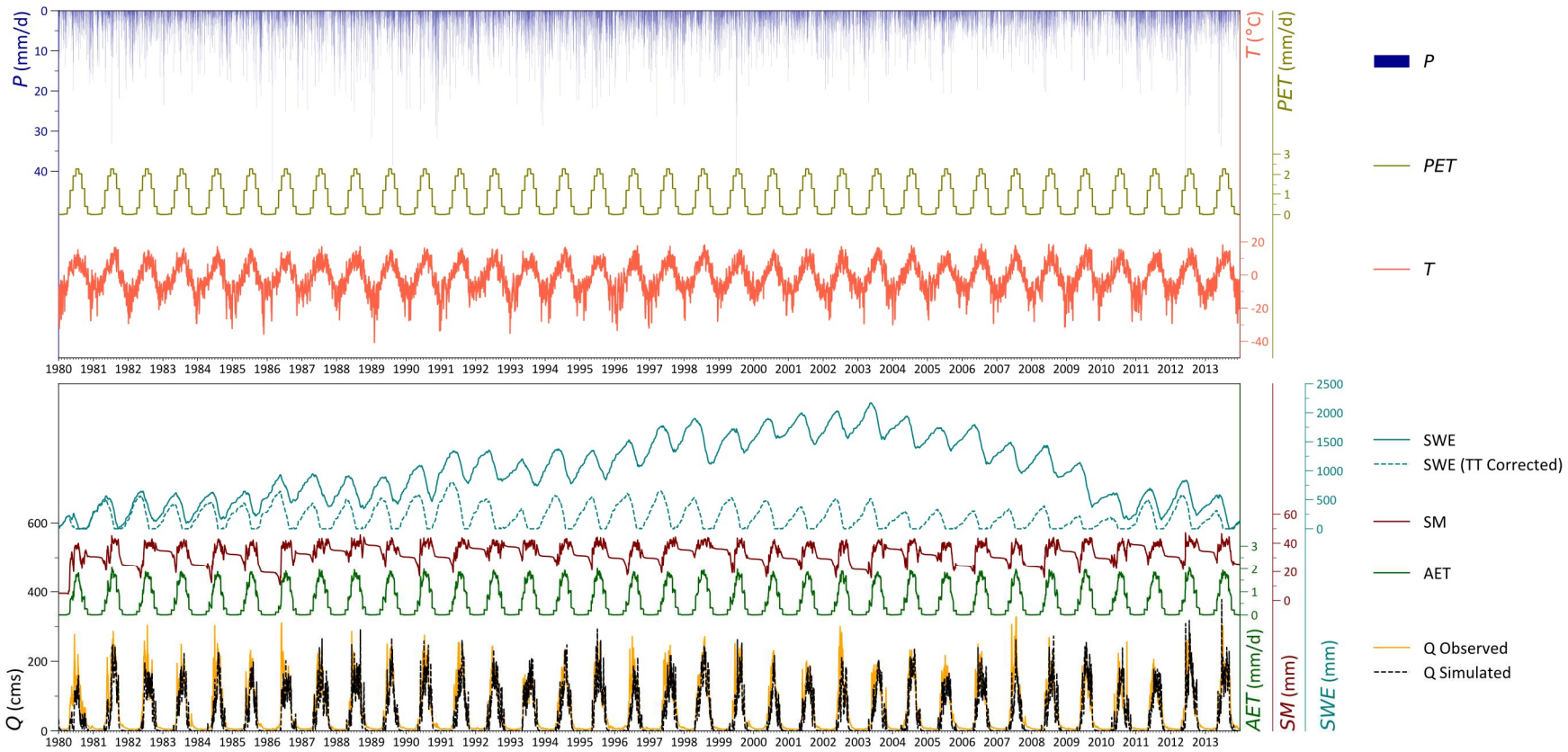

Figure 5.28. The daily hyeto- and hydrograph of the North Saskatchewan River (at Whirlpool Point, 05DA009) catchment from 1980 to the end of 2013. The top panel shows the amounts of observed mean daily precipitation (P), temperature (T) and computed Hamon's PET (see Section 4.2.4). The bottom panel shows the observed flow ($Q\ Observed$), as well as the calibrated flow ($Q\ Simulated$). The time-series of the simulated snow water equivalent (SWE), soil moisture (SM), and actual evapotranspiration (AET) components of the model are demonstrated, too. The suggested TT parameter from the calibration experiment ($TT = 2.83$) caused the SWE component to behave abnormally. By setting the TT parameter to zero, the SWE behaves as expected (shown with dashed line in the bottom panel.) The corresponding simulated streamflow is not shown. By this correction, the NSE value has been lowered to 0.53 (from 0.8), but the $|BIAS|$ remained unchanged. The styling of the graph is adopted from Széles et al. (2020). (The format of the figure is vector-based; in case of software incompatibility, the author should be contacted.)

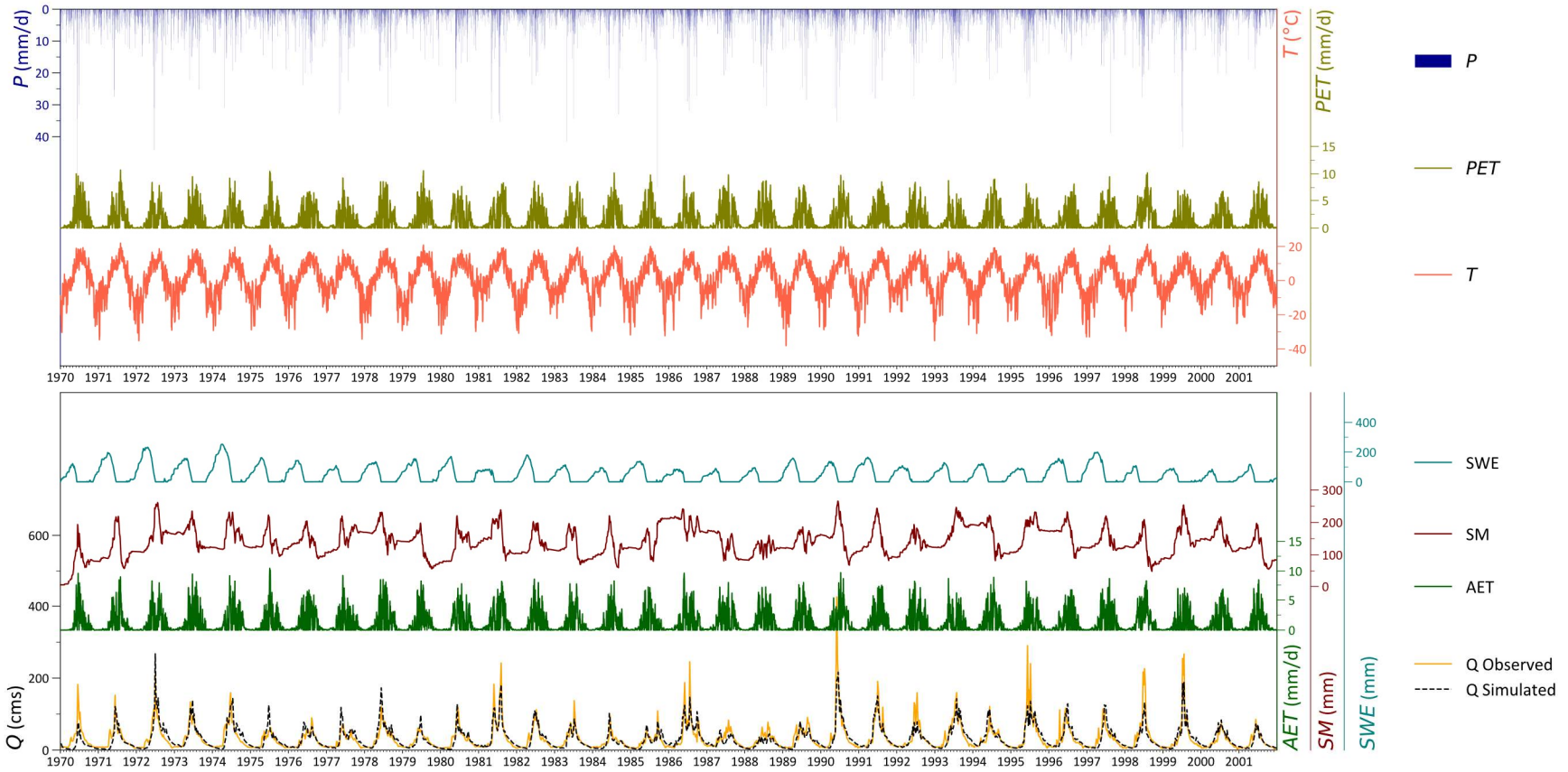

Figure 5.29. The daily hyeto- and hydrograph of the Red Deer River (Dickson Dam Tunnel Outlet, 05CB007) catchment from 1980 to the end of 2013. The top panel shows the amounts of observed mean daily precipitation (P), temperature (T) and computed Hamon's PET (see Section 4.2.4). The bottom panel shows the observed flow ($Q\ Observed$), as well as the calibrated flow ($Q\ Simulated$). The time-series of the simulated snow water equivalent (SWE), soil moisture (SM), and actual evapotranspiration (AET) components of the model are demonstrated, too. The styling of the graph is adopted from Széles et al. (2020). (The format of the figure is vector-based; in case of software incompatibility, the author should be contacted.)

5.3.2 Multi-objective Trade-off Analysis

To further examine the calibration quality described in Section 5.3.1, the trade-offs between the NSE and $|BIAS|$ are analyzed for those catchments for which the fitted HBV-SASK model shows poor performance. In doing so, the Pareto Archived Dynamically Dimensioned Search (PA-DDS, Asadzadeh et al. (2013)) was employed to derive the Pareto Front of optimal solutions. This algorithm is the multi-objective version of the DDS method that was used in the calibration process of the HBV-SASK model. Figure 5.30 shows the trade-off between the two measures for those catchments. It could be seen that the members of the Front do not significantly show an improvement in NSE at the expense of increasing $|BIAS|$ values. Similarly, Figure 5.31 demonstrates the trade-offs for calibration experiments with poor $|BIAS|$ measures.

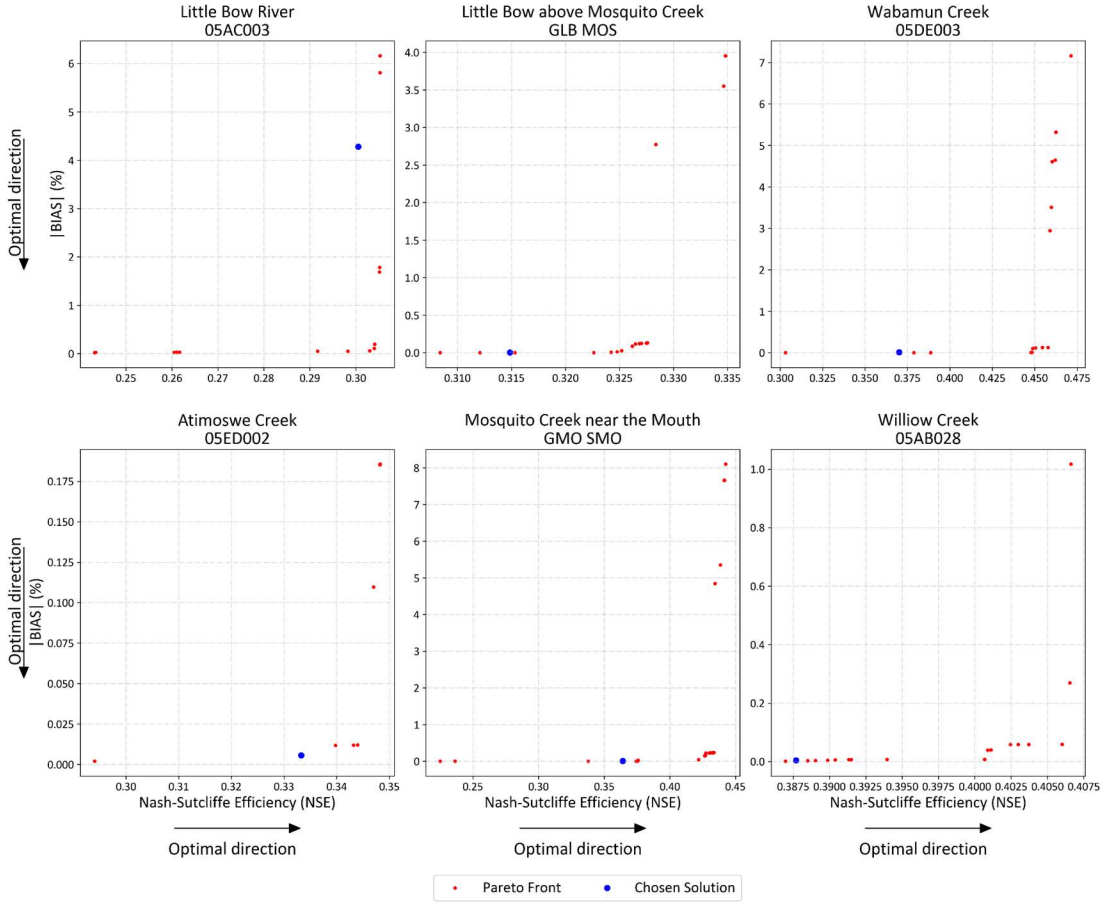

Figure 5.30. The trade-off between NSE and $|BIAS|$ for 6 selected catchments, where the calibrated HBV-SASK model shows poor NSE values. The chosen solution is indicated with a blue circle, whereas all other Pareto Front members are shown with a red one.

Likewise, compromising NSE values does not result in remarkable improvements in the other measure.

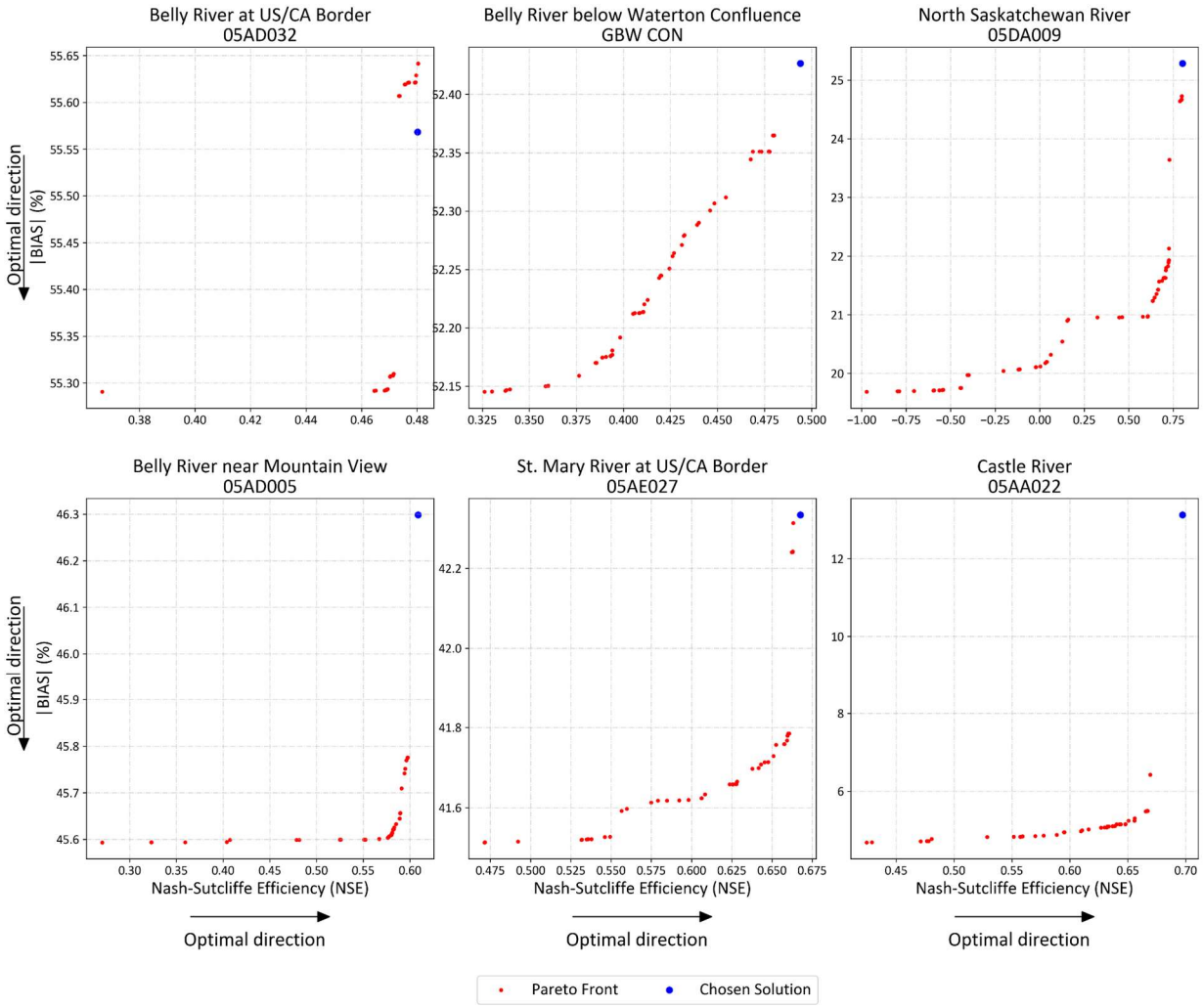

Figure 5.31. The trade-off between NSE and $|BIAS|$ for 6 selected catchments, where the calibrated HBV-SASK model shows poor $|BIAS|$ values. The chosen solution is indicated with a blue circle, whereas all other Pareto Front members are shown with a red one.

To obtain the Pareto Fronts, the PA-DDS algorithm was run 5 times (using a different seed number), each with 2,000 iterations. The figures above show the best Pareto Front attained from the best optimization trial. It should be noted that the chosen solutions were obtained separately by the DDS algorithm and were not chosen from the Pareto Front members, which were produced by multi-objective optimization algorithm. Therefore, the chosen solution might be sub-optimal

compared to the Front members. The overall objective of illustrating the Pareto Front was to examine whether a higher quality calibration result was possible. These results indicate that in the future works, the focus should be on the multi-objective optimization in the first place.

5.3.3 Actual Evapotranspiration (AET) Validation

Figure 5.32 depicts the comparison between the HBV-SASK AET and the MODIS ET estimates for each month over two headwater catchments of this study: 1) Bow River at Banff (outlet gauge of 05BB001) and 2) North Saskatchewan River (NSR) at Whirlpool Point (outlet gauge of 05DA009).

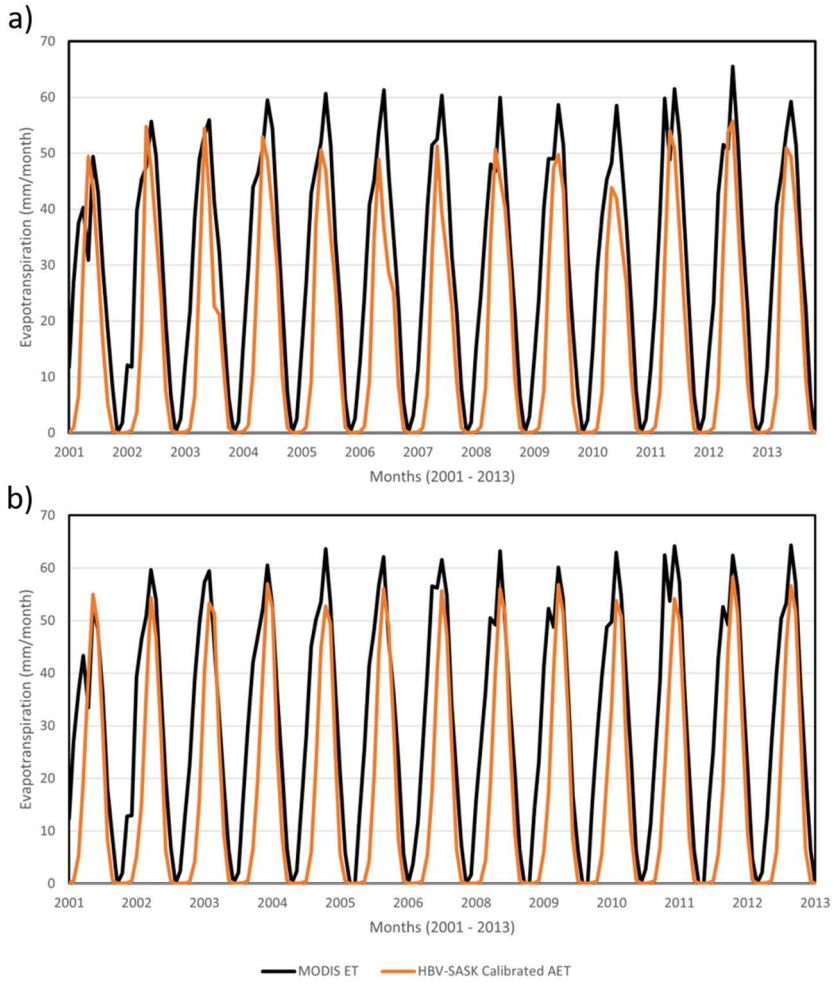

Figure 5.32. Comparison of evapotranspiration for each month from 2001 to 2018 obtained from MODIS and computed by the HBV-SASK model for a) Bow river at Banff (05BB001) and b) North Saskatchewan River (NSR) at Whirlpool Point (05DA009) catchments.

From the figure, it could be viewed that the ET values of the HBV-SASK model and MODIS Terra estimates are not in agreement in their rising limbs. Nevertheless, the results are more comparable in the falling limbs of the ET values. According to MODIS estimates, ET is significant in this region all year round except for the months of December and January, when it approaches zero. In this region, however, the temperature is typically below zero degrees Celsius from November through March, inclusive. HBV-SASK, consistent with other conceptual models, assumes that ET is very small when the temperature is below zero. Therefore, the below-zero temperature in February and March explains the lag in the rising limb generated by HBV-SASK. Further research requires looking at possible in-situ observations (e.g., via flux towers), particularly in light of the fact that MODIS estimates may also be prone to errors and biases.

Moreover, it could be viewed that the HBV-SASK AET values have underestimated the peak values of the MODIS ET estimates. There could be two reasons behind these behaviors. Firstly, the HBV-SASK model, like any other conceptual hydrological model, should be calibrated, during which, for the sake of satisfying the water balance, the model might be forced to underestimate the AET value to compensate for the missing input precipitation values. Secondly, the AET component of the HBV-SASK model is calculated based on the long-term monthly-averaged PET values, that were again calculated using the Hamon's equation relying only on mean daily temperature values. However, "evapotranspiration is a combined process of evaporation of liquid water from various surfaces, transpiration from the leaves of plants and trees, and sublimation from ice and snow surfaces" (Safaei 2018). Therefore, in order to accurately calculate evapotranspiration from different landscapes, many other environmental variables and fluxes should be considered. In contrary to the simplistic estimation of AET in the HBV-SASK model, the MODIS values were computed considering a broad number of factors, such as relative humidity, actual vapor pressure, and incoming solar radiation which can potentially result in more accurate ET estimates. These justifications were also mentioned in Safaei (2018).

It is worth mentioning that, in some HBV variants, a snowfall correction factor is defined to account for the underestimated evaporation from snow accumulations and snow sublimation (e.g., Seibert (1997)). The aforementioned reasons can potentially explain the mismatch between MODIS and HBV-SASK ET estimations in general. Further research is needed to make the AET estimates of the HBV-SASK model more accurate.

5.3.4 Overall Performance Evaluation

The overall performance of the HBV-SASK model is evaluated for the four selected catchments used in Section 5.2.1. In doing so, the flow duration curves (FDCs) are plotted for the observed and calibrated flows of each catchment. Furthermore, the 40 sample scenarios used in this research to verify the applicability of different components of the methodology were fed to the HBV-SASK model for each catchment.

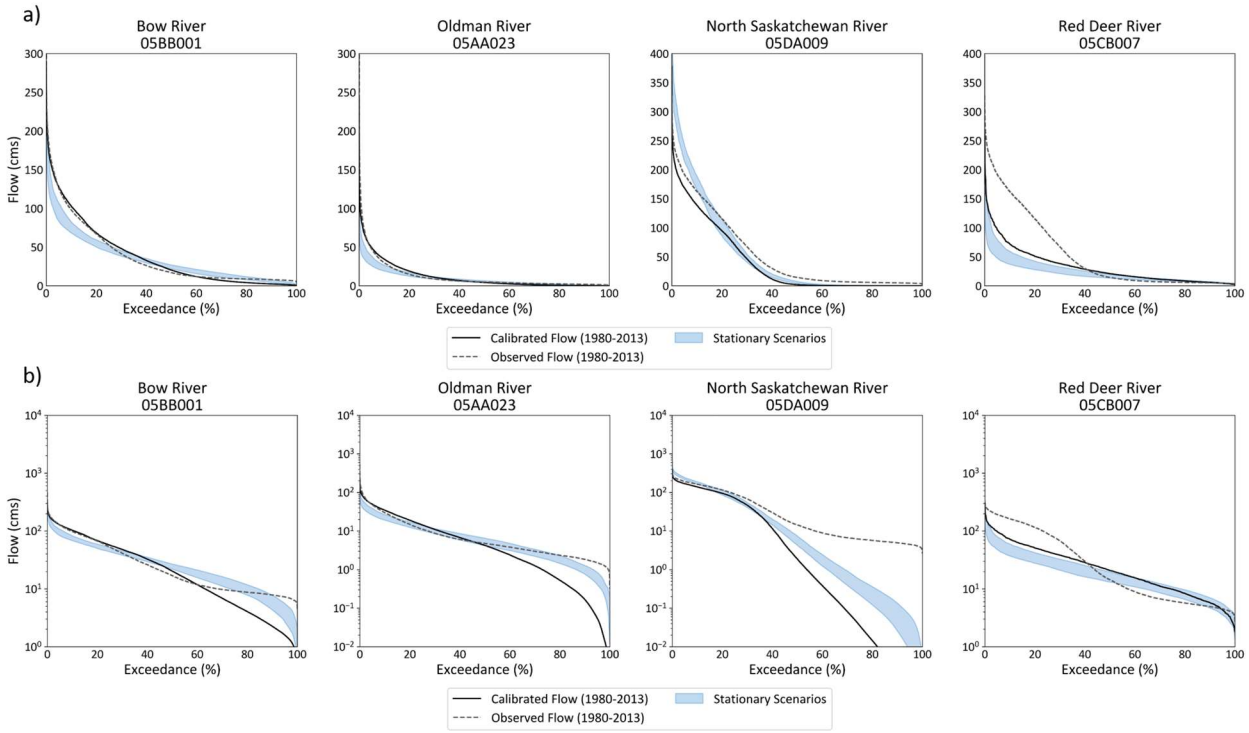

Figure 5.33. Overall assessment of the HBV-SASK model in face of the 40 sample scenarios using FDCs in a) normal and b) logarithmic scales. The blue patch displays the ranges of flows modelled from the sample realizations. It may be noted that for observed flows of the Red Deer River catchment the naturalized values were used as the outlet is located downstream of the Dickson Dam regulating Glennifer Lake (See Section 4.6 for data sources). The other three catchments shown have unregulated flow and the exact daily observations were used. Stationary scenarios refer to the 40 sample scenarios generated for the validation process.

From the figure, it can be viewed that, the blue surface approximately envelops the calibrated flow of the HBV-SASK for each site. However, there is a difference between the calibrated and the observed line which can be traced back to the calibration performance of the HBV-SASK

model. The difference is much more visible for the Red Deer River case where naturalized flow were used to demonstrate the observed values.

5.4 Vulnerability Assessment

5.4.1 Validation of the Water Resources Management Model

To assess the overall performance of the IWMSask model, the sample scenarios used in Sections 5.2 and 5.3 were further employed to simulate the flows at the chosen SaskRB control points (see Figure 4.2). The FDCs of the observed and simulated flows for the baseline period, as well as the FDC range for the sample scenarios, are computed and summarized in Figure 5.34. Looking only at the output of the IWMSask for the baseline period (i.e., simulated flow for 1999–2018), it could be visually interpreted that the model perfectly replicates the observed FDC for the SSR control point, and acceptably reproduces the observed FDCs for the NSR and SR control points. However, the ranges of the sample scenarios underestimate the baseline period flows for the NSR and SR ones. This underestimation could be traced back to the biases and shortcomings of the weather generation and hydrology models detailed earlier in this chapter. This flaw can potentially result in an overestimation of discovered vulnerabilities. It is worth noting that the observed flows for each control point are calculated based on PPWB guidelines detailed in Table 5.2.

Table 5.1. The methods to calculate the observed flow at the three control points of this study.

Number #	River and Control Point	Method of Calculation (based on gauge code)	Reference
1	SSR at the AB-SK border	(05CK004) + (05AJ001)	PPWB (2020a)
2	NSR at the AB-SK border	(05EF001)	PPWB (2020b)
3	SR at the SK-MB border	(05KJ001) – 1.31(05KH007)	PPWB (2020c)

5.4.2 Vulnerability Assessment Results

In this section, the results of the scenario-neutral vulnerability assessment are presented. As mentioned in Section 4.4, four different requirements of the Master Agreement are evaluated, the areas of vulnerability are illustrated, and a discussion is further developed to provide insights into

how sensitive the Master Agreement is to the perturbations of the exposure space climate attributes. Thereby, first, Section 5.4.2.1 reports on the SSR minimum flow requirement, and afterwards, details on the vulnerabilities of the annual apportionment of the SSR, NSR, and SR are presented (Section 5.4.2.2).

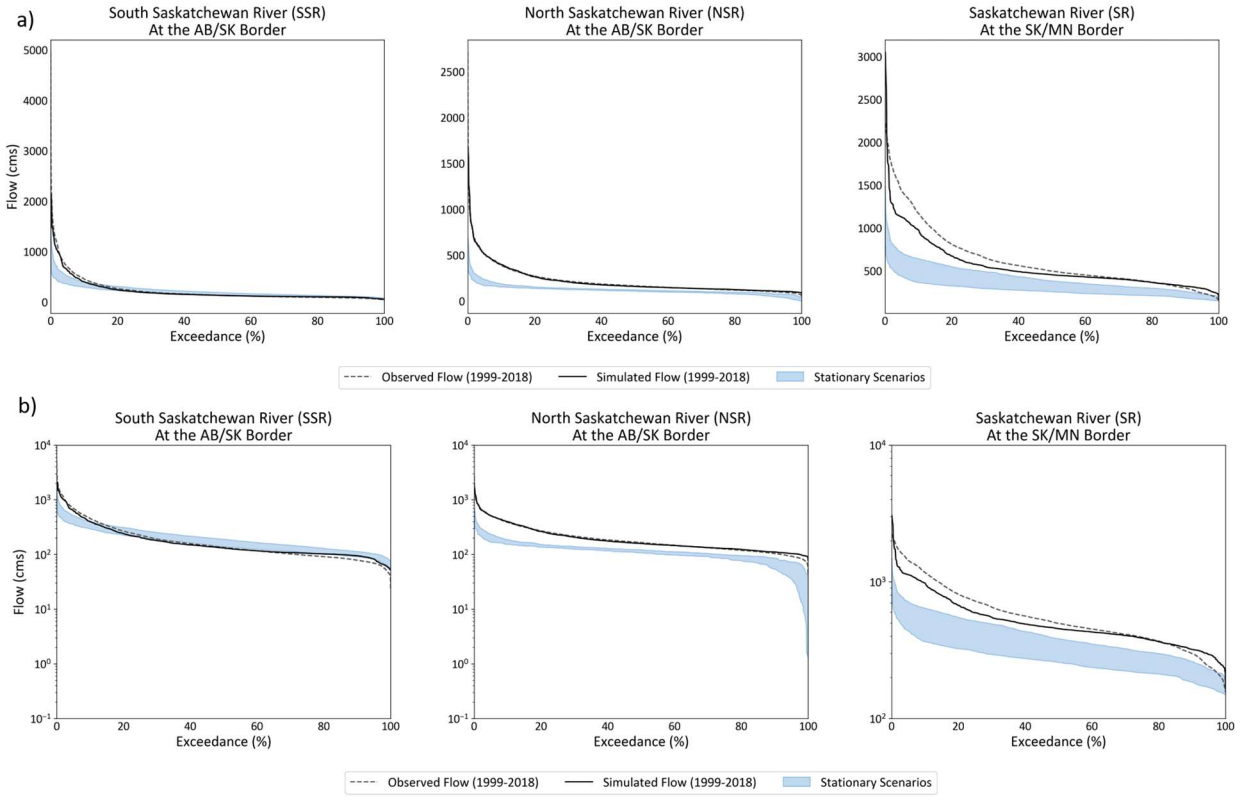

Figure 5.34. Overall assessment of the IWMSask model. The FDCs of the 40 sample weather scenarios in a) normal and b) logarithmic scales are compared to the simulated and observed flow for the baseline period of water management (i.e., 1999–2018). Stationary scenarios refer to the 40 sample scenarios generated for the validation process.

5.4.2.1 Minimum Flow Requirement

Figure 5.35 shows the general picture of the SSR minimum flow requirement vulnerabilities to the generated, perturbed climate change scenarios. Each subfigure indicates different cross-sections of the response surface sliced by discrete incremental temperature values; the horizontal and vertical axes of each subfigure indicate P_{JJA} and P_{DJF} deviations (in percent) from the baseline period values, respectively. The scenarios are scattered over each cross-section shown by four

different markers representing their associated N_{dry} values. The contour lines of each cross-section are plotted to distinguish vulnerable regions.

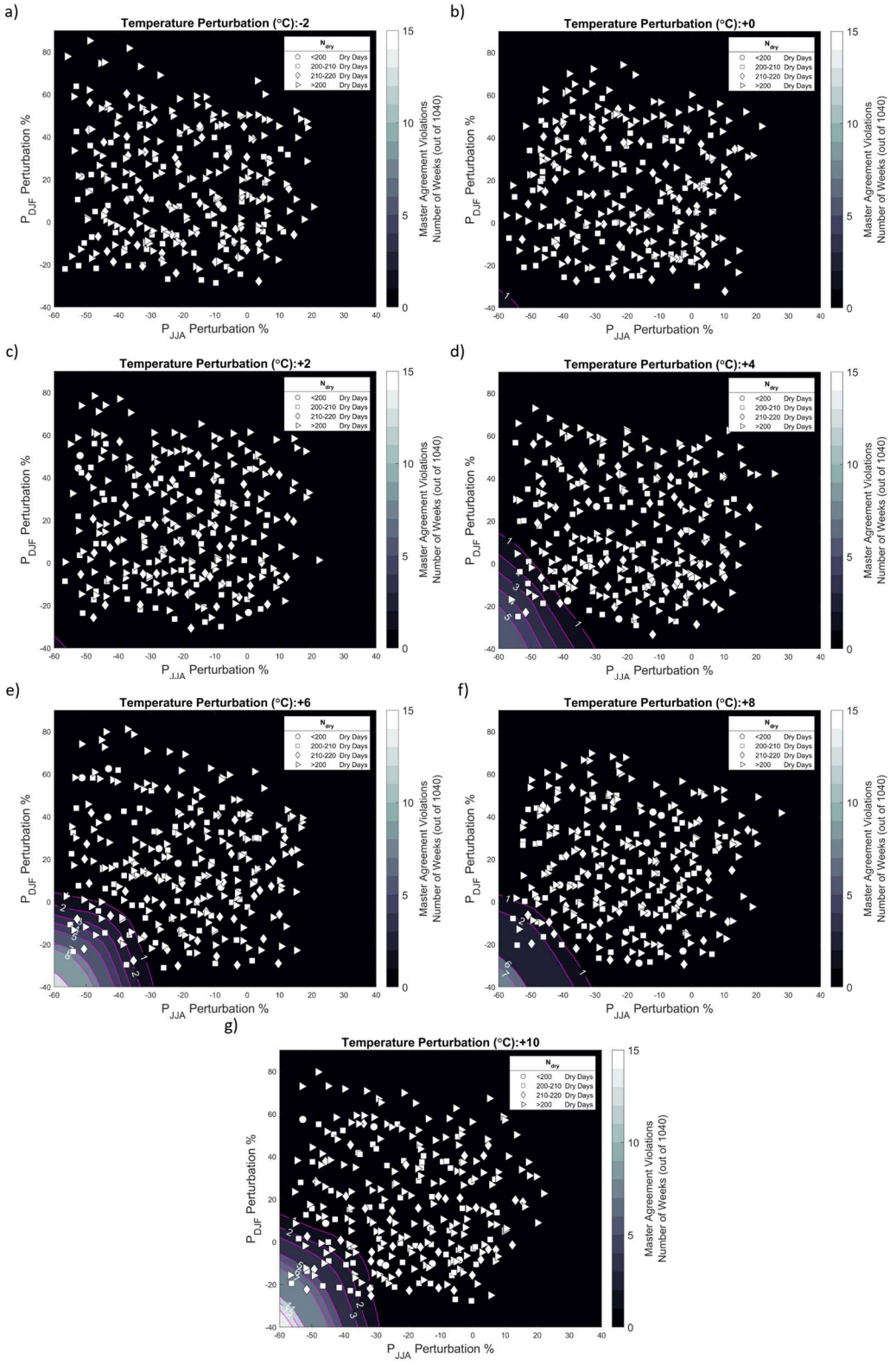

Figure 5.35. The vulnerability of the SSR minimum flow requirement to a wide range of climate change scenarios. The minimum flow of 42.5 $m^3 s^{-1}$, or half of the natural flow, whichever is less, is mandated by the Master Agreement that must be always satisfied, on the point where the SSR crosses the border of AB and SK.

As expected, the system seems to be resilient in cold (i.e., ΔT_{Ann} = -2 °C), no change (i.e., ΔT_{Ann} = 0 °C), and slightly warm (i.e., ΔT_{Ann} = +2 °C) temperature scenarios, regardless of precipitation perturbations. However, with an increase of +4 °C, the system starts violating the minimum flow requirement for a number of weeks. The bottom left corner of Figure 5.35d, which indicates an extreme deficit of summer and winter precipitations, shows the system can violate the requirement for up to 6 weeks (out of the overall 1,040 time-steps). The number of violations (in the same region) increases in warmer scenarios (Figure 5.35e-g); ΔT_{Ann} of +10 °C induces the system to miss the minimum flow requirement for up to 13 weeks. Moreover, the pattern of the vulnerable region indicates vulnerability to changes in P_{JJA} and P_{DJF}; a decrease of 15% to 25% in P_{JJA} can exert stress on the system even if the P_{DJF} value is increased to 10% in warm scenarios (i.e., +4 °C and beyond). Nevertheless, the response surface seems to be less sensitive to the N_{dry}, as this attribute seems to have minimal impact on the formation of the vulnerable region in the bottom left area of each cross-section.

To better understand how impactful each factor is, the Spearman's rank correlation coefficient (ρ) is calculated to better understand the relationship between the perturbed climate attributes and several outputs of this vulnerability assessment study (following Guo et al. (2017)). The selected outputs are the annual averaged natural ($Q_{nat\ R}$) and actual flows (Q_R) of each river (R) as well as the minimum flow requirement objective $J_{minflow,SSR}$. Table 5.2 details the mentioned correlations (with significant values, p-value < 0.05, distinguished with an asterisk), and Figure 5.36 shows the responses of the selected outputs to the perturbed attributes. It may be noted that for the case of $J_{minflow,SSR}$, only scenarios experiencing violations are depicted in the figure.

Looking at the near-zero ρs for N_{dry} in the table, it reaffirms the minimal impact of perturbed dry days, as stated earlier, on the natural and actual flows. Also, $J_{minflow,SSR}$ shows less sensitivity to the perturbations of this climate attribute. Nevertheless, other correlations listed in the table show expected behaviours; percent changes in summer and winter precipitations show a significant impact on the flows and violations of the minimum flow requirement. Moreover, as implied above, changes in annual temperature are negatively correlated with the flows indicating warmer climates results in lower flows and higher chances of violating the SSR minimum flow requirement.

Table 5.2. Spearman's rank correlation coefficients (ρ) between the perturbed climate attributes (Figure 5.24) and the selected outputs of the vulnerability assessment study: $Q_{nat\ R}$ and Q_R refers to the natural and actual flow of river R at the control points, and $J_{minflow,SSR}$ is the minimum flow objective of the SSR. An asterisk indicates the correlation is significant at the 0.05 level.

	$\mathbf{P_{JJA}}$	$\mathbf{P_{DJF}}$	$\mathbf{T_{Ann}}$	$\mathbf{N_{dry}}$	$\mathbf{P_{Ann}}$
$\boldsymbol{Q_{nat\ SSR}}$	0.66*	0.57*	-0.29*	0.00	0.92*
$\boldsymbol{Q_{SSR}}$	0.64*	0.55*	-0.27*	0.00	0.90*
$\boldsymbol{Q_{nat\ NSR}}$	0.57*	0.52*	-0.49*	0.00	0.82
$\boldsymbol{Q_{NSR}}$	0.57*	0.52*	-0.49*	0.00	0.82*
$\boldsymbol{Q_{nat\ SR}}$	0.62*	0.53*	-0.34*	0.00	0.87*
$\boldsymbol{Q_{SR}}$	0.62*	0.54*	0.35*	0.00	0.87*
$\boldsymbol{J_{minflow,SSR}}$	-0.23*	-0.21*	0.14*	0.02	-0.29*

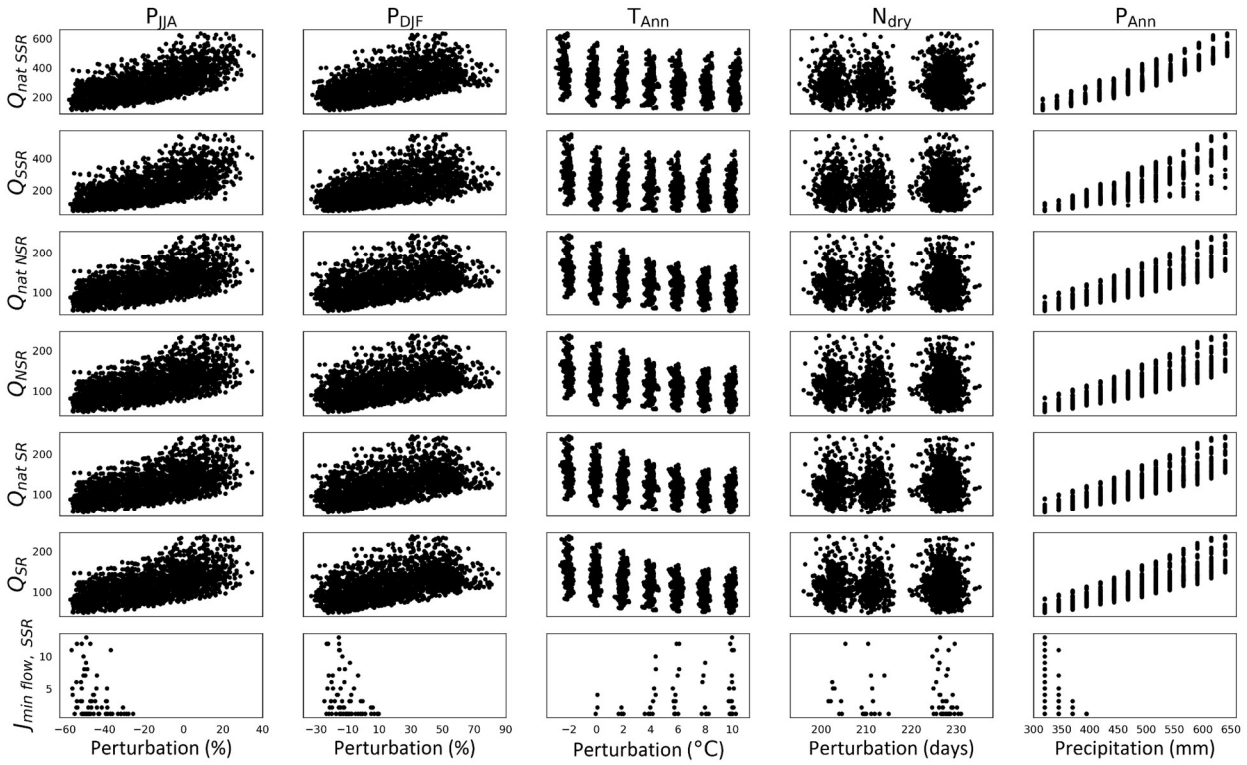

Figure 5.36. Responses of the scenario assessment output to the five climate attributes of the exposure space (Table 4.2): $Q_{nat\ R}$ and Q_R refers to the natural and actual flow of river R at its control point and $J_{minflow,SSR}$ is the minimum flow objective of the SSR at the AB-SK border. The unit of $Q_{nat\ R}$ and Q_R is in m^3s^{-1} and for $J_{minflow,SSR}$, the number failed time-steps for each scenario. Each dot in the figure represents the properties of one scenario.

Additionally, as a result of decreased natural flow at the AB-SK border, the magnitude of the minimum flow requirements is unsurprisingly impacted, as detailed in Table 5.3. From the table, it could be pointed out that in around 8 percent of the time, the requirement was reduced to less than 42.5 m^3s^{-1} as the natural flow at the border was lower than the 85 m^3s^{-1} threshold (see Equation 4.25). Although this compromise is legally permitted by the Master Agreement, it can potentially result in violations of other requirements in the immediate downstream, such as minimums of environmental or cultural flows in different river reaches. Furthermore, as could be viewed from the table, with smaller requirement amounts, the risk of failing to meet the objective increases.

Table 5.3. The magnitude of the minimum flow requirement of the SSR in all perturbed scenarios categorized in decile brackets, along with their corresponding risk of failure.

Minimum Flow Requirement ($Q_{(min.flow),SSR}$, **in** m^3s^{-1})	**Frequency of Occurrence** **(in all scenarios)**	**Risk of Failure** (**i.e.,** $J_{minflow,SSR}$ **in percent)**
$Q_{(min.flow),SSR} = 42.5$	92.3 %	~ 0.001 %
$40.0 \leq Q_{(min.flow),SSR} < 42.5$	1.4 %	~ 0.050 %
$30.0 \leq Q_{(min.flow),SSR} < 40.0$	4.3 %	~ 0.090 %
$20.0 \leq Q_{(min.flow),SSR} < 30.0$	1.8 %	~ 0.281 %
$10.0 \leq Q_{(min.flow),SSR} < 20.0$	0.2 %	~ 3.939 %

5.4.2.2 Annual Apportionment Requirements

Moving to the $J_{0.5(nat.flow),SSR}$ requirement, in only 10 scenarios (out of 1,960), violations of the annual apportionment for the SSR are observed, the details of which are listed in Table 5.4. It should be noted that in each case, the risk of failure is 5 percent (i.e., 1 year out of the total 20 years). However, looking at the weekly deficits of flow that were required to meet the annual apportionment, for all cases, it could be interpreted that they were less than 5% of the natural flow of that year. These amounts seem relatively small compared to the total inflow of water. Nevertheless, from Table 5.4, it could be viewed that the natural flow at the SSR control point was significantly decreased, while the apportionment agreement was met at 95 % of the time for the listed scenarios. This can be attributed to the method implemented in the IWMSask model (Section 4.4.1) that assures the annual apportionment is met as much as possible.

Table 5.4. Attributes of scenarios in which the SSR annual apportionment failed.

#	P_{JJA} (%)	P_{DJF} (%)	T_{Ann} (°C)	N_{dry} (days)	P_{Ann} (mm)	The scenario annual average $Q_{nat\ SSR}$ (m^3s^{-1})	The scenario annual average Q_{SSR} (m^3s^{-1})	Weekly deficit (for the failed year, m^3s^{-1})	Percent of average natural flow (of the failed year, %)
1	-47.74	-25.64	+1.71	212.76	319.86	133.90	77.64	1.90	1.42
2	-51.14	-23.54	+1.64	204.56	319.87	134.41	76.88	2.20	1.64
3	-47.06	-15.21	+1.85	228.34	319.87	138.19	81.14	6.07	4.40
4	-51.56	-14.64	+1.84	230.99	319.86	142.84	84.76	5.96	4.17
5	-43.94	-15.70	+1.85	229.17	319.85	133.44	77.61	4.01	3.01
6	-38.33	-11.53	+3.54	229.54	344.46	142.05	84.11	1.30	0.91
7	-41.55	-18.69	-1.99	212.07	344.48	205.09	133.93	1.06	0.52
8	-52.09	-20.91	-0.13	202.02	319.86	145.32	82.34	0.91	0.63
9	-45.82	-16.35	0.07	319.86	319.86	142.93	81.21	0.90	0.63
10	-33.32	-12.26	-0.03	228.65	344.47	160.17	94.42	0.85	0.53

Although the annual apportionment is nearly met in all scenarios, other users in the basin, such as irrigation and non-irrigation demand nodes, environmental flows, etc. are experiencing water shortages. The shortage in a demand node is defined as the difference between the demand and amount of water supplied to that node. To understand the general picture of stresses imposed on different users, the water shortage for irrigation users, non-irrigation users, and environmental flows are depicted in Figure 5.37–Figure 5.39. Further vulnerability analysis of these users is beyond the scope of this thesis and should be addressed in future studies.

For the case of $J_{0.5(nat.flow),NSR}$ and $J_{0.5(nat.flow),SR}$, no violation of the annual apportionment is observed. This is due to the fact that the water usage in central Alberta and Saskatchewan is much lower than that of southern Alberta where the SSR flows, according to Shah (2020). Thereby, no more analyses are shown for these two rivers.

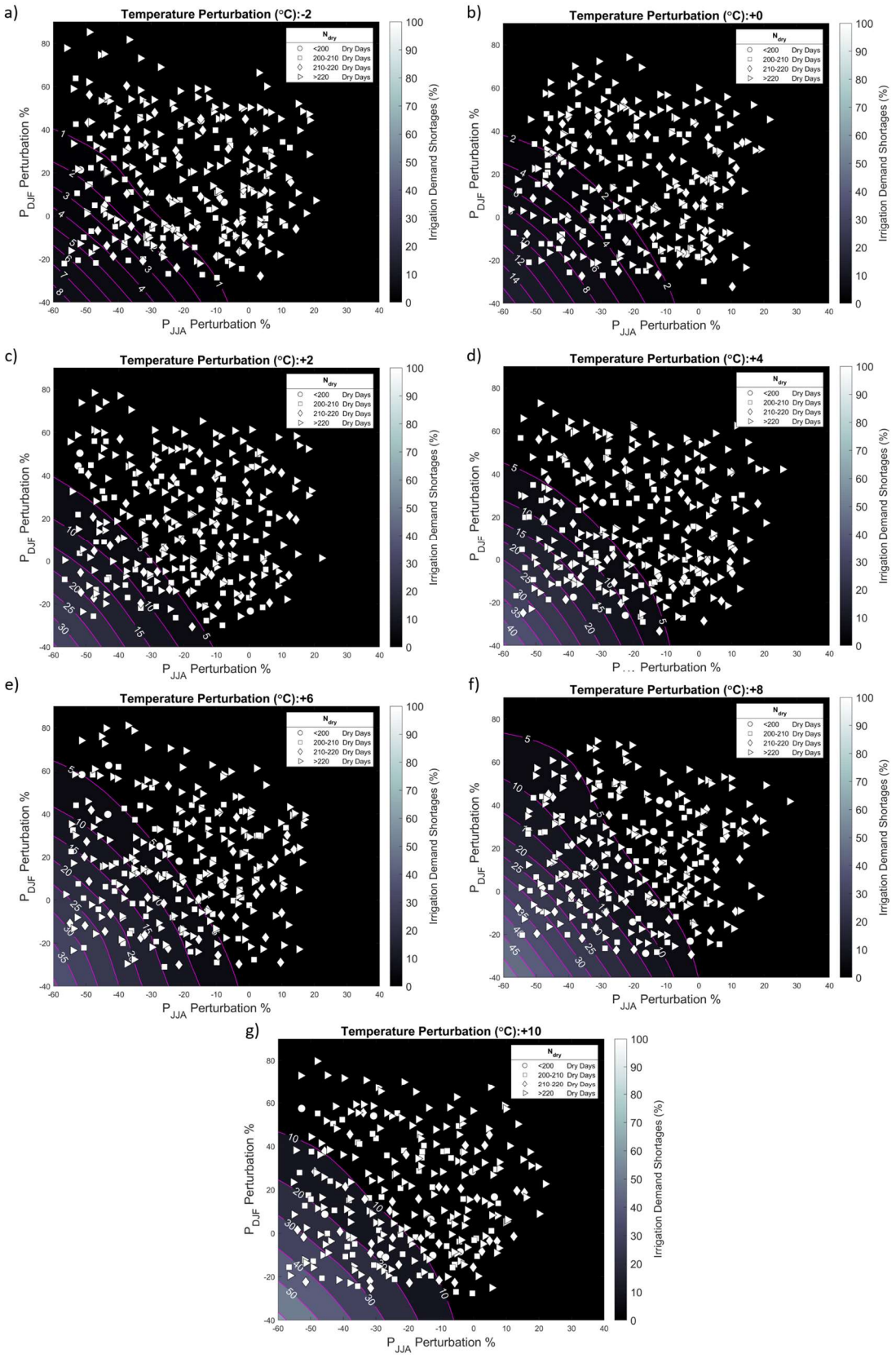

Figure 5.37. Irrigation demand shortage in the face of perturbed climate change scenarios.

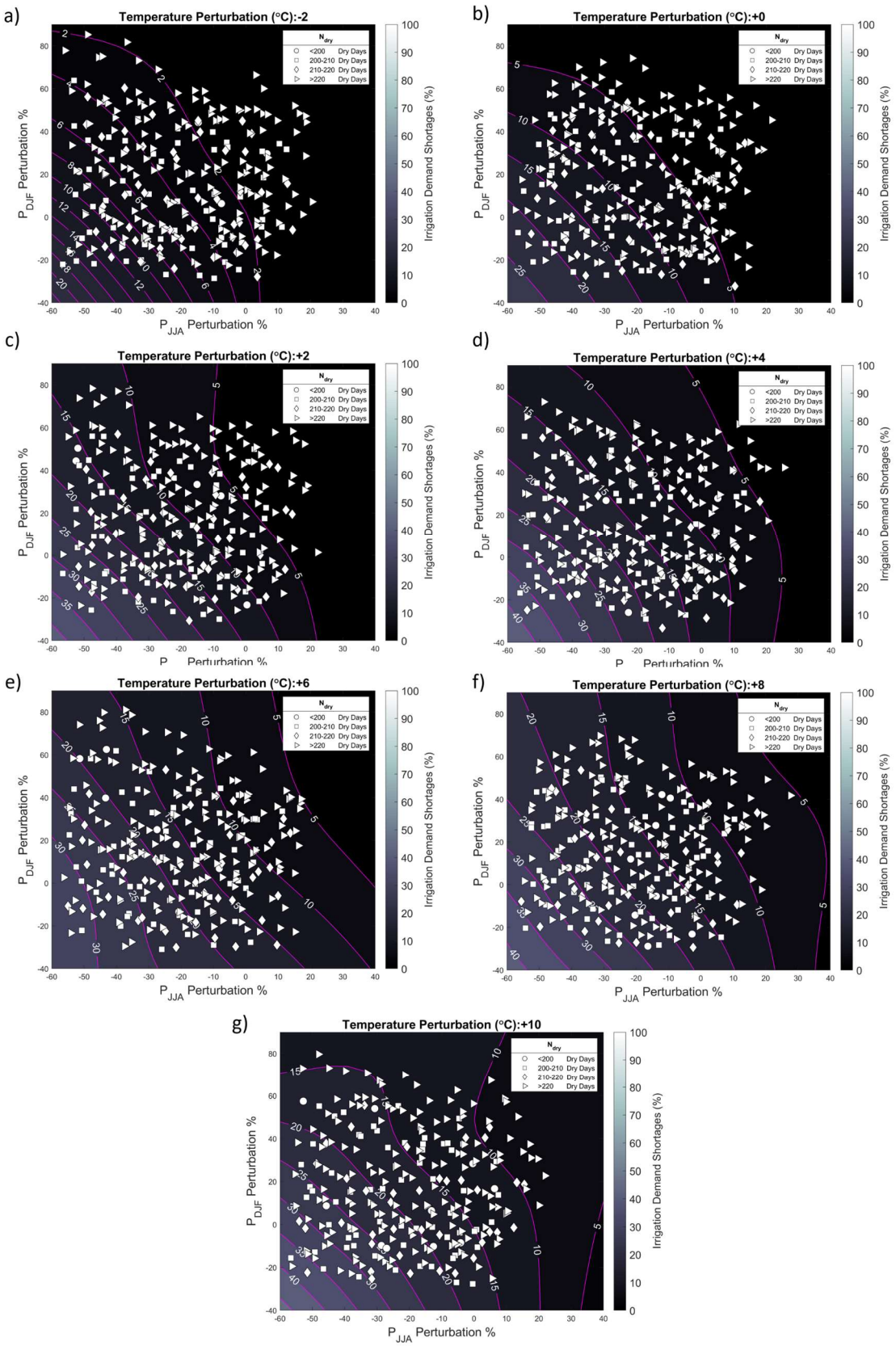

Figure 5.38. Non-irrigation shortages in the face of perturbed climate change scenarios.

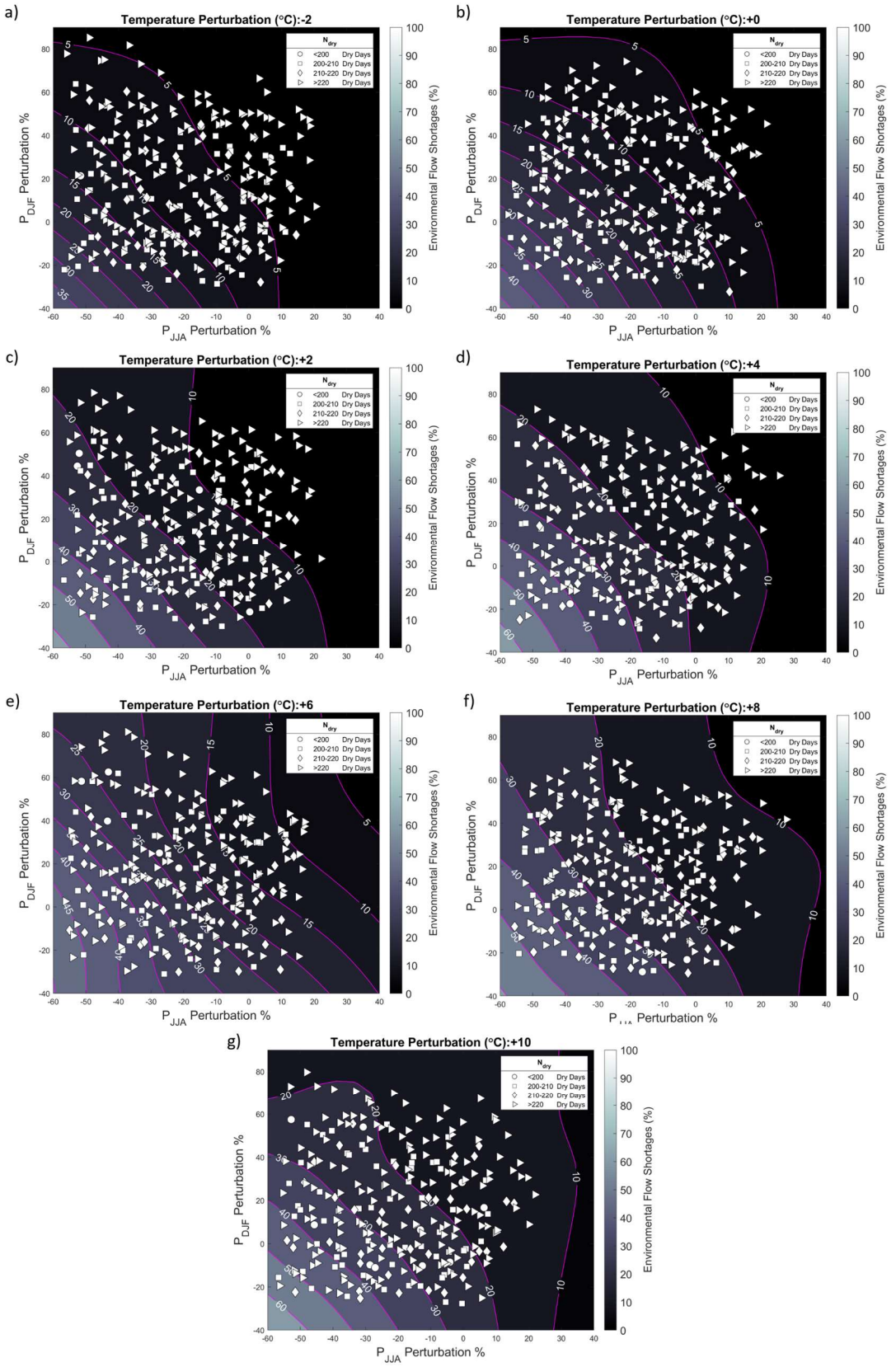

Figure 5.39. Environmental flow shortages in the face of perturbed climate change scenarios.

5.4.2.3 Trade-offs between Different Water Sectors

In this sub-section, further investigation on the trade-offs between the shortages of each water sector, i.e., irrigation, non-irrigation, and environmental flows, in response to the climate change scenarios of this study is carried on. As violations of the Master Agreement were only observed upstream of the SSR crossing the AB and SK border, the results of this sub-section are only shown for the water sectors located in southern Alberta.

Figure 5.40 shows the relationship between the shortages of the aforementioned sectors located within southern Alberta and annual average inflow to the basin. It could be viewed that the relationships between shortages of all sectors show an exponential behavior. As could be seen, environmental flows suffer most amongst other sectors in response to a decrease in inflow followed by non-irrigation and irrigation sectors. However, the irrigation sector shortage surpasses the non-irrigation one in a number of extremely dry scenarios as could be viewed in the upper left tail of the scenario clusters shown in the figure. These behaviours can be explained by the wide and non-uniform distributions of water rights among the different users, as shown in Figure 4.7. In addition, it is worth mentioning that apart from the priorities, the location of each node and the magnitude of demand are important factors in the water allocation simulation process.

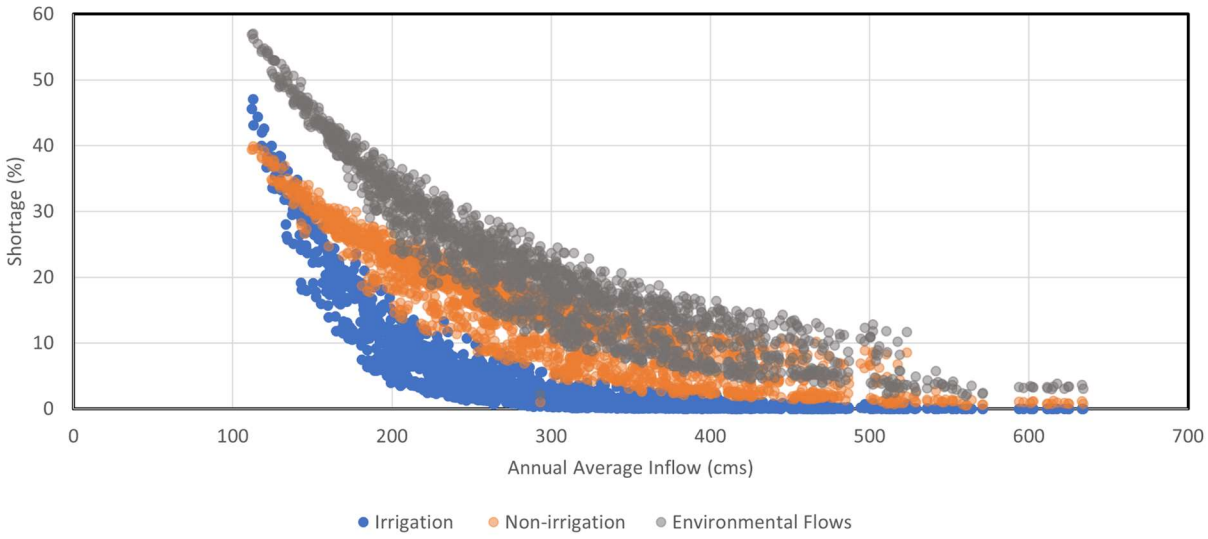

Figure 5.40. The trade-offs between shortages of irrigation (blue), non-irrigation (orange), and environmental flows (gray) and the annual average inflow for each climate change scenario (shown with a circle).

The same behaviour can also be viewed in the trade-offs between the shortages of each sector and the annual averaged flow passing the AB and SK border (Figure 5.41), as well as the ratio of annual average inflow passing that boarder (Figure 5.42).

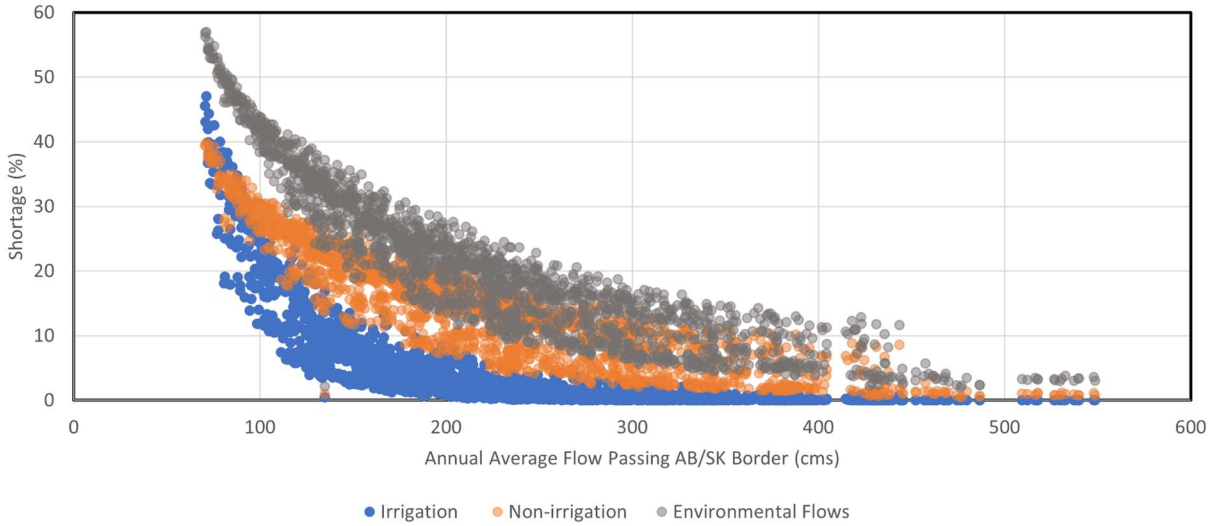

Figure 5.41. The trade-offs between shortages of irrigation (blue), non-irrigation (orange), and environmental flows (gray) and the annual average flow passing the AB and SK border for each climate change scenario (shown with a circle).

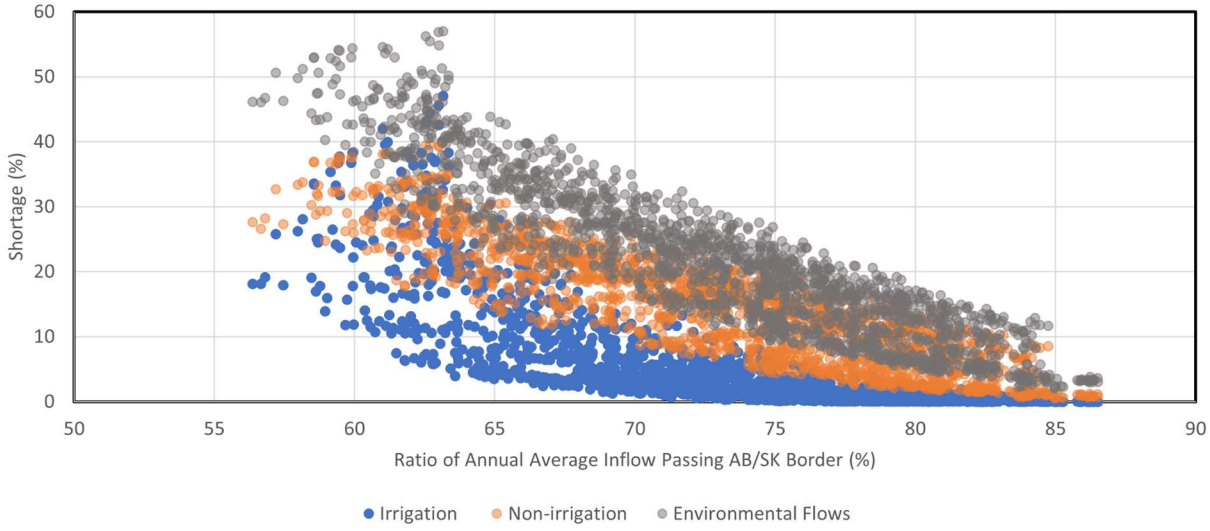

Figure 5.42. The trade-offs between shortages of irrigation (blue), non-irrigation (orange), and environmental flows (gray) and the ratio of annual average inflow passing the AB and SK border for each climate change scenario (shown with a circle).

To further understand the relationship between shortages of different sectors, the trade-offs between each of them are plotted in Figure 5.43 to Figure 5.45. As could be viewed in the figures, the irrigation shortages show a logarithmic behavior in relation to other sectors' shortages, while the trade-off between non-irrigation and environmental flow shortage follows a linear pattern.

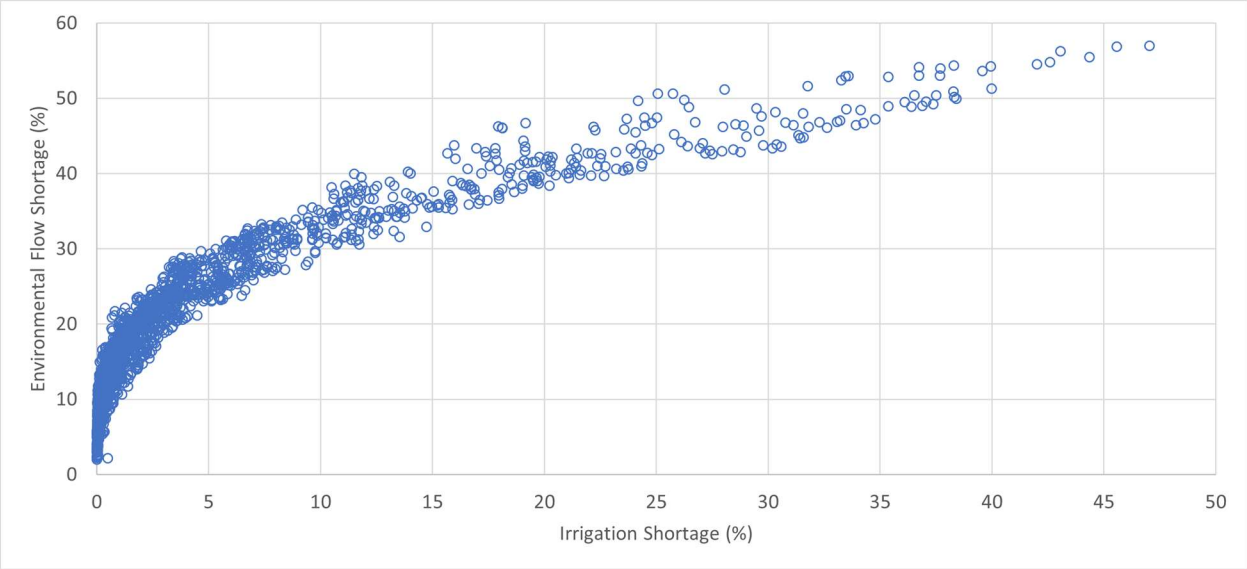

Figure 5.43. The trade-off between environmental flows and irrigation shortages facing climate change scenarios (each shown with a circle).

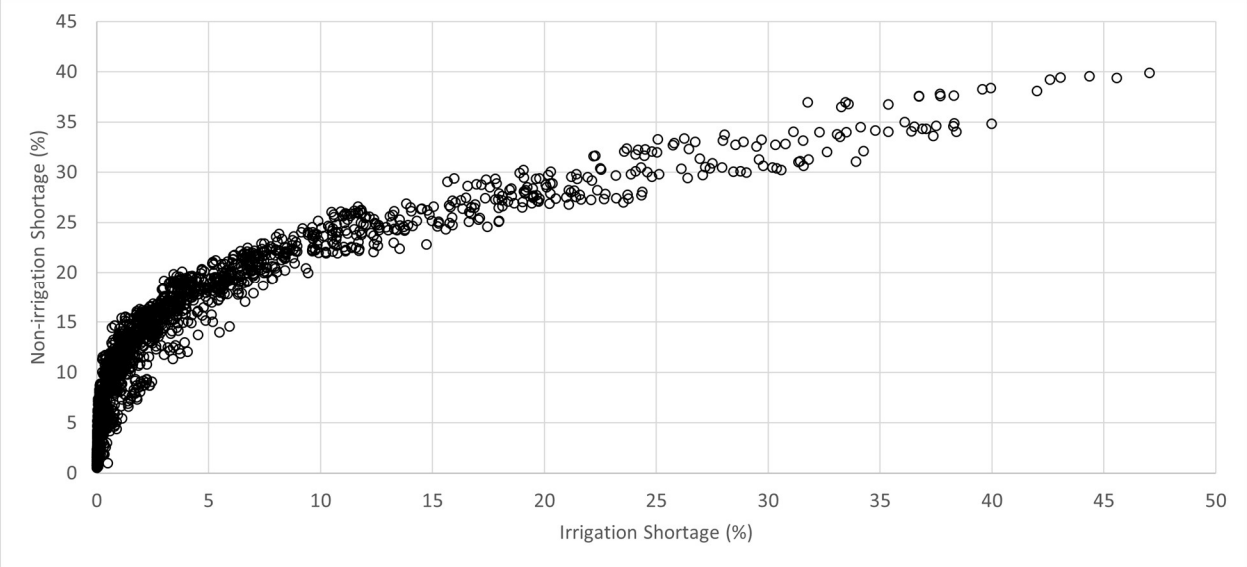

Figure 5.44. The trade-off between irrigation and non-irrigation shortages facing climate change scenarios (each shown with a circle).

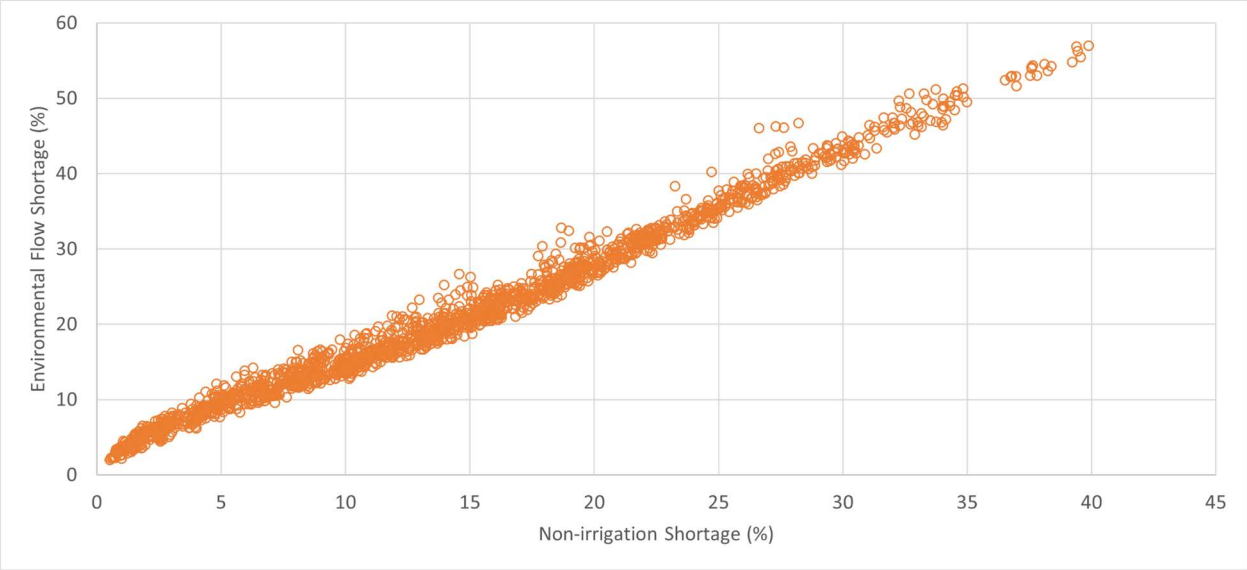

Figure 5.45. The trade-off between environmental flows and non-irrigation shortages facing climate change scenarios (each shown with a circle).

These differences in pattern could be due to several reasons. Firstly, the timing of the demand for each sector is different; the irrigation sector usually demands water between weeks 13 and 40, whereas other sectors usually have constant demand values throughout the year. Secondly, the priorities associated with each sector could impact the shape of the trade-offs; as mentioned earlier, each sector follows a different distribution of priorities (see Figure 4.7). Thirdly, the location of each sector is important in the allocation of water; the irrigation sectors are usually clustered within an irrigation district in southern Alberta, while the non-irrigation and environmental flows are spread throughout the province.

To further investigate the logarithmic behaviour that is seen in Figure 5.43, the scenarios with a similar amount of annual precipitation (see Figure 5.24) were chosen, and similar plots were drawn once again. For example, in Figure 5.46, the relationship between the shortages of irrigation and non-irrigation sectors are depicted for scenarios with 319 mm of annual precipitation. As could be viewed in the figure, a perfect logarithmic regression curve with an R^2 of 0.98 fits the clusters of scenarios. To understand where these clusters come from and why the increase follows a logarithmic pattern, the relationship between the irrigation shortage and the temperature perturbation values was drawn. It was found out that in scenarios with an equal amount of annual precipitation, increasing temperature increments impose more shortage on the irrigation (Figure 5.47) as well as non-irrigation and environmental flows (not shown). The same behaviour could

also be seen in each class of scenario with an equal amount of annual precipitation. A detailed investigation of the shortages that are seen in response to the climate change scenarios could be further pursued in future research.

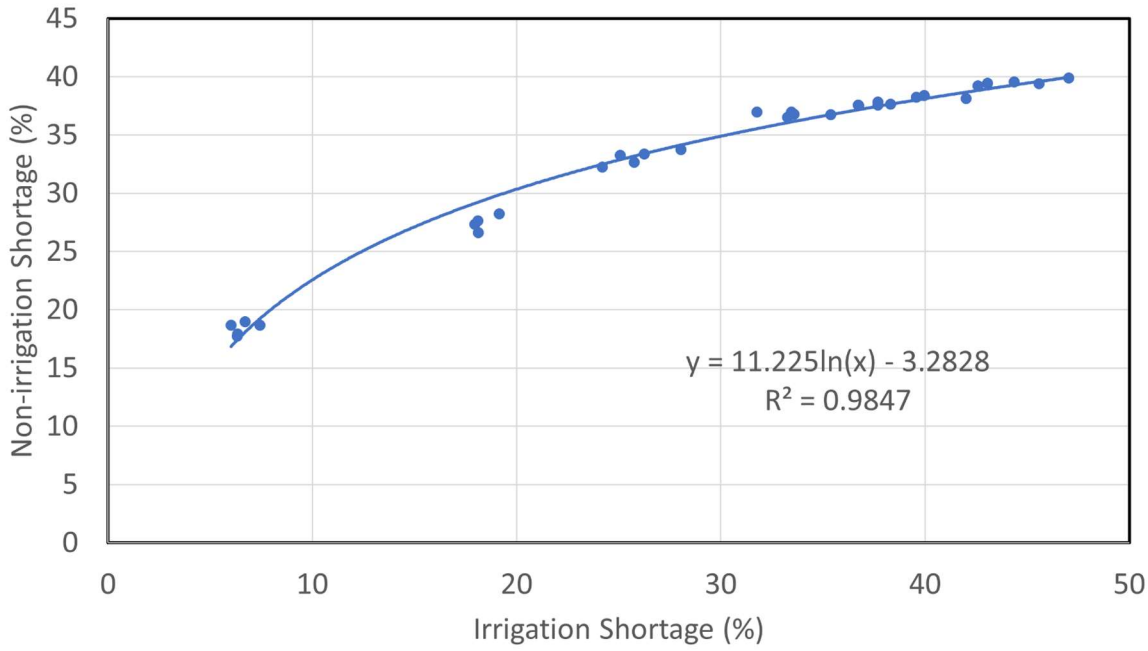

Figure 5.46. The trade-off between irrigation and non-irrigation shortages for scenarios with annual precipitation amount of 319mm. The trade-off follows a logarithmic behavior with the mathematical relationship shown as above. Each circle corresponds to one scenario.

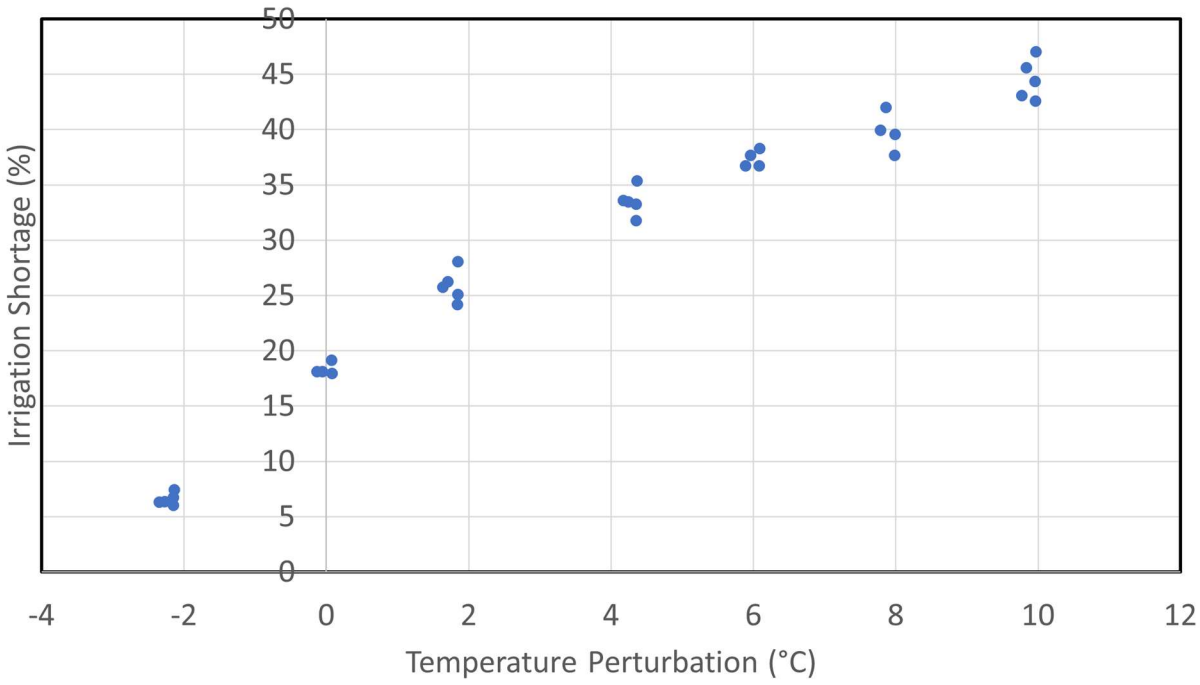

Figure 5.47. The trade-off between the irrigation shortage (%) and the temperature perturbations (℃) of scenarios with annual precipitation amount of 319mm.

6 CHAPTER 6: OVERALL DISCUSSION

6.1 General Overview

This thesis investigated the impact of climate change by perturbing four attributes, which are: 1) annual temperature (T_{Ann}), summer precipitation (P_{JJA}), winter precipitation (P_{DJF}), and the total number of dry days in a year (N_{dry}). The ranges of perturbations for the first three attributes were informed by all the climate projections of CMIP5. For the last one, two well-regarded Canadian RCMs were used. These could provide a comprehensive picture of what might happen to the hydrology and water resources system of the Saskatchewan River Basin.

From a hydrologic point of view, the change in generated streamflow is expected to be significant if any of the first three attributes were to change in the future. However, the change in generated flows were shown to be less sensitive (or even insensitive) to changes in the total number of dry days. This appeared to be rather counter-intuitive and further research is warranted to quantify the possible impacts of change more accurately in the timing regime of storms.

Form a water resources point of view, this section tries to address three critical questions, as outlined in the following.

6.2 Is the Master Agreement Viable under Climate Change?

This question can be addressed from two different angles, theoretical and practical. From a theoretical point of view, the modelling work of this study shows that the requirements (in terms of both annual apportionment and minimum flow requirements) stated in the Master Agreement can generally be met, even under severely dry scenarios. However, from a practical point of view, this comes with the fact that the water supply to both irrigation and non-irrigation sectors in southern Alberta could drop significantly to an alarming degree under some of the plausible future scenarios. Perhaps more importantly, the decline in flows to conserve the environmental flows

would be substantial. Therefore, the Master Agreement can become very vulnerable under certain futures scenarios.

6.3 What Sectors Will Suffer the Most in Extremely Dry Scenarios?

The cost of satisfying the Master Agreement imposed on the other sectors in the southern Alberta is significant. Irrigation and non-irrigation sectors as well as environmental flows each could face up to 30 to 40 percent of water shortage annually in moderate warming scenarios (i.e., +2 to +4°C) and even higher in severe warming scenarios (i.e., +6°C and above). These shortages can potentially result in negative social and economic impacts (Eamen et al. 2020). Furthermore, environmental flow shortages in the different river reaches can potentially violate several water quality objectives detailed in the Schedule E of the Master Agreement (not investigated in this thesis).

Overall, both irrigation and non-irrigation sectors as well as environmental flows appear to be more sensitive to possible declines in summer precipitation. In some cases, an increase in winter precipitation cannot offset the negative impacts of a decline in P_{JJA}. This observation is very important because the impact of climate change on precipitation regime is expected to be different for summer and winter. In many of the projected scenarios showing an overall increase in annual precipitation, summer precipitation would decrease while winter precipitation would increase. Thus, such scenarios should be carefully investigated in further studies.

6.4 What Can be Done to Alleviate the Impact of Climate Change?

First of all, the results highlighted the need for an integrated modelling and management framework to enable a system-wide assessment of the impact of climate change. A localized study might miss to consider the complexity of the water management of this system and the trade-offs between competitive objectives and stakeholders across the basin. Building resilience in this basin against climate change requires work across three fronts: 1) initiating an inclusive and basin-wide dialogue about priorities, vulnerabilities, and values, informed by an integrated model, 2) demand management, improvement in irrigation efficiency, possibly establishing a water market, and 3)

revisiting the operation strategy of the water infrastructure, including reservoirs, across the entire basin such that the well-being of the entire basin is maximized.

7 CHAPTER 7: CONCLUSIONS AND FURTHER REMARKS

This research addressed concerns around vulnerabilities of transboundary river basins, as demanded by UNECE (2016). As mentioned throughout this research, many stressors are negatively affecting the institutional and ecosystem capacities of these basins around the globe. Covering nearly half of the Earth's land surface, these basins are vital to the survival of societies and humankind. One of the existential threats that is already stressing transboundary river systems is climate change. Understanding the vulnerabilities imposed by this biophysical stressor on transboundary basins can give a clearer picture of what measures must be taken to alleviate such susceptibilities. In doing so, many vulnerability assessments in the literature use the traditional, predict-then-act top-down vulnerability assessments and planning. Although this method brings many advantages to the table, a localized, detailed vulnerability assessment at the basin scale is a mandate to scope possible climate-change-induced susceptibilities. This research used a methodology to conduct a thorough, scenario-neutral vulnerability assessment at the basin scale and address this issue. Needless to say, in several steps of the methodology, the information derived from the top-down technique was used to complement the current vulnerability study.

In this study, a set of plausible, future weather scenarios was employed and was used to test a water management system using several modelling components. An important advantage of this type of scenario is that the detected vulnerabilities could be associated with the changes in climate variables and attributes. The proposed methodology of this thesis was demonstrated on the Saskatchewan River Basin (SaskRB) in western Canada to evaluate how different plausible scenarios of future climate change can affect the transboundary rivers' flow crossing interprovincial borders within Canada. Four climate attributes, which were deemed to change in the future were perturbed to stress test the water management system of the SaskRB. While a wide range of change is suggested in CMIP5 in the value of precipitation and temperature over the horizon of 2080–2099, the analysis of the thesis showed that the two Canadian RCMs suggested equal or more wet days for the end of the 21st century. This information was used to inform the

annual average number of dry days of the produced weather scenarios. A weather generator capable of producing scenarios with differing number of dry days was employed. In doing so, the parameters of the weather generator were perturbed to reflect these desired changes. Nevertheless, as the RCMs projections are most often biased, a simple delta method was utilized to inform the parameter perturbation procedure. In future research, a larger set of RCMs (and other sources of knowledge) could be employed to inform this attribute of scenarios.

Moreover, the uncertainty ranges proposed by the CMIP5 climate models were used to perturb the seasonal precipitation and annual temperature values of scenarios. These ranges, proposed by Asong et al. (2020), were 0 to +10°C for the annual temperature change, −45 to +15% change for the summer precipitation, and −5 to +40% for the winter precipitation for the SaskRB (Asong et al. 2020). These perturbations were mirrored in the synthetic scenarios using a post-processing procedure. However, in future research other lines of evidence could be used in informing the exposure space formation (see Section 4.2.2), such as paleo-hydrological and paleoclimate data (Elshorbagy et al. 2016; e.g. Razavi et al. 2015, 2016; Slaughter and Razavi 2020).

Using a simple conceptual hydrological model, i.e., HBV-SASK, the weather scenarios were further translating into river flows that were further fed into a water management model of the SaskRB. The quantities of water crossing the provincial political border within the SaskRB were measured in each scenario and further investigated. The analyses of the thesis found that the requirements of the Master Agreement are potentially sensitive to changes in the seasonal perturbations of summer and winter precipitation. With an increase in temperature, the intensity of violations increases too. The number of dry days was found to have a minimal impact on the vulnerability of the system.

Moreover, it was found that water use can contribute significantly to the vulnerability of the system. In parts of the basin where water abstraction is high, specifically the southern parts of AB, the consumptive water users (irrigation and non-irrigation users) show more vulnerability compared to parts where water abstraction is tolerable by the system. Although the Master Agreement is not significantly violated in much of the perturbed scenarios, however, a significant risk is posed to the consumptive users in the southern part of AB where SSR flows. The northern parts of AB and the whole portion of the SaskRB located within SK seem to be less vulnerable to climatic changes due to lower water management interventions and less water demand. This signifies the importance of sustainable use of freshwater resources which can add another layer of

safety in terms of political tensions between the states. It is acknowledged that the system's demand in this study was that of the recent last 20 years (1999–2018) and was not adjusted to reflect the impacts of climate change. In further research, an irrigation demand model is deemed needed to estimate the demands for each irrigation node under different climate conditions.

REFERENCES

Abdolvand, B., Mez, L., Winter, K., Mirsaeedi-Gloßner, S., Schütt, B., Rost, K. T., and Bar, J. (2015). "The dimension of water in Central Asia: security concerns and the long road of capacity building." *Environmental Earth Sciences*, 73(2), 897–912. doi:10.1007/s12665-014-3579-9.

Abu, R., Reed, M. G., and Jardine, T. D. (2020). "Using two-eyed seeing to bridge Western science and Indigenous knowledge systems and understand long-term change in the Saskatchewan River Delta, Canada." *International Journal of Water Resources Development*, Routledge, 36(5), 757–776. doi:10.1080/07900627.2018.1558050.

Aghakouchak, A., and Habib, E. (2010). "Application of a Conceptual Hydrologic Model in Teaching Hydrologic Processes." *Int. J. Engng Ed.*, 26(4), 963–973.

Ahmed, K. F., Wang, G., Silander, J., Wilson, A. M., Allen, J. M., Horton, R., and Anyah, R. (2013). "Statistical downscaling and bias correction of climate model outputs for climate change impact assessment in the U.S. northeast." *Global and Planetary Change*, 100, 320–332. doi:10.1016/j.gloplacha.2012.11.003.

Al-Faraj, F. A. M., and Scholz, M. (2015). "Impact of upstream anthropogenic river regulation on downstream water availability in transboundary river watersheds." *International Journal of Water Resources Development*, Taylor & Francis, 31(1), 28–49. doi:10.1080/07900627.2014.924395.

Alberta Environmental Protection. (1993). "WRMM (Water Resources Management Model), Program Description." Calgary, Canada.

Andrews, E. S., Chung, F. I., and Lund, J. R. (1992). "Multilayered, Priority-Based Simulation Of Conjunctive Facilities." *Journal of Water Resources Planning and Management*, 118(1), 32–53. doi:10.1061/(ASCE)0733-9496(1992)118:1(32).

Apipattanavis, S., Podestá, G., Rajagopalan, B., and Katz, R. W. (2007). "A semiparametric multivariate and multisite weather generator." *Water Resources Research*, 43(11). doi:10.1029/2006WR005714.

Asadzadeh, M., Razavi, S., Tolson, B. A., and Fay, D. (2014). "Pre-emption strategies for efficient multi-objective optimization: Application to the development of Lake Superior regulation plan." *Environmental Modelling and Software*, Elsevier Ltd, 54, 128–141. doi:10.1016/j.envsoft.2014.01.005.

Asadzadeh, M., and Tolson, B. (2013). "Pareto archived dynamically dimensioned search with hypervolume-based selection for multi-objective optimization." *Engineering Optimization*, 45(12), 1489–1509. doi:10.1080/0305215X.2012.748046.

Asong, Z. E., Hawkins, E., Razavi, S., Wheater, H. S., Pomeroy, J., Pietroniro, A., and Elshamy, M. E. (2020). "Climate projections for scenario-led adaptation strategies for water resources: Rethinking how to represent and interpret the cascade of uncertainty." *Climatic Change*, (unpublished).

Asong, Z. E., Khaliq, M. N., and Wheater, H. S. (2014). "Regionalization of precipitation

characteristics in the Canadian Prairie Provinces using large-scale atmospheric covariates and geophysical attributes." *Stochastic Environmental Research and Risk Assessment*, 29(3), 875–892. doi:10.1007/s00477-014-0918-z.

Asong, Z. E., Khaliq, M. N., and Wheater, H. S. (2016). "Multisite multivariate modeling of daily precipitation and temperature in the Canadian Prairie Provinces using generalized linear models." *Climate Dynamics*, 47(9–10), 2901–2921. doi:10.1007/s00382-016-3004-z.

Atef, S. S., Sadeqinazhad, F., Farjaad, F., and Amatya, D. M. (2019). "Water conflict management and cooperation between Afghanistan and Pakistan." *Journal of Hydrology*, 570, 875–892. doi:10.1016/j.jhydrol.2018.12.075.

Bakker, M. H. N. (2009). "Transboundary river floods: examining countries, international river basins and continents." *Water Policy*, 11(3), 269–288. doi:10.2166/wp.2009.041.

Bakker, M. H. N., and Duncan, J. A. (2017). "Future bottlenecks in international river basins: where transboundary institutions, population growth and hydrological variability intersect." *Water International*, Routledge, 42(4), 400–424. doi:10.1080/02508060.2017.1331412.

Bankes, S. (1993). "Exploratory Modeling for Policy Analysis." *Operations Research*, 41(3), 435–449. doi:10.1287/opre.41.3.435.

Bardossy, A., and Plate, E. J. (1992). "Space-time model for daily rainfall using atmospheric circulation patterns." *Water Resources Research*, 28(5), 1247–1259. doi:10.1029/91WR02589.

Bartholomew, E., and Kwakkel, J. H. (2020). "On considering robustness in the search phase of Robust Decision Making : A comparison of Many-Objective Robust Decision Making , multi-scenario Many-Objective Robust Decision Making , and Many Objective Robust Optimization." *Environmental Modelling and Software*, Elsevier Ltd, 127(December 2019), 104699. doi:10.1016/j.envsoft.2020.104699.

Barua, A., ter Horst, R., Sehring, J., Bréthaut, C., Salamé, L., Wolf, A., Pawletta, B. J., Manzungu, E., and Nicol, A. (2019). "Universities' partnership: the role of academic institutions in water cooperation and diplomacy." *International Journal of Water Resources Development*, Routledge, 1–7. doi:10.1080/07900627.2019.1657002.

Ben-Haim, Y. (2001). *Information-gap decision theory: decisions under severe uncertainty*. Academic Press London.

Bergström, S. (1995). "The HBV model." *Computer Models of Watershed Hydrology*, V. P. Singh, ed., Water resources publications, Highland Ranch, CO, USA, 443–476.

Bergström, S., and Forsman, A. (1973). "Development of a conceptual deterministic rainfall-runoff model." *Nordic Hydrology*, 4, 147–170.

Berry, D. J. (1979). "Interprovincial water resource concerns." *Canadian Water Resources Journal*, 4(1), 33–39. doi:10.4296/cwrj0401033.

Bhatti, A. M., Koike, T., and Shrestha, M. (2016). "Climate change impact assessment on mountain snow hydrology by water and energy budget-based distributed hydrological model." *Journal of Hydrology*, Elsevier B.V., 543, 523–541. doi:10.1016/j.jhydrol.2016.10.025.

Bonsal, B. R., Peters, D. L., Seglenieks, F., Rivera, A., and Berg, A. (2019). "Changes in Freshwater Availability Across Canada." *Canada's Changing Climate Report*, E. Bush and D. S. Lemmen, eds., Ottawa, Ontario, 261–342.

Borgomeo, E., Farmer, C. L., and Hall, J. W. (2015). "Numerical rivers: A synthetic streamflow generator for water resources vulnerability assessments." *Water Resources Research*, 51(7), 5382–5405. doi:10.1002/2014WR016827.

Brichieri-Colombi, S., and Bradnock, R. W. (2003). “Geopolitics, water and development in South Asia: cooperative development in the Ganges-Brahmaputra delta.” *The Geographical Journal*, 169(1), 43–64. doi:10.1111/1475-4959.t01-1-00002.

Brissette, F. P., Khalili, M., and Leconte, R. (2007). “Efficient stochastic generation of multi-site synthetic precipitation data.” *Journal of Hydrology*, 345(3–4), 121–133. doi:10.1016/j.jhydrol.2007.06.035.

Brown, C., Ghile, Y., Laverty, M., and Li, K. (2012). “Decision scaling: Linking bottom-up vulnerability analysis with climate projections in the water sector.” *Water Resources Research*, 48(9), 1–12. doi:10.1029/2011WR011212.

Brown, C., Werick, W., Leger, W., and Fay, D. (2011). “A Decision-analytic approach to managing climate risks: application to the Upper Great Lakes.” *JAWRA Journal of the American Water Resources Association*, 47(3), 524–534. doi:10.1111/j.1752-1688.2011.00552.x.

Burn, D. H. (1994). “Hydrologic effects of climatic change in west-central Canada.” *Journal of Hydrology*, 160, 53–70. doi:10.1016/0022-1694(94)90033-7.

Bush, E., Gillett, N., Watson, E., Fyfe, J., Vogel, F., and Swart, N. (2018). “Understanding Observed Global Climate Change.” *Canada’s Changing Climate Report*, E. Bush and D. S. Lemmen, eds., Government of Canada, Ottawa, Ontario, 24–72.

Cannon, A. J., Piani, C., and Sippel, S. (2020). “Bias correction of climate model output for impact models.” *Climate Extremes and Their Implications for Impact and Risk Assessment*, Elsevier, 77–104. doi:10.1016/B978-0-12-814895-2.00005-7.

Caponera, D. A. (1985). “Patterns of cooperation in international water law: principles and institutions.” *Natural Resources Journal*, 25(3), 563–587.

Caron, A., Leconte, R., and Brissette, F. (2008). “An improved stochastic weather generator for hydrological impact studies.” *Canadian Water Resources Journal*, 33(3), 233–256. doi:10.4296/cwrj3303233.

Chandler, R. (2014). “A multisite, multivariate daily weather generator - user guide.”

Chandler, R. E., and Wheater, H. S. (2002). “Analysis of rainfall variability using generalized linear models: A case study from the west of Ireland.” *Water Resources Research*, 38(10), 10-1-10–11. doi:10.1029/2001WR000906.

Chen, J., Arsenault, R., Brissette, F. P., Côté, P., and Su, T. (2019). “Coupling annual, monthly and daily weather generators to simulate multisite and multivariate climate variables with low-frequency variability for hydrological modelling.” *Climate Dynamics*. doi:10.1007/s00382-019-04750-z.

Chen, J., Brissette, F. P., and Leconte, R. (2010). “A daily stochastic weather generator for preserving low-frequency of climate variability.” *Journal of Hydrology*, 388, 480–490. doi:10.1016/j.jhydrol.2010.05.032.

Chen, J., Brissette, F. P., and Leconte, R. (2011). “Uncertainty of downscaling method in quantifying the impact of climate change on hydrology.” *Journal of Hydrology*, 401, 190–202. doi:10.1016/j.jhydrol.2011.02.020.

Chen, J., Brissette, F., and Zhang, X. J. (2014). “Multi-site stochastic weather generator for daily precipitation and temperature.” *Transactions of the ASABE*, 57(5), 1375–1391. doi:10.13031/trans.57.10685.

Cleugh, H. A., Leuning, R., Mu, Q., and Running, S. W. (2007). “Regional evaporation estimates from flux tower and MODIS satellite data.” *Remote Sensing of Environment*, 106(3), 285–304. doi:10.1016/j.rse.2006.07.007.

Cohen, S. J. (1991). “Possible impacts of climatic warming scenarios on water resources in the Saskatchewan River Sub-basin, Canada.” *Climatic Change*, 19(3), 291–317. doi:10.1007/BF00140168.

Conway, D., Nicholls, R. J., Brown, S., Tebboth, M. G. L., Adger, W. N., Ahmad, B., Biemans, H., Crick, F., Lutz, A. F., De Campos, R. S., Said, M., Singh, C., Zaroug, M. A. H., Ludi, E., New, M., and Wester, P. (2019). “The need for bottom-up assessments of climate risks and adaptation in climate-sensitive regions.” *Nature Climate Change*, 9(7), 503–511. doi:10.1038/s41558-019-0502-0.

Cooley, H., and Gleick, P. H. (2011). “Climate-proofing transboundary water agreements.” *Hydrological Sciences Journal*, 56(4), 711–718. doi:10.1080/02626667.2011.576651.

Dai, C., and Qin, X. S. (2019). “Assessment of the effectiveness of a multi-site stochastic weather generator on hydrological modelling in the Red Deer River watershed, Canada.” *Hydrological Sciences Journal*, 64(13), 1616–1628. doi:10.1080/02626667.2019.1661416.

Dessai, S., and Hulme, M. (2004). “Does climate adaptation policy need probabilities?” *Climate Policy*, 4(2), 107–128. doi:10.1080/14693062.2004.9685515.

Dibike, Y., Prowse, T., Bonsal, B., and O’Neil, H. (2017). “Implications of future climate on water availability in the western Canadian river basins.” *International Journal of Climatology*, 37(7), 3247–3263. doi:10.1002/joc.4912.

Dinar, S., Katz, D., De Stefano, L., and Blankespoor, B. (2015). “Climate change, conflict, and cooperation: Global analysis of the effectiveness of international river treaties in addressing water variability.” *Political Geography*, 45, 55–66. doi:10.1016/j.polgeo.2014.08.003.

Dinar, S., Katz, D., De Stefano, L., and Blankespoor, B. (2019). “Do treaties matter? Climate change, water variability, and cooperation along transboundary river basins.” *Political Geography*, 69, 162–172. doi:10.1016/j.polgeo.2018.08.007.

Dittrich, R., Wreford, A., and Moran, D. (2016). “A survey of decision-making approaches for climate change adaptation: Are robust methods the way forward?” *Ecological Economics*, Elsevier B.V., 122, 79–89. doi:10.1016/j.ecolecon.2015.12.006.

Dommenget, D., and Rezny, M. (2018). “A caveat note on tuning in the development of coupled climate models.” *Journal of Advances in Modeling Earth Systems*, 10(1), 78–97. doi:10.1002/2017MS000947.

Dong, L., Leung, L. R., Lu, J., and Gao, Y. (2019). “Contributions of extreme and non-extreme precipitation to California precipitation seasonality changes under warming.” *Geophysical Research Letters*, 46(22), 13470–13478. doi:10.1029/2019GL084225.

Eamen, L., Brouwer, R., and Razavi, S. (2020). “The economic impacts of water supply restrictions due to climate and policy change: A transboundary river basin supply-side input-output analysis.” *Ecological Economics*, 172, 106532. doi:10.1016/j.ecolecon.2019.106532.

Efstratiadis, A., and Koutsoyiannis, D. (2010). “One decade of multi-objective calibration approaches in hydrological modelling: a review.” *Hydrological Sciences Journal*, 55(1), 58–78. doi:10.1080/02626660903526292.

Ehret, U., Zehe, E., Wulfmeyer, V., Warrach-Sagi, K., and Liebert, J. (2012). “HESS Opinions ‘should we apply bias correction to global and regional climate model data?’” *Hydrology and Earth System Sciences*, 16(9), 3391–3404. doi:10.5194/hess-16-3391-2012.

Elshorbagy, A., Wagener, T., Razavi, S., and Sauchyn, D. (2016). “Correlation and causation in tree-ring-based reconstruction of paleohydrology in cold semiarid regions.” *Water Resources Research*, 52(9), 7053–7069. doi:10.1002/2016WR018985.

Fang, X., and Pomeroy, J. (2020). “Diagnosis of future changes in hydrology for a Canadian Rocky Mountain headwater basin.” *Hydrology and Earth System Sciences Discussions*, under disc, 1–40. doi:10.5194/hess-2019-640.

Farinosi, F., Giupponi, C., Reynaud, A., Ceccherini, G., Carmona-Moreno, C., De Roo, A., Gonzalez-Sanchez, D., and Bidoglio, G. (2018). “An innovative approach to the assessment of hydro-political risk: A spatially explicit, data driven indicator of hydro-political issues.” *Global Environmental Change*, 52, 286–313. doi:10.1016/j.gloenvcha.2018.07.001.

Farjad, B., Gupta, A., Razavi, S., Faramarzi, M., and Marceau, D. J. (2017). “An integrated modelling system to predict hydrological processes under climate and land-use/cover change scenarios.” *Water (Switzerland)*, 9(10). doi:10.3390/w9100767.

Fatichi, S., Ivanov, V. Y., and Caporali, E. (2012). “Investigating interannual variability of precipitation at the global scale: is there a connection with seasonality?” *Journal of Climate*, 25(16), 5512–5523. doi:10.1175/JCLI-D-11-00356.1.

Feng, X., Porporato, A., and Rodriguez-Iturbe, I. (2013). “Changes in rainfall seasonality in the tropics.” *Nature Climate Change*, 3(9), 811–815. doi:10.1038/nclimate1907.

Feser, F., Rockel, B., von Storch, H., Winterfeldt, J., and Zahn, M. (2011). “Regional climate models add value to global model data: a review and selected examples.” *Bulletin of the American Meteorological Society*, 92(9), 1181–1192. doi:10.1175/2011BAMS3061.1.

Fischer, E. M., and Knutti, R. (2015). “Anthropogenic contribution to global occurrence of heavy-precipitation and high-temperature extremes.” *Nature Climate Change*, 5(6), 560–564. doi:10.1038/nclimate2617.

Foley, A. M. (2010). “Uncertainty in regional climate modelling: A review.” *Progress in Physical Geography*, 34(5), 647–670. doi:10.1177/0309133310375654.

Forsythe, W. C., Rykiel, E. J., Stahl, R. S., Wu, H., and Schoolfield, R. M. (1995). “A model comparison for daylength as a function of latitude and day of year.” *Ecological Modelling*, 80(1), 87–95. doi:10.1016/0304-3800(94)00034-F.

Foufoula-Georgiou, E., and Lettenmaier, D. P. (1987). “A Markov Renewal Model for rainfall occurrences.” *Water Resources Research*, 23(5), 875–884. doi:10.1029/WR023i005p00875.

Fulkerson, D. R. (1961). “An Out-of-Kilter Method for Minimal-Cost Flow Problems.” *Journal of the Society for Industrial and Applied Mathematics*, 9(1), 18–27. doi:10.1137/0109002.

Gaborit, É., Fortin, V., Xu, X., Seglenieks, F., Tolson, B., Fry, L. M., Hunter, T., Anctil, F., and Gronewold, A. D. (2017). “A hydrological prediction system based on the SVS land-surface scheme: efficient calibration of GEM-Hydro for streamflow simulation over the Lake Ontario basin.” *Hydrology and Earth System Sciences*, 21(9), 4825–4839. doi:10.5194/hess-21-4825-2017.

Gerlak, A. K. (2004). “Strengthening river basin institutions: The global environment facility and the Danube River Basin.” *Water Resources Research*, 40(8), 1–11. doi:10.1029/2003WR002936.

Gerlak, A. K., Lautze, J., and Giordano, M. (2011). “Water resources data and information exchange in transboundary water treaties.” *International Environmental Agreements: Politics, Law and Economics*, 11(2), 179–199. doi:10.1007/s10784-010-9144-4.

Giordano, M. A., and Wolf, A. T. (2003). “Sharing waters: Post-Rio international water management.” *Natural Resources Forum*, 27(2), 163–171. doi:10.1111/1477-8947.00051.

Giordano, M., Drieschova, A., Duncan, J. A., Sayama, Y., De Stefano, L., and Wolf, A. T. (2014). “A review of the evolution and state of transboundary freshwater treaties.” *International Environmental Agreements: Politics, Law and Economics*, 14(3), 245–264.

doi:10.1007/s10784-013-9211-8.
Giorgi, F., Raffaele, F., and Coppola, E. (2018). “The response of precipitation characteristics to global warming from global and regional climate projections.” *Earth System Dynamics Discussions*, 1–41. doi:10.5194/esd-2018-64.
Gleick, P. H. (2003). “Global freshwater resources: soft-path solutions for the 21st century.” *Science*, 302(5650), 1524–1528. doi:10.1126/science.1089967.
Gober, P. (2014). “Decision Making Under Uncertainty: A New Paradigm for Water Resources Planning and Management.” *Modern Water Resources Engineering*, L. K. Wang and C. T. Yang, eds., Humana Press, Totowa, NJ, 411–436. doi:10.1007/978-1-62703-595-8_8.
Government of Alberta. (2020a). *St . Mary River and Milk River Basins - Canadian and American Entitlements*.
Government of Alberta. (2020b). “Master Agreement on Apportionment | Alberta.ca.” <https://www.alberta.ca/master-agreement-on-apportionment.aspx>.
Grover, V. I., and Krantzberg, G. (2015). “Transboundary water management: lessons learnt from North America.” *Water International*, Routledge, 40(1), 183–198. doi:10.1080/02508060.2014.984962.
Guo, D., Westra, S., and Maier, H. R. (2017). “Use of a scenario-neutral approach to identify the key hydro-meteorological attributes that impact runoff from a natural catchment.” *Journal of Hydrology*, Elsevier B.V., 554, 317–330. doi:10.1016/j.jhydrol.2017.09.021.
Guo, D., Westra, S., and Maier, H. R. (2018). “An inverse approach to perturb historical rainfall data for scenario-neutral climate impact studies.” *Journal of Hydrology*, Elsevier B.V., 556, 877–890. doi:10.1016/j.jhydrol.2016.03.025.
Gupta, H. V., and Razavi, S. (2018). “Revisiting the Basis of Sensitivity Analysis for Dynamical Earth System Models.” *Water Resources Research*, 54(11), 8692–8717. doi:10.1029/2018WR022668.
Gupta, H. V., Sorooshian, S., and Yapo, P. O. (1998). “Toward improved calibration of hydrologic models: Multiple and noncommensurable measures of information.” *Water Resources Research*, 34(4), 751–763. doi:10.1029/97WR03495.
Haasnoot, M., Kwakkel, J. H., Walker, W. E., and ter Maat, J. (2013). “Dynamic adaptive policy pathways: A method for crafting robust decisions for a deeply uncertain world.” *Global Environmental Change*, Elsevier Ltd, 23(2), 485–498. doi:10.1016/j.gloenvcha.2012.12.006.
Hadjimichael, A., Quinn, J., and Reed, P. (2020a). “Advancing Diagnostic Model Evaluation to Better Understand Water Shortage Mechanisms in Institutionally Complex River Basins.” *Water Resources Research*, 56(10), 1–25. doi:10.1029/2020WR028079.
Hadjimichael, A., Quinn, J., Wilson, E., Reed, P., Basdekas, L., Yates, D., and Garrison, M. (2020b). “Defining Robustness, Vulnerabilities, and Consequential Scenarios for Diverse Stakeholder Interests in Institutionally Complex River Basins.” *Earth’s Future*, 8(7), 1–22. doi:10.1029/2020EF001503.
Hagemann, S., Chen, C., Clark, D. B., Folwell, S., Gosling, S. N., Haddeland, I., Hanasaki, N., Heinke, J., Ludwig, F., Voss, F., and Wiltshire, A. J. (2013). “Climate change impact on available water resources obtained using multiple global climate and hydrology models.” *Earth System Dynamics*, 4(1), 129–144. doi:10.5194/esd-4-129-2013.
Haghnegahdar, A., Tolson, B. A., Craig, J. R., and Paya, K. T. (2015). “Assessing the performance of a semi-distributed hydrological model under various watershed discretization schemes.” *Hydrological Processes*, 29(18), 4018–4031.

doi:10.1002/hyp.10550.
Haghnegahdar, A., Tolson, B. A., Davison, B., Seglenieks, F. R., Klyszejko, E., Soulis, E. D., Fortin, V., and Matott, L. S. (2014). "Calibrating environment Canada's MESH modelling system over the Great Lakes Basin." *Atmosphere - Ocean*, Taylor & Francis, 52(4), 281–293. doi:10.1080/07055900.2014.939131.
Hall, J. W., Lempert, R. J., Keller, K., Hackbarth, A., Mijere, C., and McInerney, D. J. (2012). "Robust climate policies under uncertainty: a comparison of robust decision making and info-gap methods." *Risk Analysis*, 32(10), 1657–1672. doi:10.1111/j.1539-6924.2012.01802.x.
Halliday, R., and Faveri, G. (2007a). "The St. Mary and Milk Rivers: The 1921 Order Revisited." *Canadian Water Resources Journal*, 32(1), 75–92. doi:10.4296/cwrj3201075.
Halliday, R., and Faveri, G. (2007b). "Response to Comments by S.B. Rood and L.S. Dolan on 'The St. Mary and Milk Rivers: The 1921 Order Revisited.'" *Canadian Water Resources Journal*, 32(4), 339–342. doi:10.4296/cwrj3204339.
Hamon, W. R. (1960). "Estimating Potential Evapotranspiration." Massachusetts Institute of Technology (MIT).
Hamon, W. R. (1963). "Computation of direct runoff amounts from storm rainfall." *International Association of Scientific Hydrology Publication*.
Hanesiak, J. M., Stewart, R. E., Bonsal, B. R., Harder, P., Lawford, R., Aider, R., Amiro, B. D., Atallah, E., Barr, A. G., Black, T. A., Bullock, P., Brimelow, J. C., Brown, R., Carmichael, H., Derksen, C., Flanagan, L. B., Gachon, P., Greene, H., Gyakum, J., Henson, W., Hogg, E. H., Kochtubajda, B., Leighton, H., Lin, C., Luo, Y., McCaughey, J. H., Meinert, A., Shabbar, A., Snelgrove, K., Szeto, K., Trishchenko, A., Van Der Kamp, G., Wang, S., Wen, L., Wheaton, E., Wielki, C., Yang, Y., Yirdaw, S., and Zha, T. (2011). "Characterization and summary of the 1999-2005 Canadian prairie drought." *Atmosphere - Ocean*, 49(4), 421–452. doi:10.1080/07055900.2011.626757.
Harris, C. R., Millman, K. J., van der Walt, S. J., Gommers, R., Virtanen, P., Cournapeau, D., Wieser, E., Taylor, J., Berg, S., Smith, N. J., Kern, R., Picus, M., Hoyer, S., van Kerkwijk, M. H., Brett, M., Haldane, A., del Río, J. F., Wiebe, M., Peterson, P., Gérard-Marchant, P., Sheppard, K., Reddy, T., Weckesser, W., Abbasi, H., Gohlke, C., and Oliphant, T. E. (2020). "Array programming with NumPy." *Nature*, Springer US, 585(7825), 357–362. doi:10.1038/s41586-020-2649-2.
Hashimoto, T., Stedinger, J. R., and Loucks, D. P. (1982). "Reliability, resiliency, and vulnerability criteria for water resource system performance evaluation." *Water Resources Research*, 18(1), 14–20. doi:10.1029/WR018i001p00014.
Hassanzadeh, E., Elshorbagy, A., Wheater, H., Gober, P., and Nazemi, A. (2016). "Integrating supply uncertainties from stochastic modeling into integrated water resource management: case study of the Saskatchewan River Basin." *Journal of Water Resources Planning and Management*, 142(2), 05015006. doi:10.1061/(ASCE)WR.1943-5452.0000581.
Heinmiller, B. T. (2020). "The Boundary Waters Treaty and the International Joint Commission in the St. Mary-Milk Basin." *The first century of the international joint commission*, University of Calgary Press, University of Calgary, AB, 143–164.
Hensel, P. R., McLaughlin Mitchell, S., Sowers, T. E., and Thyne, C. L. (2008). "Bones of contention." *Journal of Conflict Resolution*, 52(1), 117–143. doi:10.1177/0022002707310425.
Herman, J. D., Reed, P. M., Zeff, H. B., and Characklis, G. W. (2015). "How should robustness

be defined for water systems planning under change?" *Journal of Water Resources Planning and Management*, 141(10), 04015012. doi:10.1061/(ASCE)WR.1943-5452.0000509.
Herman, J. D., Zeff, H. B., Lamontagne, J. R., Reed, P. M., and Characklis, G. W. (2016). "Synthetic drought scenario generation to support bottom-up water supply vulnerability assessments." *Journal of Water Resources Planning and Management*, 142(11), 04016050. doi:10.1061/(ASCE)WR.1943-5452.0000701.
Hutchinson, M. F., McKenney, D. W., Lawrence, K., Pedlar, J. H., Hopkinson, R. F., Milewska, E., and Papadopol, P. (2009). "Development and testing of Canada-wide interpolated spatial models of daily minimum-maximum temperature and precipitation for 1961-2003." *Journal of Applied Meteorology and Climatology*, 48(4), 725–741. doi:10.1175/2008JAMC1979.1.
IJC. (1909). *The Boundary Waters Treaty*. *IJC*. doi:10.1111/j.1540-6563.1954.tb00169.x.
IJC. (1921). *International Joint Commission Order - 4 October 1921*. Ottawa, Canada.
IJC. (1948). "IJC Docket No. 57R." <https://www.ijc.org/en/57r> (Jan. 1, 2020).
IJC. (2020). "St. Mary and Milk River Basins | International Joint Commission." <https://ijc.org/en/st-mary-milk-rivers> (Jan. 11, 2021).
ILA. (1966). *Report of the Fifty-Second Conference*. Helsinki.
ILA. (2004). *Report of the Seventy-First Conference*. Berlin.
Ilich, N. (1992). "Improvement of the return flow allocation in the Water Resources Management Model of Alberta Environment." *Canadian Journal of Civil Engineering*, 27(1), 613–621. doi:https://doi-org.cyber.usask.ca/10.1139/l93-078.
Ilich, N. (2008). "Shortcomings of linear programming in optimizing river basin allocation." *Water Resources Research*, 44(2), 1–14. doi:10.1029/2007WR006192.
Ilich, N. (2009). "Limitations of network flow algorithms in river basin modeling." *Journal of Water Resources Planning and Management*, 135(1), 48–55. doi:10.1061/(ASCE)0733-9496(2009)135:1(48).
IPCC. (2018). "Summary for Policymakers." *Global warming of 1.5°C. An IPCC Special Report on the impacts of global warming of 1.5°C above pre-industrial levels and related global greenhouse gas emission pathways, in the context of strengthening the global response to the threat of climate change,* P. Masson-Delmotte, V., H.-O. Zhai, D. Pörtner, J. Roberts, P. R. Skea, and and T. W. Shukla, A. Pirani, W. Moufouma-Okia, C. Péan, R. Pidcock, S. Connors, J.B.R. Matthews, Y. Chen, X. Zhou, M.I. Gomis, E. Lonnoy, T. Maycock, M. Tignor, eds., 1–21.
IPCC Panel. (2014). *Climate Change 2014 Synthesis Report*. Geneva, Switzerland.
Islam, S., and Repella, A. C. (2015). "Water diplomacy: a negotiated approach to manage complex water problems." *Journal of Contemporary Water Research & Education*, 155(1), 1–10. doi:10.1111/j.1936-704X.2015.03190.x.
Islam, Z., and Gan, T. Y. (2012). "Effects of climate change on the surface-water management of the South Saskatchewan River Basin." *Journal of Water Resources Planning and Management*, 140(3), 332–342. doi:10.1061/(asce)wr.1943-5452.0000326.
Islam, Z., and Gan, T. Y. (2015a). "Potential combined hydrologic impacts of climate change and El Niño Southern Oscillation to South Saskatchewan River Basin." *Journal of Hydrology*, Elsevier B.V., 523, 34–48. doi:10.1016/j.jhydrol.2015.01.043.
Islam, Z., and Gan, T. Y. (2015b). "Future irrigation demand of South Saskatchewan River Basin under the combined impacts of climate change and El Niño southern oscillation." *Water Resources Management*, 29(6), 2091–2105. doi:10.1007/s11269-015-0930-1.

Islam, Z., and Gan, T. Y. (2016). “Water allocation challenges of South Saskatchewan River Basin under the combined impacts of climate change and El Nino southern oscillation.” *Journal of Water Resources Planning and Management*, 142(10), 1–11. doi:10.1061/(ASCE)WR.1943-5452 .0000683.

Iyob, B. (2010). “Resilience and adaptability of transboundary rivers: the principle of equitable distribution of benefits and the institutional capacity of the Nile Basin.” Oregon State University.

Jetoo, S., Thorn, A., Friedman, K., Gosman, S., and Krantzberg, G. (2015). “Governance and geopolitics as drivers of change in the Great Lakes-St. Lawrence basin.” *Journal of Great Lakes Research*, International Association for Great Lakes Research., 41(S1), 108–118. doi:10.1016/j.jglr.2014.11.011.

Judgment. (1997). *Gabĉìkovo-Nagymaros Project (Hungary/Slovakia)*. *I.C.J. Reports*.

Kalbhenn, A., and Bernauer, T. (2012). “International Water Cooperation and Conflict: a new event dataset.” *SSRN Electronic Journal*. doi:10.2139/ssrn.2176609.

Kasprzyk, J. R., Reed, P. M., Characklis, G. W., and Kirsch, B. R. (2012). “Many-objective de Novo water supply portfolio planning under deep uncertainty.” *Environmental Modelling & Software*, 34, 87–104. doi:10.1016/j.envsoft.2011.04.003.

Kienzle, S. W., Nemeth, M. W., Byrne, J. M., and MacDonald, R. J. (2012). “Simulating the hydrological impacts of climate change in the upper North Saskatchewan River basin, Alberta, Canada.” *Journal of Hydrology*, 412–413, 76–89. doi:10.1016/j.jhydrol.2011.01.058.

Kim, H. W., Hwang, K., Mu, Q., Lee, S. O., and Choi, M. (2012). “Validation of MODIS 16 global terrestrial evapotranspiration products in various climates and land cover types in Asia.” *KSCE Journal of Civil Engineering*, 16(2), 229–238. doi:10.1007/s12205-012-0006-1.

Kirsch, B. R., Characklis, G. W., and Zeff, H. B. (2013). “Evaluating the impact of alternative hydro-climate scenarios on transfer agreements: practical improvement for generating synthetic streamflows.” *Journal of Water Resources Planning and Management*, 139(4), 396–406. doi:10.1061/(ASCE)WR.1943-5452.0000287.

Knight, F. H. (1921). *Risk, Uncertainty and Profit*. Schaffner & Marx, New York.

Knutti, R., and Sedláček, J. (2013). “Robustness and uncertainties in the new CMIP5 climate model projections.” *Nature Climate Change*, Nature Publishing Group, 3(4), 369–373. doi:10.1038/nclimate1716.

Kuenzer, C., Campbell, I., Roch, M., Leinenkugel, P., Tuan, V. Q., and Dech, S. (2013). “Understanding the impact of hydropower developments in the context of upstream–downstream relations in the Mekong river basin.” *Sustainability Science*, 8(4), 565–584. doi:10.1007/s11625-012-0195-z.

Kwakkel, J. H., Haasnoot, M., and Walker, W. E. (2016). “Comparing robust decision-making and dynamic adaptive policy pathways for model-based decision support under deep uncertainty.” *Environmental Modelling and Software*, 86, 168–183. doi:10.1016/j.envsoft.2016.09.017.

Kwakkel, J. H., Walker, W. E., and Marchau, V. A. W. J. (2010). “Classifying and communicating uncertainties in model-based policy analysis.” *International Journal of Technology, Policy and Management*, 10(4), 299. doi:10.1504/IJTPM.2010.036918.

Labadie, J. W. (2010). *MODSIM: River basin management decision support system*. *Users Manual and Documentation*, Fort Collins, CO.

Landovsky, J. (2006). *Institutional assessment of transboundary water resources management - human development report*.
Landovsky, J. (2011). "Conflict and cooperation in transboundary watersheds." Charles University.
Lempert, R. J., and Collins, M. T. (2007). "Managing the risk of uncertain threshold responses: Comparison of robust, optimum, and precautionary approaches." *Risk Analysis*, 27(4), 1009–1026. doi:10.1111/j.1539-6924.2007.00940.x.
Lempert, R. J., Popper, S. W., and Bankes, S. C. (2003). *Shaping the next one hundred years: new methods for quantitative, long-term policy analysis*. RAND, Santa Monica, CA.
Lempert, R. J., Popper, S. W., and Bankes, S. C. (2010). "Robust decision making: coping with uncertainty." *Futurist*, 44(1), 47–48.
Lempert, R., Nakicenovic, N., Sarewitz, D., and Schlesinger, M. (2004). "Characterizing climate-change uncertainties for decision-makers. An editorial essay." *Climatic Change*, 65, 1–9. doi:10.1023/B:CLIM.0000037561.75281.b3.
Lindström, G., Johansson, B., Persson, M., Gardelin, M., and Bergström, S. (1997). "Development and test of the distributed HBV-96 hydrological model." *Journal of Hydrology*, 201(1–4), 272–288. doi:10.1016/S0022-1694(97)00041-3.
Lu, J., Sun, G., McNulty, S. G., and Amatya, D. M. (2005). "A comparison of six potential evapotranspiration methods for regional use in the southeastern United States." *Journal of the American Water Resources Association*, 41(3), 621–633. doi:10.1111/j.1752-1688.2005.tb03759.x.
MacDonald, R. J., Byrne, J. M., Boon, S., and Kienzle, S. W. (2012). "Modelling the potential impacts of climate change on snowpack in the North Saskatchewan River watershed, Alberta." *Water Resources Management*, 26(11), 3053–3076. doi:10.1007/s11269-012-0016-2.
MacKinnon, B. D., Sagin, J., Baulch, H. M., Lindenschmidt, K. E., and Jardine, T. D. (2015). "Influence of hydrological connectivity on winter limnology in floodplain lakes of the Saskatchewan River Delta, Saskatchewan." *Canadian Journal of Fisheries and Aquatic Sciences*, 73(1), 140–152. doi:10.1139/cjfas-2015-0210.
Maier, H. R., Guillaume, J. H. A., van Delden, H., Riddell, G. A., Haasnoot, M., and Kwakkel, J. H. (2016). "An uncertain future, deep uncertainty, scenarios, robustness and adaptation: How do they fit together?" *Environmental Modelling & Software*, 81, 154–164. doi:10.1016/j.envsoft.2016.03.014.
Maraun, D. (2016). "Bias correcting climate change simulations - a critical review." *Current Climate Change Reports*, Current Climate Change Reports, 2(4), 211–220. doi:10.1007/s40641-016-0050-x.
Maraun, D., Shepherd, T. G., Widmann, M., Zappa, G., Walton, D., Gutiérrez, J. M., Hagemann, S., Richter, I., Soares, P. M. M., Hall, A., and Mearns, L. O. (2017). "Towards process-informed bias correction of climate change simulations." *Nature Climate Change*, 7(11), 764–773. doi:10.1038/nclimate3418.
Matalas, N. C. (1967). "Mathematical assessment of synthetic hydrology." *Water Resources Research*, 3(4), 937–945. doi:10.1029/WR003i004p00937.
Matrosov, E. S., Woods, A. M., and Harou, J. J. (2013). "Robust Decision Making and Info-Gap Decision Theory for water resource system planning." *Journal of Hydrology*, 494, 43–58. doi:10.1016/j.jhydrol.2013.03.006.
McCabe, G. J., Hay, L. E., Bock, A., Markstrom, S. L., and Atkinson, R. D. (2015). "Inter-

annual and spatial variability of Hamon potential evapotranspiration model coefficients." *Journal of Hydrology*, Elsevier B.V., 521, 389–394. doi:10.1016/j.jhydrol.2014.12.006.
McCracken, M., and Meyer, C. (2018). "Monitoring of transboundary water cooperation: Review of Sustainable Development Goal Indicator 6.5.2 methodology." *Journal of Hydrology*, 563, 1–12. doi:10.1016/j.jhydrol.2018.05.013.
McCracken, M., and Wolf, A. T. (2019). "Updating the register of international river basins of the world." *International Journal of Water Resources Development*, 35(5), 732–782. doi:10.1080/07900627.2019.1572497.
McKague, K., Rudra, R., Ogilvie, J., Ahmed, I., and Gharabaghi, B. (2005). "Evaluation of weather generator climgen for southern ontario." *Canadian Water Resources Journal*, 30(4), 315–330. doi:10.4296/cwrj3004315.
McLane, R. P. (2010). "The St. Mary River and the Milk River: Two Rivers, One Stream." *University of Denver Water Law Review*, 14, 131–158.
McNally, A., Magee, D., and Wolf, A. T. (2009). "Hydropower and sustainability: Resilience and vulnerability in China's powersheds." *Journal of Environmental Management*, 90(SUPPL. 3), S286–S293. doi:10.1016/j.jenvman.2008.07.029.
McPhail, C., Maier, H. R., Kwakkel, J. H., Giuliani, M., Castelletti, A., and Westra, S. (2018). "Robustness metrics: how are they calculated, when should they be used and why do they give different results?" *Earth's Future*, 6(2), 169–191. doi:10.1002/2017EF000649.
Mearns, L., McGinnis, S., Korytina, D., Arritt, R., Biner, S., Bukovsky, M., Chang, H.-I., Christensen, O., Herzmann, D., Jiao, Y., Kharin, S., Lazare, M., Nikulin, G., Qian, M., Scinocca, J., Winger, K., Castro, C., Frigon, A., and Gutowski, W. (2020). "The NA-CORDEX dataset, Version 1.0." *NCAR Climate Data Gateway, Boulder CO*. doi:10.5065/D6SJ1JCH.
Milly, P. C. D., Betancourt, J., Falkenmark, M., Hirsch, R. M., Kundzewicz, Z. W., Lettenmaier, D. P., and Stouffer, R. J. (2008). "Stationarity is dead: whither water management?" *Science*, 319(5863), 573–574. doi:10.1126/science.1151915.
Milly, P. C. D., and Dunne, K. A. (2017). "A hydrologic drying bias in water-resource impact analyses of anthropogenic climate change." *Journal of the American Water Resources Association*, 53(4), 822–838. doi:10.1111/1752-1688.12538.
Miner, M., Patankar, G., Gamkhar, S., and Eaton, D. J. (2009). "Water sharing between India and Pakistan: A critical evaluation of the Indus Water Treaty." *Water International*, 34(2), 204–216. doi:10.1080/02508060902902193.
Mitchell, S. M., and Zawahri, N. A. (2015). "The effectiveness of treaty design in addressing water disputes." *Journal of Peace Research*, 52(2), 187–200. doi:10.1177/0022343314559623.
Moallemi, E. A., Elsawah, S., and Ryan, M. J. (2020a). "Robust decision making and Epoch–Era analysis: A comparison of two robustness frameworks for decision-making under uncertainty." *Technological Forecasting and Social Change*, Elsevier, 151, 119797. doi:10.1016/j.techfore.2019.119797.
Moallemi, E. A., Kwakkel, J., de Haan, F. J., and Bryan, B. A. (2020b). "Exploratory modeling for analyzing coupled human-natural systems under uncertainty." *Global Environmental Change*, Elsevier Ltd, 65(November 2019), 102186. doi:10.1016/j.gloenvcha.2020.102186.
Morales-Marín, L., Wheater, H., and Lindenschmidt, K. E. (2018). "Potential changes of annual-averaged nutrient export in the South Saskatchewan River Basin under climate and land-use change scenarios." *Water (Switzerland)*, 10(10). doi:10.3390/w10101438.

Mu, Q., Zhao, M., and Running, S. W. (2011). “Improvements to a MODIS global terrestrial evapotranspiration algorithm.” *Remote Sensing of Environment*, Elsevier Inc., 115(8), 1781–1800. doi:10.1016/j.rse.2011.02.019.

Mu, Q., Zhao, M., and Running, S. W. (2013). *MODIS Global Terrestrial Evapotranspiration (ET) Product (NASA MOD16A2/A3) Algorithm Theoretical Basis Document Collection 5*. *Numerical Terradynamic Simulation Group*, Missoula, MT.

Nagheeby, M., and Warner, J. (2018). “The geopolitical overlay of the hydropolitics of the Harirud River Basin.” *International Environmental Agreements: Politics, Law and Economics*, Springer Netherlands, 18(6), 839–860. doi:10.1007/s10784-018-9418-9.

Nash, J. E., and Sutcliffe, J. V. (1970). “River flow forecasting through conceptual models part I — A discussion of principles.” *Journal of Hydrology*, 10(3), 282–290. doi:10.1016/0022-1694(70)90255-6.

Navarro-Racines, C., Tarapues, J., Thornton, P., Jarvis, A., and Ramirez-Villegas, J. (2020). “High-resolution and bias-corrected CMIP5 projections for climate change impact assessments.” *Scientific Data*, 7(1), 1–14. doi:10.1038/s41597-019-0343-8.

Nazemi, A., Wheater, H. S., Chun, K. P., and Elshorbagy, A. (2013). “A stochastic reconstruction framework for analysis of water resource system vulnerability to climate-induced changes in river flow regime.” *Water Resources Research*, 49(1), 291–305. doi:10.1029/2012WR012755.

Norman, E. S., and Bakker, K. (2015). “Do good fences make good neighbours? Canada–United States transboundary water governance, the Boundary Waters Treaty, and twenty-first-century challenges.” *Water International*, Routledge, 40(1), 199–213. doi:10.1080/02508060.2014.978973.

O’Gorman, P. A. (2015). “Precipitation extremes under climate change.” *Current Climate Change Reports*, 1(2), 49–59. doi:10.1007/s40641-015-0009-3.

Do Ó, A. (2012). “Drought planning and management in transboundary river basins: The case of the Iberian Guadiana.” *Water Policy*, 14(5), 784–799. doi:10.2166/wp.2012.173.

Odom, O., and Wolf, A. T. (2011). “Institutional resilience and climate variability in international water treaties: the Jordan River Basin as ‘proof-of-concept.’” *Hydrological Sciences Journal*, 56(4), 703–710. doi:10.1080/02626667.2011.574138.

Olsson, T., Jakkila, J., Veijalainen, N., Backman, L., Kaurola, J., and Vehviläinen, B. (2015). “Impacts of climate change on temperature, precipitation and hydrology in Finland - Studies using bias corrected Regional Climate Model data.” *Hydrology and Earth System Sciences*, 19(7), 3217–3238. doi:10.5194/hess-19-3217-2015.

Oregan State University Institute for Water and Watersheds. (2017). “Transboundary Freshwater Dispute Database.”

Oreskes, N., Shrader-Frechette, K., and Belitz, K. (1994). “Verification, validation, and confirmation of numerical models in the Earth sciences.” *Science*, 263(5147), 641–646. doi:10.1126/science.263.5147.641.

Parker, A. M., Srinivasan, S. V., Lempert, R. J., and Berry, S. H. (2015). “Evaluating simulation-derived scenarios for effective decision support.” *Technological Forecasting and Social Change*, Elsevier Inc., 91, 64–77. doi:10.1016/j.techfore.2014.01.010.

Patt, A. G., and Schrag, D. P. (2003). “Using specific language to describe risk.” *Climate Change*, 61, 17–30. doi:10.1023/A:1026314523443.

Petersen-Perlman, J. D., Veilleux, J. C., and Wolf, A. T. (2017). “International water conflict and cooperation: challenges and opportunities.” *Water International*, Routledge, 42(2), 105–

120. doi:10.1080/02508060.2017.1276041.
Pietroniro, A., and Kilpatrick, J. (2020). *Report to the International Joint Commission on the Division of the Waters of the St. Mary and Milk Rivers*.
Pingale, S. M., Jat, M. K., and Khare, D. (2014). "Integrated urban water management modelling under climate change scenarios." *Resources, Conservation and Recycling*, 83, 176–189. doi:10.1016/j.resconrec.2013.10.006.
Pomeroy, J. W., de Boer, D., and Martz, L. W. (2005). *Hydrology and water resources of Saskatchewan*. Saskatoon.
Pomeroy, J. W., Fang, X., and Williams, B. (2009). *Impacts of Climate Change on Saskatchewan's Water Resources*. *University of Saskatchewan*.
PPWB. (1976). *Determination of Natural Flow for Apportionment Purposes*.
PPWB. (2015). "The 1969 Master Agreement on Apportionment and By-laws, Rules and Procedures." Prairie Provinces Water Board, Regina, SK.
PPWB. (2020a). "Prairie Provinces Water Board - South Saskatchewan River." <https://www.ppwb.ca/surface-water-quantity-activities/goal-1-achieve-apportionment-requirements/ppwb-water-quantity-monitoring-sites-and-data/south-saskatchewan-river> (Jan. 6, 2021).
PPWB. (2020b). "Prairie Provinces Water Board - North Saskatchewan River." <https://www.ppwb.ca/surface-water-quantity-activities/goal-1-achieve-apportionment-requirements/ppwb-water-quantity-monitoring-sites-and-data/north-saskatchewan-river> (Jan. 6, 2021).
PPWB. (2020c). "Prairie Provinces Water Board - Saskatchewan River." <https://www.ppwb.ca/surface-water-quantity-activities/goal-1-achieve-apportionment-requirements/ppwb-water-quantity-monitoring-sites-and-data/saskatchewan-river> (Jan. 6, 2021).
Prudhomme, C., Wilby, R. L., Crooks, S., Kay, A. L., and Reynard, N. S. (2010). "Scenario-neutral approach to climate change impact studies: Application to flood risk." *Journal of Hydrology*, 390, 198–209. doi:10.1016/j.jhydrol.2010.06.043.
Quinn, J. D., Hadjimichael, A., Reed, P. M., and Steinschneider, S. (2020). "Can exploratory modeling of water scarcity vulnerabilities and robustness be scenario neutral?" *Earth's Future*, 8, 1–25. doi:10.1029/2020EF001650.
Quinn, J. D., Reed, P. M., Giuliani, M., Castelletti, A., Oyler, J. W., and Nicholas, R. E. (2018). "Exploring how changing Monsoonal dynamics and human pressures challenge multireservoir management for flood protection, hydropower production, and agricultural water supply." *Water Resources Research*, 54(7), 4638–4662. doi:10.1029/2018WR022743.
Racsko, P., Szeidl, L., and Semenov, M. (1991). "A serial approach to local stochastic weather models." *Ecological Modelling*, 57(1–2), 27–41. doi:10.1016/0304-3800(91)90053-4.
Ray, P. A., Bonzanigo, L., Wi, S., Yang, Y.-C. E., Karki, P., García, L. E., Rodriguez, D. J., and Brown, C. M. (2018). "Multidimensional stress test for hydropower investments facing climate, geophysical and financial uncertainty." *Global Environmental Change*, 48, 168–181. doi:10.1016/j.gloenvcha.2017.11.013.
Ray, P. A., and Brown, C. M. (2015). *Confronting Climate Uncertainty in Water Resources Planning and Project Design: The Decision Tree Framework*. The World Bank, Washington, D. C. doi:10.1596/978-1-4648-0477-9.
Razavi, S., Asadzadeh, M., Tolson, B., Fay, D., Moin, S., Bruxer, J., and Fan, Y. (2014). "Evaluation of New Control Structures for Regulating the Great Lakes System:

Multiscenario, Multireservoir Optimization Approach." *Journal of Water Resources Planning and Management*, 140(8), 04014018. doi:10.1061/(ASCE)WR.1943-5452.0000375.

Razavi, S., Elshorbagy, A., Wheater, H., and Sauchyn, D. (2015). "Toward understanding nonstationarity in climate and hydrology through tree ring proxy records." *Water Resources Research*, 51(3), 1813–1830. doi:10.1002/2014WR015696.

Razavi, S., Elshorbagy, A., Wheater, H., and Sauchyn, D. (2016). "Time scale effect and uncertainty in reconstruction of paleo-hydrology." *Hydrological Processes*, 30(13), 1985–1999. doi:10.1002/hyp.10754.

Razavi, S., and Gupta, H. V. (2019). "A multi-method Generalized Global Sensitivity Matrix approach to accounting for the dynamical nature of earth and environmental systems models." *Environmental Modelling and Software*, Elsevier, 114(April 2018), 1–11. doi:10.1016/j.envsoft.2018.12.002.

Razavi, S., Sheikholeslami, R., Gupta, H. V., and Haghnegahdar, A. (2019). "VARS-TOOL: A toolbox for comprehensive, efficient, and robust sensitivity and uncertainty analysis." *Environmental Modelling and Software*, Elsevier, 112(October 2018), 95–107. doi:10.1016/j.envsoft.2018.10.005.

Reed, P. M., and Kasprzyk, J. (2009). "Water resources management: the myth, the wicked, and the future." *Journal of Water Resources Planning and Management*, 135(6), 411–413. doi:10.1061/(ASCE)WR.1943-5452.0000047.

Refsgaard, J. C., Sonnenborg, T. O., Butts, M. B., Christensen, J. H., Christensen, S., Drews, M., Jensen, K. H., Jørgensen, F., Jørgensen, L. F., Larsen, M. A. D., Rasmussen, S. H., Seaby, L. P., Seifert, D., and Vilhelmsen, T. N. (2016). "Climate change impacts on groundwater hydrology – where are the main uncertainties and can they be reduced?" *Hydrological Sciences Journal*, Taylor & Francis, 61(13), 2312–2324. doi:10.1080/02626667.2015.1131899.

Richardson, C. W. (1981). "Stochastic simulation of daily precipitation, temperature, and solar radiation." *Water Resources Research*, 17(1), 182–190. doi:10.1029/WR017i001p00182.

Richardson, C. W., and Wright, D. A. (1984). *WGEN : A Model for Generating Daily Weather Variables*. *U. S. Department of Agriculture, Agricultural Research Service, ARS-8*, Washington, D. C.

Rieu-Clarke, A. (2019). "From treaty practice to the UN Watercourses Convention." *Research Handbook on International Water Law*, S. C. Mccaffrey, C. Leb, and R. T. Denoon, eds., Edward Elgar, 11–25.

Rittel, H. W. J., and Webber, M. M. (1973). "Dilemmas in a general theory of planning." *Policy Sciences*, 4(2), 155–169. doi:10.1007/BF01405730.

Roach, T., Kapelan, Z., Ledbetter, R., and Ledbetter, M. (2016). "Comparison of robust optimization and info-gap methods for water resource management under deep uncertainty." *Journal of Water Resources Planning and Management*, 142(9), 04016028. doi:10.1061/(ASCE)WR.1943-5452.0000660.

Safaei, S. (2018). "Characterization of uncertainty in model parameter and precipitation data across several headwater catchments in the Canadian Rockies: a large-sample hydrology approach." University of Saskatchewan.

Salman, S. M. A. (2007). "The Helsinki Rules, the UN Watercourses Convention and the Berlin Rules: perspectives on international water law." *International Journal of Water Resources Development*, 23(4), 625–640. doi:10.1080/07900620701488562.

Sapountzaki, K., and Daskalakis, I. (2016). “Transboundary resilience: the case of social-hydrological systems facing water scarcity or drought.” *Journal of Risk Research*, Routledge, 19(7), 829–846. doi:10.1080/13669877.2015.1057202.

Sauchyn, D. J., St-Jacques, J. M., Barrow, E., Nemeth, M. W., Macdonald, R. J., Sheer, A. M. S., and Sheer, D. P. (2016). “Adaptive water resource planning in the South Saskatchewan River Basin: use of scenarios of hydroclimatic variability and extremes.” *Journal of the American Water Resources Association*, 52(1), 222–240. doi:10.1111/1752-1688.12378.

Schindler, D. W., Hecky, R. E., and McCullough, G. K. (2012). “The rapid eutrophication of Lake Winnipeg: Greening under global change.” *Journal of Great Lakes Research*, 38(SUPPL. 3), 6–13. doi:10.1016/j.jglr.2012.04.003.

Schlabing, D., Frassl, M. A., Eder, M. M., Rinke, K., and Bárdossy, A. (2014). “Use of a weather generator for simulating climate change effects on ecosystems: A case study on Lake Constance.” *Environmental Modelling & Software*, 61, 326–338. doi:10.1016/j.envsoft.2014.06.028.

Schlef, K. E., Steinschneider, S., and Brown, C. M. (2018). “Spatiotemporal impacts of climate and demand on water supply in the Apalachicola-Chattahoochee-Flint Basin.” *Journal of Water Resources Planning and Management*, 144(2), 05017020. doi:10.1061/(ASCE)WR.1943-5452.0000865.

Schmeier, S., Gerlak, A. K., and Blumstein, S. (2016). “Clearing the muddy waters of shared watercourses governance: conceptualizing international River Basin Organizations.” *International Environmental Agreements: Politics, Law and Economics*, 16(4), 597–619. doi:10.1007/s10784-015-9287-4.

Schmeier, S., and Shubber, Z. (2018). “Anchoring water diplomacy – The legal nature of international river basin organizations.” *Journal of Hydrology*, 567, 114–120. doi:10.1016/j.jhydrol.2018.09.054.

Schoof, J. T. (2013). “Statistical downscaling in climatology.” *Geography Compass*, 7(4), 249–265. doi:10.1111/gec3.12036.

Scinocca, J. F., Kharin, V. V., Jiao, Y., Qian, M. W., Lazare, M., Solheim, L., Flato, G. M., Biner, S., Desgagne, M., and Dugas, B. (2016). “Coordinated global and regional climate modeling.” *Journal of Climate*, 29(1), 17–35. doi:10.1175/JCLI-D-15-0161.1.

Seibert, J. (1997). “Estimation of parameter uncertainty in the HBV model.” *Nordic Hydrology*, 28(4–5), 247–262. doi:10.2166/nh.1998.15.

Shabbar, A., and Bonsal, B. (2003). “An assessment of changes in winter cold and warm spells over Canada.” *Natural Hazards*, 29(2), 173–188. doi:10.1023/A:1023639209987.

Shah, S. M. A. (2020). “Integrated water resources management in a transboundary river basin: model development and sensitivity analysis.” University of Saskatchewan.

Shah, S. M. A., Razavi, S., Slaughter, A. R., Do, N. C., Carlson, H., Keshavarz, K., Eamen, L., Elshorbagy, A., Wheater, H. S., and Asadzadeh, M. (2021). “Integrated Modelling and Management of Complex Transboundary River Systems.” *Water Resources Management*, under revi.

Sheffield, J., Goteti, G., and Wood, E. F. (2006). “Development of a 50-year high-resolution global dataset of meteorological forcings for land surface modeling.” *Journal of Climate*, 19(13), 3088–3111. doi:10.1175/JCLI3790.1.

Shen, M., Chen, J., Zhuan, M., Chen, H., Xu, C. Y., and Xiong, L. (2018). “Estimating uncertainty and its temporal variation related to global climate models in quantifying climate change impacts on hydrology.” *Journal of Hydrology*, 556, 10–24.

doi:10.1016/j.jhydrol.2017.11.004.
Shiklomanov, I. A. (1993). "World fresh water resources." *Water in crisis: a guide to the world's fresh water resources*, P. H. Gleick, ed., Oxford University Press, New York, 13–23.
Shmueli, D. F. (1999). "Water quality in international river basins." *Political Geography*, 18(4), 437–476. doi:10.1016/S0962-6298(98)00106-1.
Shook, K., and Pomeroy, J. (2012). "Changes in the hydrological character of rainfall on the Canadian prairies." *Hydrological Processes*, 26(12), 1752–1766. doi:10.1002/hyp.9383.
Shrestha, S., Shrestha, M., and Babel, M. S. (2016). "Modelling the potential impacts of climate change on hydrology and water resources in the Indrawati River Basin, Nepal." *Environmental Earth Sciences*, 75(4), 1–13. doi:10.1007/s12665-015-5150-8.
Slaughter, A. R., and Razavi, S. (2020). "Paleo-hydrologic reconstruction of 400 years of past flows at a weekly time step for major rivers of Western Canada." *Earth System Science Data*, 12(1), 231–243. doi:10.5194/essd-12-231-2020.
Smith, K. A., Wilby, R. L., Broderick, C., Prudhomme, C., Matthews, T., Harrigan, S., and Murphy, C. (2018). "Navigating cascades of uncertainty — as easy as ABC? not quite…." *Journal of Extreme Events*, 5(1), 1850007. doi:10.1142/S2345737618500070.
Spector, B. I. (2000). "Motivating water diplomacy: finding the situational incentives to negotiate." *International Negotiation*, 5(2), 223–236. doi:10.1163/15718060020848749.
Stainforth, D. A., Downing, T. E., Washington, R., Lopez, A., and New, M. (2007). "Issues in the interpretation of climate model ensembles to inform decisions." *Philosophical Transactions of the Royal Society A: Mathematical, Physical and Engineering Sciences*, 365(1857), 2163–2177. doi:10.1098/rsta.2007.2073.
Steele-Dunne, S., Lynch, P., McGrath, R., Semmler, T., Wang, S., Hanafin, J., and Nolan, P. (2008). "The impacts of climate change on hydrology in Ireland." *Journal of Hydrology*, 356, 28–45. doi:10.1016/j.jhydrol.2008.03.025.
De Stefano, L., Duncan, J., Dinar, S., Stahl, K., Strzepek, K. M., and Wolf, A. T. (2012). "Climate change and the institutional resilience of international river basins." *Journal of Peace Research*, 49(1), 193–209. doi:10.1177/0022343311427416.
De Stefano, L., Edwards, P., De Silva, L., and Wolf, A. T. (2010). "Tracking cooperation and conflict in international basins: Historic and recent trends." *Water Policy*, 12(6), 871–884. doi:10.2166/wp.2010.137.
De Stefano, L., Petersen-Perlman, J. D., Sproles, E. A., Eynard, J., and Wolf, A. T. (2017). "Assessment of transboundary river basins for potential hydro-political tensions." *Global Environmental Change*, 45, 35–46. doi:10.1016/j.gloenvcha.2017.04.008.
Steinschneider, S., and Brown, C. (2013). "A semiparametric multivariate, multisite weather generator with low-frequency variability for use in climate risk assessments." *Water Resources Research*, 49(11), 7205–7220. doi:10.1002/wrcr.20528.
Stockholm Water Institute (SEI). (2020). "Water Evaluation and Planning."
Subramanian, A., Brown, B., and Wolf, A. T. (2014). "Understanding and overcoming risks to cooperation along transboundary rivers." *Water Policy*, 16(5), 824–843. doi:10.2166/wp.2014.010.
Sushama, L., Khaliq, N., and Laprise, R. (2010). "Dry spell characteristics over Canada in a changing climate as simulated by the Canadian RCM." *Global and Planetary Change*, Elsevier B.V., 74(1), 1–14. doi:10.1016/j.gloplacha.2010.07.004.
Széles, B., Parajka, J., Hogan, P., Silasari, R., Pavlin, L., Strauss, P., and Blöschl, G. (2020). "The added value of different data types for calibrating and testing a hydrologic model in a

small catchment." *Water Resources Research*. doi:10.1029/2019wr026153.
Taleb, N. N. (2007). *The Black Swan*. Random House, New York.
Tanzeeba, S., and Gan, T. Y. (2012). "Potential impact of climate change on the water availability of South Saskatchewan River Basin." *Climatic Change*, 112(2), 355–386. doi:10.1007/s10584-011-0221-7.
Tariku, T. B., and Gan, T. Y. (2018). "Sensitivity of the weather research and forecasting model to parameterization schemes for regional climate of Nile River Basin." *Climate Dynamics*, 50, 4231–4247. doi:10.1007/s00382-017-3870-z.
Thissen, W., Kwakkel, J., Mens, M., van der Sluijs, J., Stemberger, S., Wardekker, A., and Wildschut, D. (2017). "Dealing with uncertainties in fresh water supply: experiences in the Netherlands." *Water Resources Management*, Water Resources Management, 31(2), 703–725. doi:10.1007/s11269-015-1198-1.
Tir, J., and Stinnett, D. M. (2012). "Weathering climate change: Can institutions mitigate international water conflict?" *Journal of Peace Research*, 49(1), 211–225. doi:10.1177/0022343311427066.
Tolson, B. A., and Shoemaker, C. A. (2007). "Dynamically dimensioned search algorithm for computationally efficient watershed model calibration." *Water Resources Research*, 43(1), 1–16. doi:10.1029/2005WR004723.
Trenberth, K. E. (2011). "Changes in precipitation with climate change." *Climate Research*, 47(1–2), 123–138. doi:10.3354/cr00953.
Troell, J., and Swanson, G. (2014). "Adaptive water governance and the principles of international water law." *Transboundary Water Governance: Adaptation to Climate Change*, J. C. Sanchez and R. Joshua, eds., Gland, Switzerland, 23–50.
UN. (1997). *Convention on the Law of the Non-Navigational Uses of International Watercourses*. New york.
UNECE. (2013). *Convention on the Protection and Use of Transboundary Watercourses and International Lakes*. New York and Geneva.
UNECE. (2016). *Water and Climate Change Adaptation in Transboundary Basins*. *Water and Climate Change Adaptation in Transboundary Basins*. doi:10.18356/ad5d8295-en.
UNEP-DHI, and UNEP. (2016). *Transboundary River Basins: Status and Trends, Summary for Policy Makers*. Nairobi.
Virtanen, P., Gommers, R., Oliphant, T. E., Haberland, M., Reddy, T., Cournapeau, D., Burovski, E., Peterson, P., Weckesser, W., Bright, J., van der Walt, S. J., Brett, M., Wilson, J., Millman, K. J., Mayorov, N., Nelson, A. R. J., Jones, E., Kern, R., Larson, E., Carey, C. J., Polat, İ., Feng, Y., Moore, E. W., VanderPlas, J., Laxalde, D., Perktold, J., Cimrman, R., Henriksen, I., Quintero, E. A., Harris, C. R., Archibald, A. M., Ribeiro, A. H., Pedregosa, F., van Mulbregt, P., Vijaykumar, A., Bardelli, A. Pietro, Rothberg, A., Hilboll, A., Kloeckner, A., Scopatz, A., Lee, A., Rokem, A., Woods, C. N., Fulton, C., Masson, C., Häggström, C., Fitzgerald, C., Nicholson, D. A., Hagen, D. R., Pasechnik, D. V., Olivetti, E., Martin, E., Wieser, E., Silva, F., Lenders, F., Wilhelm, F., Young, G., Price, G. A., Ingold, G. L., Allen, G. E., Lee, G. R., Audren, H., Probst, I., Dietrich, J. P., Silterra, J., Webber, J. T., Slavič, J., Nothman, J., Buchner, J., Kulick, J., Schönberger, J. L., de Miranda Cardoso, J. V., Reimer, J., Harrington, J., Rodríguez, J. L. C., Nunez-Iglesias, J., Kuczynski, J., Tritz, K., Thoma, M., Newville, M., Kümmerer, M., Bolingbroke, M., Tartre, M., Pak, M., Smith, N. J., Nowaczyk, N., Shebanov, N., Pavlyk, O., Brodtkorb, P. A., Lee, P., McGibbon, R. T., Feldbauer, R., Lewis, S., Tygier, S., Sievert, S., Vigna, S., Peterson,

S., More, S., Pudlik, T., Oshima, T., Pingel, T. J., Robitaille, T. P., Spura, T., Jones, T. R., Cera, T., Leslie, T., Zito, T., Krauss, T., Upadhyay, U., Halchenko, Y. O., and Vázquez-Baeza, Y. (2020). "SciPy 1.0: fundamental algorithms for scientific computing in Python." *Nature Methods*, 17(3), 261–272. doi:10.1038/s41592-019-0686-2.

Walker, W. E., Lempert, R. J., and Kwakkel, J. H. (2013). "Deep Uncertainty." *Encyclopedia of Operations Research and Management Science*, S. I. Gass and M. C. Fu, eds., Springer US, Boston, MA, 395–402. doi:10.1007/978-1-4419-1153-7.

Wallis, T. W. R., and Griffiths, J. F. (1995). "An assessment of the weather generator (WXGEN) used in the erosion/productivity impact calculator (EPIC)." *Agricultural and Forest Meteorology*, 73, 115–133. doi:10.1016/0168-1923(94)02172-G.

Ward, F. A. (2013). "Forging sustainable transboundary water-sharing agreements: Barriers and opportunities." *Water Policy*, 15(3), 386–417. doi:10.2166/wp.2012.003.

Weaver, C. P., Lempert, R. J., Brown, C., Hall, J. A., Revell, D., and Sarewitz, D. (2013). "Improving the contribution of climate model information to decision making: The value and demands of robust decision frameworks." *Wiley Interdisciplinary Reviews: Climate Change*, 4(1), 39–60. doi:10.1002/wcc.202.

Westmacott, J. R., and Burn, D. H. (1997). "Climate change effects on the hydrologic regime within the Churchill-Nelson River Basin." *Journal of Hydrology*, 202, 263–279. doi:10.1016/S0022-1694(97)00073-5.

Westra, S., Fowler, H. J., Evans, J. P., Alexander, L. V., Berg, P., Johnson, F., Kendon, E. J., Lenderink, G., and Roberts, N. M. (2014). "Future changes to the intensity and frequency of short-duration extreme rainfall." *Reviews of Geophysics*, 52(3), 522–555. doi:10.1002/2014RG000464.

Wheater, H., and Gober, P. (2013). "Water security in the Canadian Prairies: science and management challenges." *Philosophical Transactions of the Royal Society A: Mathematical, Physical and Engineering Sciences*, 371(2002), 20120409. doi:10.1098/rsta.2012.0409.

Wheater, H. S., Chandler, R. E., Onof, C. J., Isham, V. S., Bellone, E., Yang, C., Lekkas, D., Lourmas, G., and Segond, M. L. (2005). "Spatial-temporal rainfall modelling for flood risk estimation." *Stochastic Environmental Research and Risk Assessment*, 19(6), 403–416. doi:10.1007/s00477-005-0011-8.

Whitfield, P. H., and Pomeroy, J. W. (2016). "Changes to flood peaks of a mountain river: implications for analysis of the 2013 flood in the Upper Bow River, Canada." *Hydrological Processes*, 30(25), 4657–4673. doi:10.1002/hyp.10957.

Wilby, R. L., Conway, D., and Jones, P. D. (2002). "Prospects for downscaling seasonal precipitation variability using conditioned weather generator parameters." *Hydrological Processes*, 16(6), 1215–1234. doi:10.1002/hyp.1058.

Wilby, R. L., and Dessai, S. (2010). "Robust adaptation to climate change." *Weather*, 65(7), 180–185. doi:10.1002/wea.543.

Wild, T. B., Reed, P. M., Asce, M., Loucks, D. P., Asce, D. M., Mallen-cooper, M., and Jensen, E. D. (2019). "Balancing Hydropower Development and Ecological Impacts in the Mekong : Tradeoffs for Sambor Mega Dam." *Journal of Water Resources Planning and Management*, 145(2), 1–14. doi:10.1061/(ASCE)WR.1943-5452.0001036.

Wilks, D. S. (1998). "Multisite generalization of a daily stochastic precipitation generation model." *Journal of Hydrology*, 210, 178–191. doi:10.1016/S0022-1694(98)00186-3.

Wilks, D. S., and Wilby, R. L. (1999). "The weather generation game: a review of stochastic

weather models." *Progress in Physical Geography*, 23(3), 329–357. doi:10.1191/030913399666525256.
Winter, J. M., Yeh, P. J. F., Fu, X., and Eltahir, E. A. B. (2015). "Uncertainty in modeled and observed climate change impacts on American Midwest hydrology." *Water Resources Research*, 51(5), 3635–3646. doi:10.1002/2014WR016056.
Wolf, A. T., Kramer, A., Carius, A., and Dabelko, G. D. (2005). *Managing Water Conflict and Cooperation*. *State of the World - Redefining Global Security*.
Wolf, A. T., Yoffe, S. B., and Giordano, M. (2003). "International waters: identifying basins at risk." *Water Policy*, 5(1), 29–60. doi:10.2166/wp.2003.0002.
Wolfe, M. E. (1992). "The Milk River: Deferred Water Policy Transitions in an International Waterway." *Natural Resources Journal*, 32(1), 55–76.
Wong, J. S., Razavi, S., Bonsal, B. R., Wheater, H. S., and Asong, Z. E. (2017). "Inter-comparison of daily precipitation products for large-scale hydro-climatic applications over Canada." *Hydrology and Earth System Sciences*, 21(4), 2163–2185. doi:10.5194/hess-21-2163-2017.
World Bank. (2019). *Financing Climate Change Adaptation in Transboundary Basins*. World Bank. doi:10.1596/31224.
Wyatt, A. B., and Baird, I. G. (2007). "Transboundary impact assessment in the Sesan River Basin: The case of the Yali Falls Dam." *International Journal of Water Resources Development*, 23(3), 427–442. doi:10.1080/07900620701400443.
Yoffe, S., Wolf, A. T., and Giordano, M. (2003). "Conflict and cooperation over international freshwater resources: Indicators of basins at risk." *Journal of the American Water Resources Association*, 39(5), 1109–1126. doi:10.1111/j.1752-1688.2003.tb03696.x.
Zeff, H. B., Herman, J. D., Reed, P. M., and Characklis, G. W. (2016). "Cooperative drought adaptation: Integrating infrastructure development, conservation, and water transfers into adaptive policy pathways." *Water Resources Research*, 52(9), 7327–7346. doi:10.1002/2016WR018771.
Zeitoun, M., and Mirumachi, N. (2008). "Transboundary water interaction I: Reconsidering conflict and cooperation." *International Environmental Agreements: Politics, Law and Economics*, 8(4), 297–316. doi:10.1007/s10784-008-9083-5.
Zhang, Y. Q., Chiew, F. H. S., Zhang, L., Leuning, R., and Cleugh, H. A. (2008). "Estimating catchment evaporation and runoff using MODIS leaf area index and the Penman-Monteith equation." *Water Resources Research*, 44(10), 1–15. doi:10.1029/2007WR006563.
Zhuang, X. W., Li, Y. P., Huang, G. H., and Wang, C. X. (2017). "Evaluating climate change impacts on the hydrology of watershed in northwestern China using a stepwise-clustered downscaling approach." *International Journal of Climatology*, 37(6), 2961–2976. doi:10.1002/joc.4892.

APPENDIX A: HBV-SASK CALIBRATED PARAMETERS

The table below details all the parameters of the HBV-SASK model applied to the headwater catchments of the SaskRB.

Table A.1. The calibrated parameters of the HBV-SASK model for each headwater catchment used in this study.

#	Catchment gauge	TT	C0	ETF	LP	FC	β (beta)	FRAC	K1	α (alpha)	K2	UBAS	PM	Bias-correction factor
1	05AA002	0.96	1.84	0.43	0.73	213.83	1.00	0.10	0.66	1.00	0.03	1.00	1.00	0.99
2	05AA004	-0.25	0.56	0.43	0.65	307.47	2.33	0.79	0.10	1.64	0.05	2.57	1.00	1.01
3	05AA022	2.35	1.88	0.13	1.00	50.00	1.00	0.31	0.05	1.86	0.05	1.00	1.00	1.13
4	05AA023	0.11	1.23	0.31	0.26	347.62	1.13	0.30	0.46	1.26	0.05	1.32	1.00	1.01
5	05AA024	2.66	2.32	0.05	0.83	434.50	3.00	0.43	0.21	1.03	0.03	1.00	1.00	1.00
6	05AB002	2.28	10.00	0.00	0.08	390.31	1.66	0.64	0.17	1.18	0.05	2.81	1.00	0.97
7	05AB007	3.21	1.56	0.78	0.87	109.28	2.40	0.51	0.14	1.22	0.01	1.20	1.00	0.98
8	05AB021	2.46	5.59	0.00	0.42	449.40	2.84	0.86	0.05	1.55	0.05	1.91	1.00	1.00
9	05AB028	2.94	1.90	0.40	0.53	359.18	2.11	0.73	0.59	1.06	0.00	3.00	1.00	1.07
10	05AC003	0.76	5.78	0.74	0.32	475.20	2.36	0.65	0.28	1.00	0.00	2.70	1.00	1.04
11	05AD002	3.43	1.81	0.87	0.79	278.67	1.00	0.12	0.19	3.00	0.03	1.00	1.00	0.98
12	05AD005	1.86	2.82	0.20	1.00	50.00	1.00	0.10	1.00	3.00	0.05	1.00	1.00	1.84
13	05AD007	2.95	1.50	0.74	0.58	235.36	1.00	0.14	1.00	1.00	0.03	1.00	1.00	1.01
14	05AD008	1.39	0.99	0.14	0.51	87.25	1.00	0.17	1.00	1.00	0.03	1.00	1.00	1.00
15	05AD026	2.29	1.77	0.20	1.00	50.00	1.00	0.84	0.05	1.00	0.00	1.00	1.00	1.05
16	05AD032	2.97	6.99	0.21	1.00	50.00	1.00	0.10	1.00	1.00	0.05	1.00	1.00	2.21
17	05AD041	2.04	1.96	0.03	0.91	375.43	1.00	0.10	0.12	2.74	0.03	1.00	1.00	1.00
18	05AE006	3.59	1.03	0.07	1.00	489.40	1.26	0.11	1.00	1.00	0.04	1.00	1.00	1.00
19	05AE027	3.07	2.12	0.19	1.00	50.00	1.00	0.10	1.00	1.00	0.05	1.00	1.00	1.72
20	05BB001	1.70	3.28	0.03	0.98	76.71	1.50	0.13	0.22	1.41	0.02	1.74	1.00	0.99
21	05BC001	2.16	3.66	0.15	1.00	50.00	1.00	0.13	0.61	1.50	0.02	1.00	1.00	1.04
22	05BD002	-0.11	1.96	0.87	0.33	437.05	1.22	0.28	0.05	1.47	0.01	1.00	1.00	0.99
23	05BE006	0.34	1.81	0.18	0.41	182.90	1.02	0.13	0.05	1.65	0.02	1.00	1.00	1.00
24	05BF001	2.60	4.03	0.15	1.00	243.36	1.06	0.13	0.41	1.33	0.02	1.00	1.00	1.03
25	05BG001	2.85	1.69	0.34	0.91	141.75	1.00	0.20	0.34	1.03	0.01	1.00	1.00	1.01
26	05BG002	0.48	2.28	0.78	0.57	432.30	1.00	0.25	0.07	1.91	0.02	1.00	1.00	1.04

#	Catchment gauge	TT	C0	ETF	LP	FC	β (beta)	FRAC	K1	α (alpha)	K2	UBAS	PM	Bias-correction factor
27	05BH004	2.75	2.77	0.12	0.66	300.52	1.78	0.14	0.27	1.00	0.02	1.00	1.00	1.01
28	05BH008	0.90	1.45	0.25	0.43	163.32	1.36	0.51	0.05	1.00	0.01	1.00	1.00	1.05
29	05BH009	1.06	0.89	0.00	0.00	500.00	3.00	0.90	0.05	1.48	0.05	1.50	1.00	1.04
30	05BJ010	-3.97	0.11	0.41	0.98	194.39	3.00	0.45	0.24	1.28	0.03	1.29	1.00	0.97
31	05BL004	2.66	2.10	0.99	0.54	296.92	1.16	0.26	0.47	1.00	0.04	2.70	1.00	1.03
32	05BL009	2.93	1.66	0.88	0.39	337.24	1.00	0.34	0.29	1.08	0.04	1.37	1.00	1.01
33	05BL024	3.95	2.92	0.00	0.25	423.95	1.56	0.19	0.39	1.00	0.05	1.00	1.00	1.01
34	05CB007	-.96	0.37	0.36	0.46	325.89	1.74	0.48	0.05	1.53	0.01	2.08	1.00	1.03
35	05CC002	-1.45	2.48	0.00	0.28	429.05	2.12	0.48	0.05	1.64	0.04	3.00	1.00	1.03
36	05CD004	-0.12	4.31	0.00	0.30	347.25	2.24	0.59	0.05	1.60	0.02	3.00	1.00	1.02
37	05CE001	1.75	9.61	0.00	0.29	457.43	1.70	0.82	0.05	1.41	0.00	1.55	1.00	1.02
38	05CK004	1.83	7.95	0.01	0.49	438.86	2.68	0.83	0.06	1.31	0.00	3.00	1.00	1.05
39	05DA002	1.51	3.31	0.49	0.61	396.64	1.01	0.18	0.11	1.95	0.02	1.37	1.00	1.00
40	05DA009	2.83	0.90	0.00	1.00	50.00	1.00	0.90	0.34	1.00	0.05	1.00	1.00	1.35
41	05DB002	-2.94	0.15	0.17	0.71	222.85	1.85	0.64	0.05	1.57	0.01	2.07	1.00	0.96
42	05DB006	0.10	0.41	0.51	0.71	163.09	1.92	0.41	0.25	1.24	0.01	2.45	1.00	0.98
43	05DC006	-2.44	0.17	0.65	0.90	109.89	2.38	0.62	0.14	1.29	0.01	1.00	1.00	0.99
44	05DC012	-1.44	0.24	0.09	0.70	112.11	2.68	0.68	0.19	1.31	0.02	1.86	1.00	1.01
45	05DD004	-3.38	0.17	0.16	0.89	73.62	2.10	0.73	0.05	1.73	0.05	1.33	1.00	1.01
46	05DD007	0.24	1.07	0.42	0.61	292.89	1.02	0.27	0.13	1.69	0.02	1.59	1.00	1.01
47	05DD009	-1.40	0.27	0.45	0.91	114.09	2.67	0.71	0.19	1.35	0.01	1.53	1.00	1.00
48	05DE003	-0.40	3.91	0.57	0.29	412.38	2.34	0.35	0.32	1.00	0.01	1.64	1.00	0.97
49	05DE007	-0.51	0.35	0.11	0.24	105.61	1.27	0.71	0.09	1.65	0.00	1.76	1.00	1.08
50	05DE009	0.60	1.83	0.05	0.09	192.03	1.54	0.90	0.45	1.18	0.01	1.43	1.00	1.03
51	05DF003	0.64	3.17	0.09	0.12	299.66	1.82	0.90	0.19	1.00	0.00	1.40	1.00	0.94
52	05DF004	2.66	9.16	0.31	0.42	248.20	2.93	0.90	0.13	1.64	0.01	1.27	1.00	1.04
53	05DF006	1.26	6.99	0.00	0.22	149.77	1.67	0.43	0.06	2.43	0.00	2.56	1.00	0.98
54	05EA001	1.25	2.51	0.07	0.19	393.84	2.13	0.90	0.07	1.00	0.05	1.37	1.00	1.02
55	05EB902	1.25	4.41	0.00	0.29	139.96	3.00	0.82	0.21	1.23	0.00	1.33	1.00	1.01
56	05EC002	2.49	7.55	0.31	0.15	363.90	2.73	0.90	0.21	1.17	0.00	1.95	1.00	1.18
57	05EC005	3.82	10.00	0.41	0.02	229.58	2.57	0.53	0.18	1.01	0.00	2.83	1.00	1.04
58	05EC006	-0.30	1.74	0.02	0.05	251.74	1.99	0.60	0.11	1.00	0.05	3.00	1.00	0.82
59	05ED002	0.91	4.32	0.71	0.36	248.97	2.71	0.81	0.19	1.66	0.00	2.62	1.00	1.00
60	05ED003	1.40	4.31	0.07	0.42	291.12	2.84	0.90	0.23	1.00	0.05	1.74	1.00	0.92
61	05EE007	3.84	5.01	0.70	0.43	444.25	1.07	0.10	0.12	1.00	0.00	1.00	1.00	0.68
62	GBEMOU	3.02	1.30	0.15	0.56	171.04	1.16	0.15	0.34	3.00	0.03	1.00	1.00	0.99
63	GBWCON	4.00	1.41	0.20	1.00	50.00	1.00	0.90	0.05	1.10	0.05	1.00	1.00	2.09
64	GHISQA	2.63	2.35	0.35	0.49	458.91	1.86	0.22	0.36	1.00	0.05	1.34	1.00	1.03
65	GLBMOS	0.49	3.61	0.10	0.09	473.30	1.24	0.17	0.25	1.00	0.00	2.08	1.00	1.05
66	GMOSMO	1.76	9.76	0.51	0.32	280.60	1.51	0.24	0.22	1.05	0.00	1.56	1.00	1.05
67	GRDBIG	1.33	8.52	0.00	0.43	500.00	2.52	0.46	0.05	1.70	0.04	2.29	1.00	1.02
68	GRDJEN	1.65	7.22	0.06	0.54	497.29	3.00	0.64	0.05	1.56	0.03	3.00	1.00	1.04

#	Catchment gauge	TT	C0	ETF	LP	FC	β (beta)	FRAC	K1	α (alpha)	K2	UBAS	PM	Bias-correction factor
69	GSHMOU	0.35	0.54	0.61	0.35	320.22	1.11	0.34	0.37	1.00	0.05	3.00	1.00	1.04
70	GSTDAM	3.77	1.56	0.18	1.00	50.00	1.00	0.12	1.00	1.00	0.03	1.00	1.00	1.06

APPENDIX B: INCREMENTAL FLOW REGRESSION MODELS

In several river reaches an incremental flow is considered to better represent the water budget of the SaskRB. As these incremental flows are not hydrologically modelled, their values are simulated using a regression model in the scenario simulations. The regression model is constructed based on the historical values of the incremental flow of interest, and major upstream flows. The details of the regression models used to simulate incremental flows are described in Table B.1. The names match the IWMSask standards.

Table B.1 Details of the regression models used to simulate the incremental flows.

#	Location	Reference flows (RF)	Regression model
1	Downstream of Bow-Highwood junction	TAU outflow + Calgary Incremental flow + 05BJ010 + Highwood outflow	0.013(RF) + 0.44
2	Upstream of Belly river inflow to Oldman River	Oldman incremental flow	0.66(RF) + 0.22
3	Downstream of Belly River inflow to SSR	Belly River inflow	0.15(RF)+0.04
4	Lethbridge, Oldman River	All upstream flows	0.22(RF)+1.00
5	Inflow of Battle River to NSR	NSR outflow from AB	0.12(RF)
6	Downstream of Battle River	NSR outflow from AB	0.007(RF)
7	Downstream of Battle River	NSR outflow from AB	0.03(RF)
8	Swift Current River to SR	SSR outflow from AB	0.0008(RF)
9	Brightwater Creek to SR	SSR outflow from AB	0.002(RF)
10	Black S Creek to SR	SSR outflow from AB	0.0002(RF)
11	Little M Creek to SR	SSR outflow from AB	0.0008(RF)
12	Dell W Creek to SR	SSR outflow from AB	0.0009(RF)
13	St. Louis Creek to SR	NSR outflow from SK	0.007(RF)
14	Prince Albert to SR	NSR outflow from SK	0.003(RF)

#	Location	Reference flows (RF)	Regression model
15	SK Fork to SR	NSR outflow from SK	0.0074(RF)
16	Nipawin Lake to SR	NSR outflow from SK	0.004(RF)
17	Tobin Lake to SR	NSR outflow from SK	0.44(RF)
18	Upstream of MB to SR	SR outflow from SK	0.17(RF)
19	Before Grand Rapids	SR outflow from SK	1.2(RF)